# EXPANDING THE SCOPE OF HETEROTRIMETALLIC $MMo_2$ COMPLEXES THROUGH HARD-SOFT ACID-BASE CHEMISTRY

by

Brian S. Dolinar

A dissertation submitted in partial fulfillment of

the requirements for the degree of

Doctor of Philosophy

(Chemistry)

at the

UNIVERSITY OF WISCONSIN – MADISON

2016

Date of final oral examination: January 28, 2016

The dissertation is approved by the following members of the Final Oral Committee:

John F. Berry, Professor, Inorganic Chemistry
Shannon S. Stahl, Professor, Organic Chemistry
Clark R. Landis, Professor, Inorganic Chemistry
Daniel C. Fredrickson, Associate Professor, Inorganic Chemistry
Thomas C. Brunold, Professor, Inorganic Chemistry

**Abstract**

Extended Metal Atom Chains (EMACs) are inorganic coordination compounds in which three or more metal atoms are held together in a linear arrangement. Most EMACs and heterometallic EMACs (HEMACs) are composed exclusively of transition metals. This thesis details synthetic methods for generating HEMACs that are not confined to the transition metals through the utilization of Hard-Soft Acid-Base (HSAB) principles. In Chapter 2, the coordination chemistry of different isomers of $Mo_2(SNOX)_4$ (HSNO5 = 5, monothiosuccinimide; HSNO6 = 6-thioxo-2-piperidinone) is detailed. These compounds are structurally characterized by single crystal X-ray diffraction, electrochemically characterized by cyclic voltammetry, and their metal-metal orbitals are described by density functional theory (DFT) calculations. These compounds serve as a baseline against which the compounds synthesized in later chapters can be compared. Chapter 3 describes the synthesis and structure of $pyLiMo_2(SNO5)_4Cl$ (py = pyridine), the first HEMAC that contains a metal outside of the transition metals. Structural studies reveal an abnormally short $Mo_2$–Cl bond distance, which is brought about by polarization of the metal-metal bonding and antibonding orbitals of $[Mo_2]^{4+}$ by the $Li^+$ ion. Chapter 4 expands the results of Chapter 3 to include other examples of HEMACs containing other Group I, II, or III metals as the heterometal. Through the structural and electrochemical analysis of these compounds, it is shown that increasing the charge on the heterometal increases both the Lewis acidity of $[Mo_2]^{4+}$ and the $[Mo_2]^{4+/5+}$ oxidation potential. In Chapter 5, $[(MeOH)_xLnMo_2(SNO5)_4Cl]^{2+}$ (x = 5, Ln = Ce – Nd; x = 4, Ln = Sm – Lu) compounds are prepared. These compounds demonstrate that Ln···$Mo_2$ distance influences both the $[Mo_2]^{4+}$ Lewis acidity and $[Mo_2]^{4+/5+}$ oxidation potential. Finally,

Chapter 6 describes the synthesis of $K_3[Mo_2(SNO5)_4Cl][Mo_2(SNO5)_4]$ the first known example of a heterometallic extended metal atom node (HEMAN) in which two HEMACs intersect.

The work presented here develops the chemistry of EMACs substantially by expanding the scope to include metals from Groups I, II, and III as well as the lanthanides. The charge and M···$Mo_2$ distance of the heterometal influences the Lewis acidity and oxidation potential of the $[Mo_2]^{4+}$ unit.

To Mary Clare and Cecilia Dolinar

**Acknowledgements**

First, I would like to thank my advisor, Professor John Berry. John has been a wonderful mentor over the past five and half years. He taught me how to be successful at chemistry and how to enjoy chemistry. He has always given me leeway to follow the chemistry I want to pursue, which has been very rewarding. I have really enjoyed exploring metal-metal bonding while working for him as well as our discussions on topics unrelated to chemistry, such as music.

I would also like to thank Dr. Ilia Guzei, who has been a mentor to me in crystallography. Working for Ilia as the X-ray crystallography TA was one of the best experiences I had in graduate school. At one point, it seemed like each structure that Ilia would have me solve had a unique twist on a crystallographic problem. Through this work, I learned far more about crystallography than I thought possible.

I owe a great deal to my labmates both past and present: Michael, Mandy, George, Shu, Eugenia, Kasia, Tim, Amanda, Wes, Ryan, Tristan, Travis, Burton, Jill, Nick, and Sungho. Through the years, they have helped me to improve my laboratory skills, my presentation skills, and the way I think about chemistry through their insightful comments and discussions. The success I have experienced in chemistry would not be possible without their help.

I would like to thank Professor Shannon Stahl and Professor Clark Landis for being on my committee since the beginning. The perspective that these two have brought to my chemistry over the years has helped me to focus my research and to describe it in such a way that it appeals to a broader audience. I also would like to thank Professors

Danny Fredrickson and Thomas Brunold for agreeing to be on my final thesis committee and taking the time to read this thesis and offer thoughtful commentary.

I would like to thank Professor Seth Brown at the University of Notre Dame. Seth was my general chemistry professor for my first semester of undergrad, and he gave me the opportunity to begin undergrad research in his lab, during my freshman year. It was through the research I conducted in his lab that I decided to pursue a PhD in chemistry. He taught me a lot about inorganic synthesis, and he has always been a supportive friend.

Next, I would like to thank Stosh Kozimor at Los Alamos National Lab. Stosh gave me the opportunity to work with his group during the summer of 2015, which allowed me to try my hand at installing actinides into the compounds described in this thesis. While this chemistry did not work as planned, it was nonetheless a wonderful experience and taught me a great deal about actinide chemistry.

The chemistry described here would not be possible without the wonderful instrumentation scientists in our department, especially Dr. Charlie Fry, Dr. Monika Ivancic, Dr. Heike Hofstetter, Dr. Martha Vestling, and Dr. Robert Shanks. Thank you for keeping the instruments up and running, answering my questions over the years, and being wonderful colleagues.

Next, my friends outside of chemistry - there are too many of you to name you all individually, which is a good problem that I am very blessed to have. You all have made my time in Madison unforgettable. I would like to thank in particular Ben and Katie Drda, Nathaniel and Heather Turner, Rick Harbaugh, Lauren Poyer, Kerri Barkley, and Johanna Wilson, who have been my closest friends during these years. Thank you for all your support and friendship.

I would also like to thank my parents, Carol and Kevin Dolinar, and brother, Sean Dolinar who have supported me my whole life and taught me to work hard at whatever I choose to do. They have also made the trek from Pittsburgh to Madison numerous times over the past 5 ½ years to visit. Thank you for the love you have shown over the years.

Last, but certainly not least, I would like to thank my wife, Mary Clare, and my daughter, Cecilia. Cecilia and Mary Clare remind me every day that there is life outside of graduate school, and the love that they show for me has greatly enriched my life. Mary Clare has been supportive of my endeavors since we first met nine years ago. She has patiently put up with countless explanations of the problems I have had in chemistry through the years (especially when I have used them to make dinner conversation!). Thank you for everything.

## Table of Contents

## List of Figures

## List of Tables

## List of Schemes

## List of Charts

# Chapter 1

*Introduction and Overview*

## 1.1 Dimolybdenum Paddlewheel Compounds

Dimolybdenum paddlewheel compounds have been structurally known since the 1960s, and the synthesis and characterization of these compounds have greatly enriched the field of inorganic chemistry.[1] The two metal atoms are typically supported by a set of four anionic bridging ligands positioned at 90° increments around the metal-metal core, giving the compounds their iconic paddlewheel shape and holding the two molybdenum atoms close enough to permit metal-metal bonding (Chart 1.1a). In the paddlewheel geometry, the d-orbitals of the two metal atoms overlap, allowing the formation of metal-metal bonds between the atoms.[1a] The electronic structure of the metal-based bonding and antibonding orbitals is depicted in Chart 1.1b. Overlap between the two $d_{z^2}$ orbitals oriented along the $Mo_2$ axis results in the formation of σ-bonding and anti-bonding orbitals. The $d_{xz}$ and $d_{yz}$ orbitals overlap to form π-bonding and anti-bonding orbitals. The $d_{xy}$ orbitals overlap to form δ-bonding and anti-bonding orbitals. The $d_{x^2-y^2}$ orbitals do not typically contribute significantly to metal-metal bonding in paddlewheel compounds because they are raised too high in energy by σ-type interactions with the four bridging ligands. A $[Mo_2]^{4+}$ core has 8 metal based electrons. These 8 electrons fill the bonding orbitals of Chart 1.1b, giving a Mo≡Mo quadruple bond.

The bridging ligands are typically anionic and composed of a three-atom bridge that has a delocalized set of π electrons, such as carboxylates,[2] amidates,[2a,3] amidinates,[2a,4] thioamidates,[2a,5] or guanidinates.[6] In addition to having a σ-type

**Chart 1.1.** The metal-metal bonding manifold of bimetallic paddlewheel compounds

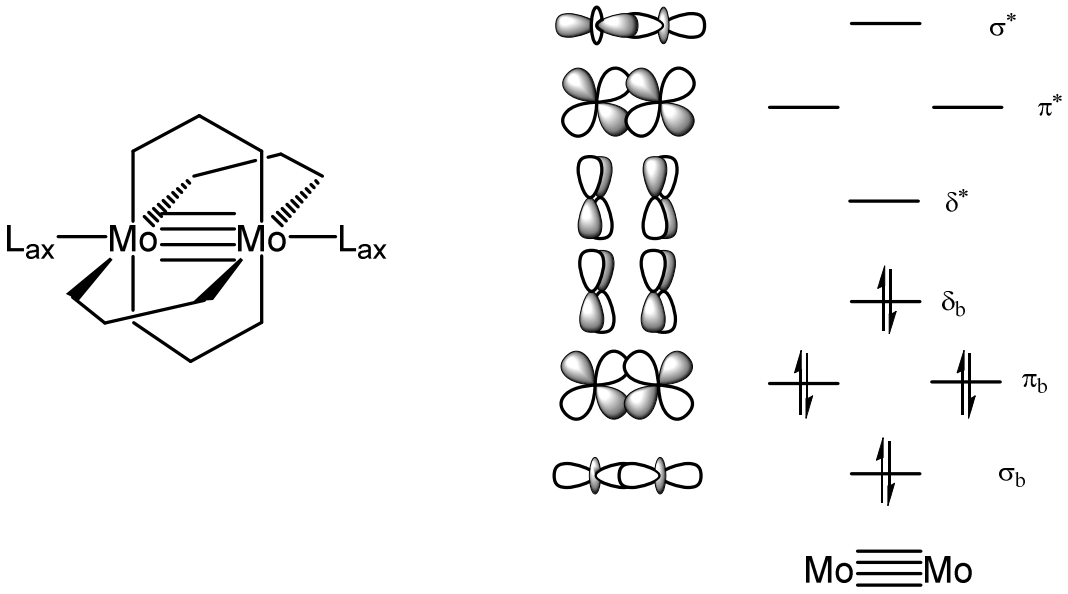


interaction with the $d_{x2-y2}$ orbital, the bridging ligand interacts with the $d_{xy}$ orbitals of the Mo atoms through a π-type interaction. Changes in the electronics and sterics of the bridging ligands influence the relative positions of the metal-metal bonding and antibonding orbitals. Exploration of the different types of ligands (and different substituents with which these ligands can be modified) has been the primary method by which the limits of dimolybdenum chemistry have been tested. Varying the equatorial ligands has led to a wide range of compounds, including the synthesis of supramolecular $[Mo_2]^{4+}$ structures[2b,2c,3b-d,4b,4e,7] with electronic coupling[3e,4a,5,8] and interesting photophysical properties.[6a,9 10] In spite of the development of a range of compounds exhibiting these physical phenomena, $[Mo_2]^{4+}$ compounds have a limited reactivity profile, since they typically reject axial ligation. Other bimetallic compounds (notably $Rh_2$ and $Ru_2$) utilize axial ligation to mediate a variety of chemical reactions.[11] Thus, other methods for modifying the Mo≡Mo quadruple bond manifold are desirable in order to promote $Mo_2$–$L_{ax}$ bonding.

## 1.2 Extended Metal Atom Chains

Changes in the electronics of the equatorial ligand are not the only avenues through which metal-metal bonds can be modified. In 1968, the world's first discrete extended metal atom chain (EMAC), $Ni_3(dpa)_4Cl_2$ (dpa = dipyridyl amide) was synthesized, although its structure would not be known until 1991.[12] An EMAC is a compound containing three or more metal atoms held in a linear arrangement. This compound is remarkable in that the inclusion of the third metal significantly alters the chemical and electronic nature of the metal-metal bonding. Since 1991, homometallic EMACs have blossomed, with trinuclear transition metal EMACs of many of the transition metals being synthesized.[13]

**Chart 1.2.** The different M-$Mo_2$ interactions possible in HEMACs.

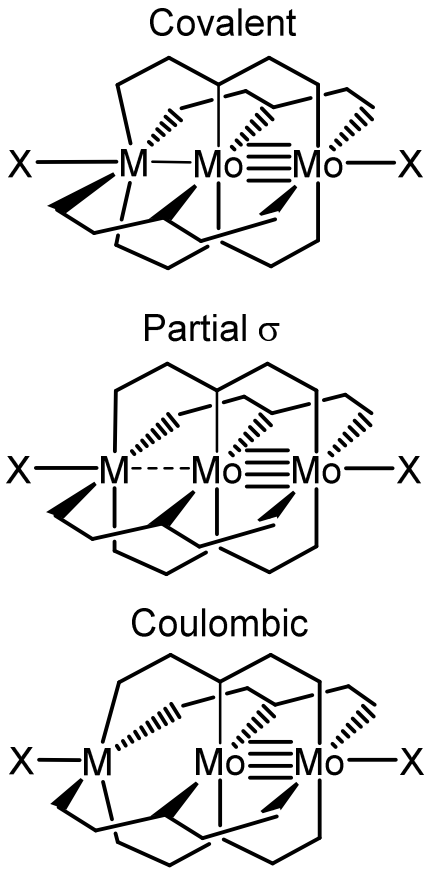

Despite the ubiquity of Mo in bimetallic chemistry, a homometallic $Mo_n$ EMAC with $n > 2$ has remained elusive. Success has instead been found in the synthesis of a number of heterometallic EMACs (HEMACs) containing a $[Mo_2]^{4+}$ bimetallic unit and additional heterometals.[14] These HEMACs have a $[Mo_2]^{4+}$ unit with an axial chloride and a $Mo_2$–Cl bond distance that is significantly shorter than the average in the Cambridge Structural Database (CSD).[15] In these compounds, the heterometal perturbs the metal-metal bonding of the original $[Mo_2]^{4+}$ bimetallic unit *via* one of several methods based on the distance and orbital overlap between the bimetallic unit and the heterometal (Chart 1.2). The first of these categories is the covalent bonding regime, where the heterometal is close enough to the $[Mo_2]^{4+}$ unit that it can form full covalent bonds between each of the metals. Interactions of this type result in delocalization of σ- and π- electrons across the three metals while maintaining localization of the δ-electrons on the $[Mo_2]^{4+}$ unit.[14f,16] The second is the partial σ-bonding regime, in which the heterometal is far enough away from the $[Mo_2]^{4+}$ unit, such that it does not form full covalent bonds, but partial overlap between the σ-symmetry orbitals of the metals is responsible for their interaction. Interactions of this type give rise to a 3-center sigma interaction allowing electrons to be delocalized over the whole metal string.[14c-e] The third is the Coulombic regime, in which the heterometal is sufficiently far enough away that it does not have appreciable orbital overlap with the bimetallic unit, but it can still interact with the metal-metal bonded unit *via* through-space Coulombic interactions. Coulombic interactions are by far the weakest of these three, but they may be able to unlock the reactivity potential of $[Mo_2]^{4+}$ in much the same way cationic activation has resulted in new chemistry of other classically inert metal centers.[17]

Primarily HEMACs containing a $[Mo_2]^{4+}$ group have fallen into the former two categories through the synthesis of $MMo_2$ compounds M = Ru (covalent)[14f,16] and M = Cr – Co (partial σ).[14c-e] Exploration of the Coulombic regime is best accomplished through the synthesis of $MMo_2$ HEMACs in which M is a traditionally redox inert main-group metal. Through the synthesis of these compounds, a systematic study of the effects of charge and cation size on the chemistry of the $[Mo_2]^{4+}$ units can be explored. Current synthetic methods for generating HEMACs most often involve the use of a polypyridyl amide ligand such as dpa.[13b] The dpa ligand is tridentate containing three N atoms that are each capable of binding a metal atom. As a result, dpa is well-tailored to synthesizing HEMACs containing metal atoms of similar Lewis acidity, such as transition metals. However, for HEMACs combining different parts of the periodic table, the lack of diversity in the donor atoms of dpa can hinder selectivity and make synthesis of the desired HEMAC much more difficult. In order to address this issue, two new ligands, 6-thioxo-1-piperidinone (HSNO6) and monothiosuccinimide (HSNO5) have been selected (Chart 1.3) that would be capable of supporting heterotrimetallic compounds. These ligands are accessible via one-step syntheses from commercially available starting materials.[18] The key advantage to these ligands lies in their asymmetry. One end of the ligands is a thioamide, while the other is an amide. Since the S atom of the thioamide is a soft base, while the O atom of the amide is a hard base, Hard-Soft Acid-Base (HSAB) theory can be utilized to synthesize HEMACs that contain both a soft metal ion and a hard metal ion. In the work explored here, it is hypothesized that the S atom will bind to the soft acid $Mo^{2+}$ while the O atom binds to a hard Lewis acid.

**Chart 1.3.** A comparison of the dpa and SNOX ligand

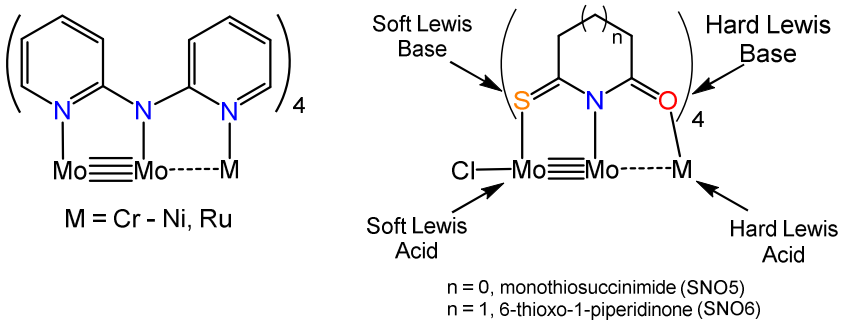


**Scheme 1.1.** Synthetic routes to HSNO6 and HSNO5

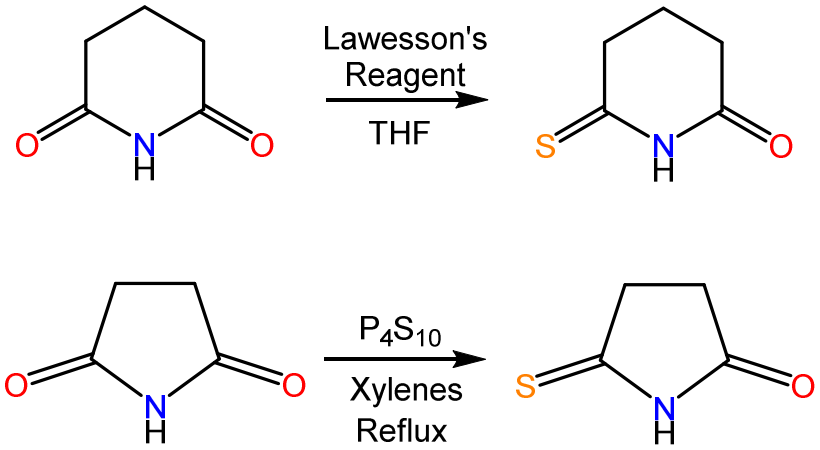


## 1.3 Outline

The work presented here is divided into five parts, focusing on the synthesis of M···Mo≡Mo heterotrimetallic compounds. In the first part, the bimetallic coordination chemistry of HSNO5 and HSNO6 with Mo≡Mo is explored. This part addresses the following questions: 1) Which group (thioamide or amide) binds to the $[Mo_2]^{4+}$ unit? 2) Is it possible to control the ligand arrangement around the $[Mo_2]^{4+}$ core? 3) How do changes to the electronics of the ligand affect the chemistry of $[Mo_2]^{4+}$? This part also provides a baseline for these compounds against which HEMACs can be compared. The

second part will focus on a synthetic method used to generate a $LiMo_2$ HEMAC. In particular, the effect of the $Li^+$ ion on the Lewis acidity and electrochemistry of $[Mo_2]^{4+}$ will be explored. The third part will explore the expansion of the $LiMo_2$ HEMAC synthetic methodology to include $Na^+$, $Ca^{2+}$, $Sr^{2+}$, and $Y^{3+}$ as the heterometals. This expansion allows the charge of the heterometal to be probed as a method for tuning electrochemical and Lewis acidic properties of these compounds. The fourth part explores the synthesis of $Ln\cdots Mo_2$ compounds. The heterometals of these compounds all have the same charge, but different ionic radii, allowing the effect of charge density on the $[Mo_2]^{4+}$ core to be examined. Finally, in the fifth part, the ability of this system to support a $K_3[Mo_2]_4$ supramolecular structure is presented. The structure uses a core of $K^+$ ions to hold together four $[Mo_2]^{4+}$ metal bonded units. These five parts demonstrate the breadth of HEMAC chemistry that can be supported by the HSNO5 ligand and impact that the choice of heterometal identity has on properties of the $[Mo_2]^{4+}$ unit.

**1.4 References**

1. (a) Cotton, F. A.; Murillo, C. A.; Walton, R. A., *Multiple Bonds Between Metal Atoms*. 3rd ed.; Springer Science and Business Media, Inc.: New York, 2005; (b) Chisholm, M. H.; Patmore, N. J., Group 6 Metal-Metal Bonds. In *Molecular Metal-Metal Bonds*, Liddle, S. T., Ed. Wiley-VCH Verlag GmbH & Co. KGaA: Weinheim, Germany, 2015; pp 139-174.

2. (a) Hicks, J.; Ring, S. P.; Patmore, N. J. *Dalton Trans.* **2012**, *41*, 6641. (b) Cotton, F. A.; Murillo, C. A.; Yu, R. *Inorg. Chim. Acta* **2006**, *359*, 4811. (c) Han, L. J.; Fan, L. Y.; Meng, M.; Wang, X.; Liu, C. Y. *Dalton Trans.* **2011**, *40*, 12832.

3. (a) Cotton, F. A.; Li, Z.; Liu, C. Y.; Murillo, C. A. *Inorg. Chem.* **2006**, *45*, 9765. (b) Cotton, F. A.; Liu, C. Y.; Murillo, C. A.; Wang, X. *Inorg. Chem.* **2006**, *45*, 2619. (c) Cotton, F. A.; Murillo, C. A.; Yu, R. *Dalton Trans.* **2006**, 3900. (d) Wilkinson, L. A.; McNeill, L.; Meijer, A. J.; Patmore, N. J. *J. Am. Chem. Soc.* **2013**, *135*, 1723. (e) Wilkinson, L. A.; McNeill, L.; Scattergood, P. A.; Patmore, N. J. *Inorg. Chem.* **2013**, *52*, 9683.

4. (a) Cotton, F. A.; Donahue, J. P.; Huang, P.; Murillo, C. A.; Villagrán, D. *Z. Anorg. Allg. Chem.* **2005**, *631*, 2606. (b) Cotton, F. A.; Donahue, J. P.; Murillo, C. A.; Yu, R. *Inorg. Chim. Acta* **2005**, *358*, 1373. (c) Chan, Z.-K.; Chen, T.-R.; Tsai, Y.-F.; Chen, J.-D.; Wang, J.-C. *Polyhedron* **2007**, *26*, 3715. (d) Krackl, S.; Inoue, S.; Driess, M.; Enthaler, S. *Eur. J. Inorg. Chem.* **2011**, 2103. (e) Hsu, W.; Li, Y.-S.; He, H.-Y.; Chen, K.-T.; Wu, H.-S.; Proserpio, D. M.; Chen, J.-D.; Wang, J.-C. *CrystEngComm* **2014**, *16*, 7385.

5. Cotton, F. A.; Li, Z.; Liu, C. Y.; Murillo, C. A. *Inorg. Chem.* **2007**, *49*, 7840.

6. (a) Cotton, F. A.; Durivage, J. C.; Gruhn, N. E.; Lichtenberger, D. L.; Murillo, C. A.; Van Dorn, L. O.; Wilkinson, C. C. *J. Phys. Chem. B* **2006**, *110*, 19793. (b) Cotton, F. A.; Murillo, C. A.; Wang, X.; Wilkinson, C. C. *Dalton Trans.* **2006**, 4623. (c) Cotton, F. A.; Murillo, C. A.; Wang, X.; Wilkinson, C. C. *Inorg. Chem.* **2006**, *45*, 5493. (d) Cotton, F. A.; Murillo, C. A.; Wang, X.; Wilkinson, C. C. *Dalton Trans.* **2007**, 3943.

7. (a) Byrnes, M. J.; Chisholm, M. H.; Patmore, N. J. *Inorg. Chem.* **2005**, *44*, 9347. (b) Cotton, F. A.; Jin, J. Y.; Li, Z.; Liu, C. Y.; Murillo, C. A. *Dalton Trans.* **2007**, 2328. (c) Cai, X.-M.; Höhne, D.; Köberl, M.; Cokoja, M.; Pöthig, A.; Herdtweck, E.; Haslinger, S.; Herrmann, W. A.; Kühn, F. E. *Organometallics* **2013**, *32*, 6004. (d) Le Gall, B.; Conan,

F.; Kerbaol, J.-M.; Pala Sala, J.; Vigier, E.; Kubicki, M. M.; Le Mest, Y. *C. R. Chim.* **2005**, *8*, 977.

8. (a) Cotton, F. A.; Murillo, C. A.; Villagran, D.; Yu, R., *J. Am. Chem. Soc.* **2006**, *128*, 3281. (b) Cotton, F. A.; Li, Z.; Liu, C. Y.; Murillo, C. A.; Villagran, D. *Inorg. Chem.* **2006**, *45*, 767. (c) Cotton, F. A.; Jin, J. Y.; Li, Z.; Murillo, C. A.; Reibenspies, J. H. *Chem. Commun.* **2008**, 211. (d) Cotton, F. A.; Murillo, C. A.; Young, M. D.; Yu, R.; Zhao, Q. *Inorg. Chem.* **2008**, *47*, 219. (e) Han, M. J.; Liu, C. Y.; Tian, P. F. *Inorg. Chem.* **2009**, *48*, 6347. (f) Shu, Y.; Lei, H.; Tan, Y. N.; Meng, M.; Zhang, X. C.; Liu, C. Y. *Dalton Trans.* **2014**, *43*, 14756.

9. (a) Byrnes, M. J.; Chisholm, M. H.; Gallucci, J. A.; Liu, Y.; Ramnauth, R.; Turro, C. *J. Am. Chem. Soc.* **2005**, *127*, 17343. (b) Burdzinski, G. T.; Chisholm, M. H.; Chou, P. T.; Chou, Y. H.; Feil, F.; Gallucci, J. C.; Ghosh, Y.; Gustafson, T. L.; Ho, M. L.; Liu, Y.; Ramnauth, R.; Turro, C. *Proc. Nat. Acad. Sci. U. S. A.* **2008**, *105*, 15247. (c) Cotton, F. A.; Li, Z.; Murillo, C. A. *Inorg. Chem.* **2009**, *48*, 11847. (d) Cotton, F. A.; Dalal, N. S.; Kaur, N.; Murillo, C. A.; Young, M. D.; Zhao, Q. *J. Cluster Sci.* **2010**, *21*, 301. (e) Bunting, P.; Chisholm, M. H.; Gallucci, J. C.; Lear, B. J. *J. Am. Chem. Soc.* **2011**, *133*, 5873. (f) Alberding, B. G.; Chisholm, M. H.; Gallucci, J. A.; Ghosh, Y.; Gustafson, T. L. *Proc. Nat. Acad. Sci. U. S. A.* **2011**, *108*, 8152. (g) Alberding, B. G.; Chisholm, M. H.; Lear, B. J.; Naseri, V.; Reed, C. R. *Dalton Trans.* **2011**, *40*, 10658. (h) Brown-Xu, S. E.; Chisholm, M. H.; Gallucci, J. C.; Ghosh, Y.; Gustafson, T. L.; Reed, C. R. *Dalton Trans.* **2012**, *41*, 2257. (i) Brown-Xu, S. E.; Chisholm, M. H.; Durr, C. B.; Spilker, T. F. *J. Am. Chem. Soc.* **2013**, *135*, 8254. (j) Brown-Xu, S. E.; Chisholm, M. H.; Durr, C. B.; Lewis, S. A.; Spilker, T. F.; Young, P. J. *Inorg. Chem.* **2014**, *53*, 637. (k) Brown-Xu, S. E.;

Chisholm, M. H.; Durr, C. B.; Lewis, S. A.; Spilker, T. F.; Young, P. J. *Chem. Sci.* **2014**, *5*, 2657. (l) Alberding, B. G.; Chisholm, M. H.; Durr, C. B.; Gallucci, J. C.; Ghosh, Y.; Spilker, T. F. *Dalton Trans.* **2014**, *43*, 11397.

10. Brown-Xu, S. E.; Chisholm, M. H.; Durr, C. B.; Lewis, S. A.; Naseri, V.; Spilker, T. F. *Chem. Sci.* **2013**, *4*, 2105.

11. (a) Berry, J. F. *Dalton Trans.* **2012**, *41*, 700. (b) Berry, J. F. *J. Chem. Sci.* **2015**, *127*, 209.

12. (a) Hurley, T. J.; Robinson, M. A. *Inorg. Chem.* **1968**, *7*, 33. (b) Aduldecha, S.; Hathaway, B. *J. Chem. Soc. Dalton Trans.* **1991**, 993.

13. (a) Berry, J. F. *Multiple Bonds Between Metal Atoms*. 3rd ed.; Springer Science and Business Media, Inc.: New York, 2005; (b) Brogden, D. W.; Berry, J. F. *Comments Inorg. Chem.* **2016**, *36*, 17.

14. (a) Mashima, K.; Shimoyama, Y.; Kusumi, Y.; Fukumoto, A.; Yamagata, T.; Ohashi, M. *Eur. J. Inorg. Chem.* **2007**, *2007*, 235. (b) Ohashi, M.; Shima, A.; Rüffer, T.; Mizomoto, H.; Kaneda, Y.; Mashima, K. *Inorg. Chem.* **2007**, *46*, 6702. (c) Nippe, M.; Bill, E.; Berry, J. F. *Inorg. Chem.* **2011**, *50*, 7650. (d) Nippe, M.; Victor, E.; Berry, J. F. *Eur. J. Inorg. Chem.* **2008**, *2008*, 5569. (e) Brogden, D. W.; Christian, J. H.; Dalal, N. S.; Berry, J. F. *Inorg. Chim. Acta* **2015**, *424*, 241. (f) Brogden, D. W.; Berry, J. F. *Inorg. Chem.* **2015**, *54*, 7660.

15. Allen, F. H., *Acta Crystallogr., Sect. B: Struct. Sci.* **2002**, *B58*, 380-388.

16. Brogden, D. W.; Berry, J. F. *Inorg. Chem.* **2014**, *53*, 11354.

17. (a) Krogman, J. P.; Bezpalko, M. W.; Foxman, B. M.; Thomas, C. M. *Inorg. Chem.* **2013**, *52*, 3022. (b) Kuppuswamy, S.; Bezpalko, M. W.; Powers, T. M.; Turnbull, M. M.;

Foxman, B. M.; Thomas, C. M. *Inorg. Chem.* **2012**, *51*, 8225. (c) Kuppuswamy, S.; Bezpalko, M. W.; Powers, T. M.; Wilding, M. J. T.; Brozek, C. K.; Foxman, B. M.; Thomas, C. M. *Chem. Sci.* **2014**, *5*, 1617. (d) Kuppuswamy, S.; Powers, T. M.; Johnson, B. M.; Bezpalko, M. W.; Brozek, C. K.; Foxman, B. M.; Berben, L. A.; Thomas, C. M. *Inorg. Chem.* **2013**, *52*, 4802. (e) Kuppuswamy, S.; Powers, T. M.; Krogman, J. P.; Bezpalko, M. W.; Foxman, B. M.; Thomas, C. M., *Chem. Sci.* **2013**, *4*, 3557; (f) Marquard, S. L.; Bezpalko, M. W.; Foxman, B. M.; Thomas, C. M. *Organometallics* **2014**, *33*, 2071. (g) Wu, B.; Hernandez Sanchez, R.; Bezpalko, M. W.; Foxman, B. M.; Thomas, C. M. *Inorg. Chem.* **2014**, *53*, 10021. (h) Zhou, W.; Marquard, S. L.; Bezpalko, M. W.; Foxman, B. M.; Thomas, C. M. *Organometallics* **2013**, *32*, 1766.

18. (a) Berg, U.; Sandström, J. *Acta Chem. Scand.* **1966**, *20*, 689. (b) Zhu, X.; Giordano, T.; Yu, Q.-S.; Holloway, H. W.; Perry, T. A.; Lahiri, D. K.; Brossi, A.; Greig, N. H. *J. Med. Chem.* **2003**, *46*, 5222.

# Chapter 2

*Electronic Tuning of $Mo_2$(thioamidate)$_4$ Complexes through π-system Substituents and cis/trans Isomerism*



## 2.1 Abstract

We report an exploration of the coordination chemistry of a systematic series of cyclic thioamidate ligands with the quadruply-bonded $[Mo_2]^{4+}$ core. In addition to the S and N donor atoms that bind to Mo, the ligands utilized in this study have an additional O or S atom in conjugation with the thioamidate π system. The preparation of four new $Mo_2$ complexes is described, and these compounds are characterized by X-ray crystallography, NMR and UV-vis spectroscopy, electrochemistry, and DFT calculations. These complexes provide a means to interrogate the electronics of $Mo_2$(thioamidate)$_4$ systems. Notably, we describe the first two examples of $Mo_2$(thioamidate)$_4$ complexes in their *cis*-2,2-regioisomer. By varying the π-system substituent and regioisomerism of these compounds, the electronics of the dimolybdenum core is shown to be altered with varying degrees of effect. Cyclic voltammetry results show that changing the π-system substituent from O to S results in an increase in the $[Mo_2]^{4+/5+}$ oxidation potential by 170 mV. Changing the arrangement of ligands around the dimolybdenum core from *trans*-2,2 to *cis*-2,2 slightly weakens the metal-ligand bonds, raising the oxidation potential by a more modest 30-100 mV. MO diagrams of each compound derived from DFT calculations support these conclusions as well; the identity of the π-system substituent

alters the δ-δ* (HOMO-LUMO) gap by up to 0.4 eV, whereas regioisomerism yields smaller changes in the electronic structure.

**2.2 Introduction**

Metal-metal bonded bimetallic paddlewheel compounds of the transition metals have been a rich source of diverse chemistry for the past 50 years,[1] and are currently of interest with regards to their reactivity,[2] catalytic,[3] electronic,[4] photophysical,[5] and structural properties.[6] Most notable among these compounds are a plethora of $[Mo_2]^{4+}$ paddlewheel complexes supported by carboxylate, amidate, and amidinate equatorial bridging ligands that have been synthesized, and whose properties have been studied in great detail.[1] The difference in the basicity of these ligands has been demonstrated to tune properties such as the $[Mo_2]^{4+/5+}$ redox potential and the HOMO/LUMO gap.[7] In contrast, only a small handful of $[Mo_2]^{4+}$ compounds containing thioamidate bridging ligands have been reported.[7-8] Thioamidate ligands have been shown to have electronic properties intermediate between carboxylates, amidates, and amidinates.[7] Yet, there has been no systematic study of $Mo_2$(thioamidate)$_4$ compounds to determine how changes to the ligand architecture or ligand arrangement in the complex affect the electronics of the $[Mo_2]^{4+}$ core.

The thioamide ligands monothiosuccinimide (HSNO5), dithiosuccinimide (HSNS5), 6-thioxo-2-piperidinone (HSNO6), and 2,6-piperidinedithione (HSNS6) used in this study are shown in Scheme 2.1. These ligands consist of a thioamide group that can readily bind to the $[Mo_2]^{4+}$ core as well as an O or S atom in conjugation with the thioamidate unit that can alter the electronics of the ligand. The ligands that contain oxygen as the π-substituent in principle could bind to $[Mo_2]^{4+}$ either through S or O, but

we have shown previously that these ligands preferentially bind through S in agreement with predictions from hard-soft acid-base (HSAB) theory.[8a]

**Scheme 2.1.** The ligands used in this project.

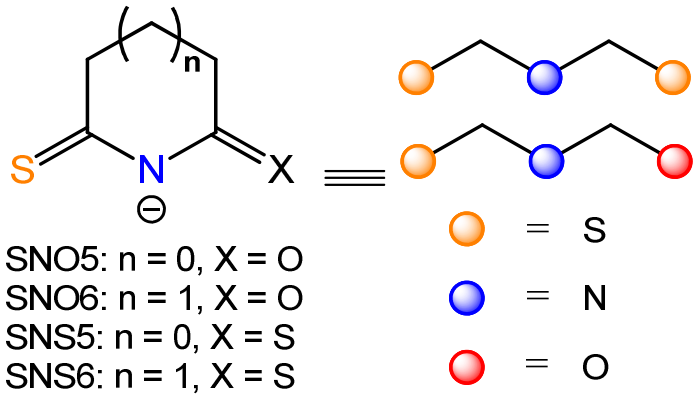


In addition to changes to the ligand composition, the electronics of $[Mo_2]^{4+}$ paddlewheel complexes can be altered by changing the arrangement of the ligands around the $[Mo_2]^{4+}$ core. In bridging ligands like amidates and thioamidates that contain two different donor atoms, four different regioisomers are possible as shown in Scheme 2.2.[7] For analogous $Mo_2(amidate)_4$ complexes the *trans*-2,2 arrangement predominates, but a number of compounds with *cis*-2,2 arrangements are known.[7,9] The few $Mo_2(thioamidate)_4$ compounds that are known adopt the *trans*-2,2 arrangement around the $[Mo_2]^{4+}$ core exclusively, where two thioamidate ligands *trans* to each other are oriented in the same direction along the Mo≡Mo vector, while the other two thioamidate ligands are oriented in the opposite direction.[7-8] The *trans*-2,2 arrangement is the thermodynamically favored regioisomer, presumably due to sterics.[7] Previous experiments with the HSNOX ligands have yielded compounds with the *trans*-2,2-

$Mo_2(SNOX)_4$ (Scheme 2.3, compounds **1a** and **1b**) when the deprotonated ligand was allowed to react with $Mo_2(OAc)_4$ or $Mo_2(TFA)_4$. However, when the thermodynamics of the reaction were altered by inclusion of a Lewis acidic cation as a template, the 4,0 arrangement was observed.[8a]

**Scheme 2.2.** The regioisomers of $Mo_2(thioamidate)_4$ complexes.

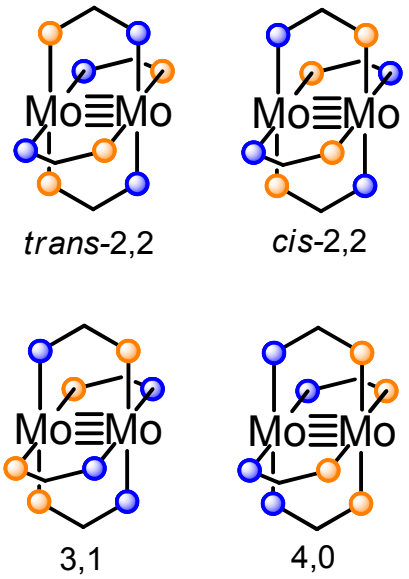


**Scheme 2.3.** The syntheses of a) $Mo_2(SNOX)_4$ complexes and b) $Mo_2(SNSX)_4$ complexes.

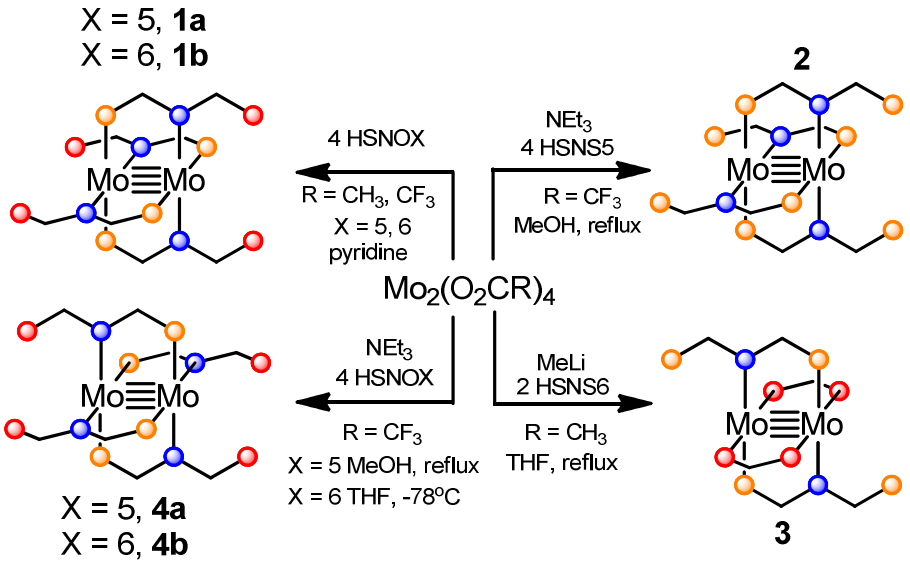

We now report the synthesis and characterization of four new dimolybdenum paddlewheel complexes that contain thioamidate supporting ligands including the first two examples of *cis*-2,2 isomers: *trans*-2,2-$Mo_2(SNS5)_4$ (**2**), *trans*-1,1-$Mo_2(OAc)_2(SNS6)_2$ (**3**), *cis*-2,2-$Mo_2(SNO5)_4$ (**4a**), and *cis*-2,2-$Mo_2(SNO6)_4$ (**4b**). Within this series of compounds it is possible now to examine the role that the π-substituent identity (O vs S) and regioisomerism (*cis* vs *trans*) play in the electronic structure of the $Mo_2$(thioamidate)$_4$ core. These compounds are studied structurally using X-ray crystallography, and their electronics are probed by electrochemistry, UV-vis spectroscopy, and DFT calculations.

## 2.3 Experimental

### 2.3.1 General

All synthetic manipulations were carried out under an inert $N_2$ atmosphere using standard Schlenk and glovebox techniques unless otherwise stated. $CH_2Cl_2$ and 1,2-$C_2H_4Cl_2$ were dried sequentially over molecular sieves and $CaH_2$ and distilled under $N_2$ prior to use. Hexane was dried using a Vacuum Atmospheres solvent purification system and degassed with $N_2$ prior to use. Pyridine was dried sequentially over molecular sieves and barium oxide. It was then distilled under $N_2$ and stored in a glovebox prior to use. All other commercial reagents were used as received without further purification. Acetic acid, acetic anhydride, Lawesson's reagent, glutarimide, succinimide, $P_2S_5$, lithium hexafluorophosphate, tetrabutyl ammonium hexafluorophosphate, trifluoroacetic acid and molybdenum carbonyl were purchased from Sigma Aldrich. Molybdenum acetate ($Mo_2(OAc)_4$) was synthesized from molybdenum carbonyl, acetic acid, and acetic anhydride.[10] Molybdenum trifluoroacetate ($Mo_2(TFA)_4$) was synthesized from

$Mo_2(OAc)_4$ and trifluoroacetic acid.[11] Monothiosuccinimide (HSNO5) and dithiosuccinimide (HSNS5) were prepared from succinimide and $P_2S_5$.[12] 2,6-piperidinedithione (HSNS6) was prepared from glutarimide and Lawesson's reagent.[13] 6-thioxo-2-piperidinone (HSNO6) was prepared from glutarimide and either Lawesson's reagent or $P_2S_5$.[12-13] Elemental analysis was carried out by Midwest Microlabs in Indianapolis, IN, USA. Mass spectrometry data were recorded at the Mass Spectrometry Facility of the Chemistry Instrument Center of the University of Wisconsin—Madison. Matrix-assisted laser desorption/ionization (MALDI) mass spectra were obtained using a Bruker REFLEX II spectrometer equipped with a 337 nm laser, a reflectron, delayed extraction, and a time-of-flight (TOF) analyzer or a Bruker ULTRAFLEX spectrometer equipped with a SmartBeam laser. The IR spectra were taken on a Bruker TENSOR 27 spectrometer using ATR techniques. $^1H$ and $^{13}C$ NMR spectra were recorded on either a Bruker AC-360 or Bruker Avance-500 spectrometer.

**2.3.2 Syntheses**

***trans*-2,2-tetrakis(dithiosuccinimidato)dimolybdenum(II) (*trans*-2,2-$Mo_2(SNS5)_4$) (2)**

A 50 mL Schlenk flask was charged with 84.7 mg HSNS5 (0.645 mmol) and 101.0 mg $Mo_2(TFA)_4$ (0.1591 mmol). These were dissolved in 20 mL MeOH, immediately giving an orange solution. Then, 150 μL $NEt_3$ (1.1 mmol) was added *via* syringe, and a purple-brown solid immediately precipitated. The reaction mixture was heated to 71° C for 24 h and subsequently cooled to room temperature. The purple-brown microcrystalline solid was collected by filtration, washed with 2 x 25 mL MeOH, and dried under vacuum overnight. Yield 99.1 mg (87.4%). X-ray quality crystals were obtained by slow diffusion of hexanes into a $CH_2Cl_2$ solution of **2**. Anal. calcd. for

$C_{17}H_{18}Cl_2Mo_2N_4S_8$ ($Mo_2(SNS5)_4 \cdot CH_2Cl_2$): C, 25.60%; H 2.27%; N, 7.02%. Found C, 25.79%; H, 2.24%; N, 6.93%. $^1$H NMR (500 MHz, $CDCl_3$) δ 3.64 (m, 2H) 3.36 (m, 2H). $^{13}$C NMR (125 MHz, $CDCl_3$) δ 224.58, 215.55, 45.15, 42.20. IR (ATR, $cm^{-1}$) 2911 vw, 1421 w, 1372 m 1302 s, 1210 vs (C=S), 1175 s, 1111 m, 1035 vw, 975 vw, 937 vw, 787 vw. MALDI-TOF Mass Spectrum (m/z) 712 $[M]^+$. UV-vis ($CH_2Cl_2$, $\lambda_{max}$, nm [$\varepsilon(M^{-1}, cm^{-1})$]): 375 [17,000], 505 [5,100])

***trans*-1,1-*bis*(2,6-piperidinedithionato)*bis*(acetato)dimolybdenum(II) ($Mo_2(SNS6)_2(OAc)_2$) (3)**

A 100 mL Schlenk flask was charged with 1.06 g 2,6-piperidinedithione (7.30 mol) dissolved in 30 mL anhydrous THF. After cooling this solution to -78° C, 4.6 mL (7.4 mmol) of a 1.6 M solution of MeLi in $Et_2O$ was added via syringe, and the solution turned a brilliant orange color and evolved a gas. Once gas evolution ceased, the solution was allowed to warm to room temperature over a period of 30 minutes. Then, this solution was transferred via cannula to a flask containing 1.57 g $Mo_2(OAc)_4$ (3.67 mmol). The reaction mixture immediately became a deep shade of emerald green, and a similarly colored green precipitate formed. The reaction mixture was allowed to stir at room temperature for 5.5 h. The resulting solid was collected by filtration in air and was washed with methanol (3 x 50 mL). The solid was then dissolved in $CH_2Cl_2$ by continuous extraction under nitrogen. The $CH_2Cl_2$ was then removed under vacuum. The resulting green solid was washed with hexanes and collected by gravity filtration in air. Yield: 553 mg (25.3%). Suitable crystals for X-ray diffraction were obtained by slow diffusion of hexanes into a saturated solution of $Mo_2(SNS)_2(OAc)_2$ in $CH_2Cl_2$. Anal. calcd. for $C_{14}H_{18}Mo_2N_2O_4S_4$ : C, 28.10 %; H, 3.03%; N, 4.68%. Found: C, 27.97%; H,

3.09%; N, 4.61%. $^1$H NMR ($CDCl_3$, 300 MHz, ppm): δ 3.35 (t, *J* = 6.3 Hz, 2H, CSC*H*$_2$CH$_2$CH$_2$CS), 2.94 (t, *J* = 6.3 Hz, 2H, CSCH$_2$CH$_2$C*H*$_2$CS), 2.87 (s, 3H, C*H*$_3$CO$_2$), 2.10 (p, *J* = 6.3 Hz, 2H, CSCH$_2$C*H*$_2$CH$_2$CS). MALDI-TOF Mass Spectrum (m/z): 598.8 m/z $[M]^+$. IR (ATR, $cm^{-1}$): 2933 vw, 2851 vw, 1487 w, 1433 m, 1412 m, 1362 s, 1331 s, 1266 s, 1238 m, 1203 w, 1165 w, 1102 vs (C=S), 1034 w, 1020 m, 961 m, 921 m, 906 m, 852 w, 791 m, 738 w, 731 w, 669 s, 632 w, 628 w. UV-Vis ($CH_2Cl_2$, $\lambda_{max}$, nm [ε($M^{-1}$, $cm^{-1}$)]): 371 [17000], 477 [1200], 648 [2400].

***cis*-2,2-tetrakis(monothiosuccinimidato)dimolybdenum(II) (*cis*-2,2-Mo$_2$(SNO5)$_4$)(4a)**

A 50 mL Schlenk flask was charged with 196 mg HSNO5 (1.70 mmol) and 268 mg $Mo_2(TFA)_4$ (0.422 mmol). These were dissolved in 20 mL MeOH. Then, 350 µL $NEt_3$ (2.5 mmol) was added, and immediately the solution became a brilliant orange color. Within a minute, a red-orange precipitate formed. The reaction was then heated to 71° C for 16 hours, and then cooled to room temperature. The solid was collected by filtration, washed with 3 x 25 mL MeOH and dried overnight under vacuum. Yield: 215 mg (78.6%). Suitable crystals for X-ray diffraction were obtained by dissolving the compound in $CH_2Cl_2$ and layering with hexanes. Crystals of the bis-methanol solvate could be obtained in the same manner except with the omission of the vacuum drying step of the procedure. Anal. calcd. for $C_{16}H_{16}S_4N_4O_4Mo_2$: C, 29.63%; H, 2.49%; N, 8.64%. Found C, 29.62%; H, 2.54%; N, 8.38%. $^1$H NMR (500 MHz, $CDCl_3$) δ 3.52 (dt, *J*=20, 5 Hz, 4H, OCCH$_2$C*H*HCS), 3.47 (dt, *J*=20, 5Hz, 4H, OCCH$_2$CH*H*CS), 2.81 (t, *J* = 5 Hz, 8H, OCC*H*$_2$CH$_2$CS). $^{13}$C NMR (500 MHz, $CDCl_3$) δ 216.31, 187.38, 39.48, 32.43. IR (ATR, $cm^{-1}$): 2938 (vw), 1722 (m) (C=O), 1430 (w), 1411 (w), 1400 (s), 1242 (m),

1200 (vs) (C=S), 1115 (w), 1020 (m), 1000 (w), 916 (w), 811 (w), 668 (w). MALDI-TOF MS (m/z): 649 [$M^+$]. UV-vis ($CH_2Cl_2$, λ(nm) [ε($M^{-1}cm^{-1}$)]): 410 [8560], 498 [1100].

**_cis_-2,2-tetrakis(monothiopiperidinonato)dimolybdenum(II) (_cis_-2,2-$Mo_2$(SNO6)$_4$, (4b)**

A 50 mL Schlenk flask was charged with 298 mg HSNO6 (2.31 mmol) and 440 mg LiCl (10.4 mmol) dissolved in 20 mL THF. A separate 100 mL Schlenk flask was charged with 367 mg $Mo_2(TFA)_4$ (0.578 mmol) and 460 mg LiCl (10.85 mmol) dissolved in 20 mL THF. To the ligand solution was added 500 μL $NEt_3$. Then, both of these solutions were cooled to -78°C. The ligand solution was added to the metal solution *via* cannula. Immediately, the reaction changed to a deep, red-violet color. After 30 s - 1 min, the THF solvent was removed under vacuum. The residue was extracted by 20 mL $CH_2Cl_2$ at room tempearture. Upon layering with hexanes, a red-orange solid appeared. The solid was then washed with 3 x 20 mL degassed $H_2O$ and 3 x 30 mL $Et_2O$. The remaining solid was recrystallized from 1,2-$C_2H_4Cl_4$ by layering with $Et_2O$, yielding an orange powder. Yield: 34.8 mg (8.56%). Suitable crystals for X-ray diffraction were obtained by further recrystallization of the powder from 1,2-$C_2H_4Cl_2$ layered with hexanes. The low yield of this reaction precluded characterization by elemental analysis. $^1$H NMR ($CDCl_3$, 500 MHz, ppm) δ 3.42 (dt, *J* = 18, 5.5 Hz, 4H, SCC*H*HCH$_2$CH$_2$CO), 3.29 (ddd, *J* = 18, 8.5, 5 Hz, 4H, SCCH*H*CH$_2$CH$_2$CO), 2.59 (dt, *J* = 18, 5.5 Hz, 4H, SCCH$_2$CH$_2$C*H*HCO), 2.49 (ddd, *J* = 18, 9.5, 5.5 Hz. 4H, SCCH$_2$CH$_2$CH*H*CO), 2.13 (m, 8H, SCCH$_2$C*H*$_2$CH$_2$CO). $^{13}$C NMR ($CDCl_3$, 125 MHz, ppm) δ 208.4, 177.7, 39.6, 32.1, 21.6. IR (ATR, $cm^{-1}$) 1687 m (C=O), 1441 m, 1404 s, 1331 m, 1256 vs, 1240 vs, 1177 vs, 1119 vs, 1054 vw, 976 m, 941 w, 913 w, 885 w, 847 w, 765 w, 664 m, 645 m, MALDI-

TOF Mass Spectrum (m/z) 704 $[M]^+$ UV-vis ($CH_2Cl_2$, $\lambda_{max}$, nm [ε ($M^{-1}$, $cm^{-1}$)]): 449 [6910], 502 [2100].

**2.3.3 X-ray Crystallography**

Suitable single crystals of **2**·$CH_2Cl_2$, **4a**·$CH_2Cl_2$, and **4b**·1,2-$C_2H_4Cl_2$ and twinned crystals for **3** and **4a**·2MeOH were selected under oil and ambient conditions. The crystals were attached to the tip of a MiTeGen MicroMount and mounted in a stream of cold nitrogen at 100(1) K (**2**·$CH_2Cl_2$, **3**, **4a**·$CH_2Cl_2$, **4a**·2MeOH , **4b**·1,2-$C_2H_4Cl_2$) or 200(1) K (**4a**·2MeOH ) and centered in the X-ray beam using a video monitoring system. The crystal evaluation and data collection were performed on a Bruker Quazar SMART APEX-II diffractometer with Mo Kα (λ = 0.71073 Å) (**2**·$CH_2Cl_2$, **3**, **4a**·$CH_2Cl_2$, **4a**·2MeOH (100 K), **4b**·1,2-$C_2H_4Cl_2$) or Cu Kα (λ = 1.54178Å) (**4a**·2MeOH (200 K)) radiation. The data were collected using a routine to survey an entire sphere of reciprocal space and were indexed by the SAINT program.[14] The structures were solved *via* direct methods and refined by iterative cycles of least-squares refinement on $F^2$ followed by difference Fourier synthesis using the SHELX2013 program.[15] In structures **4a**·2MeOH (100 K) and **4a**·2MeOH (200 K), the MeOH hydrogen atom of the major component was located from the Fourier difference map and refined independently. All other hydrogen atoms were included in the final structure factor calculation at idealized positions and were allowed to ride on the neighboring atoms with relative isotropic displacement coefficients. The unit cell for **4a**·2MeOH was also determined at several temperatures between 100K to 200K using Cu Kα (λ = 1.54178Å) radiation.

**Table 2.1**. The crystallographic details of compounds **1-4**.

| Compound | **2** | **3** | **4a**·$CH_2Cl_2$ | **4a**·2MeOH | **4a**·2MeOH | **4b**·2 1,2-DCE |
|---|---|---|---|---|---|---|
| Empirical formula | $C_{17}H_{18}Cl_2Mo_2N_4S_8$ | $C_{14}H_{18}Mo_2N_2O_4S_4$ | $C_{18}H_{20}Cl_4Mo_2N_4O_4S_4$ | $C_{18}H_{24}Mo_2N_4O_6S_4$ | $C_{18}H_{24}Mo_2N_4O_6S_4$ | $C_{24}H_{32}Cl_4Mo_2N_4O_4S_4$ |
| Formula weight | 797.61 | 598.42 | 818.30 | 712.53 | 712.53 | 902.46 |
| Temperature/K | 100(1) | 100(1) | 100(1) | 100(1) | 200(1) | 100(1) |
| λ/Å | 0.71073 | 0.71073 | 0.71073 | 0.71073 | 1.54178 | 0.71073 |
| Crystal system | monoclinic | monoclinic | monoclinic | triclinic | monoclinic | monoclinic |
| Space group | $P2_1/c$ | $P2_1/c$ | $P2_1/c$ | $P\bar{1}$ | $P2_1/c$ | $P2_1/c$ |
| *a*/Å | 16.322(6) | 8.4950(2) | 9.101(4) | 8.990(3) | 9.0133(5) | 9.7312(2) |
| *b*/Å | 10.791(4) | 7.4672(2) | 20.55(1) | 14.717(7) | 14.716(1) | 9.0334(2) |
| *c*/Å | 16.081(7) | 15.4637(4) | 7.445(4) | 10.048(4) | 10.0976(7) | 19.1659(4) |
| α/° | 90 | 90 | 90 | 89.65(2) | 90 | 90 |
| β/° | 105.44(3) | 104.634(1) | 110.31(2) | 112.53(1) | 111.403(4) | 103.771(1) |
| γ/° | 90 | 90 | 90 | 88.73(2) | 90 | 90 |
| Volume/$Å^3$ | 2730(2) | 949.10(4) | 1306(1) | 1227.6(9) | 1247.0(2) | 1636.36(6) |
| Z | 4 | 2 | 2 | 2 | 2 | 2 |
| $\rho_{calc}mg/mm^3$ | 1.940 | 2.094 | 2.081 | 1.928 | 1.898 | 1.832 |
| 2Θ range for data collection | 2.588 to 51.884° | 4.96 to 61.08° | 3.964 to 54.952° | 7.014 to 55.056° | 10.542 to 144.784° | 4.3 to 63.22° |
| Independent reflections | 5323 | 2908 | 2981 | 8926 | 2451 | 5496 |
| R(int) | 0.0599 | 0.0549 | 0.0542 | 0.0618 | 0.0219 | 0.0408 |
| Data/restraints/parameters | 5323/0/298 | 2908/0/119 | 2981/10/173 | 8926/0/336 | 2451/39/180 | 5496/0/217 |
| Goodness-of-fit on $F^2$ | 1.296 | 1.099 | 1.060 | 0.978 | 1.060 | 1.048 |
| Final R indexes [I>=2σ (I)][a,b] | $R_1$ = 0.0480 $wR_2$ = 0.1090 | $R_1$ = 0.0241 $wR_2$ = 0.0551 | $R_1$ = 0.0366 $wR_2$ = 0.0833 | $R_1$ = 0.0516, $wR_2$ = 0.1176 | $R_1$ = 0.0182 $wR_2$ = 0.0447 | $R_1$ = 0.0220 $wR_2$ = 0.0551 |
| Final R indexes [all data] | $R_1$ = 0.0658 $wR_2$ = 0.1167 | $R_1$ = 0.0326 $wR_2$ = 0.0573 | $R_1$ = 0.0509 $wR_2$ = 0.0884 | $R_1$ = 0.0740 $wR_2$ = 0.1269 | $R_1$ = 0.0196 $wR_2$ = 0.0453 | $R_1$ = 0.0293 $wR_2$ = 0.0577 |

[a]$R_1 = \Sigma||F_o| - |F_c||/[\Sigma|F_o|]$. [b]$wR_2 = |[\Sigma[w(F_o^2 - F_c^2)^2]/[\Sigma[w(F_o^2)^2]]]^{1/2}$, $w = 1/\sigma^2(F_o^2) + (aP)^2 + bP$, where $P = [\max(0 \text{ or } F_o^2) + 2(F_c^2)]/3$.

The details concerning X-ray crystallographic structure solutions and refinement for **2**·$CH_2Cl_2$, **3**, **4a**·$CH_2Cl_2$, **4a**·2MeOH (100 K), **4a**·2MeOH (200 K), and **4b**·1,2-$C_2H_4Cl_2$ are tabulated in Table 2.1. For each structure, the model was refined to a low wR2 value (< 0.15 for all data in each case).

### 2.3.4 Electrochemistry

Cyclic voltammetry was performed for compounds **2**, **4a**, and **4b** on solutions of 1 mM analyte and 100 mM electrolyte ($NBu_4PF_6$) in $CH_2Cl_2$ at 20°C using a standard glassy carbon electrode for the working electrode, a platinum wire for the auxiliary electrode, and an $Ag/Ag^+$ electrode as the reference electrode. All electrochemical potentials were internally referenced to the ferrocene/ferrocenium couple. The voltammetry was performed in the range of 1200 mV to -1200 mV at a scan rate of 100 mV/s.

### 2.3.5 Calculations

Restricted Kohn-Sham geometry optimization and single-point calculations were carried out on **1a**, **1b**, **2**, **4a**, and **4b** through the ORCA electronic structure package using the B3LYP functional.[16] The def3 basis sets from the Karlsruhe group were used,[17] which are automatically recontracted in ORCA for use with the scalar relativistic zeroth-order regular approximation (ZORA). Optimized structures for these compounds were calculated using initial atomic coordinates taken from the crystal structures and then optimized until the energy change between steps was less than $10^{-6}$ Hartree. All calculations were optimized with a Grid4 optimization grid and tight SCF convergence criteria.

## 2.4 Results and Discussion

### 2.4.1 Syntheses

We recently reported the preparation of compounds **1a** and **1b** by reaction of $Mo_2(TFA)_4$ with HSNO5 and $Mo_2(OAc)_4$ with HSNO6, respectively, in pyridine.[8a] However, in the course of our work here, we have determined that the previously reported preparation of **1a** yields a mixture containing predominantly **1a** with small amounts of other isomeric impurities.[18]

Compound **2** was synthesized in good yield (87%) by the reaction of $Mo_2(TFA)_4$ with a stoichiometric amount of HSNS5 and an excess of $NEt_3$ in MeOH as shown in Scheme 2.3. The compound is not very soluble in MeOH and precipitates directly from the reaction mixture upon addition of $NEt_3$. Compound **2** is more soluble in halogenated solvents, such as $CH_2Cl_2$ and $CHCl_3$, and is somewhat soluble in MeCN. It can be easily purified by washing with MeOH and recrystallizing from $CH_2Cl_2$ by layering with hexanes.

Compound **3** was synthesized in moderate yield (25 %) by reacting $Mo_2(OAc)_4$ with a stoichiometric amount of LiSNS6. Immediately a green solid precipitates upon addition of the deprotonated ligand to $Mo_2(OAc)_4$. Preparation of the tetra-substituted complex, $Mo_2(SNS6)_4$, was attempted in numerous ways, including using a synthetic method analogous to that of **2** as well as forcing conditions such as excess ligand and reaction temperatures as high as 140° C in diglyme. In our hands, these reactions routinely yielded a mixture of di-, tri-, and tetra-substituted compounds as evidenced by MALDI-MS, but these were not separable. It is likely that the sterics of the HSNS6

ligand make the tri- and tetra-substituted compounds thermodynamically disfavored in comparison to the di-substituted compound.

Compound **4a** forms under similar reaction conditions as **2**, using the HSNO5 ligand in place of HSNS5. In this case, the *cis*-2,2 regioisomer is favored instead of the *trans*-2,2 isomer, and can be synthesized in 79% isolated yield. In comparison with the synthesis of **1a**, it is evident that changing the solvent from pyridine to methanol provides selectivity for one regioisomer over the other.

Formation of tetra-substitued **4a** requires the use of $Mo_2(TFA)_4$ as a starting material and an external base, such as $NEt_3$, in order achieve reaction completion. Using $Mo_2(OAc)_4$ as a starting material and omitting the base causes the reaction not to go to completion. Rather, the reaction stops at the disubstituted species **5** (Figure 2.S1), which is the SNO5 analogue of **3**.

The preparation of **4b** is not nearly as facile as that of **4a**. When the same reaction conditions for preparing **4a** are used with the HSNO6 ligand, the result is predominantly *trans*-2,2-$Mo_2(SNO6)_4$, compound **1b**. Compound **4b** can be isolated as a minor, kinetic product from the reaction of $Mo_2(TFA)_4$ with HSNO6 and $NEt_3$ in THF at -78°C (Scheme 2.3). Indeed, the major product from this reaction has also proven to be **1b**, but the two isomers can be separated by washing with water, in which **1b** is soluble, and ether followed by extraction with 1,2-$C_2H_4Cl_2$.

Compound **4b** is soluble in halogenated solvents such as $CH_2Cl_2$, 1,2-$C_2H_4Cl_2$, and chloroform as well as alcohols. It is sparingly soluble in acetonitrile, water, toluene, and diethyl ether. It is insoluble in hexanes.

### 2.4.2 NMR Spectroscopy

The *trans*-2,2 SNX5 complexes have idealized $D_{2d}$ point symmetry and have mirror planes coplanar with the plane of the ligands, which makes both geminal methylene protons chemically equivalent. In *cis*-2,2-$Mo_2(SNO5)_4$, the symmetry is $C_{2h}$, and the mirror plane passes between adjacent ligands, rather than through the ligands. Molecules of *cis*-2,2-$Mo_2(SNO6)_4$, while not rigidly held to $C_{2h}$ symmetry, can nonetheless adopt a conformation that has $C_{2h}$ symmetry in solution. For both cases of the *cis*-2,2 regioisomer, this leads us to expect that the geminal methylene protons are not chemically equivalent, which distinguishes the *cis*-2,2 complexes from their corresponding *trans*-2,2 complexes.

The $^1$H NMR spectrum of **2** consists of two signals at 3.64 and 3.36 ppm. These signals show no sign of geminal coupling that would be indicative of chemically independent methylene protons. Thus, this spectrum is consistent with the *trans*-2,2 regioisomer of $Mo_2(SNS5)_4$.

The $^1$H NMR spectrum of **4a** consists of three signals that show coupling in an $ABX_2$ type pattern, and it is distinct from the spectrum of **1a** based on this coupling.[18] There are two partially overlapping, yet chemically distinct signals around 3.5 ppm, which show a strong geminal coupling constant ($J$=20 Hz). These signals are assigned to two protons on the methylene group closest to the C=S bond based on where those protons appear in the spectrum of the free HSNO5 ligand. The other signal around 2.8 ppm belongs to the $CH_2$ adjacent to the C=O bond. These two protons coincidentally have the same chemical shift. This spectrum is only consistent with the *cis*-2,2 regioisomer of $Mo_2(SNO5)_4$.

Likewise, the $^1$H NMR spectrum of **4b** shows 6 distinct signals, one for each of the 6 ligand protons. There are two signals at 3.42 and 3.25 ppm that correspond to the methylene protons adjacent to the C=S group, as well as two signals at 2.59 and 2.49 ppm that correspond to the methylene protons adjacent to the C=O group. A group of overlapping signals at 2.13 ppm corresponds to the methylene spacer. Like the $^1$H NMR spectrum of **4a**, this spectrum is consistent with the *cis*-2,2 ligand arrangement.

### 2.4.3 X-ray Crystallography

The relevant bond distances for structures of **1a**, **1b**, **2**, **3**, **4a**, and **4b** are listed in Table 2.2. Structures **2**·$CH_2Cl_2$, **3**, **4a**·$CH_2Cl_2$, and **4b**·1,2-$C_2H_4Cl_2$ all crystallized in the monoclinic space group $P2_1/c$. Crystals of **4a**·2MeOH were formed by recrystallizing solid **4a** that had precipitated from the reaction mixture without first drying it *in vacuo*. Crystals of **4a**·2MeOH were found to undergo a phase transition and were either monoclinic $P2_1/c$ or triclinic $P\bar{1}$ depending on the temperature at which the data were collected (*vide infra*).

**Table 2.2**. The relevant bond distances for compounds **1-4**

| Compound | Mo-Mo (Å) | | Mo-N (Å) | | Mo-S (Å) | | Reference |
|---|---|---|---|---|---|---|---|
| | Exp. | DFT | Exp. | DFT | Exp. | DFT | |
| **1a** | 2.1112(4) | 2.0862 | 2.145[2] | 2.1493 | 2.4753[8] | 2.5231 | 8a |
| **1b** | 2.1150(2) | 2.0746 | 2.153[3] | 2.2167 | 2.481[8] | 2.5379 | 8a |
| **2**·$CH_2Cl_2$ | 2.1242(6) | 2.1336 | 2.155[6] | 2.1482 | 2.485[2] | 2.4925 | This work |
| **3** | 2.108(2) | - | 2.160(2) | - | 2.4813(6) | - | This work |
| **4a**·$CH_2Cl_2$ | 2.145(2) | 2.0824 | 2.166[3] | 2.1597 | 2.496[2] | 2.5206 | This work |
| **4a**·2MeOH (100 K) | 2.153[2] | 2.1313 | 2.164[5] | 2.1868 | 2.499[2] | 2.5116 | This work |
| **4a**·2MeOH (200 K) | 2.1408(3) | | 2.159[2] | | 2.4942[5] | | This work |
| **4b**·1,2-$C_2H_4Cl_2$ | 2.1061(2) | 2.0832 | 2.162[2] | 2.1917 | 2.4790[4] | 2.5016 | This work |

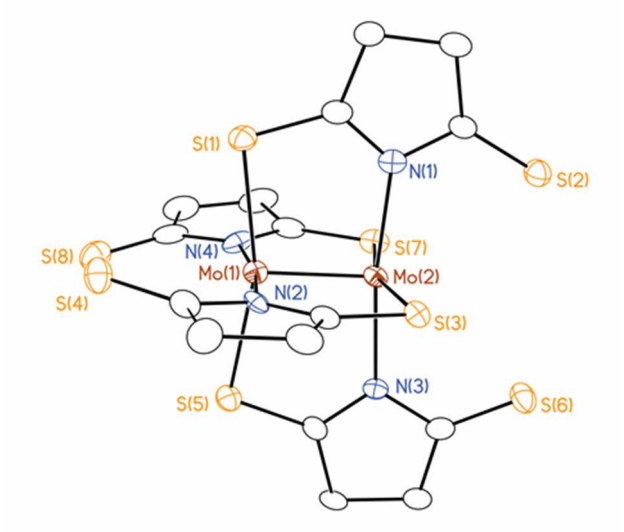


**Figure 2.1.** The crystal structure of *trans*-2,2-$Mo_2(SNS5)_4$ (**2**). All atoms are drawn as 50% probability thermal ellipsoids. All hydrogen atoms and solvents of crystallization are omitted for clarity. The compound crystallizes with a molecule of $CH_2Cl_2$ in the asymmetric unit.

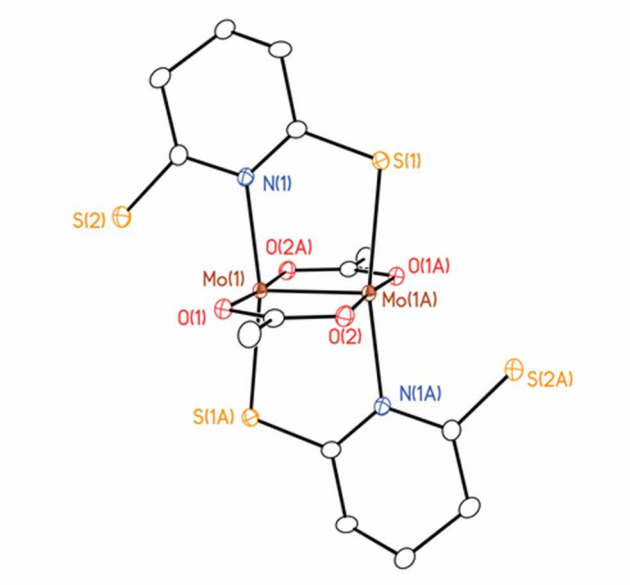


**Figure 2.2.** The crystal structure of *trans*-1,1-$Mo_2(OAc)_2(SNS6)_2$ (**3**). All atoms are drawn as 50% probability thermal ellipsoids. All hydrogen atoms are omitted for clarity.

The X-ray crystal structures of **2**, **3**, **4a**·$CH_2Cl_2$, **4a**·2MeOH, and **4b**·1,2-$C_2H_4Cl_2$ (Figures 2.1-2.5, respectively) each confirmed the identification of the regioisomers determined by NMR spectroscopy (*vide supra*). **2**·$CH_2Cl_2$, is in the *trans*-2,2 arrangement, **3**, is the *trans*-1,1 isomer,[19] **4a**·$CH_2Cl_2$ is the *cis*-2,2 isomer, and **4b**·1,2-DCE, is also the *cis*-2,2 isomer. There is significant variation in the Mo≡Mo bond length among compounds **2-4**. Compounds **2**, **3** and **4b**, have Mo≡Mo bond lengths of 2.1242(6) Å, 2.108(2) Å, and 2.1061(2) Å, respectively, which are typical for Mo≡Mo quadruple bonds. Compound **4a**, on the other hand, has a Mo≡Mo bond length of 2.145(2) Å, which is longer than most Mo≡Mo bonds, especially those containing thioamidate bridging ligands.[1,7-8] The arrangement of molecules in the unit cell of **4a** results in an oxygen atom from one molecule being in close proximity (2.607(3) Å) to the axial position of an adjacent molecule of **4a**. This close Mo···O interaction likely elongates the Mo≡Mo bond slightly by donating some electron density into the σ-antibonding orbital of the $[Mo_2]^{4+}$ unit.

The crystallographically determined metal-ligand bond distances are less varied than the Mo≡Mo bond distances for complexes **2** - **4**. The Mo–N bond distances range from 2.155[6] Å to 2.166[3] Å, and the Mo–S distances range from 2.4790[4] Å to 2.499[2] Å, both of which are typical for $Mo_2$(thioamidate)$_4$ complexes. The Mo–N bond distances for complexes **4a** and **4b** are slightly, yet statistically significantly longer than those of **1a** and **1b** by ~0.02 Å and 0.01 Å, respectively.[8a] The pendant oxygen atoms of the ligand are much closer to each other in the *cis*-2,2 complexes (O···O distance: **4a** = 3.28 Å, **4b** = 2.98 Å) than they are in the corresponding *trans*-2,2 complexes (O···O distance: **1a** = 4.60 Å, **1b** = 3.28 Å), which results in this slight elongation of the *cis*-2,2

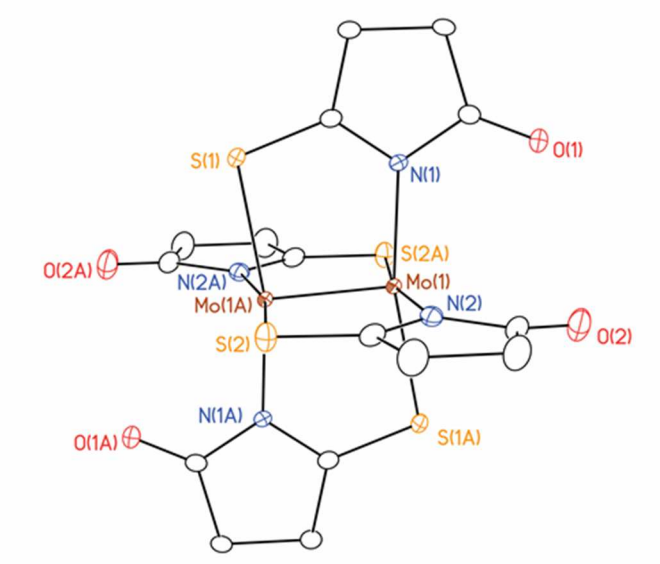


**Figure 2.3.** The crystal structure of *cis*-2,2-$Mo_2(SNO5)_4$ (**4a**). All atoms are drawn as 50% probability thermal ellipsoids. All hydrogen atoms are omitted for clarity.

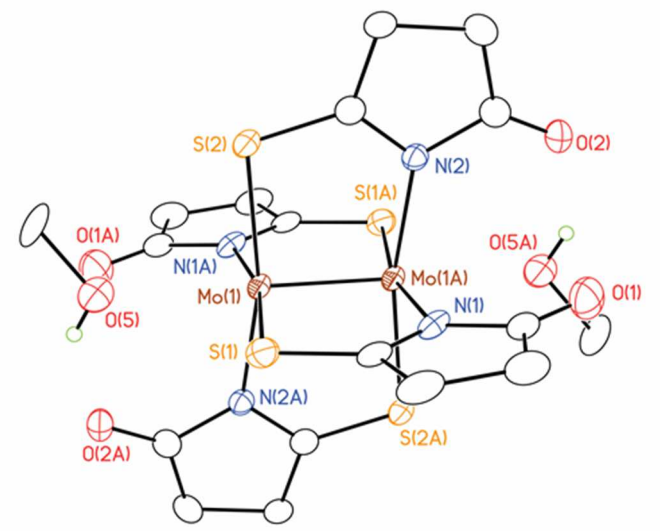


**Figure 2.4.** The 100 K crystal structure of one molecule of **4a**·2MeOH. All atoms are drawn as 50% probability thermal ellipsoids. All hydrogen atoms except the alcohol protons of the MeOH solvate are omitted for clarity.

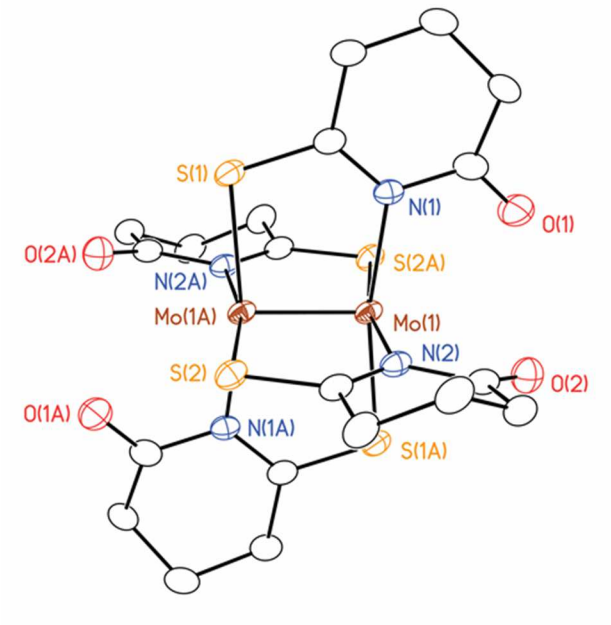


**Figure 2.5.** The X-ray crystal structure of *cis-2,2*-$Mo_2(SNO6)_4$ (**4b**). All atoms are drawn as 50% probability thermal ellipsoids. All hydrogen atoms and solvent molecules are omitted for clarity.

Mo–N and, to a lesser extent, the Mo–S bond distances. This metal-ligand bond weakening in the *cis*-2,2 isomer will be further discussed in relation to the observed trends in the electrochemical data (*vide infra*).

Compound **4a** also crystallizes as a MeOH solvate, **4a**·2MeOH. In this solvate, the MeOH molecules occupy the axial position of **4a**, but the Mo···O distances are long, 2.653(9) Å . Like its unsolvated counterpart, this long Mo···O axial interaction likely elongates the Mo≡Mo bond (2.153[2] Å). The crystallographic data also show that the OH group of the MeOH molecule forms a hydrogen bond with the carbonyl group of a coordinated $SNO5^-$ ligand. In the *cis*-2,2 isomer, the ligand arrangement allows the MeOH to form this close contact with the $[Mo_2]^{4+}$ core as well as the hydrogen bond,

whereas in the *trans*-2,2 isomer, the arrangement of the ligands sterically prevents MeOH from forming a close contact with the $[Mo_2]^{4+}$ core, and thus prevents this interaction. This set of interactions likely causes the *cis*-2,2 regioisomer to be the thermodynamically favored product over the *trans*-2,2 regioisomer when the formation of **4a** is carried out in MeOH.

### 2.4.4 Phase Change of 4a·MeOH

Two complete crystallographic data sets were taken on crystals of **4a**·2MeOH, one at 100 K and one at 200 K. At 200 K, the unit cell was determined to be a monoclinic *P* cell with the dimensions $a$ = 9.0133(5) Å, $b$ = 14.716(1) Å, $c$ = 10.0976(7) Å, $\alpha = \gamma = 90°$, $\beta = 111.403(4)°$, and at 100 K, the unit cell was determined to be a triclinic *P* cell with the dimensions $a$ = 8.990(3) Å, $b$ = 14.717(7) Å, $c$ = 10.048(4) Å, $\alpha = 89.646(17)°$, $\beta = 112.528(13)°$, $\gamma = 88.73(2)°$. The 200 K structure has an asymmetric unit that consists of 1/2 of one molecule of **4a** with a MeOH molecule occupying the axial position. A crystallographic center of symmetry lies at the midpoint of the Mo≡Mo bond. At 100 K, the asymmetric unit consists of two symmetry independent half molecules of **4a** with corresponding MeOH molecules in each axial position.

The unit cell was measured at various temperatures between 200 K and 100 K. Figure 2.6 shows the deviation of the unconstrained α angle from 90°. At temperatures > 160 K, the α angle is very close to 90°. However, between 160 K and 150 K, the deviation of α from 90° rapidly increases to 0.25°. From the inflection point of this graph, the transition temperature was determined to be 153 ± 1 K. In addition to the loss of symmetry from monoclinic P to triclinic P, twinning occurs upon cooling the crystal below 153 K. The two twin components are related by a 2-fold rotation around the *b* axis

(twin law: $\begin{bmatrix} \bar{1} & 0 & 0 \\ 0 & 1 & 0 \\ 0 & 0 & \bar{1} \end{bmatrix}$). The twinning reverses itself upon warming. The same crystal was able to undergo this phase transition several times.

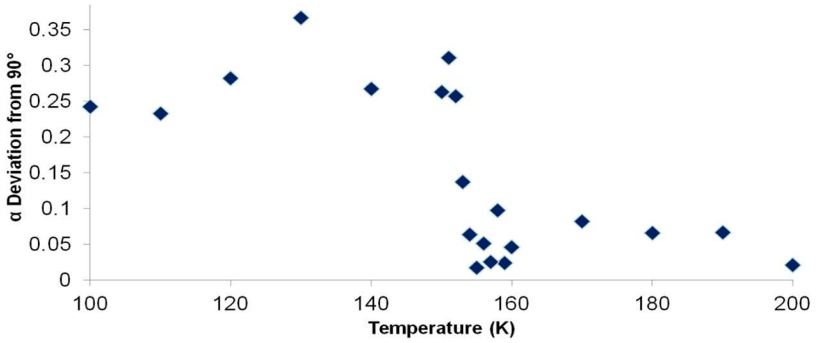


**Figure 2.6.** The temperature dependence of the deviation of the α unit cell parameter from 90° of 4a·MeOH. This is an unconstrained parameter.

A side-by-side comparison of the 200 K and 100 K structures suggests a reason for the phase change (Figure 2.7). At 200 K, the MeOH in the axial position of the $[Mo_2]^{4+}$ complex is positionally disordered such that 86% of the time it forms a hydrogen bond with atom O1 and 14% of the time it forms a hydrogen bond with atom O2 where O1 and O2 are the oxygen atoms of adjacent SNO5 ligands. At 100 K, one of the symmetry independent molecules of **4a** has a MeOH that is disordered much like the 200 K structure, while the other independent molecule of **4a** has an ordered MeOH that forms a hydrogen bond with only one ligand oxygen atom. This difference in MeOH hydrogen bonding behavior prevents these two symmetry independent molecules from being related to each other by a two-fold screw axis as they are in the 200 K structure. The ordering of one of the MeOH molecules upon cooling further supports the suggestion that hydrogen bonding plays an important role in the formation of the *cis*-2,2 isomer of $Mo_2(SNO5)_4$.

a)

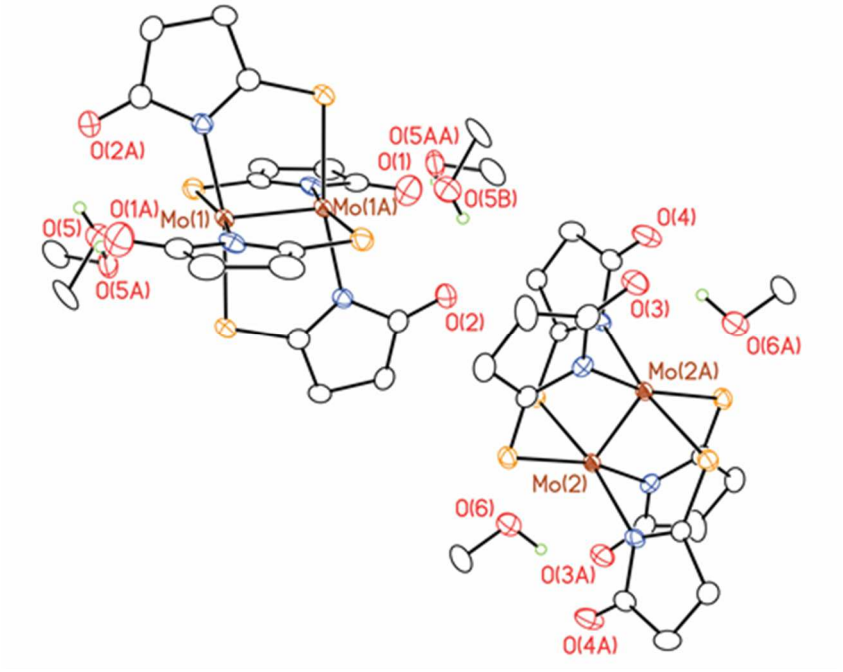


b)

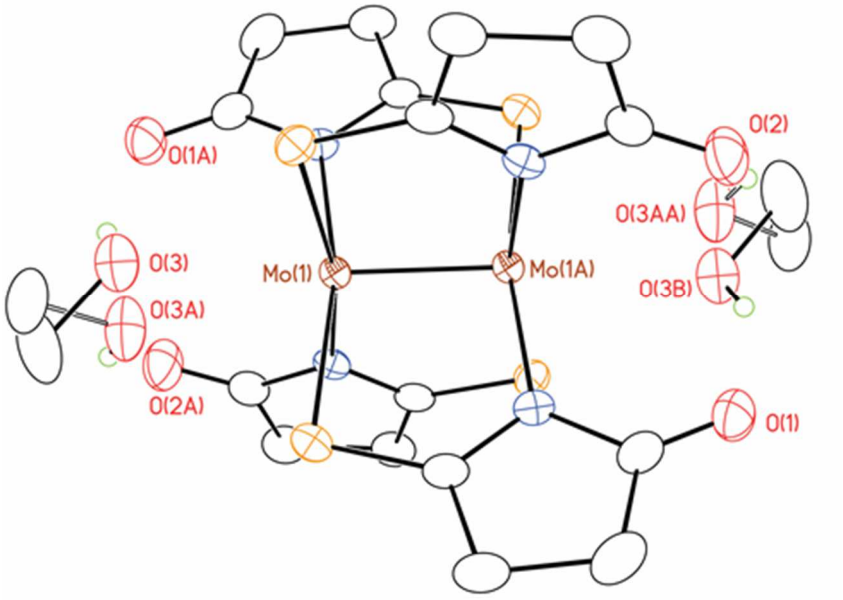


**Figure 2.7.** A comparison of the (a) 100 K and (b) 200 K structures of **4a**, illustrating the disorder present in both complexes. The atoms are drawn as either 50% (100 K) or 40% (200 K) thermal ellipsoids. All hydrogen atoms, except those on the MeOH solvate molecules has been omitted for clarity.

### 2.4.5 Electrochemistry

**Table 2.3**. The $E_{1/2}$ and $E_a$ of the $Mo_2(SN)_4$ compounds studied in this project. All potentials are referenced to $Fc/Fc^+$ couple.

| Compound | $E_{1/2}$ (mV) | $E_a$ (mV) | Solvent | Reference |
|---|---|---|---|---|
| (**3**) | - | 693 | $CH_2Cl_2$ | This work |
| (**4a**) | - | 520 | $CH_2Cl_2$ | This work |
| (**4b**) | - | 443 | $CH_2Cl_2$ | This work |
| (**1a**) | 388 | 425 | MeCN | 8a |
| (**1b**) | 351 | 415 | $CH_2Cl_2$ | 8a |

The electrochemical oxidation potentials of compounds **2**, **4a**, and **4b** are presented in Table 2.3 alongside the *trans*-2,2-$Mo_2(SNO5)_4$ and *trans*-2,2-$Mo_2(SNO6)_4$ complexes. For each of these compounds, the CV showed an irreversible signal between 400 mV and 700 mV vs. $Fc/Fc^+$, which is attributed to the $[Mo_2]^{4+/5+}$ oxidation potential and is among the highest oxidation potentials reported for this redox process in $Mo_2$(thioamidate)$_4$ complexes (literature range: 92 - 520 mV vs. $Fc/Fc^+$).[7,8a,8c,8d] While these waves are irreversible, preventing an accurate determination of the $E_{1/2}$ of the redox couple, the anodic peak potentials for these compounds can be compared since they were taken at the same scan rate of 100 mV/s. The *trans*-2,2 complexes have the lowest potential; the *cis*-2,2 complexes have oxidation potentials that are approximately 30 - 100 mV higher than their *trans*-2,2 counterparts. The oxidation potential of **2** has a potential that is 170 mV higher than the highest of the $Mo_2(SNOX)_4$ complexes (Figure 2.8).

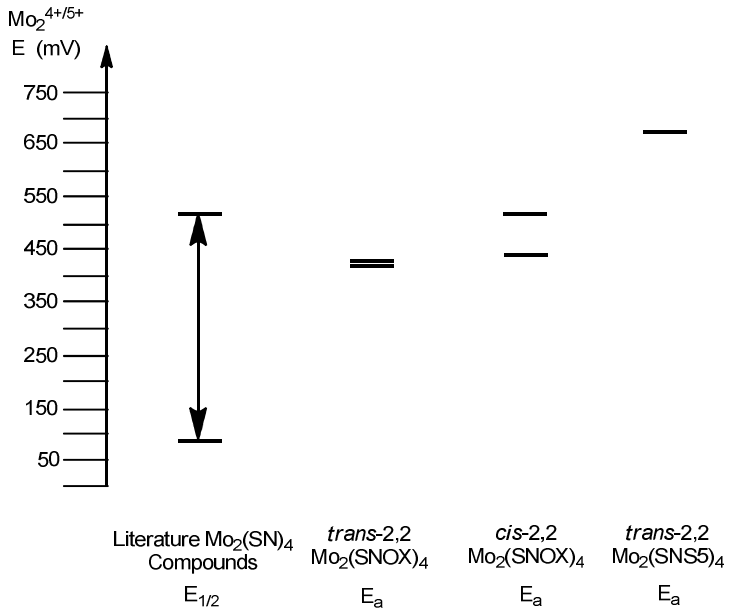


**Figure 2.8.** A comparison of the oxidation potentials of $Mo_2(SN)_4$ complexes.

This trend in oxidation potentials is related to the degree to which the equatorial thioamidate ligands can donate electron density to the $[Mo_2]^{4+}$ core in order to stabilize the $[Mo_2]^{5+}$ oxidation state. In the *trans*-2,2 complexes, the ligands are the least sterically crowded, and thus are able to form the strongest bonds with the $[Mo_2]^{4+}$ core. The slightly weaker metal-ligand bonds in the *cis*-2,2 complexes are not able to stabilize the $[Mo_2]^{5+}$ core as well as those of the *trans*-2,2 complex, and may be responsible for the slight increase in oxidation potential.

Despite being a *trans*-2,2 complex, **2** has by far the highest oxidation potential of all the compounds compared here. The main difference between **2** and the other compounds is that it bears SN*S* rather than SN*O* ligands. Thus, the inherent electronic differences between SNS and SNO ligands must be taken into account. In the SNS ligand, the valence 3p orbitals of the pendant S atom do not overlap as well in a $\pi$ sense with the 2p orbitals of the adjacent C atom as does the O 2p orbital of the SNO ligand. Thus there is less C=S double bond character in the SNS ligands than there is with the C

and O atoms of the SNOX complexes. If we keep in mind the limiting resonance structures, **A** and **B**, shown in Scheme 2.4, we would expect the zwitterionic resonance structure (**B**) for the SNS5 ligand to be more predominant than in the SNO ligand. Thus, SNS5 is less π-basic than its SNO counterpart, which results in a higher oxidation potential for the $[Mo_2]^{4+}$ complex.

### 2.4.6 Electronic Spectra

The UV-vis spectra of **1-4** are shown overlaid in Figure 2.9, and the spectral data are summarized in Table 2.4. For $Mo_2(SNOX)_4$ complexes **1a**, **4a**, and **4b**, the spectra each consist of one band around 410-450 nm with a high extinction coefficient (> 5,000 $M^{-1}$ $cm^{-1}$), and a second peak at ~ 500 nm with an extinction coefficient that is roughly an order of magnitude less intense. Because of its intensity, the former band is attributed to a Mo δ to ligand π* charge transfer band, and the latter may be attributed to a δ-δ* transition based on comparison with UV-vis spectra of similar $[Mo_2]^{4+}$ complexes.[7] Complex **1b** has only one MLCT band at 460 nm that likely masks the δ-δ* transition.

**Table 2.4.** The peak wavelength and extinction coefficients of **1 - 4**.

| Compound | $\lambda_{max}$ (nm) | ε ($M^{-1}cm^{-1}$) | $\lambda_{max}$ (nm) | ε ($M^{-1}cm^{-1}$) | $\lambda_{max}$ (nm) | ε ($M^{-1}cm^{-1}$) |
|---|---|---|---|---|---|---|
| **1a** | - | - | 414 | 5400 | 495 | 830 |
| **1b** | - | - | 460 | 12000 | - | - |
| **2** | 375 | 17000 | 505 | 5100 | - | - |
| **3** | 371 | 17000 | 477 | 1200 | 648 | 2400 |
| **4a** | - | - | 410 | 8600 | 498 | 1100 |
| **4b** | - | | 449 | 6900 | 502 | 2100 |

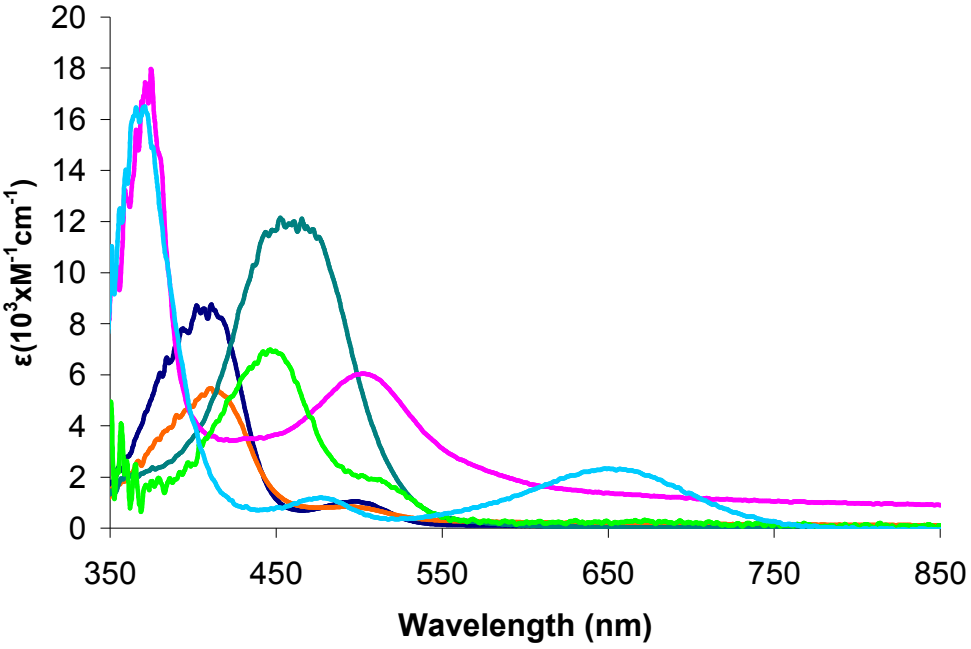


**Figure 2.9.** The UV-vis spectra of **1-4**. Compound **1a** is navy, **1b** is teal, **2** is pink, **3** is light blue, **4a** is orange, **4b** is green.

**Scheme 2.4.** The resonance structures of $SNS5^-$ and $SNO5^-$ ligands.

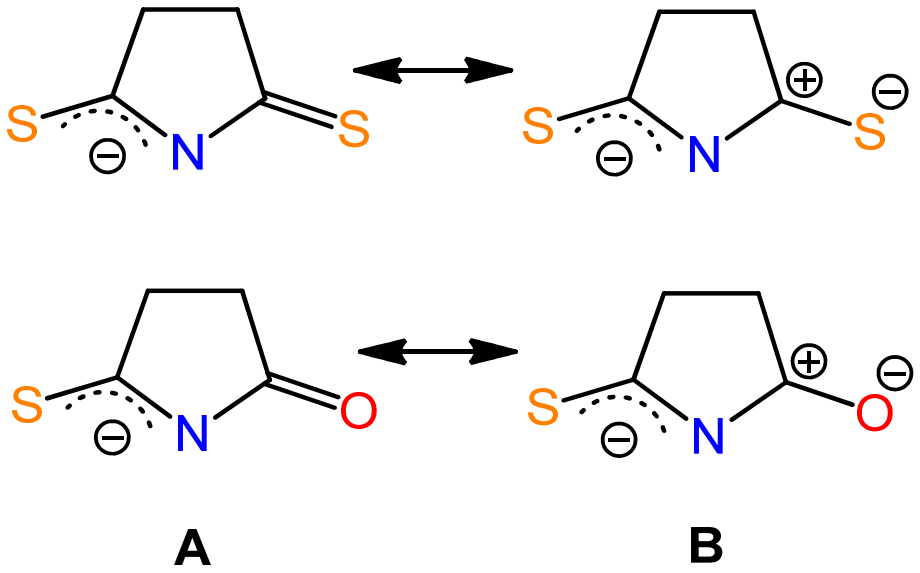

The spectra of the $SNSX^-$ complexes **2** and **3** both contain very intense bands around 375 nm with an extinction coefficient around 17,000 $M^{-1}$ $cm^{-1}$, attributed to a ligand π-π* transition. These spectra also contain the same Mo δ to ligand π* transition as the $Mo_2(SNOX)_4$ complexes, but these occur much lower in energy (505 and 648 nm, respectively) than those of **1a**, **1b**, **4a**, and **4b**. Compound **3** also contains an easily distinguished δ-δ* transition at 477 nm that is close in energy to those of the SNOX complexes. From these data, it is evident that the MLCT moves to a dramatically lower energy when S is substituted for O as the π-system substituent. However, changing the regioisomerism from *trans*-2,2 to *cis*-2,2 has only minimal effect on the electronic spectra of these complexes.

**2.4.7 DFT Calculations**

DFT geometry optimization and single point calculations were used to investigate the nature of the Mo≡Mo bonding manifold in complexes **1**, **2**, and **4**. The optimized Mo ≡Mo, Mo–N, and Mo–S bond distances are given in Table 2.2 alongside the crystallographically determined experimental values. The calculated geometries are very close to the experimental geometries. The Mo≡Mo bond distances are calculated to be shorter than the crystallographic values with differences ranging from ~0.023 Å for **4b** to 0.063 Å for **4a**. For the former, this is an acceptable difference. However, for the latter, this difference is large enough to cause concern.

The calculated structure of **4a** does not take packing effects into account in determining the Mo≡Mo bond length. The calculated structure of **4a**·2MeOH, which includes both axial MeOH molecules, has a Mo≡Mo bond length of 2.131 Å, which is much closer to the experimentally determined value for **4a** (2.153[2] Å), supporting our

earlier premise that the weak Mo···O axial interaction can serve to elongate a Mo≡Mo bond.

The relative thermodynamic energies of **1a** and **4a** as well as **1b** and **4b** were determined. As expected, the *trans*-2,2 complexes (**1a** and **1b**) are lower in energy than the *cis*-2,2 complexes, with the energy differences being 31.7 kJ/mol and 32.4 kJ/mol, respectively. This difference in energy is small enough that the MeOH axial interaction with the $[Mo_2]^{4+}$ core as well as hydrogen bonding between MeOH and the equatorial ligands seen in **4a** can be enough to make **4a** more thermodynamically favorable than **1a** when the compound is prepared in the presence of MeOH.

Diagrams of the metal frontier orbitals for complexes **1**, **2**, and **4** are shown in Figure 2.10. These MO diagrams show the same order of Mo≡Mo bonding and antibonding orbitals that has been found in other $Mo_2$(thioamidate)$_4$ complexes.[7,8a] In complexes **1a**, **1b**, and **2**, the π-symmetry orbitals are degenerate, while in **4a** and **4b**, the π-symmetry orbitals lose their degeneracy. The loss of π degeneracy occurs due to a reduction of symmetry from idealized $D_{2d}$ for the *trans*-2,2 regioisomer to $C_{2h}$ for the *cis*-2,2 regioisomer. In the $C_{2h}$ point group, the π orbitals are not equivalent by symmetry and hence are non-degenerate.

In each compound, the HOMO is the Mo≡Mo δ orbital, and the LUMO is the Mo ≡Mo δ* orbital. The HOMO-LUMO gap decreases depending on the π-basicity of the equatorial ligands. For the compounds with SNOX ligands, the HOMO-LUMO gap is approximately the same at ~3 eV: Neither geometrical isomerism nor ligand sterics has much of an effect on the HOMO-LUMO gap. However, **2** with the SNS5 ligand has a HOMO-LUMO gap that is smaller than that of the SNOX compounds by about 0.4 eV.

Ligand based $\pi_{nb}$ orbitals have an antibonding interaction with the δ* LUMO of the *trans*-2,2 complexes. Since the SNS5 ligand has a more electron poor π-system than do the SNOX ligands (vide supra), SNS5 destabilizes the δ* orbital less than its SNOX counterparts, leading to the reduced HOMO-LUMO gap.

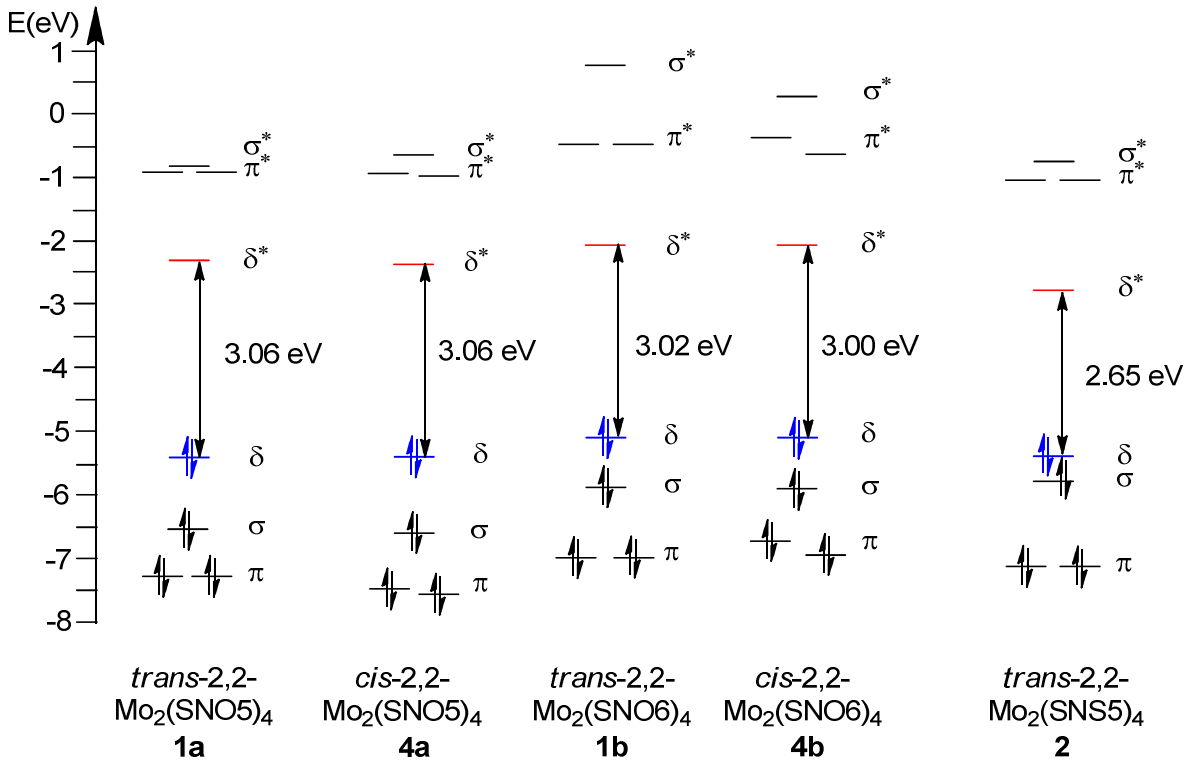


**Figure 2.10.** The MO diagrams of compounds **1-4** with orbital energies based on the results of DFT (B3LYP) calculations.

**2.5 Conclusions**

The electronics of $Mo_2$(thioamidate)$_4$ complexes can be tuned by changing the nature of the π-system substituents on the thioamidate ligands as well as altering the arrangement of the ligands around the $[Mo_2]^{4+}$ core. Changing the π-system substituents from oxygen to sulfur reduces the amount of electron density that is available to the π-system of the ligand, which results in large changes to electronics of the $[Mo_2]^{4+}$ core

stabilized by the ligand. Upon substituting S for O as the π-system substituent, the $[Mo_2]^{4+}$ core becomes more difficult to oxidize, the HOMO-LUMO gap decreases, and the metal to ligand charge transfer becomes lower in energy by lowering the energy of the ligand-based π* orbital. Changing the regioisomerism of the complex has a much smaller effect on the overall electronics. The increased steric clash between adjacent, uncoordinated O atoms in the *cis*-2,2 SNO equatorial ligands lengthens the metal ligand bonds, causing the ligands to be slightly less able to stabilize the $[Mo_2]^{4+}$ core. This results in small increases in the electrochemical $[Mo_2]^{4+/5+}$ potential but minimal changes in the electronic structure of the compounds. Used in tandem, these two strategies could provide methods for the rational design of $Mo_2$(thioamidate)$_4$ complexes that have precisely tuned electronic properties.

## 2.6 Acknowledgements

We thank Ilia A. Guzei for his help in conducting the variable temperature crystallography experiment as well as Momo Fredrickson and Daniel Fredrickson for providing us with the photograph of the violin in the TOC-graphic. The authors also wish to acknowledge financial support under NSF Grants CHE-1300464, CHE-9208463 (Bruker AC 360), and CHE-0840494 (computational facilities) as well as a generous bequest from Paul J. Bender (Bruker Avance 500).

## 2.7 Supporting Information

### 2.7.1 Crystal Structure of 5

*Data Collection*

An orange crystal with approximate dimensions 0.055 x 0.053 x 0.025 $mm^3$ was selected under oil under ambient conditions and attached to the tip of a MiTeGen

MicroMount©. The crystal was mounted in a stream of cold nitrogen at 100(1) K and centered in the X-ray beam by using a video camera.

The crystal evaluation and data collection were performed on a Bruker Quazar SMART APEXII diffractometer with Mo $K_\alpha$ ($\lambda$ = 0.71073 Å) radiation and the diffractometer to crystal distance of 4.96 cm.

The initial cell constants were obtained from three series of ω scans at different starting angles. Each series consisted of 12 frames collected at intervals of 0.5º in a 6º range about ω with the exposure time of 20 seconds per frame. The reflections were successfully indexed by an automated indexing routine built in the APEXII program suite.

The data were collected by using a full sphere data collection routine to survey reciprocal space to the extent of a full sphere to a resolution of 0.70 Å. A total of 10362 data were harvested by collecting 6 sets of frames with 0.5º scans in ω and φ with exposure times of 40 sec per frame. These highly redundant datasets were corrected for Lorentz and polarization effects. The absorption correction was based on fitting a function to the empirical transmission surface as sampled by multiple equivalent measurements.[14]

*Structure Solution and Refinement*

The systematic absences in the diffraction data were uniquely consistent for the space group $P2_1/n$ that yielded chemically reasonable and computationally stable results of refinement.[15]

A successful solution by charge flipping provided most non-hydrogen atoms from the *E*-map.[15,20] The remaining non-hydrogen atoms were located in an alternating series

of least-squares cycles and difference Fourier maps. All non-hydrogen atoms were refined with anisotropic displacement coefficients. All hydrogen atoms were included in the structure factor calculation at idealized positions and were allowed to ride on the neighboring atoms with relative isotropic displacement coefficients.

The dimolybdenum compound (Figure 2.S1) resides on a crystallographic inversion center. Thermal parameter restraints were required on the monothiosuccinimidato and acetate ligands to enable a computationally stable refinement.

The final least-squares refinement of 110 parameters against 1548 data resulted in residuals $R$ (based on $F^2$ for $I \geq 2\sigma$) and $wR$ (based on $F^2$ for all data) of 0.0570 and 0.1337, respectively.

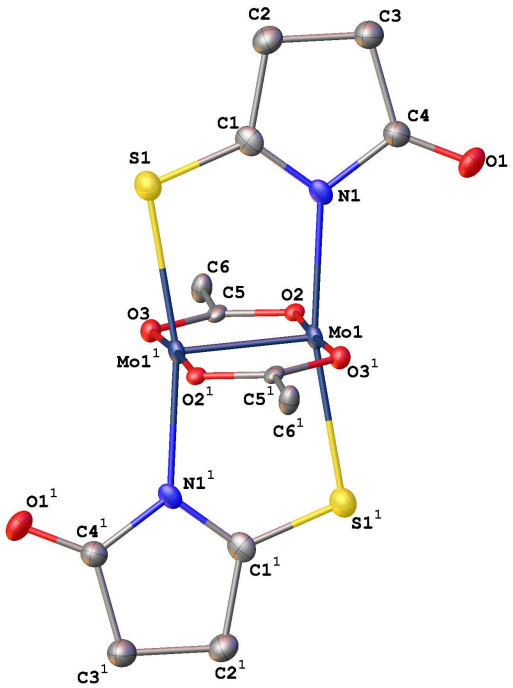


**Figure 2.S1.** The structure of **5**. All atoms are drawn as 50% thermal probability ellipsoids. All hydrogen atoms are omitted for clarity.

**Table 2.S1.** Crystal data and structure refinement for **5**.

| | |
|---|---|
| Empirical formula | $C_{12}H_{14}Mo_2N_2O_6S_2$ |
| Formula weight | 538.25 |
| Temperature/K | 100.0 |
| λ/Å | 0.71073 |
| Crystal system | monoclinic |
| Space group | $P2_1/n$ |
| a/Å | 5.450(2) |
| b/Å | 8.227(3) |
| c/Å | 18.268(8) |
| α/° | 90 |
| β/° | 96.805(15) |
| γ/° | 90 |
| Volume/Å$^3$ | 813.3(6) |
| Z | 2 |
| $\rho_{calc}$ mg/mm$^3$ | 2.198 |
| μ/mm$^{-1}$ | 1.831 |
| F(000) | 528.0 |
| 2Θ range for data collection | 4.492 to 51.472° |
| Reflections collected | 10362 |
| Independent reflections | 1548[R(int) = 0.0395] |
| Data/restraints/parameters | 1548/60/110 |
| Goodness-of-fit on $F^2$ | 1.509 |
| Final R indexes [I>=2σ (I)] | $R_1$ = 0.0570, $wR_2$ = 0.1328 |
| Final R indexes [all data] | $R_1$ = 0.0606, $wR_2$ = 0.1337 |
| Largest diff. peak/hole / e Å$^{-3}$ | 1.09/-1.08 |

### 2.7.2 DFT Calculations

*MO Picture*

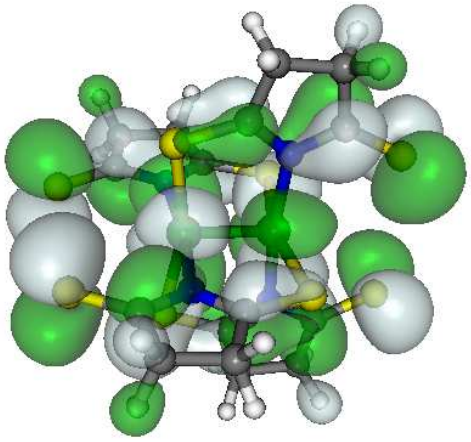

**Figure 2.S2.** The δ* (LUMO) orbital of *trans*-2,2-$Mo_2(SNS5)_4$ (**2**).

*Coordinates*

*trans*-2,2-$Mo_2(SNO5)_4$ (**1a**)

| | | | |
|---|---|---|---|
| Mo | 0.00000 | -0.00000 | 2.08617 |
| S | -0.12019 | 2.49451 | -0.35749 |
| S | 2.49432 | 0.12586 | 2.43783 |
| O | -0.10854 | 2.26149 | 4.56953 |
| O | 2.26173 | 0.09972 | -2.48931 |
| N | -0.10531 | 2.13935 | 2.26663 |
| N | 2.13925 | 0.10267 | -0.18615 |
| C | -0.14560 | 3.00273 | 1.26238 |
| C | -0.21277 | 4.44539 | 1.71773 |
| H | -1.10927 | 4.92493 | 1.32167 |
| H | 0.64136 | 5.00280 | 1.32987 |
| C | -0.21358 | 4.32409 | 3.24565 |
| H | 0.63716 | 4.81073 | 3.72367 |
| H | -1.11581 | 4.71919 | 3.71389 |
| C | -0.13793 | 2.82313 | 3.50359 |
| C | 3.00261 | 0.14578 | 0.81795 |
| C | 4.44541 | 0.21149 | 0.36271 |
| H | 5.00408 | -0.63880 | 0.75711 |
| H | 4.92334 | 1.11167 | 0.75242 |
| C | 4.32457 | 0.20160 | -1.16524 |
| H | 4.72458 | 1.09778 | -1.64072 |
| H | 4.80714 | -0.65564 | -1.63587 |
| C | 2.82320 | 0.13025 | -1.42328 |
| Mo | 0.00000 | 0.00000 | 0.00000 |
| S | -2.49575 | -0.12697 | 2.43991 |

| | | | |
|---|---|---|---|
| S | 0.12110 | -2.49599 | -0.34824 |
| O | -2.25636 | -0.12170 | -2.48670 |
| O | 0.11760 | -2.25684 | 4.57855 |
| N | -2.13820 | -0.10865 | -0.18366 |
| N | 0.10693 | -2.13814 | 2.27524 |
| C | -3.00252 | -0.15400 | 0.81955 |
| C | -4.44404 | -0.23185 | 0.36204 |
| H | -5.00999 | 0.61533 | 0.75264 |
| H | -4.91561 | -1.13453 | 0.75365 |
| C | -4.32087 | -0.22628 | -1.16578 |
| H | -4.71551 | -1.12583 | -1.63935 |
| H | -4.80683 | 0.62716 | -1.63988 |
| C | -2.81976 | -0.14787 | -1.42160 |
| C | 0.14923 | -3.00261 | 1.27208 |
| C | 0.22407 | -4.44441 | 1.72927 |
| H | 1.12789 | -4.91622 | 1.34037 |
| H | -0.62197 | -5.00990 | 1.33563 |
| C | 0.21438 | -4.32163 | 3.25713 |
| H | -0.64350 | -4.80302 | 3.72792 |
| H | 1.10995 | -4.72161 | 3.73368 |
| C | 0.14271 | -2.82000 | 3.51326 |

*trans*-2,2-$Mo_2(SNO6)_4$ (**1b**)

| | | | |
|---|---|---|---|
| Mo | 0.00000 | 0.00000 | 0.00000 |
| Mo | 0.00000 | 0.00000 | 2.07456 |
| S | 1.42158 | 2.07493 | -0.32682 |
| S | -2.07351 | 1.42586 | 2.39692 |
| S | -1.43546 | -2.07121 | -0.31669 |
| S | 2.07644 | -1.42478 | 2.39501 |
| O | 1.01879 | 1.43518 | 4.49566 |
| O | -1.46269 | 0.97018 | -2.42411 |
| O | -0.97193 | -1.45584 | 4.50330 |
| O | 1.41864 | -1.03050 | -2.42533 |
| N | 1.25056 | 1.81875 | 2.28907 |
| N | -1.81994 | 1.24680 | -0.21848 |
| N | -1.25133 | -1.81495 | 2.29806 |
| N | 1.81113 | -1.25816 | -0.21986 |
| C | 1.74781 | 2.53436 | 1.28680 |
| C | 2.62237 | 3.74380 | 1.52807 |
| H | 3.66696 | 3.40811 | 1.53238 |
| H | 2.52318 | 4.42854 | 0.68650 |
| C | 2.29218 | 4.41697 | 2.85698 |
| H | 1.29814 | 4.87039 | 2.80188 |
| H | 2.99943 | 5.22299 | 3.06298 |
| C | 2.32413 | 3.37239 | 3.96661 |
| H | 1.97378 | 3.75785 | 4.92398 |
| H | 3.35102 | 3.02169 | 4.12559 |
| C | 1.48911 | 2.15308 | 3.63520 |
| C | -2.54259 | 1.73549 | 0.78279 |
| C | -3.79412 | 2.54809 | 0.53932 |

| | | | |
|---|---|---|---|
| H | -3.94984 | 3.22308 | 1.38021 |
| H | -4.64739 | 1.85832 | 0.53383 |
| C | -3.72650 | 3.29422 | -0.79000 |
| H | -4.67607 | 3.79174 | -0.99756 |
| H | -2.96220 | 4.07494 | -0.73440 |
| C | -3.37914 | 2.30742 | -1.89862 |
| H | -4.21062 | 1.61019 | -2.05766 |
| H | -3.19036 | 2.79236 | -2.85625 |
| C | -2.16132 | 1.47119 | -1.56511 |
| C | -1.74683 | -2.53523 | 1.29796 |
| C | -2.57004 | -3.77910 | 1.54444 |
| H | -1.88778 | -4.63836 | 1.55376 |
| H | -3.24528 | -3.93175 | 0.70320 |
| C | -3.31717 | -3.70029 | 2.87253 |
| H | -3.82470 | -4.64409 | 3.08217 |
| H | -4.08989 | -2.92811 | 2.81371 |
| C | -2.32814 | -3.35974 | 3.98124 |
| H | -2.81234 | -3.16303 | 4.93766 |
| H | -1.63976 | -4.19787 | 4.14367 |
| C | -1.47923 | -2.15122 | 3.64531 |
| C | 2.52608 | -1.75969 | 0.78109 |
| C | 3.72485 | -2.64815 | 0.53774 |
| H | 3.37813 | -3.68917 | 0.54385 |
| H | 4.41617 | -2.55010 | 1.37409 |
| C | 4.39247 | -2.33554 | -0.79809 |
| H | 4.85908 | -1.34713 | -0.75315 |
| H | 5.18778 | -3.05454 | -1.00498 |
| C | 3.33961 | -2.36158 | -1.90010 |
| H | 2.97311 | -3.38470 | -2.04762 |
| H | 3.72315 | -2.02494 | -2.86308 |
| C | 2.13471 | -1.50685 | -1.56660 |

*trans*-2,2-$Mo_2(SNS5)_4$ (**2**)

| | | | |
|---|---|---|---|
| Mo | 0.00000 | -0.00000 | 2.13360 |
| Mo | 0.00000 | 0.00000 | -0.00000 |
| S | -0.62741 | 2.38420 | 2.50093 |
| S | -1.97312 | -0.52803 | 4.93500 |
| S | -2.38155 | -0.63443 | -0.37090 |
| S | 1.96828 | 0.51080 | 4.94169 |
| S | 2.38378 | 0.63394 | -0.36277 |
| S | -0.51641 | 1.97188 | -2.80458 |
| S | 0.63202 | -2.38245 | 2.50109 |
| S | 0.53234 | -1.96836 | -2.80409 |
| N | 0.55453 | -2.07112 | -0.13916 |
| N | -0.54801 | 2.07211 | -0.13950 |
| N | -2.07188 | -0.55372 | 2.26989 |
| C | 2.73059 | 0.71230 | 3.48693 |
| C | -2.72991 | -0.73512 | 3.47819 |

| | | | |
|---|---|---|---|
| N | 2.07227 | 0.54448 | 2.27688 |
| C | 1.12682 | -4.17446 | -1.09571 |
| H | 2.09785 | -4.38150 | -1.56727 |
| H | 0.39674 | -4.84393 | -1.57195 |
| C | -4.17391 | -1.13479 | 3.22400 |
| H | -4.84857 | -0.41260 | 3.70466 |
| H | -4.37334 | -2.11026 | 3.68981 |
| C | 1.15732 | -4.30086 | 0.43942 |
| H | 0.44371 | -5.04267 | 0.82795 |
| H | 2.14665 | -4.57952 | 0.83197 |
| C | 2.91207 | 0.76660 | 1.24523 |
| C | -4.30039 | -1.15886 | 1.68888 |
| H | -4.58038 | -2.14589 | 1.29160 |
| H | -5.04101 | -0.44228 | 1.30346 |
| C | 4.30759 | 1.12850 | 1.70151 |
| H | 4.59622 | 2.11769 | 1.31590 |
| H | 5.04185 | 0.41003 | 1.30765 |
| C | -1.13581 | 4.30569 | 0.43901 |
| H | -0.41763 | 5.04156 | 0.83036 |
| H | -2.12412 | 4.59137 | 0.82903 |
| C | -0.76840 | 2.91111 | 0.89324 |
| C | -0.71972 | 2.73130 | -1.34860 |
| C | 0.77832 | -2.90917 | 0.89365 |
| C | -1.10177 | 4.18021 | -1.09601 |
| H | -2.06970 | 4.39490 | -1.57043 |
| H | -0.36499 | 4.84439 | -1.56933 |
| C | 4.18144 | 1.08831 | 3.23647 |
| H | 4.84148 | 0.34551 | 3.70633 |
| H | 4.40148 | 2.05263 | 3.71566 |
| C | -2.90858 | -0.77928 | 1.23635 |
| C | 0.73489 | -2.72815 | -1.34819 |

*cis*-2,2-$Mo_2(SNO5)_4$ (**4a**)

| | | | |
|---|---|---|---|
| Mo | -0.00000 | 0.00000 | 2.08248 |
| S | 0.56201 | -2.43233 | -0.34436 |
| S | 2.41782 | 0.63133 | -0.33489 |
| O | 0.36729 | -2.26609 | 4.58387 |
| O | 2.17198 | 0.72947 | 4.59268 |
| N | 0.49692 | -2.09259 | 2.28279 |
| N | 2.08266 | 0.53024 | 2.29156 |
| C | 0.68439 | -2.93076 | 1.27040 |
| C | 0.99426 | -4.34392 | 1.72020 |
| H | 1.97286 | -4.65034 | 1.34690 |
| H | 0.26507 | -5.04080 | 1.30447 |
| C | 0.93205 | -4.24258 | 3.24782 |
| H | 0.17326 | -4.88279 | 3.69842 |
| H | 1.87889 | -4.47168 | 3.73865 |
| C | 0.57541 | -2.78352 | 3.51683 |

| | | | |
|---|---|---|---|
| C | 2.91368 | 0.75355 | 1.28060 |
| C | 4.30813 | 1.13630 | 1.73295 |
| H | 4.57894 | 2.11341 | 1.32995 |
| H | 5.03822 | 0.42233 | 1.34853 |
| C | 4.19160 | 1.12599 | 3.26071 |
| H | 4.82439 | 0.37710 | 3.73918 |
| H | 4.42090 | 2.08501 | 3.72556 |
| C | 2.72982 | 0.77862 | 3.52695 |
| Mo | 0.00000 | 0.00000 | 0.00000 |
| S | -0.56202 | 2.43234 | 2.42684 |
| S | -2.41782 | -0.63133 | 2.41737 |
| O | -0.36730 | 2.26609 | -2.50139 |
| O | -2.17198 | -0.72945 | -2.51020 |
| N | -0.49692 | 2.09259 | -0.20031 |
| N | -2.08266 | -0.53024 | -0.20907 |
| C | -0.68439 | 2.93076 | 0.81208 |
| C | -0.99427 | 4.34392 | 0.36228 |
| H | -1.97286 | 4.65033 | 0.73558 |
| H | -0.26508 | 5.04080 | 0.77801 |
| C | -0.93207 | 4.24258 | -1.16533 |
| H | -0.17328 | 4.88279 | -1.61594 |
| H | -1.87891 | 4.47167 | -1.65616 |
| C | -0.57540 | 2.78352 | -1.43435 |
| C | -2.91368 | -0.75354 | 0.80188 |
| C | -4.30813 | -1.13628 | 0.34954 |
| H | -4.57895 | -2.11340 | 0.75253 |
| H | -5.03822 | -0.42232 | 0.73396 |
| C | -4.19160 | -1.12597 | -1.17822 |
| H | -4.82439 | -0.37708 | -1.65670 |
| H | -4.42092 | -2.08499 | -1.64308 |
| C | -2.72982 | -0.77862 | -1.44447 |

*cis*-2,2-$Mo_2(SNO5)_4 \cdot 2MeOH$ (**4a**·2MeOH)

| | | | |
|---|---|---|---|
| Mo | 0.00000 | -0.00000 | 0.00000 |
| S | -0.32348 | -2.48129 | 2.30886 |
| S | 2.45617 | -0.46880 | -0.18739 |
| O | -0.39174 | -2.32547 | -2.63518 |
| O | 2.34901 | -0.32684 | 4.75673 |
| N | -0.35637 | -2.12808 | -0.31846 |
| N | 2.13701 | -0.32496 | 2.44106 |
| C | -0.43620 | -2.98350 | 0.69988 |
| C | -0.63572 | -4.42119 | 0.26708 |
| H | -1.56788 | -4.81222 | 0.67827 |
| H | 0.16884 | -5.04713 | 0.65607 |
| C | -0.64204 | -4.32090 | -1.25821 |
| H | 0.16715 | -4.87422 | -1.73624 |
| H | -1.57363 | -4.65402 | -1.71726 |
| C | -0.45468 | -2.83296 | -1.54353 |
| C | 2.97130 | -0.51818 | 1.42040 |
| C | 4.40132 | -0.77462 | 1.84833 |

| | | | |
|---|---|---|---|
| H | 5.05648 | 0.00177 | 1.44922 |
| H | 4.75349 | -1.72445 | 1.44355 |
| C | 4.30889 | -0.75831 | 3.37381 |
| H | 4.55873 | -1.71512 | 3.83439 |
| H | 4.93421 | -0.00091 | 3.84748 |
| C | 2.84275 | -0.44653 | 3.66351 |
| Mo | 0.00000 | 0.00000 | 2.13129 |
| S | 0.34193 | 2.48781 | -0.15462 |
| S | -2.46782 | 0.45067 | 2.29704 |
| O | 0.33854 | 2.34054 | 4.79127 |
| O | -2.34803 | 0.39175 | -2.64986 |
| N | 0.33399 | 2.13605 | 2.47709 |
| N | -2.13854 | 0.34886 | -0.33630 |
| C | 0.42480 | 2.99122 | 1.45060 |
| C | 0.61100 | 4.42903 | 1.88970 |
| H | 1.52363 | 4.84304 | 1.45900 |
| H | -0.21658 | 5.04087 | 1.52673 |
| C | 0.65034 | 4.32081 | 3.41431 |
| H | -0.12392 | 4.89779 | 3.92077 |
| H | 1.60652 | 4.61682 | 3.84870 |
| C | 0.42659 | 2.83988 | 3.68886 |
| C | -2.97539 | 0.53066 | 0.69331 |
| C | -4.40177 | 0.80046 | 0.26081 |
| H | -5.07397 | 0.05370 | 0.68573 |
| H | -4.72994 | 1.77142 | 0.63531 |
| C | -4.31539 | 0.74286 | -1.26435 |
| H | -4.60892 | 1.66907 | -1.75951 |
| H | -4.90791 | -0.05901 | -1.70727 |
| C | -2.84232 | 0.47733 | -1.54487 |
| O | -0.65133 | -0.21374 | 4.64545 |
| H | -0.17091 | 0.57411 | 4.96583 |
| C | -0.66381 | -1.23111 | 5.64217 |
| H | -1.17368 | -0.88471 | 6.54637 |
| H | 0.34980 | -1.54913 | 5.89606 |
| H | -1.21523 | -2.07834 | 5.23772 |
| O | 0.38214 | 0.57653 | -2.50938 |
| H | -0.51258 | 0.35161 | -2.83024 |
| C | 1.35686 | 0.29939 | -3.51029 |
| H | 2.32947 | 0.57132 | -3.10345 |
| H | 1.17555 | 0.89937 | -4.40732 |
| H | 1.36087 | -0.75996 | -3.77605 |

*cis*-2,2-$Mo_2(SNO6)_4$ (**4b**)

| | | | |
|---|---|---|---|
| Mo | 0.00000 | -0.00000 | 2.08315 |
| S | 1.28562 | 2.12342 | 2.39091 |
| S | -2.14131 | 1.25795 | 2.38644 |
| O | 1.17895 | 1.34255 | -2.41322 |

| | | | |
|---|---|---|---|
| O | -1.74418 | 0.53331 | -2.41071 |
| N | 1.13893 | 1.85882 | -0.21948 |
| N | -1.89674 | 1.07608 | -0.22556 |
| C | 1.56980 | 2.61811 | 0.78841 |
| C | 2.30078 | 3.91938 | 0.55444 |
| H | 2.91853 | 4.14312 | 1.42306 |
| H | 1.55164 | 4.71879 | 0.49140 |
| C | 3.11590 | 3.88152 | -0.73414 |
| H | 3.54863 | 4.86196 | -0.94279 |
| H | 3.94840 | 3.18073 | -0.62236 |
| C | 2.21403 | 3.43279 | -1.87804 |
| H | 1.45347 | 4.19795 | -2.07570 |
| H | 2.75554 | 3.27541 | -2.81009 |
| C | 1.48242 | 2.14674 | -1.55503 |
| C | -2.64589 | 1.52180 | 0.78245 |
| C | -3.95975 | 2.23026 | 0.54784 |
| H | -4.14501 | 2.91409 | 1.37549 |
| H | -4.76312 | 1.48379 | 0.57650 |
| C | -3.96973 | 2.94149 | -0.80084 |
| H | -4.94893 | 3.38378 | -0.99472 |
| H | -3.24536 | 3.76122 | -0.78958 |
| C | -3.60552 | 1.93600 | -1.88454 |
| H | -3.44855 | 2.39647 | -2.86034 |
| H | -4.41516 | 1.20821 | -2.01290 |
| C | -2.35677 | 1.14077 | -1.55672 |
| Mo | 0.00000 | 0.00000 | 0.00000 |
| S | -1.28562 | -2.12342 | -0.30776 |
| S | 2.14131 | -1.25795 | -0.30329 |
| O | -1.17886 | -1.34260 | 4.49639 |
| O | 1.74416 | -0.53334 | 4.49387 |
| N | -1.13893 | -1.85882 | 2.30264 |
| N | 1.89674 | -1.07608 | 2.30871 |
| C | -1.56980 | -2.61811 | 1.29474 |
| C | -2.30075 | -3.91940 | 1.52871 |
| H | -2.91852 | -4.14314 | 0.66010 |
| H | -1.55160 | -4.71880 | 1.59173 |
| C | -3.11585 | -3.88156 | 2.81731 |
| H | -3.54855 | -4.86201 | 3.02597 |
| H | -3.94837 | -3.18078 | 2.70555 |
| C | -2.21397 | -3.43281 | 3.96120 |
| H | -1.45338 | -4.19796 | 4.15883 |
| H | -2.75546 | -3.27546 | 4.89327 |
| C | -1.48241 | -2.14674 | 3.63818 |
| C | 2.64589 | -1.52180 | 1.30070 |
| C | 3.95975 | -2.23026 | 1.53531 |
| H | 4.14501 | -2.91409 | 0.70766 |
| H | 4.76312 | -1.48379 | 1.50666 |
| C | 3.96972 | -2.94150 | 2.88399 |
| H | 4.94892 | -3.38379 | 3.07787 |
| H | 3.24535 | -3.76123 | 2.87272 |
| C | 3.60551 | -1.93602 | 3.96769 |

| | | | |
|---|---|---|---|
| H | 3.44853 | -2.39650 | 4.94349 |
| H | 4.41514 | -1.20824 | 4.09606 |
| C | 2.35676 | -1.14078 | 3.63987 |

## 2.8 References

1. Cotton, F. A.; Murillo, C. A.; Walton, R. A. *Multiple Bonds Between Metal Atoms.* 3rd ed.; Springer Science and Business Media, Inc.: New York, 2005.

2. (a) Zhou, W.; Saper, N. I.; Krogman, J. P.; Foxman, B. M.; Thomas, C. M. *Dalton Trans.* **2014**, *43*, 1984. (b) Napoline, J. W.; Krogman, J. P.; Shi, R.; Kuppuswamy, S.; Bezpalko, M. W.; Foxman, B. M.; Thomas, C. M. *Eur. J. Inorg. Chem.* **2013**, 3874. (c) Krogman, J. P.; Bezpalko, M. W.; Foxman, B. M.; Thomas, C. M. *Inorg. Chem.* **2013**, *52*, 3022. (d) Napoline, J. W.; Bezpalko, M. W.; Foxman, B. M.; Thomas, C. M. *Chem. Commun.* **2013**, *49*, 4388. (e) Corcos, A. R.; Long, A. K. M.; Guzei, I. A.; Berry, J. F. *Eur. J. Inorg. Chem.* **2013**, 3808. (f) Nippe, M.; Timmer, G. H.; Berry, J. F. *Chem. Commun*. **2009**, 4357. (g) Nippe, M.; Victor, E.; Berry, J. F. *Inorg. Chem*. **2009**, *48*, 11889. (h) Long, A. K. M.; Yu, R. P.; Timmer, G. H.; Berry, J. F. *J. Am. Chem. Soc*. **2010**, *132*, 12228. (i) Nippe, M.; Goodman, S. M.; Fry, C. G.; Berry, J. F. *J. Am. Chem. Soc*. **2011**, *133*, 2856. (j) Long, A. K. M.; Timmer, G. H.; Pap, J. S.; Snyder, J. L.; Yu R. P.; Berry, J. F. *J. Am. Chem. Soc*. **2011**, *133*, 13138. (k) Nippe, M.; Turov, Y.; Berry J. F. *Inorg. Chem*. **2011**, *50*, 10592. (l) Turov, Y.; Berry, J. F. *Dalton Trans*. **2012**, *41*, 8153. (m) Timmer, G. H.; Berry, J. F. *Chem. Sci.* **2012**, *3*, 3038.

3. (a) Kornecki, K. P.; Berry, J. F.; Powers, D. C.; Ritter, T. Metal-Metal Bond-Containing Complexes as Catalysts for C-H Functionalization. In *Prog. Inorg. Chem.*, Karlin, K. D., Ed. 2014; Vol. 58, pp 225. (b) Berry, J. F. *Dalton Trans*. **2012**, *41*, 700. (c) Davies, H. M. L.; Manning, J. R. *Nature*, **2008**, *451*, 417. (d) DuBois, J. *Org. Proc. Res.*

*Dev.* **2011**, *15*, 758. (e) Doyle, M. P.; Duffy, R.; Ratnikov, M.; Zhou, L. *Chem. Rev.* **2010**, *110*, 704. (f) Powers, D. C.; Ritter, T. *Acc. Chem. Res*. **2012**, *45*, 840. (g) Villalobs, L.; Cao, Z.; Fanwick P. E.; Ren, T. *Dalton Trans*. **2012**, *41*, 644. (h) Teets, T. S.; Nocera, D. G. *Chem. Commun*. **2011**, *47*, 9268. (i) Sinha, A.; Majumdar, M.; Sarkar, M.; Ghatak, T.; Bera, J. K. *Organometallics* **2013**, *32*, 340.

4. (a) Chiarella, G. M.; Cotton, F. A.; Durivage, J. C.; Lichtenberger, D. L.; Murillo, C. A. *J. Am. Chem. Soc.* **2013**, *135*, 17889. (b) Zhou, W.; Marquard, S. L.; Bezpalko, M. W.; Foxman, B. M.; Thomas, C. M. *Organometallics* **2013**, *32*, 1766. (c) Hua, S.-A.; Tsai, Y.-C.; Peng, S.-M. *J. Chin. Chem. Soc.* **2014**, *61*, 9. (d) Cummings, S. P.; Savchenko, J.; Fanwick, P. E.; Kharlamova, A.; Ren, T. *Organometallics* **2013**, *32*, 1129. (e) Xiao, X.; Liu, C. Y.; He, Q.; Han, M. J.; Meng, M.; Lei, H.; Lu, X. *Inorg. Chem.* **2013**, *52*, 12624. (f) Liu, C. Y.; Xiao, X.; Meng, M.; Zhang, Y.; Han, M. J. *J. Phys. Chem. C* **2013**, *117*, 19859. (g) Cai, X.-M.; Zhang, X.-Y.; Savchenko, J.; Cao, Z.; Ren, T.; Zuo, J.-L. *Organometallics* **2012**, *31*, 8591. (h) Cummings, S. P.; Cao, Z.; Fanwick, P. E.; Kharlamova, A.; Ren, T. *Inorg. Chem.* **2012**, *51*, 7561. (i) Forrest, W. P.; Cao, Z.; Hassel, K. M.; Prentice, B. M.; Fanwick, P. E.; Ren, T. *Inorg. Chem.* **2012**, *51*, 3261. (j) Xi, B.; Liu, I. P.-C.; Xu, G.-L.; Choudhuri, M. M. R.; DeRosa, M. C.; Crutchley, R. J.; Ren, T. *J. Am. Chem. Soc.* **2011**, *133*, 15094. (k) Chisholm, M. H. in *Structure and Bonding* ed. Parkin, G. Springer, **2010**, vol. 136, pp. *29.* (l) Chisholm, M. H.; Patmore, N. S. *Acc. Chem. Res.* **2007**, *40*, 19. (m) Berry, J. F. in *Structure and Bonding* ed. Parkin, G. Springer, **2010**, vol. 136, pp. 1. (n) Mohan, P. J.; Georgiev V. P.; McGrady, J. E. *Chem. Sci.* **2012**, *3*, 1319. (o) Manni, G. L.; Dzubak, A.; Mulla, A.; Brogden, D. W.; Berry, J. F.; Gagliardi, L. *Chem. Eur. J.* **2012**, *18*, 1737.

5. (a) Powers, D. C.; Chambers, M. B.; Teets, T. S.; Elgrishi, N.; Anderson, B. L.; Nocera, D. *Chem. Sci.* **2013**, *4*, 2880. (b) Teets, T. S.; Neumann, M. P.; Nocera, D. G. *Chem. Commun.* **2011**, *47*, 1485. (c) Teets, T. S.; Nocera, D. G. *J. Am. Chem. Soc.* **2011**, *133*, 17796. (d) Chisholm, M. H. *Macromol. Chem. Phys.* **2012**, *213*, 800. (e) Chisholm, M. H.; Lear, B. J. *Chem. Soc. Rev.* **2011**, *40*, 5254. (f) Alberding, B. G.; Chisholm, M. H.; Gallucii, J. C.; Ghosh, Y.; Gustafson, T. L. *Proc. Nat. Acad. Sci. USA*, **2011**, *108*, 8152. (g) Bradley, P. M.; Fu, P. K.-L.; Turro, C. *Comments Inorg. Chem.* **2001**, *22*, 393.

6. (a) Tereniak, S. J.; Carlson, R. K.; Clouston, L. J.; Young Jr., V. G.; Bill, E.; Maurice, R.; Chen, Y.-S.; Kim, H. J.; Gagliardi, L.; Lu, C. C. *J. Am. Chem. Soc.* **2014**, *136*, 1842. (b) Clouston, L. J.; Siedschlag, R. B.; Rudd, P. A.; Planas, N.; Hu, S.; Miller, A. D.; Gagliardi, L.; Lu, C. C. *J. Am. Chem. Soc.* **2013**, *135*, 13142. (c) Rudd, P. A.; Liu, S.; Planas, N.; Bill, E.; Gagliardi, L.; Lu, C. C. *Angew. Chem. Int. Ed.* **2013**, *52*, 4449. (d) Tan, Z. F.; Liu, C. Y.; Li, Z.; Meng, M.; Weng, N. S. *Inorg. Chem.* **2012**, *51*, 2212. (e) Rudd, P. A.; Liu, S.; Gagliardi, L.; Young, V. G., Jr.; Lu, C. C. *J. Am. Chem. Soc.* **2011**, *133*, 20724. (f) Filatov, A. S.; Napier, M.; Vreshch, V. D.; Sumner, N. J.; Dikarev, E. V.; Petrukhina, M. A. *Inorg. Chem.* **2012**, *51*, 566. (g) Filatov, A. S.; Petrukhina, M. A. *Coord. Chem. Rev.* **2010**, *254*, 2234. (h) Majumdar, M.; Patra, S. K.; Bera, J. K. *Polyhedron*, **2006**, *26*, 1597. (i) Chisholm, M. H.; Macintosh, A. M. *Chem. Rev.* **2005**, *105*, 2949. (j) Manke, D. R.; Loh, Z.-H.; Nocera, D. G. *Inorg. Chem.* **2004**, *43*, 3618. (k) Cotton, F. A.; Lin, C.; Murillo, C. A. *Acc. Chem. Res.* **2001**, *34*, 759.

7. Hicks, J.; Ring, S. P.; Patmore, N. J. *Dalton Trans.* **2012**, *41*, 6641.

8. (a) Dolinar, B. S.; Berry, J. F. *Inorg. Chem.* **2013**, *52*, 4658. (b) Cotton, F. A.; Niswander, R. H.; Sekutowski, J. C. *Inorg. Chem.* **1979**, *18*, 1149. (c) Ambrosius, H. P.

M. M.; Cotton, F. A.; Falvello, L. R.; Hintzen, H. T. J. M.; Melton, T. J.; Schwotzer, W.; Tomas, M.; van der Linden, J. G. M. *Inorg. Chem.* **1984**, *23*, 1611. (d) Fanwick, P. E.; Ju-Sheng, Q.; Yi-Ping, W.; Walton, R. A. *Inorg. Chim. Acta*, **1990**, *168*, 159. (e) Sheldrick, W. S.; Mintert, M. *Inorg. Chim. Acta,* **1994**, *219*, 23.

9. (a) Cotton, F. A.; Niswander, R. H.; Sekutowski, J. C. *Inorg. Chem.* **1979**, *18*, 1152. (b) Cotton, F. A.; Ilsley, W. H.; Kaim, W. *J. Am. Chem. Soc.* **1980**, *102*, 3475. (c) Bing, A.; Cotton, F. A.; Kaim, W. *Inorg. Chem.* **1979**, *18*, 3030. (d) Cotton, F. A.; Ilsley, W. H.; Kaim, W. *Inorg. Chem.* **1980**, *19*, 1453. (e) Baral, S.; Cotton, F. A.; Ilsley, W. H.; Kaim, W. *Inorg. Chem.* **1982**, *21*, 1644. (f) Clegg, W.; Garner, C. D.; Akhter, L.; Al-Samman, M. H. *Inorg. Chem.* **1983**, *22*, 2466. (g) Lichtenberger, D. L.; Kristofzski, J. G.; Bruck, M. A. *Acta Crystallogr., Sect. C: Cryst. Struct. Commun.* **1988**, *C44*, 1523. (h) Abbott, R. G.; Cotton, F. A.; Falvello, L. R. *Inorg. Chem.* **1990**, *29*, 514. (i) Mashima, K.; Nakano, H.; Mori, T.; Takaya, H.; Nakamura, A. *Chem. Lett.* **1992**, 185. (j) Mintert, M.; Sheldrick, W. S. *Chem. Ber.* **1996**, *129*, 683. (k) Pal, K.; Nakao, K.; Mashima, K. *E. J. Inorg. Chem.* **2010**, 5668. (l) Wilkinson, L. A.; McNeill, L.; Scattergood, P. A.; Patmore, N. J. *Inorg. Chem.* **2013**, *52*, 9683.

10. Holste, G.; Schäfer H. *Z. anorg. allg. Chem.*, **1972**, *391*, 263.

11. Cotton, F. A.; Norman, G. J. *J. Coord. Chem.* **1971**, *1*, 161.

12. Berg, U.; Sandström J. *Acta Chem. Scand.* **1966**, *20*, 689.

13. Zhu, X.; Giordano, T.; Yu, Q. -S.; Holloway, H. W.; Perry, T. A.; Lahiri, D. K.; Brossi, A.; Greig, N. H. *J. Med. Chem.* **2003**, *46*, 5222.

14. SAINT; Bruker-AXS: Madison, WI, 2009.

15. Sheldrick, G. M. *Acta Crystallogr., Sect. A: Found. Crystallogr.* **2008**, *A64*, 112.

16. (a) Neese, F. ORCA-an ab inito DFT and Semi-empirical Electronic Structure Package, version 2.8.0; University of Bonn: Germany, 2010. (b) Perdew, J. P.; *Phys. Rev. B: Condens. Matter*, **1986**, *33*, 8822. (c) Becke, A. D.; *Phys. Rev. A: At. Mol. Opt.* **1988**, *38*, 3098.

17. Weigend, F.; Ahlrichs, R. *Phys. Chem. Chem. Phys.* **2005**, *7*, 3297.

18. The $^{13}$C NMR of **4a** also is distinct from that of **1a**. We reported previously[8a] the $^{13}$C NMR spectra of **1a**, but in the course of the work described in this paper, we realized that our reported $^{13}$C spectrum of **1a** also containedas well as possibly the 3,1 isomer. Our previous report therefore notes additional (erroneous) peaks. We have been unable to obtain perfectly clean spectra of **1a**, but the $^{13}$C signals of **1a** are clearly the following: δ 215.65, 186.96, 39.55, 32.30.

19. The *trans*-1,1 notation refers to a paddlewheel complex having two different equatorial ligands, one of which has asymmetric donor atoms (e.g. N, S). The asymmetric ligands are *trans* to each other with their donor atoms oriented in opposite directions along the Mo≡Mo vector. For further discussion of this, see reference 9(l).

20. Dolomanov, O. V.; Bourhis, L. J.; Gildea, R. J.; Howard, J. A. K.; Puschmann, H. *J. Appl. Crystallogr.* **2009**, 42, 339.

# Chapter 3

*Lewis Acid Enhanced Axial Ligation of $[Mo_2]^{4+}$ Complexes*

Reprinted with permission. *Inorg. Chem.*, **2013**, *52*, 4658 – 4667. 

## 3.1 Abstract

We report here the synthesis, X-ray crystal structures, electrochemistry, and DFT single point calculations of three new complexes: tetrakis(monothiosuccinimidato)dimolybdenum(II) ($Mo_2(SNO5)_4$) (**1a**), tetrakis(6-thioxo-2-piperidinonato)dimolybdenum(II) ($Mo_2(SNO6)_4$ (**1b**), and chlorotetrakis(monothiosuccinimidato)pyridinelithiumdimolybdenum(II) ($pyLiMo_2(SNO5)_4Cl$) (**2-py**). X-ray crystallography shows unusually short axial $Mo_2$-Cl bond lengths in **2-py**, 2.6533(6) Å, and dimeric **2-dim**, 2.644(1) Å, which we propose result from an increased Lewis acidity of the $Mo_2$ unit in the presence of the proximal $Li^+$ ion. When **2-py** is dissolved in MeCN, the lithium reversibly dissociates, forming an equilibrium mixture of ($MeCNLiMo_2(SNO5)_4Cl$) (**2-MeCN**) and $[Li(MeCN)_4]^+[Mo_2(SNO5)_4Cl]^-$ (**3**). Cyclic voltammetry was used to determine the equilibrium lithium binding constant (room temperature $K_{eq} = 95 \pm 1$). From analysis of the temperature dependence of the equilibrium constant thermodynamic parameters for formation of **2-MeCN** from **3** ($\Delta H° = -6.96 \pm 0.93$ kJ mol$^{-1}$ and $\Delta S° = 13.9 \pm 3.5$ J mol$^{-1}$ K$^{-1}$) were extracted. DFT calculations indicate that $Li^+$ affects the $Mo_2$–Cl bond length through polarization of metal-metal bonding/antibonding molecular orbitals when lithium and chloride are added to the dimolybdenum core.

## 3.2 Introduction

Metal-metal bonded compounds having the paddlewheel-type structure, shown in Chart 3.1a, have played a major role in the development of coordination chemistry,[1] and continue to be of interest for their catalytic,[2] photophysical,[3] electronic,[4] structural properties,[5] and reactivity.[6] The reactivity of ligands in the axial position of these complexes is very important and plays a key role in applications such as catalysis. Only few $[Mo_2]^{4+}$ compounds are known that are axially ligated with either neutral ligands, such as THF, nitriles, and a pyrazole derivative,[7] or with anionic ligands, including $Cl^-$, $Br^-$, $I^-$, and $[BF_4]^-$.[8] $[Mo_2]^{4+}$ carboxylates can also associate through intermolecular axial interactions with O atoms from an adjacent molecule.[9] In all of these cases, however, these axial ligands are bound exceptionally weakly with $Mo_2–L_{ax}$ bond lengths often up to 0.4 - 0.6 Å longer than corresponding $Mo–L_{eq}$ bond lengths; more often, $[Mo_2]^{4+}$ complexes eschew axial ligands entirely. Thus, new strategies for axial functionalization of $[Mo_2]^{4+}$ complexes are of interest.

**Chart 3.1.** a) Paddlewheel-type structure supported by bridging anionic equatorial ligands $[X\text{-}Y\text{-}Z]^-$ The metal-metal bond order, *n*, can range from 0-4, and $L_{ax}$ are axial donor ligands. b) A qualitative molecular orbital diagram of metal-metal interactions for $[Mo_2]^{4+}$ .

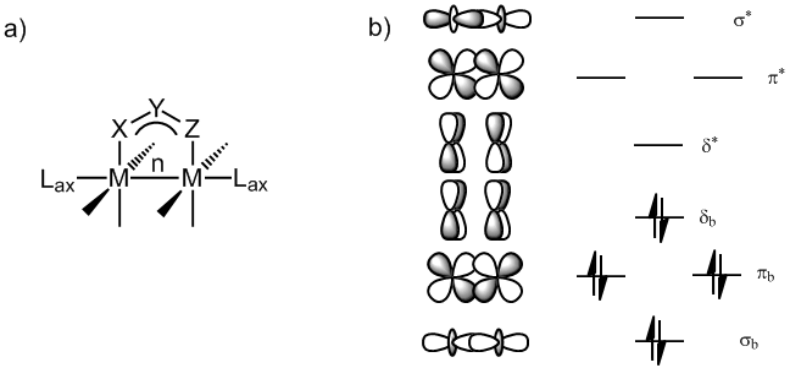

The indifference of the $[Mo_2]^{4+}$ unit towards axial ligands has its origin in the electronic structure of the $[Mo_2]^{4+}$ unit. Chart 3.1b depicts a qualitative MO diagram of a $[Mo_2]^{4+}$ species. The principal empty Mo-centered orbital that would have the correct symmetry to overlap with a σ-type lone pair orbital on a Lewis base is the Mo-Mo σ* orbital. This σ* orbital is elevated in energy by the strong interaction between the $d_{z2}$ orbitals of the two Mo atoms, resulting in a poor energetic matching, and hence, poor overlap with ligand-based σ-type lone pair orbitals. Thus, axial ligands bind weakly to $[Mo_2]^{4+}$ complexes.

Because of our interest in the reactivity of $M_2$ complexes, we wanted to see if it were possible to increase the Lewis acidity of $[Mo_2]^{4+}$ species and strengthen $Mo_2$–$L_{ax}$ bond. An attractive approach to this would be to design complexes that bring a Lewis acid into close proximity with the $[Mo_2]^{4+}$ unit, thus activating it and making it more susceptible to attack by a Lewis base. A similar strategy was recently explored by the Gabbaï group, in which inert $Hg^{2+}$ and $Au^{+}$ ions were activated by conjoining them to a proximal $Ar_4Sb^{+}$ ion as a Lewis acid, resulting in further ligation of these metals.[10] Also, the Thomas group has recently demonstrated that Lewis acidic $Zr^{4+}$ ions can activate Co, yielding a complex capable of splitting C=O bonds in $CO_2$.[11]

With regard to Lewis acid activation of $[Mo_2]^{4+}$ systems, the closest examples were reported by us on linear heterotrinuclear M···Mo≡Mo complexes using either $Co^{2+}$ or $Fe^{2+}$, in which chloride ligands bind the open $[Mo_2]^{4+}$ axial position, resulting in $Mo_2$–Cl bond distances significantly shorter than those of unactivated $[Mo_2]^{4+}$ units.[8g,h] We hypothesized, therefore, that stronger Lewis acids, such as alkali metals should result in more Lewis acidic $[Mo_2]^{4+}$ units and stronger bonds between Mo and axial ligands.

**Chart 3.2.** The ligands monothiosuccinimide and 6-thioxo-2-pipiridinone

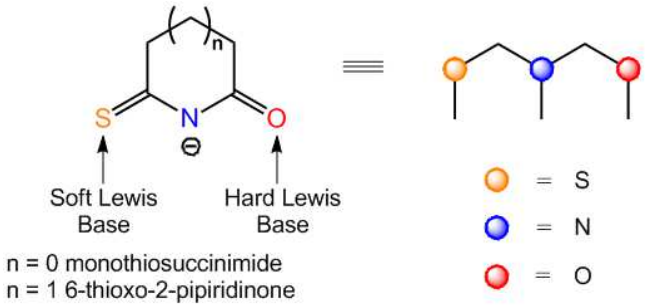


In order to promote the formation of such complexes, a new type of ligand capable of forming trimetallic complexes was designed. As opposed to dipyridylamine ligands used in our earlier M···Mo≡Mo work, which have three nitrogen bases, we have designed a ligand containing a combination of hard and soft bases so that Hard-Soft Acid-Base (HSAB) theory could be used to design heterometallic compounds with element-specific structures. Alkoxyalkylphosphines,[12] phosphinoamides[11,13] and thiopyridines[14] have been used to synthesize heterometallic complexes using a similar concept. Monothiosuccinimide (HSNO5) and 6-thioxo-2-piperidinone (HSNO6), shown in Chart 3.2, are two ligands that are ideal for this type of chemistry. These two ligands differ only in their ring size, and they incorporate hard and soft bases that would facilitate the synthesis of a heterometallic complex containing a hard Lewis acidic fragment and a $[Mo_2]^{4+}$ unit. The sulfur on this ligand is a soft base, and it is able to effectively bind $Mo^{2+}$, while the oxygen is a hard base, making it ideal to bind alkali ions.

Herein we report the synthesis and characterization of two unactivated dimolybdenum complexes, *trans*-2,2-$Mo_2(SNO5)_4$ (**1a**) and *trans*-2,2-$Mo_2(SNO6)_4$ (**1b**), and a dimolybdenum complex that is activated by the presence of a Lewis acidic lithium cation, py$LiMo_2(SNO5)_4Cl$ (**2-py**) (Scheme 3.1a). These complexes have been

structurally characterized by X-ray crystallography. We also provide electrochemical evidence that **2-py** reversibly dissociates $Li^+$ when dissolved in MeCN to form $(MeCN)LiMo_2(SNO5)_4Cl$ (**2-MeCN**) in equilibrium with $[Li(MeCN)_4]^+[Mo_2(SNO5)_4Cl]^-$ (**3**) (Scheme 3.1b). To gain more insight into the electronic structure of this complex, DFT geometry optimizations and single point calculations were performed on these complexes.

**Scheme 3.1.** a) The synthesis pathway for forming *trans*-2,2-$Mo_2(SNOX)_4$ complexes as well as $pyLiMo_2(SNO5)_4Cl$. b) The proposed equilibrium involving $Li^+$ dissociation from compound **2-MeCN**.

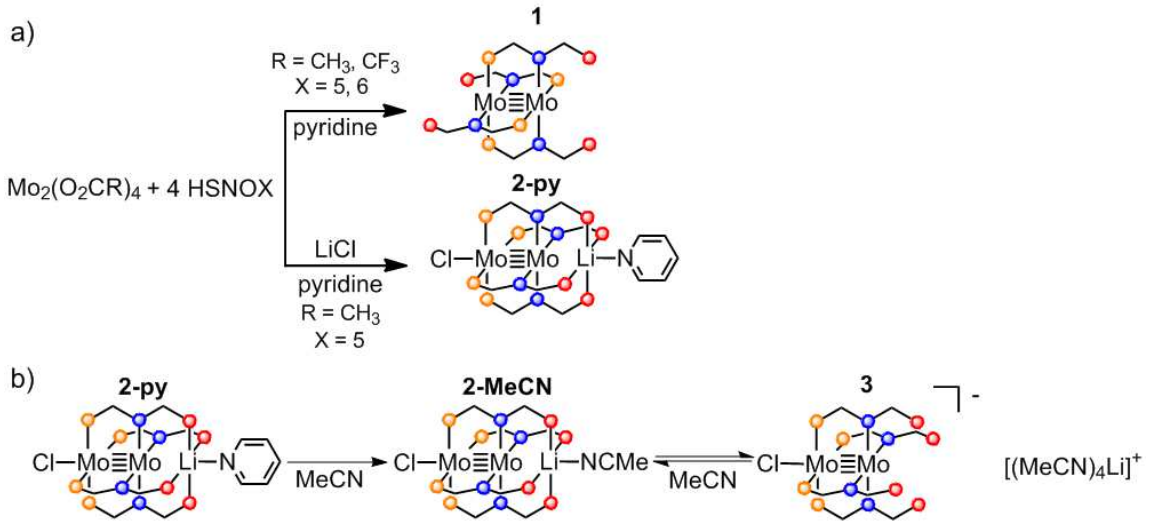


## 3.3 Experimental

### 3.3.1 General

All synthetic manipulations were carried out under an inert $N_2$ atmosphere using standard Schlenk and glovebox techniques unless otherwise stated. $CH_2Cl_2$ and $C_2H_4Cl_2$ were dried sequentially over molecular sieves and $CaH_2$ and distilled under $N_2$ prior to

use. THF was dried using a Vacuum Atmospheres solvent purification system and degassed with $N_2$ prior to use. Pyridine was dried sequentially over molecular sieves and barium oxide. It was then distilled under $N_2$ and stored in a glovebox prior to use. All other commercial reagents were used as received without further purification. Lawesson's reagent, glutarimide, succinimide, $P_2S_5$, lithium hexafluorophosphate, tetrabutyl ammonium hexafluorophosphate, trifluoroacetic acid and molybdenum carbonyl were purchased from Sigma Aldrich. Molybdenum acetate ($Mo_2(OAc)_4$) was synthesized from molybdenum carbonyl and acetic acid.[15] Molybdenum trifluoroacetate ($Mo_2(TFA)_4$) was synthesized from $Mo_2(OAc)_4$ and trifluoroacetic acid.[16] Monothiosuccinimide (HSNO5) was prepared from succinimide and $P_2S_5$.[17] 6-thioxo-2-piperidionone (HSNO6) was prepared from glutarimide and Lawesson's reagent.[18] Elemental analysis was carried out by Midwest Microlabs in Indianapolis, IN, USA. Mass spectrometry data were recorded at the Mass Spectrometry Facility of the Chemistry Instrument Center of the University of Wisconsin—Madison. Matrix-assisted laser desorption/ionization (MALDI) mass spectra were obtained using a Bruker REFLEX II spectrometer equipped with a 337 nm laser, a reflectron, delayed extraction, and a time-of-flight (TOF) analyzer. In the positive ion mode, the acceleration voltage was 25 kV. The IR spectra were taken on a BRUKER TENSOR 27 using ATR techniques. $^1$H NMR spectra were recorded on a Bruker AC+ 300 spectrometer. $^{13}$C and $^7$Li NMR spectra were recorded on a Bruker Avance-500 spectrometer.

### 3.3.2 Syntheses

***trans*-2,2-tetrakis(monothiosuccinimidato)dimolybdenum(II) (*trans*-2,2-$Mo_2(SNO5)_4$) (1a).**

A flask was charged with 246 mg HSNO5 (2.14 mmol), 331 mg $Mo_2(TFA)_4$ (0.333 mmol), and 30 mL of pyridine. The resulting reaction mixture was heated to reflux with stirring for 3 h. The reaction mixture was then allowed to cool to room temperature, and the solvent was removed under vacuum. The resulting residue was washed with 3 x 20 mL $Et_2O$. This gave an orange-brown powder, which was extracted with 20 mL hot $CH_2Cl_2$. Layering this extract with hexanes gave **1a** as a brown powder. The solid was filtered in air and washed with 3 x 20 mL hexanes and 1 x 20 mL $Et_2O$. Yield: 199 mg (59.0 %). $^1$H NMR (300 MHz, $CDCl_3$) δ 3.563 (m, 2H), 2.885 (m, 2H). $^{13}$C NMR (125 MHz, $CDCl_3$) δ 215.85, 215.57, 186.91, 186.58, 39.55, 32.30. (Duplicates in $^{13}$C NMR likely due to multiple conformers present in solution) MALDI-MS: (**1a**$^+$) 651 m/z. IR (ATR, $cm^{-1}$) 1755 w, 1725 m, 1438 m, 1415, m, 1398 m, 1248 m, 1191 vs, 990 vw, 963 w, 917 m, 804 m, 733 m. UV-vis ($CH_2Cl_2$, , λ(nm) [ε($M^{-1}cm^{-1}$)]): 414 [5400], 495 [830]. Elemental Analysis: Calculated for $C_{16}H_{16}S_4N_4O_4Mo_2$ (**1a**) C: 29.63%, H: 2.49%, N: 8.64%. Found: C: 29.64%, H: 2.57%, N: 7.96%.

***trans*-2,2-tetrakis(6-thioxo-2-piperidinonato)dimolybdenum(II) (*trans*-2,2-$Mo_2(SNO6)_4$) (1b).**

A flask was charged with 320 mg HSNO6 (2.48 mmol), 264 mg $Mo_2(OAc)_4$ (0.572 mmol), 148 mg LiCl and 15 mL of pyridine, and the resulting reaction mixture was heated to reflux with stirring for 16 h. The solvent was then removed under vacuum, leaving a red oily residue. The residue was triturated with 2 x 15 mL $Et_2O$, yielding a fine

red solid. The solid was extracted with 20 mL 1,2-dichloroethane and crystals were grown from the resulting solution by layering with 80 mL hexanes. Compound **1b** was isolated by filtration as a red, microcrystalline solid. Yield: 201 mg (46.2%). $^{1}$H NMR (300 MHz, $CDCl_3$) δ 3.325 (t, J = 6 Hz, 2H), 2.521 (t, J = 6.6 Hz, 2H), 2.156 (p, J = 6.3 Hz, 2H). $^{13}$C (125 MHz, $CDCl_3$) δ 207.96, 177.53, 39.13, 21.86. MALDI-MS: (**1b**$^{+}$) 705 m/z. IR (ATR, cm$^{-1}$) 2959 vw, 1675 m, 1604 w, 1521 w, 1485 w, 1441 s, 1407 s, 1333 m, 1323 m, 1261 vs, 1245 vs, 1181 vs, 1115 vs, 1070 w, 1042 w, 1012 w, 975 m, 962 m, 912 m, 846 w, 758 m, 677 s, 651 s. UV-vis (THF, λ(nm) [ε(M$^{-1}$cm$^{-1}$)]): 460 [12,000]. Elemental Analysis: Calculated for $C_{20}H_{24}S_4N_4O_4Mo_2$ (**1b**) C: 34.09%, H: 3.43%, N:7.95% Found: C: 34.03%, H: 3.41%, N: 7.84%.

**4,0-chlorotetrakis(monothiosuccinimidato)pyridinedimolybdenum(II)lithium ($pyLiMo_2(SNO5)_4Cl$) (2-py)**.

A flask was charged with 326 mg HSNO5 (2.83 mmol), 303 mg $Mo_2(OAc)_4$ (0.706 mmol), and 320 mg LiCl (7.6 mmol) were dissolved in 20 mL of pyridine. The resulting solution was heated to 110° C without stirring. Within a few hours, red-orange crystalline **2-py** began to precipitate from the solution. After 16 h the reaction was cooled to room temperature. Compound **2-py** was collected by filtration, washed with 3 x 20 mL THF, 2 x 20 mL of hexanes, and dried under vacuum. Yield: 369 mg (61.6%). $^{1}$H NMR (300 MHz, MeCN-d3) δ 8.59 (m, 2H), 7.745 (tt, J = 7.8, 1.8 Hz, 1H), 7.34 (m, 2H), 3.58 (m, 8H), 2.78 (m, 8H). $^{13}$C NMR (125 MHz, MeCN-d3) δ 192.73, 150.76, 137.04, 124.83, 95.74, 41.29, 33.39. $^{7}$Li NMR (194 MHz, DMF) δ 0.547. IR (ATR, cm$^{-1}$) 2963 vw, 1724 m, 1569 vw, 1441 w 1429 w, 1390 w, 1259 s, 1236 s, 1217 s, 1086 m, 1034 s, 1018 s, 962 w, 937 w, 863 w, 797 vs, 753 w, 703 m, 684 m, 665 m, 629 w. UV-vis

(MeCN, λ(nm) [ε($M^{-1}cm^{-1}$)]): 433 [5300], 521 [530]. Elemental Analysis: Calculated for $C_{26}H_{26}N_6S_4O_4Mo_2Li$ (**2-py**·py). C: 36.78%, H: 3.09%, N: 9.90%. Found: C: 36.64%, H: 3.09%, N: 9.80%. X-ray quality crystals were also obtained of dimeric $[LiMo_2(SNO5)_4Cl]_2$ (**2-dim**) by crystallizing **2-py** from $CH_2Cl_2$/py/hexanes.

### 3.3.3 X-ray Crystallography

Suitable crystals of **1a**, **1b**, **2-py** and **2-dim** were selected under oil and ambient conditions. For **1a** an orange plate shaped single crystal with dimensions 0.118 x 0.087 x 0.075 $mm^3$ was selected. For **1b** an orange-yellow block shaped crystal with dimensions 0.370 x 0.190 x 0.090 $mm^3$ was selected. For **2-py**, a red plate shaped crystal with dimensions 0.210 x 0.184 x 0.029 $mm^3$ was selected. For **2-dim** an orange rod shaped crystal with dimensions 0.100 x 0.050 x 0.030 $mm^3$ was selected. Crystals were attached to the tip of a MiTeGen MicroMount and mounted in a stream of cold nitrogen at 100(1) K and centered in the X-ray beam using a video monitoring system. The crystal evaluation and data collection were performed on a Bruker Quazar SMART APEX-II diffractometer with Cu Kα (λ = 1.54178 Å) (**1a**) or Mo Kα (λ = 0.71073 Å) (**1b**, **2-py**, **2-dim**) radiation. The data were collected using a routine to survey an entire sphere of reciprocal space and were indexed by the SAINT routine in APEX-II.[19] The structures were solved *via* direct methods and refined by iterative cycles of least-squares refinement on $F^2$ followed by difference Fourier synthesis. All hydrogen atoms were included in the final structure factor calculation at idealized positions and were allowed to ride on the neighboring atoms with relative isotropic displacement coefficients.

**Table 3.1**. The X-ray crystallographic solution details for compounds **1** and **2-py**.

| Compound | **1a** | **1b** | **2-py** | **2-dim** |
|---|---|---|---|---|
| Empirical formula | $C_{16}H_{16}Mo_2N_4O_4S_4$ | $C_{23}H_{30}N_4O_4S_4Cl_3Mo_2$ | $C_{26}H_{26}LiN_6O_4S_4ClMo_2$ | $C_{34}H_{36}Cl_6Li_2Mo_4N_8O_8S_8$ |
| Formula weight | 648.45 | 852.98 | 849.04 | 1551.53 |
| Temperature/K | 100(1) | 100(1) | 100(1) | 100(1) |
| λ/ Å | 1.54178 | 0.71073 | 0.71073 | 0.71073 |
| Crystal system | orthorhombic | monoclinic | orthorhombic | monoclinic |
| Space group | *Pccn* | $P2_1/n$ | $P2_12_12_1$ | $P2_1/n$ |
| a/Å | 10.6032(7) | 10.6871(3) | 8.6895(3) | 8.704(3) |
| b/Å | 12.591(1) | 19.8411(6) | 13.7221(5) | 22.530(8) |
| c/Å | 15.842(2) | 15.3151(5) | 26.1281(9) | 13.543(5) |
| β/° | 90 | 106.159(1) | 90 | 108.07(2) |
| Volume/Å$^3$ | 2115.0(3) | 3119.2(2) | 3115.5(2) | 2525.1(17) |
| Z | 4 | 4 | 4 | 2 |
| $\rho_{calc}$ mg/mm$^3$ | 2.036 | 1.816 | 1.810 | 2.041 |
| Final R indexes[a,b] [I≥2σ (I)] | $R_1$ = 0.0271<br>$wR_2$ = 0.0733 | $R_1$ = 0.0290<br>$wR_2$ = 0.0664 | $R_1$ = 0.0186<br>$wR_2$ = 0.0381 | $R_1$ = 0.0309<br>$wR_2$ = 0.0621 |
| Final R indexes [all data] | $R_1$ = 0.0281<br>$wR_2$ = 0.0741 | $R_1$ = 0.0389<br>$wR_2$ = 0.0709 | $R_1$ = 0.0204<br>$wR_2$ = 0.0387 | $R_1$ = 0.0504<br>$wR_2$ = 0.0683 |
| Flack Parameter | - | - | -0.03(2) | - |

[a]$R1 = \Sigma||F_o| - |F_c||/[\Sigma|F_o|]$. [b]$wR2 = |[\Sigma[w(F_o^2 - F_c^2)^2]/[\Sigma[w(F_o^2)^2]]]^{1/2}$, $w = 1/\sigma^2(F_o^2) + (aP)^2 + bP$, where $P = [\max(0 \text{ or } F_o^2) + 2(F_c^2)]/3$.

The details concerning X-ray crystallographic solutions and refinement for compounds **1a**, **1b**, and **2-py** are tabulated in Table 3.1. For each structure, the model was refined to a low wR2 value (< 0.10 for each case). After refinement of the model, compound **2-py** had a featureless final Fourier map. For compounds **1a** and **1b**, the final Fourier maps had peaks of 1.34 e/Å$^3$ and 1.36 e/Å$^3$, respectively. These highest peaks were located closest to the heaviest atoms in the models (Mo) and were interpreted as noise. For compound **2-py**, the absolute structure was established by anomalous dispersion using the method of Flack.[20]

### 3.3.4 Electrochemistry

Compounds **2-MeCN** and **3** were prepared *in situ* by dissolving **2-py** in a 100 mM solution of $NBu_4PF_6$ in MeCN at room temperature under ambient conditions and subsequently titrating the solution with either $LiPF_6$ or 12-crown-4 ether, respectively. Cyclic voltammetry for compounds **1a**, **1b**, **2-MeCN**, and **3** was performed on solutions of 1 mM analyte and 100 mM electrolyte ($NBu_4PF_6$) at temperatures ranging from -29°C to 20°C using a standard glassy carbon electrode for the working electrode, a platinum wire for the auxiliary electrode, and an $Ag/Ag^+$ electrode as the reference electrode. All electrochemical potentials were internally referenced to the ferrocene/ferrocenium couple. The voltammetry was performed in the range of 900 mV to -500 mV for compounds **2-MeCN** and **3** or to -1700 mV for compounds **1a** and **1b** at a scan rate of 100 mV/s. The solvents used were MeCN for compounds **1a**, **2-MeCN**, and **3**, and $CH_2Cl_2$ for compound **1b**.

### 3.3.5 DFT Calculations

Restricted Kohn-Sham geometry optimization and single-point calculations were carried out on **1a** and **2-py** through the ORCA calculation package using the BP86 functional.[21] The def2-TZVP (Mo, Cl) and def2-SVP (all other atoms) basis sets from the Karlsruhe group,[22] which are automatically recontracted in ORCA for use with the scalar relativistic zeroth-order regular approximation (ZORA), were used. Structures for compounds **1a** and **2-py** were calculated using initial atomic coordinates taken from the crystal structures and then optimized until the energy change between steps was less than $10^{-6}$ Hartree. All calculations were optimized with a Grid4 optimization grid and tight SCF convergence criteria.

## 3.4 Results and Discussion

### 3.4.1 Synthesis

Compounds **1a** and **1b** were synthesized in useful yields by reacting free HSNO5 and HSNO6 ligands with $Mo_2(TFA)_4$ and $Mo_2(OAc)_4$ under $N_2$ in refluxing pyridine, respectively. For these reactions, pyridine serves two purposes. First, it is a solvent with a high boiling point (~130°C at 1.1 bar) so the reactions can be heated to a high enough temperature to proceed to completion. Second, the basicity of pyridine drives this reaction by removing the acetic or trifluoroacetic acid formed *via* ligand substitution.

Lithium chloride is an important additive that aids in purification of **1b**. The pyridinium acetate byproduct formed in the reaction is not soluble in $Et_2O$ or hexanes, but it is soluble in 1,2-dichloroethane and $CH_2Cl_2$, as is **1b**. When LiCl is added to the reaction, lithium acetate and pyridinium chloride are formed instead of pyridinium acetate, and so the purification of **1b** can be accomplished by washing the mixture with

$Et_2O$ and subsequent extraction with 1,2-dichloroethane since now only **1b** is soluble in this solvent. When LiCl is not added to the reaction mixture, only impure, non-crystalline product can be obtained from the reaction. Both compounds **1a** and **1b** are able to be handled and used under ambient conditions, but they degrade slightly after exposure to air and moisture over the course of several months.

Compound **2-py** is the product the reaction of $Mo_2(OAc)_4$ with HSNO5 and excess LiCl under $N_2$ in hot pyridine (110°C). The product precipitates from pyridine, greatly simplifying workup and leading to good yields (62%). Like **1a** and **1b**, **2-py** is air and moisture stable. **2-py** is sparingly soluble in most non-coordinating solvents such as dichloromethane and toluene, but it is more soluble in strongly coordinating solvents such as DMSO, MeCN, pyridine, and DMF. The Li-bound pyridine ligand in **2-py** is labile. Simple recrystallization of **2-py** from a mixture of $CH_2Cl_2$ and pyridine affords **2-dim** in which the py ligand is lost and is replaced by an intermolecular Li-O interaction with an O atom from an adjoining $LiMo_2(SNO5)_4Cl$ species. When **2-py** dissolved in coordinating solvents, it is assumed that the donor solvent replaces the py ligand. **2-py** can also be delithiated as evidenced by the electrochemistry of **2-py** in MeCN (*vide infra*). In solution, the lithiated and non-lithiated species are in equilibrium as illustrated in Scheme 3.1b.

The synthesis of the HSNO6 complex analogous to **2-py** ($pyLiMo_2(SNO6)_4Cl$) was attempted as well, and $LiMo_2(SNO6)_4Cl$ was obtained, but only in very poor yield.[23] Formation of this compound is likely disfavored due to the smaller binding pocket available for $Li^+$ in complexes of the SNO6 ligand as compared with complexes of the SNO5 ligand.

### 3.4.2 X-ray Crystallography

A list of relevant bond lengths and angles for compounds **1a**, **1b**, **2-py**, and **2-dim** described here is included in Table 3.2.

**Table 3.2**. Important bond distances and bond angles for the X-ray crystal structures of compounds **1a**, **1b**, **2-py**, **2-dim**.

| | $Mo_2(SNO5)_4$(1a) | $Mo_2(SNO6)_4$ (1b) | $pyLiMo_2(SNO5)_4Cl$ (2-py) | $[LiMo_2(SNO5)_4Cl]_2$ (2-dim) |
|---|---|---|---|---|
| **D(Mo-Mo) (Å)** | 2.1112(4) | 2.1150(2) | 2.1357(3) | 2.1354(8) |
| **D(Mo-N) (Å)** | 2.145[2] | 2.153[3] | 2.119[2] | 2.123[3] |
| **D(Mo-S) (Å)** | 2.4753[8] | 2.481[8] | 2.5172[6] | 2.514[1] |
| **D(Mo-Cl) (Å)** | - | - | 2.6533(6) | 2.644(1) |
| **D(Li-O) eq (Å)** | - | - | 2.182[6] | 2.185[7] |
| **D(Li···Mo) (Å)** | - | - | 3.075(5) | 3.049(6) |
| **A(Mo-Mo-Cl) (°)** | - | - | 176.24(2) | 174.95(2) |
| **A(Li-Mo-Mo) (°)** | - | - | 178.7(1) | 177.3(1) |

Compound **1a** crystallized in the orthorhombic space group *Pccn* from slow diffusion of hexane into a solution of the compound in dichloromethane (Figure 3.1). The complex has idealized $D_{2d}$ symmetry and a crystallographic two-fold axis bisects the Mo ≡Mo vector. Following the conventional nomenclature for isomeric paddlewheel type compounds bridged by ligands bearing two different donor atoms,[1] the *trans*-2,2 isomer of **1a** is observed here. This terminology means that two of the $SNO5^-$ ligands *trans* to each other are aligned one way along the Mo≡Mo bond axis while the other two ligands are aligned in the opposite direction. Each molybdenum atom in complex **1a** is therefore bound to two S atoms *trans* to each other and two N atoms *trans* to each other. The Mo≡ Mo distance of 2.1112(4) Å is typical of a Mo≡Mo quadruple bond.[15,16] The Mo-N bond lengths are within the range of reported values for similar dimolybdenum complexes containing four equatorial N-S ligands (2.130 - 2.199 Å), while the Mo-S bond lengths

are slightly longer than the range reported in the literature (2.444 - 2.468 Å).[24] The $sp^2$ hybridization of the carbonyl and thioxo carbons of each ligand in compound **1a** results in the entire SNO5 ligand being planar.

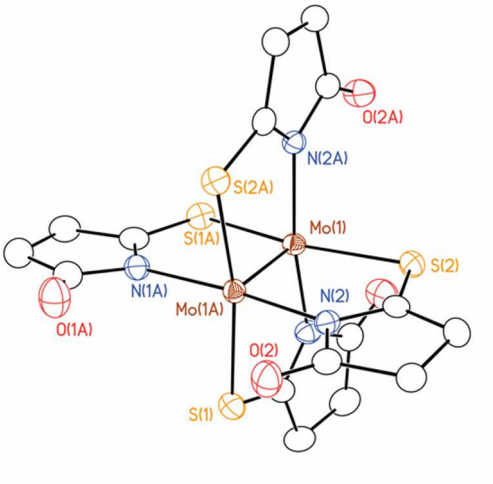


**Figure 3.1.** The X-ray crystal structures of compound **1a**. All atoms are drawn as 50% thermal probability ellipsoids, and all hydrogen atoms are omitted for clarity. The structure of the compound is the *trans*-2,2 isomer.

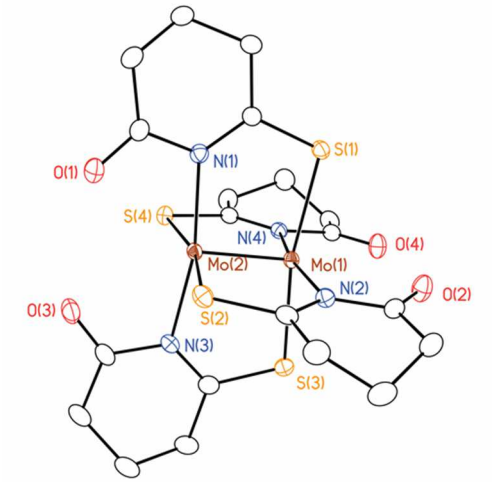


**Figure 3.2.** The crystal structure of **1b**. All atoms are drawn as 50% thermal probability ellipsoids, and all H atoms are omitted for clarity. **1b** also crystallizes with 1.5 molecules of 1,2-dichloroethane in the asymmetric unit (not shown).

The X-ray crystal structure for **1b** is shown in Figure 3.2. Compound **1b** crystallizes in the monoclinic space group $P2_1/c$ with 1.5 1,2-dichloroethane solvent molecules in the asymmetric unit. Like **1a**, **1b** adopts the *trans*-2,2 configuration. The average Mo-N, Mo-S, and Mo≡Mo bond distances are all similar to the corresponding bond distances for **1a**. Unlike the structure of compound **1a**, in **1b**, the six-membered ring of the $SNO6^-$ ligand is puckered with the carbon in the 4 position out of the plane of the ligand.

In both compounds **1a** and **1b**, the Mo-N bond distance is significantly shorter than the Mo-S bond distance primarily due to the difference between the atomic radii of N and S. The difference in these bond lengths, > 0.3 Å, results in the ligand being canted, pushing the oxygen atoms of opposite ligands closer together. In **1b** the non-bonded distance between the oxygen atoms (3.276 Å) is significantly shorter than the distance between oxygen atoms in **1a** (4.602 Å). In the $SNO6^-$ case, steric crowding by the O atoms limits the available space for $Li^+$ to bind, whereas in the $SNO5^-$ case, the O atoms are not nearly as close together, providing a much larger binding pocket to accommodate a $Li^+$ cation. It is likely that the preference for the *trans*-2,2 configuration also stems from the fact that the oxygen atoms could be too close together in the other possible isomers.

Compound **2-py** crystallizes from the pyridine reaction mixture in the non-centrosymmetric space group $P2_12_12_1$ as a monomer as shown in Figure 3.3. The compound also can crystallize from a non-coordinating solvent such as $CH_2Cl_2$ as a pyridine-free dimer (**2-dim**, Figure 3.4), which has very similar bond distances and bond angles to **2-py**. The crystal structure shows that **2-py** adopts the 4,0 isomer as opposed to

the 2,2 isomer of compounds **1a** and **1b**, as well as all previously synthesized $[Mo_2]^{4+}$ complexes with N,S equatorial ligands.[24] Also unlike **1a** and **1b**, **2-py** contains a coordinated $Li^+$ ion along the Mo≡Mo axis at a distance of 3.07 Å from the $[Mo_2]^{4+}$ unit. It therefore appears that $Li^+$ acts as a template for the $SNO5^-$ ligands, allowing the formation of the 4,0 isomer.

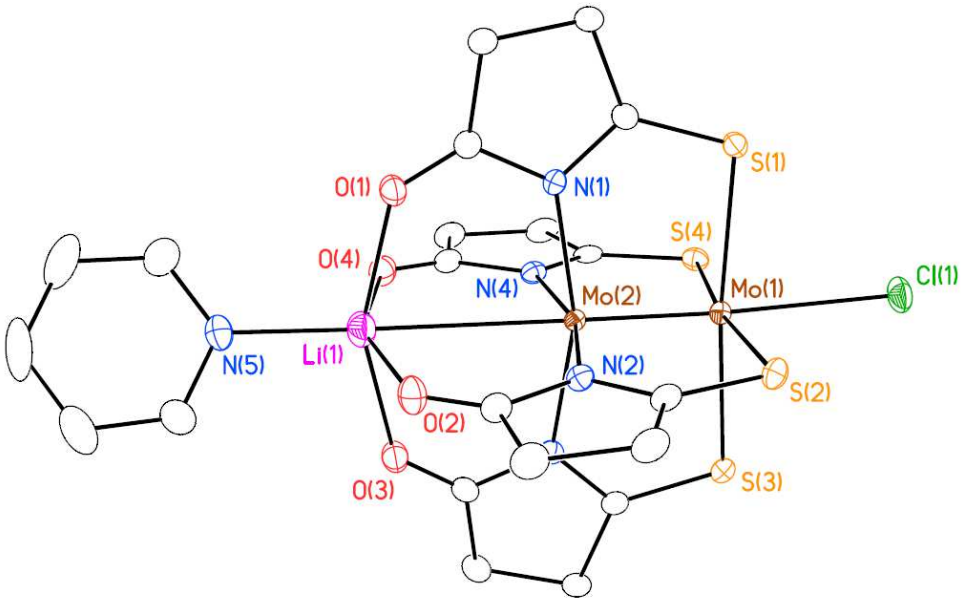


**Figure 3.3.** The X-ray crystal structure of monomeric **2-py**. All atoms are drawn as 50% thermal probability ellipsoids and all hydrogen atoms are omitted for clarity. **2-py** crystallizes with an additional molecule of pyridine in the asymmetric unit (not shown).

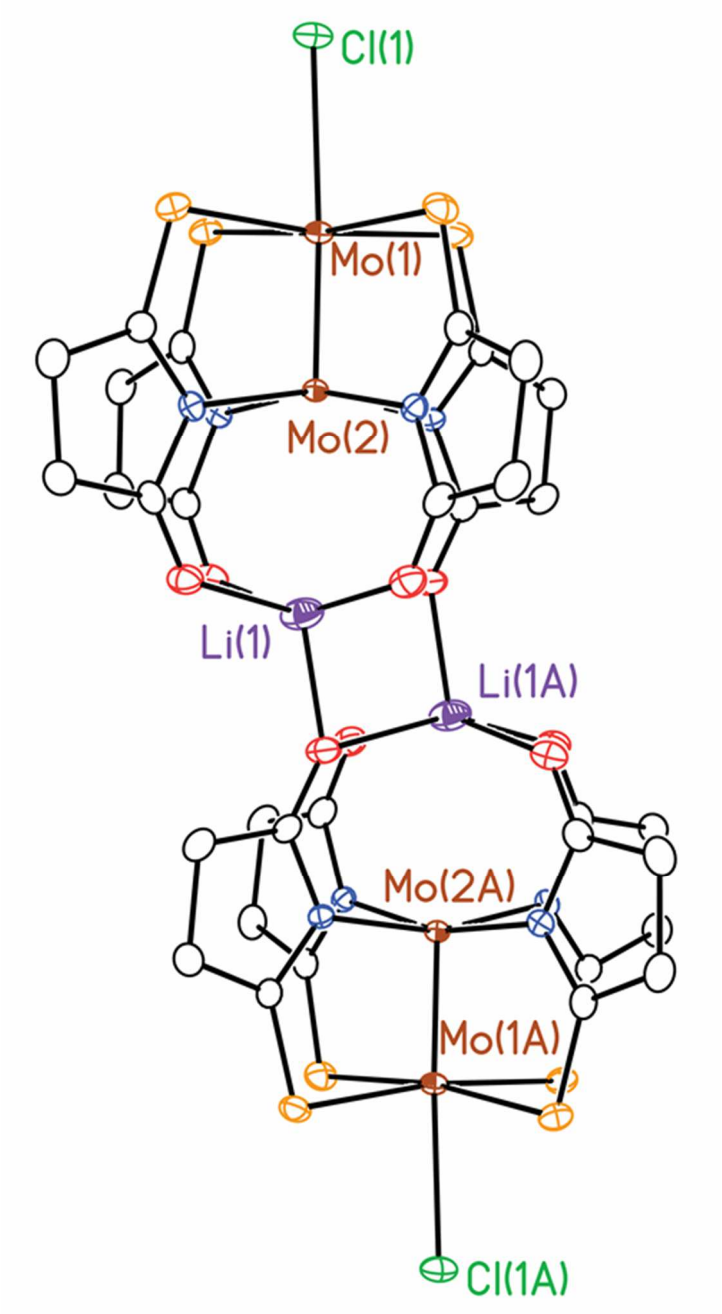


**Figure 3.4.** The X-ray crystal structure of dimeric **2-dim**. All atoms are drawn as 50% thermal probability ellipsoids and all hydrogen atoms are omitted for clarity. **2-dim** crystallizes with two additional molecules of $CH_2Cl_2$ per dimer (not shown).

**Table 3.3.** The Mo≡Mo and Mo-Cl distances of unactivated, late transition metal activated, and alkali metal activated $[Mo_2]^{4+}$–Cl complexes.

| **Compound** | **Mo≡Mo (Å)** | **$Mo_2$–Cl (Å)** |
|---|---|---|
| *Unactivated* | | |
| $Mo_2(O_2CH)_4$ KCl[8a] | 2.106[2] | 2.864[2] |
| $Mo_2Cl_2(OAc)_2$ (μ-dppa)$_2$[8b] | 2.152(2) | 2.862(3) |
| {[trans-$Mo_2(O_2CCF_3)_2$(μ-dppa)]$_3$($\mu_6$-$CO_3$)(μ-Cl)$_3$}F[8c] | 2.154[1] | 2.877[3] |
| $Mo_2(O_2CC_6H_3(NH_3)_2)_4Cl_8$[8d] | 2.107(1) | 2.854(2) |
| $[Pd_2Cl_2(CNC_6H_3Me_2\text{-}2,6)_4][Mo_2(O_2CCF_3)_4]$[8e] | 2.1312(3) | 2.7747(5) |
| $Mo_2Cl_2(OAc)_2$ (μ-dppma)$_2$[8f] | 2.1719(8) | 2.714(1) |
| *Late Transition Metal Activated* | | |
| $Mo_2Fe(dpa)_4Cl_2$[8g] | 2.168(3) | 2.707(1) |
| $Mo_2Co(dpa)_4Cl_2$ $(CH_2Cl_2)_2$[8h] | 2.1027(5) | 2.720(1) |
| *Alkali Metal Activated* | | |
| pyLi$Mo_2$(SNO5)$_4$Cl (**2-py**) | 2.1356(3) | 2.6533(6) |
| [Li$Mo_2$(SNO5)$_4$Cl]$_2$ (**2-dim**) | 2.1354(8) | 2.644(1) |

dppa = *N*,*N*-bis(diphenylphosphino)amine
dppma = *N*,*N*-bis(diphenylphosphino)methylamine
dpa = dipyridylamine.

The $Mo_2$–Cl distances in **2-py** and **2-dim** are 2.6533(6) Å and 2.644(1) Å, respectively, which are the shortest distances yet reported for an axial $Cl^-$ ion trans to a Mo≡Mo bond. The Mo≡Mo bond distances are 2.1356(3) Å and 2.1354(8) Å, respectively, which are longer than the Mo≡Mo bond distances in compounds **1a** and **1b** by 0.025 Å. The differences in Mo≡Mo bond distance are statistically significant but may not carry much chemical significance.

A comparison of the axial $Mo_2$–Cl bond distances from **2-py**, **2-dim**, and those of other known $Mo_2$–Cl compounds reported in the CSD are listed in Table 3.3. The previously synthesized $[Mo_2]^{4+}$ complexes can be divided into two categories: $[Mo_2]^{4+}$ complexes with no additional Lewis acid present and $[Mo_2]^{4+}$ complexes with a late transition metal acting to increase the $[Mo_2]^{4+}$ Lewis acidity. The $Mo_2$–Cl bond distances

in unactivated $[Mo_2]^{4+}$ complexes range from 2.714(1) Å to 2.864[2] Å with an average of 2.8242[5] Å. The $[Mo_2]^{4+}$ complexes activated by a late transition metal Lewis acid in general have shorter $Mo_2$–Cl bond lengths (2.720(1) Å and 2.707(1) Å). The axial $Mo_2$–Cl bond distances in **2-py** and **2-dim** are much shorter than those in either of these classes of compounds. Thus, the increased Lewis acidity of $Li^+$ activates the $[Mo_2]^{4+}$ core far better than even late transition metals.

### 3.4.5 Electrochemistry

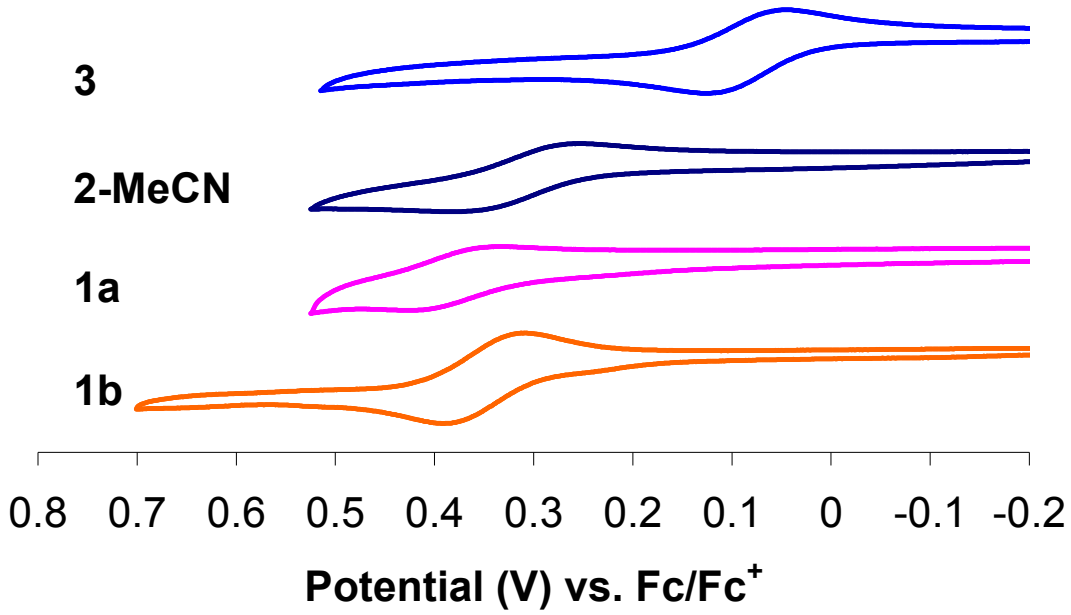


**Figure 3.5.** The cyclic voltammograms of compounds **1a** (pink), **1b** (orange), **2-MeCN** (navy), and **3** (blue).

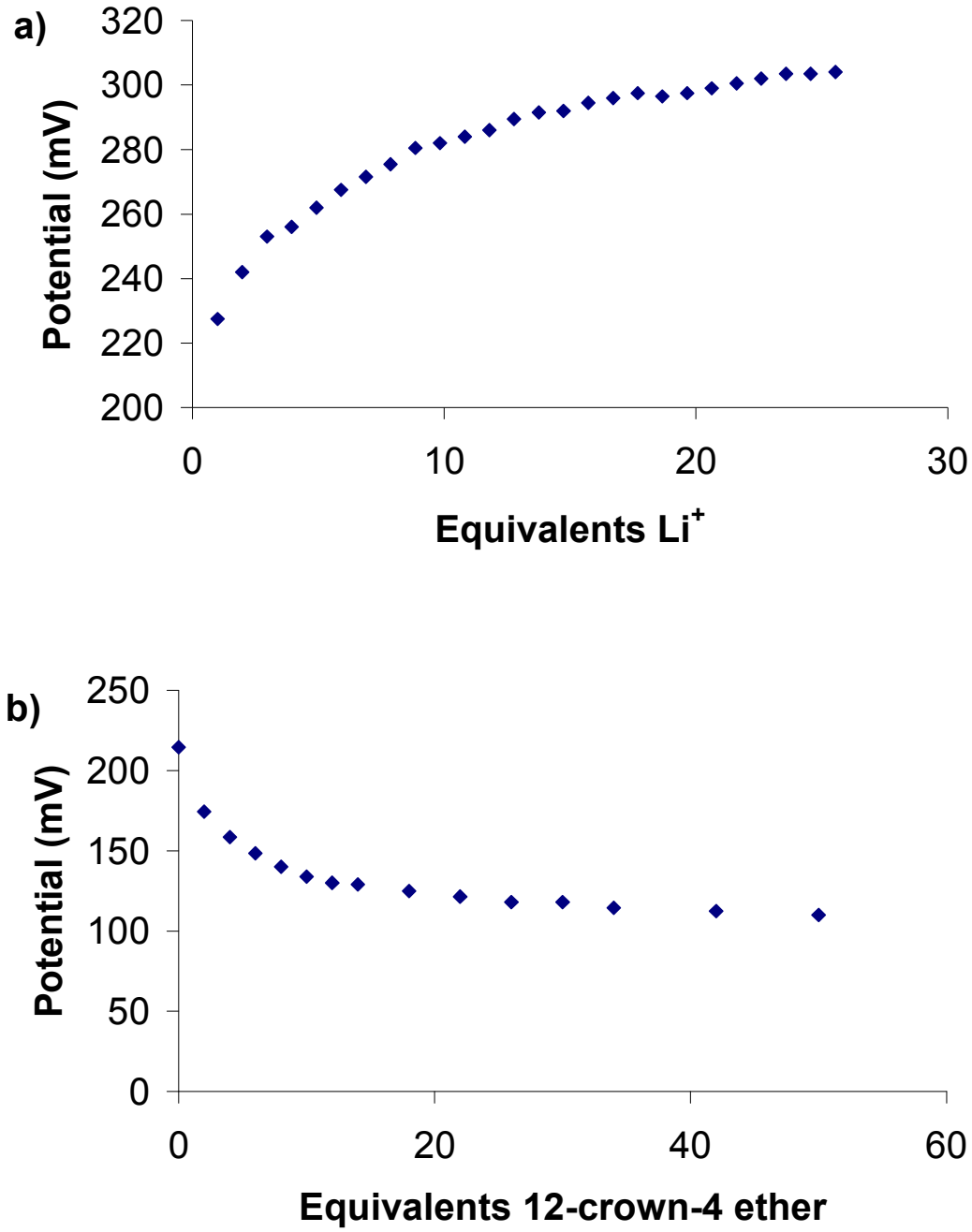


**Figure 3.6.** The potential of the MeCN solution of **2-py** as a function of a) equivalents of $Li^+$ added and b) equivalents of 12-crown-4 added. All potentials are referenced to $Fc/Fc^+$ redox couple.

Quadruply-bonded $[Mo_2]^{4+}$ compounds can often be oxidized to the corresponding $[Mo_2]^{5+}$ level in which the Mo-Mo bond order is 3.5.[25] The new compounds reported here all show one quasi reversible wave in their respective cyclic voltammograms (Figure 3.5) consistent with the $[Mo_2]^{4+/5+}$ redox couple. While **1a** and **1b** show reversible waves at 388 and 351 mV vs. $Fc/Fc^+$, respectively, the redox potential of **2-py** depends strongly on the conditions of the electrochemistry, most importantly, on the $[Li^+]$ concentration supplied by the supporting electrolyte (Figure 3.6). For example, a solution of **2-py** in 0.1 M $NBu_4PF_6$ in MeCN shows a reversible wave at 204 mV, which becomes less accessible as $LiPF_6$ is added to the supporting electrolyte, ultimately reaching a value of 319 mV. If, instead, the strong $Li^+$ chelating agent 12-crown-4 ether is added to a solution of **2-py**, the $[Mo_2]^{4+/5+}$ wave becomes drastically more accessible, reaching a plateau at 89 mV. These data are consistent with a $Li^+$ complexation/decomplexation equilibrium in which the $Li^+$ ion of **2-py** may be reversibly removed. For the species involved in this equilibrium, we propose the structures **2-MeCN** and **3** (Scheme 3.2); for the former compound we make the reasonable assumption that, upon being dissolved in MeCN, the pyridine ligand in **2-py** is quickly replaced with MeCN. For **3**, we hypothesize that the axial $Cl^-$ does not dissociate, which is consistent with the low oxidation potential of the compound. Based on the experiments described above, the $[Mo_2]^{4+/5+}$ potentials of **2-MeCN** and **3** are assigned as shown in Table 3.4.

Since the metalated and demetalated complexes have different oxidation potentials, this system is an example of metal coupled electron transfer (MCET).[26] In MCET, the redox potential of a compound behaves according to Equations 1 and 2, which are derived from the Nernst equation using Hess's Law.

$$E = E_2 - \frac{RT}{F}\left(\ln(K_{red})\right) \textbf{(Eq1)}$$

$$E = E_3 - \frac{RT}{F}\left(\ln(K_{ox})\right) \textbf{(Eq2)}$$

**Table 3.4.** The electrochemical potentials for oxidation of complexes **1** - **3** as well as other $[Mo_2]^{4+}$ complexes with N,S equatorial ligands. All potentials are given referenced to the $Fc/Fc^+$ couple.

| Compound | Potential vs. Fc/Fc+ (mV) | Solvent |
|---|---|---|
| *trans*-2,2-$Mo_2$(SNO5)$_4$ (**1a**) | 388 | MeCN |
| *trans*-2,2-$Mo_2$(SNO6)$_4$ (**1b**) | 351 | $CH_2Cl_2$ |
| 4,0-MeCNLiCl$Mo_2$(SNO5)$_4$ (**2-MeCN**) | 319 | MeCN |
| 4,0-[$Mo_2$(SNO5)$_4$Cl]$^-$ (**3**) | 89 | MeCN |
| $Mo_2$($Ph_2$PC(S)NMe)$_4$[24b] | 180 | $CH_2Cl_2$ |
| $Mo_2$($Ph_2$PC(S)NPh)$_4$[24b] | 240 | $CH_2Cl_2$ |
| $Mo_2$($Me_2$NC(S)NMe)$_4$[24b] | 210 | $CH_2Cl_2$ |
| $Mo_2$({NPh}C(S)C≡CPh)$_4$[24e] | 92 | DMF |
| | 297 | THF |
| $Mo_2$(2-mercaptoquinoline)$_4$[24c] | 520 | $CH_2Cl_2$ |
| | 1320 | $CH_2Cl_2$ |

**Scheme 3.2.** The square scheme for the electrochemistry of complexes **2-MeCN** and **3**.

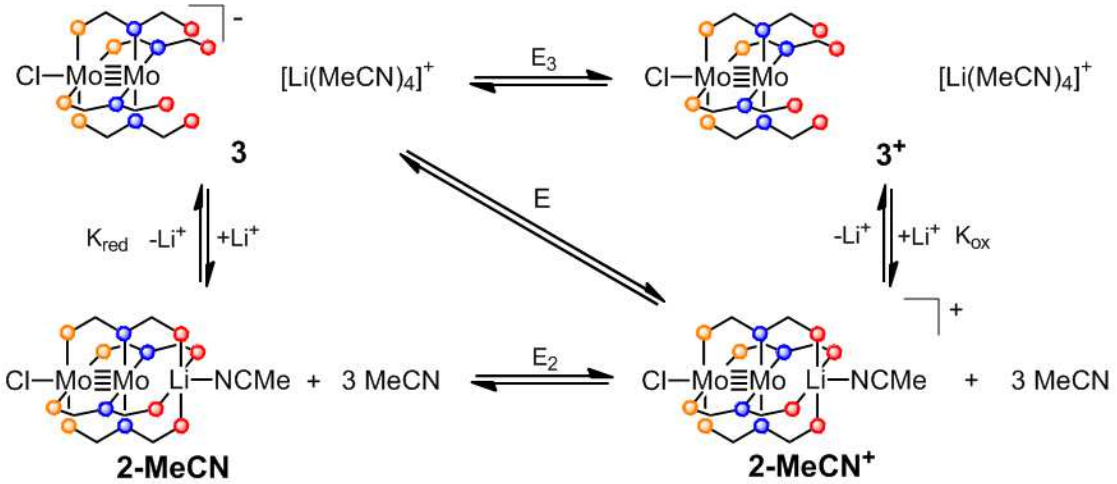

Thus, for the **2-MeCN**/**3** equilibrium, the thermodynamics of lithium binding to both **3** and $\mathbf{3}^{+}$ can be calculated using the oxidation potentials of pure **2-MeCN** and **3** as well as determining the oxidation potential of a equilibrium mixture of the two and by using the square scheme shown in Scheme 3.2. At 20°C, the oxidation potential of a solution of **2-py** in MeCN with no additional $Li^{+}$ or 12-crown-4 ether added is 204 mV, which corresponds to an equilibrium constant, $K_{red} = 95 \pm 1$. The equilibrium constants for lithium binding to the oxidized complex ($\mathbf{3}^{+}$) and non-oxidized complex (**3**) were determined at temperatures ranging from -29° C to 20° C. Van't Hoff plots of these equilibrium constants are shown in Figure 3.7. From these plots, the standard enthalpy and entropy of lithium binding to **3** and $\mathbf{3}^{+}$ were determined ($\Delta H° = -6.96 \pm 0.93$ kJ $mol^{-1}$ and $\Delta S° = 13.9 \pm 3.5$ J $mol^{-1}$ $K^{-1}$ for **3**, and $\Delta H° = 15.2 \pm 1.3$ kJ $mol^{-1}$ and $\Delta S° = 13.9 \pm 4.9$ J $mol^{-1}$ $K^{-1}$ for $\mathbf{3}^{+}$**)**. The positive value for the change in entropy in both of these cases is sensible; free lithium ions in MeCN solution are usually coordinated to four MeCN molecules in a tetrahedral fashion.[27] Binding lithium to **3** will therefore result in the net gain of two molecules in the system, increasing the entropy.

It is useful to compare the data obtained here with the complexation of $Li^{+}$ with 12-crown-4 ether in MeCN, which yields a 2:1 ligand:$Li^{+}$ complex. Formation of this complex is entropically disfavored by ~10 J $mol^{-1}$ $K^{-1}$.[28] We speculate that the negative entropy of the 12-crown-4 system is largely due to a loss of conformational flexibility of the 12-crown-4 ether upon complexation with $Li^{+}$. The ligands of **3** are already rigidly held by the $[Mo_2]^{4+}$ unit, eliminating this entropy sink.

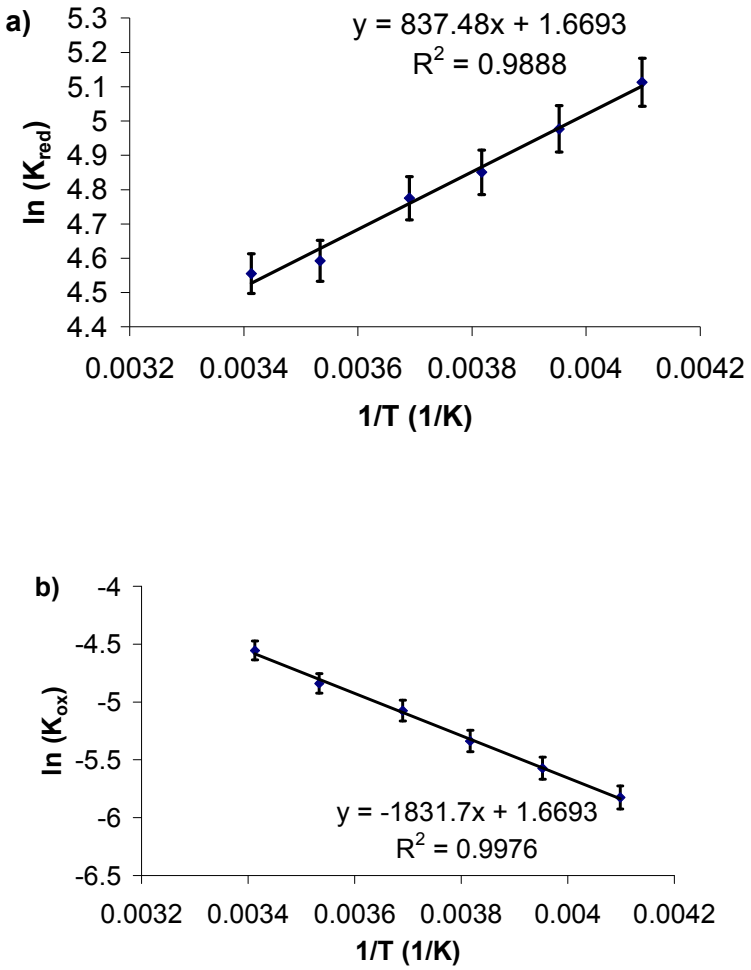


**Figure 3.7.** Van't Hoff Plots for the equilibrium between a) **2-MeCN** and **3** and b) **2-MeCN**$^+$ and **3**$^+$. Equilibrium constants were measured over a range of -29°C to 20°C.

Interestingly, the value of ΔH is negative for **3** but positive for **3**$^+$. In binding $Li^+$ to **3**, the compound is stabilized by the hard acid-hard base interaction of the four oxygen atoms and $Li^+$. When $Li^+$ binds to **3**$^+$ it is also stabilized by these same interactions, but it is destabilized to a greater degree by Coulombic repulsion between the increased charge of the $[Mo_2]^{4+}$ core and $Li^+$. This Coulombic repulsion proves to contribute more to the

overall enthalpy of the reaction than the stabilization by the Lewis acid/Lewis base interactions.

In comparison, the enthalpy of $Li^+$ binding to 12-crown-4 ether is more exothermic than $Li^+$ binding to **3** by about 17 kJ $mol^{-1}$.[28] The difference in enthalpy likely stems from the eight total Li-O bonds formed in complexation between 12-crown-4 ether and $Li^+$ as opposed to the four Li-O bonds formed when $Li^+$ binds to **3**.

### 3.4.6 DFT Calculations

The optimized bond distances and bond angles are shown in Table 3.5 and compared to the crystal structure values. For compound **1a**, the calculated structure accurately reproduces the crystal structure geometry. The calculated Mo≡Mo bond distance of 2.1077 Å only differs by 0.0035 Å from the crystal structure value of 2.1112(4) Å. The Mo≡Mo bond distance calculated here corresponds to a Mayer bond order of 3.3, slightly less than the idealized value of 4. The average Mo-N and Mo-S bond distances differ minimally from the crystal structure values. The calculated N-Mo-N bond angle is very close to the crystal structure value, but there is a more significant difference between the calculated S-Mo-S bond angle and the crystal structure value ($\Delta$(N-Mo-N) = 0.21°, $\Delta$(S-Mo-S) = 3.18°).

**Table 3.5.** Experimental and Calculated bond distances and angles for **1a** and **2-py**.

| | **1a exp** | **1a calc.** | **2-py exp** | **2-py calc.** |
|---|---|---|---|---|
| Mo-Mo (Å) | 2.1112(4) | 2.1077 | 2.1356(3) | 2.1664 |
| Mo-N avg. (Å) | 2.145[2] | 2.1325 | 2.119[2] | 2.1234 |
| Mo-S avg. (Å) | 2.4753[8] | 2.4965 | 2.5172[6] | 2.5192 |
| Mo-Li (Å) | - | - | 3.075(5) | 3.0430 |
| Mo-Cl (Å) | - | - | 2.6533(6) | 2.5066 |
| S-Mo-S avg. (°) | 168.30[2] | 165.16 | 169.60[5] | 172.56 |
| N-Mo-N avg. (°) | 168.19[6] | 168.40 | 166.7[1] | 163.92 |

For compound **2-py**, the calculated model adequately reproduces how the equatorial ligands bind to the $[Mo_2]^{4+}$ core as shown by how well the calculated Mo-N and Mo-S bond distances agree with the crystal structure values, but the axial $Mo_2$–Cl bond distance is significantly underestimated by ~0.15 Å. However, the potential energy surface (PES) for stretching the $Mo_2$–Cl bond (Figure 3.S1), indicates that elongating the $Mo_2$–Cl bond to the experimental value only increases the total energy by ~5 kJ/mol, which can be caused by crystal packing effects. It should be noted, though, that increasing the $Mo_2$–Cl distance to a "normal" value, above 2.8 Å, incurs a greater energetic penalty (> 14 kJ/mol ). Thus, the DFT results clearly indicate the stabilization of an unusually short Mo-Cl bond in **2-py**.

Single point calculations performed on the optimized structures of **1a** and **2-py** give insight into their electronic structures. MO diagrams based on the DFT results for the metal-metal bonding orbitals of **1a** and **2-py** are shown in Figure 3.8. The metal-metal bonding orbitals are the most important orbitals since they govern how these complexes interact with the axial $Li^+$ ion and $Cl^-$ ion. For **1a** the MO diagram shows a deviation from the predicted qualitative MO diagram shown in Chart 3.1 in that the Mo-Mo π bonding orbitals are lower in energy than the Mo-Mo σ bonding orbital, which is raised in energy due to antibonding interactions with the $SNO5^-$ ligand. As expected, the HOMO is a Mo-Mo δ bonding orbital, and the LUMO is a Mo-Mo δ antibonding orbital as predicted by the qualitative MO-diagram (Chart 3.1b).

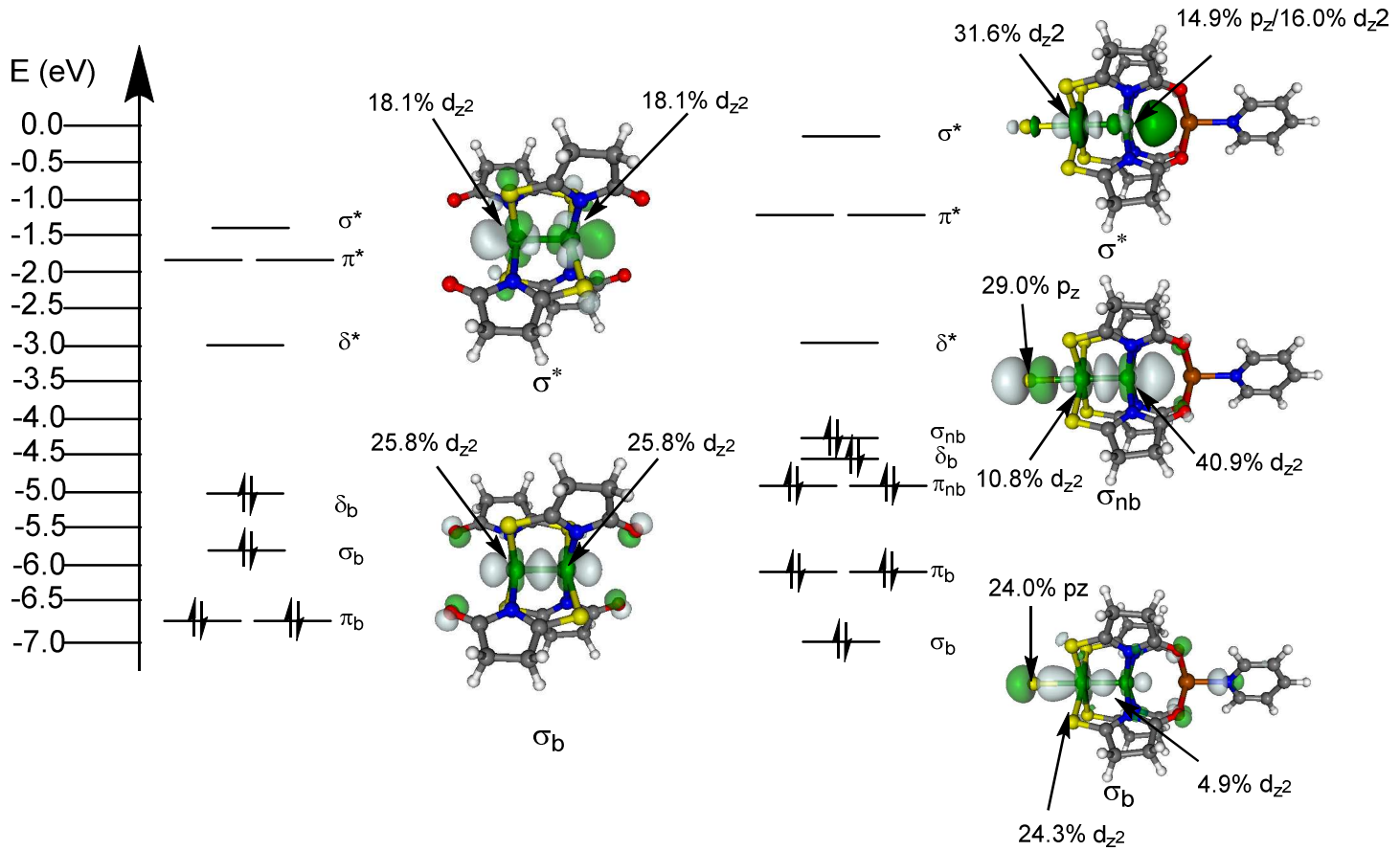


**Figure 3.8.** The MO diagrams of compounds **1a** and **2-py**. Only the orbitals with significant contributions from the Mo atoms are shown. The percent contribution of the major components of the σ-type orbitals are indicated next to the diagram of those orbitals

**Scheme 3.3.** The qualitative MO diagram illustrating the origin of the σ-type orbitals in **2-py**.

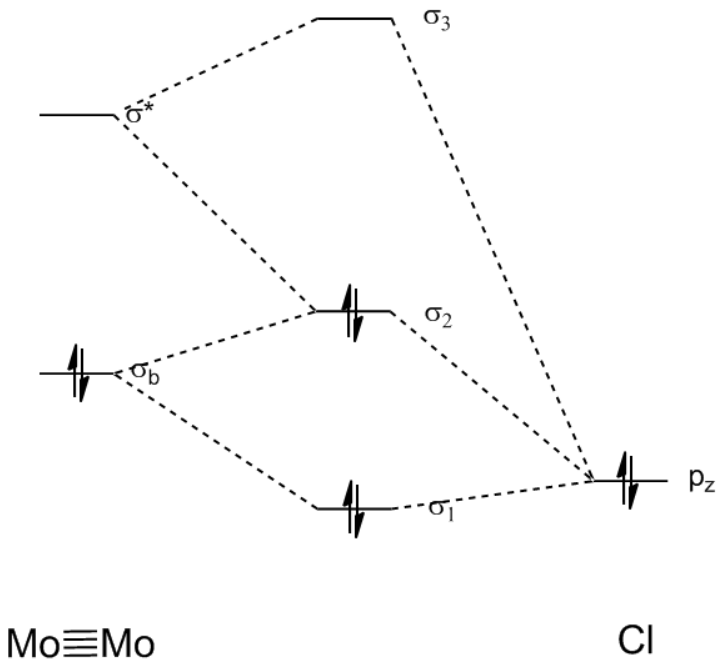


For compound **2-py**, the HOMO is a σ-type orbital ($\sigma_2$, Figure 3.8) rather than a δ-type orbital, which is a major deviation from the predicted qualitative MO diagram in Chart 3.1. The elevation of the $\sigma_2$ orbital to HOMO over the δ-type orbital results from the interaction of the $[Mo_2]^{4+}$ core with the axial $Cl^-$ as shown in Scheme 3.3. If we take the Mo-Mo-Cl vector to be the z axis, then the Cl $p_z$ lone pair orbital is energetically well situated to interact with the filled $[Mo_2]^{4+}$ σ orbital, with which it forms a bonding ($\sigma_1$) and antibonding ($\sigma_2$) combination. The $[Mo_2]^{4+}$ σ* orbital also mixes with the $Cl^-$ $p_z$ and $[Mo_2]^{4+}$ σ, yielding $\sigma_3$, which is antibonding with respect to both the Mo-Mo and the Mo-Cl interactions. Thus, the two Mo atoms and the $Cl^-$ ligand form something akin to a 3-

center 4-electron σ-bond. The $\sigma_2$ orbital is elevated in energy to become the HOMO, while the $\sigma_1$ orbital is brought down in energy by the interaction.

The most striking difference between the MO diagrams of compounds **1a** and **2-py** is shown in the polarization of the σ-type orbitals in **2-py** as compared with **1a**. In compound **1a**, each σ-type MO has a 50% contribution from each Mo atom. However, in **2-py**, the orbitals are not evenly distributed. In the $\sigma_1$ orbital, the MO is polarized 4.96:1 towards the Mo atom directly bound to the $Cl^-$, and in the $\sigma_2$ orbital, the MO is polarized 3.79:1 towards the Mo atom closest to $Li^+$. This polarization is due to the interaction of $Li^+$ and $Cl^-$ with $[Mo_2]^{4+}$ and, to a lesser extent, the 4,0 disposition of the $SNO5^-$ ligands, but the individual contribution of $Li^+$ cannot be determined by this MO diagram alone.

Geometry optimization and single point calculations were also performed on $[pyLiMo_2(SNO5)_4]^+$, which is **2-py** from which the $Cl^-$ ligand has been removed. The σ* and $\sigma_b$ orbitals are the primary orbitals with which a σ-type orbital on $Cl^-$ will interact when forming an axial $Mo_2$–Cl bond. In the σ* orbital shown in Figure 3.9, the orbital is polarized towards the open axial position by significant mixing of the Mo $5p_z$ orbital with the $4d_z2$ orbital of the exposed axial Mo atom. This polarization makes the σ* orbital much more available to interact with a $Cl^-$ σ-type orbital. In the $\sigma_b$ orbital, the polarization is less pronounced since it is too low in energy to mix with the $5p_z$ orbital. As a result of the polarization of these orbitals, the $Cl^-$ ligand forms a much stronger bond with the $[Mo_2]^{4+}$ core of **2-py** than in unactivated $[Mo_2]^{4+}$ complexes.

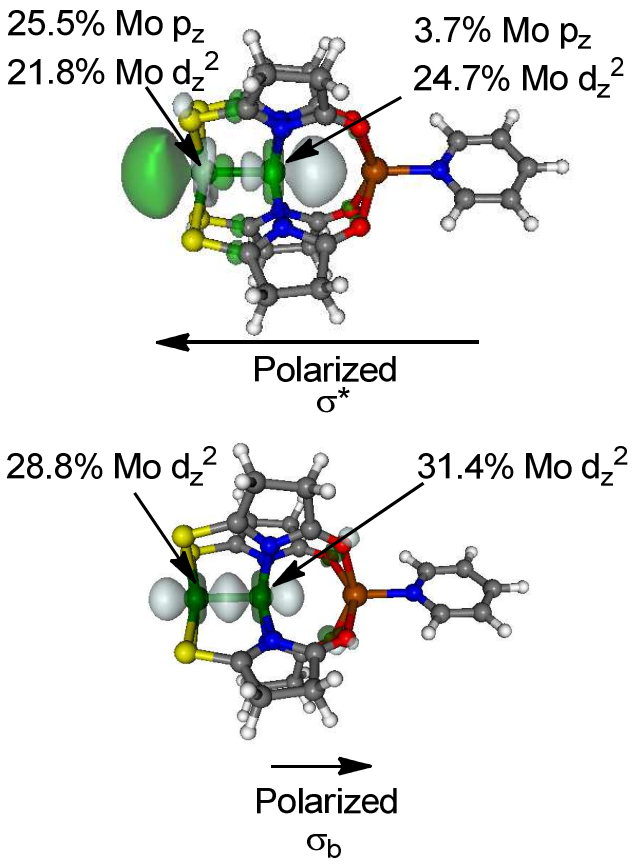


**Figure 3.9**. The σ* and $\sigma_b$ orbitals of $[pyLiMo_2(SNO5)_4]^+$ showing the polarization caused by the presence of $Li^+$.

### 3.5 Conclusions

Cationic lithium has been successfully shown by X-ray crystallography to activate an axial site of a dimolybdenum complex. The activated compound was shown to thermodynamically favor $Li^+$ binding, which is reversible in coordinating solvents. DFT calculations on these compounds gave geometries in close agreement with experiment, and they provided an electronic explanation for the increased affinity of $[Mo_2]^{4+}$ for the axial $Cl^-$ ligand in a Lewis acid activated complex. The Lewis acid activation results from a polarization of the molecular orbitals and a subsequent strengthening of the $Mo_2$–Cl

bond as evidenced by the X-ray crystal data and DFT calculations. Based on the data shown here, it is possible that these compounds could also find utility as $Li^+$ ion sensors.

## 3.6 Acknowledgements

The authors wish to acknowledge financial support from the National Science Foundation under CHE-0745500, CHE-9208463 (Bruker AC 360), CHE-0840494 (computational facilities) and a generous bequest from Paul J. Bender (Bruker Avance 500).

## 3.7 Supporting Information

### 3.7.1 Potential Energy Surface of 2-py

The $Mo_2$–Cl distance is the widest discrepancy between the experimental and calculated structures for compound **2-py**. Single point calculations were performed on the molecule with varying fixed $Mo_2$–Cl distances between 2.40 Å and 2.80 Å, yielding a one-dimensional potential energy surface for the complex. The final single point energies of these structures are shown in Figure 3.9. The potential energy surface is very shallow over this range of $Mo_2$–Cl distances. The difference in the calculated energies between the optimized structure and the experimental structure is 4.81 kJ/mol. Based on this potential energy surface, the calculated structure matches the experimental structure within error.

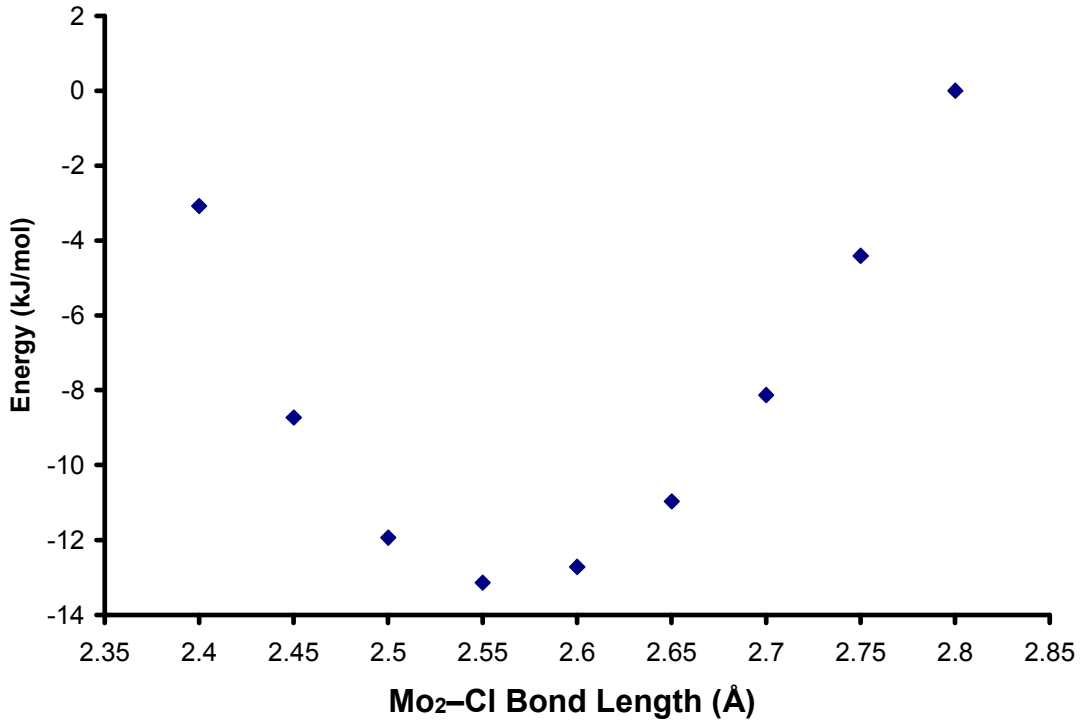


**Figure 3.S1**. The one-dimensional potential energy surface of **2a** along the Mo-Cl bond length dimension. The $Mo_2$-Cl bond length of 2.80 Å was chosen to be the zero point for the energy scale.

### 3.8 References

1. *Multiple Bonds Between Metal Atoms, 3rd edition.* Cotton, F. A.; Murillo, C. A.; Walton, R. A., Eds.; Springer Science and Business Media: New York, 2005.

2. (a) Kornecki, K. P.; Berry, J. F.; Powers, D. C.; Ritter, T. Metal-Metal Bond-Containing Complexes as Catalysts for C–H Functionalization. In *Prog. Inorg. Chem.* Karlin, K. D., Ed. 2014; Vo. 58, pp 225. (b) Berry, J. F.; *Dalton Trans.* **2012**, *41*, 700. (c) Davies, H. M. L.; Manning, J. R. *Nature*, **2008**, *451*, 417. (d) DuBois, J. *Org. Proc. Res. Dev.* **2011**, *15*, 758. (e) Doyle, M. P.; Duffy, R.; Ratnikov, M.; Zhou, L. *Chem. Rev.*

**2010**, *110*, 704. (f) Powers, D. C.; Ritter, T. *Acc. Chem. Res.* **2012**, *45*, 840. (g) Villalobos, L.; Cao, Z.; Fanwick, P. E.; Ren, T. *Dalton Trans.* **2012**, *41*, 644. (h) Teets, T. S.; Nocera, D. G. *Chem. Commun.* **2011**, *47*, 9268.

3. (a) Chisholm, M. H. *Macromol. Chem. Phys.* **2012**, *213*, 800. (b) Chisholm, M. H.; Lear, B. J.; *Chem. Soc. Rev.* **2011**, *40*, 5254. (c) Alberding, B. G.; Chisholm, M. H.; Gallucii, J. C.; Ghosh, Y.; Gustafson, T. L. *Proc. Nat. Acad. Sci. U.S.A.* **2011**, *108*, 8152. (d) Bradley, P. M.; Fu, P. K.-L.; Turro, C. *Comments Inorg. Chem.* **2001**, *22*, 393.

4. (a) Chisholm, M. H. in *Structure and Bonding*, Parkin, G., Ed. Vol. 136, 29, (2010). (b) Chisholm, M. H.; Patmore, N. S. *Acc. Chem. Res.* **2007**, *40*, 19. (c) Berry, J. F. in *Structure and Bonding*, Parkin, G., Ed. Vol. 136, 1, (2010). (d) Mohan, P. J.; Georgiev, V. P.; McGrady, J. E. *Chem. Sci.* **2012**, *3*, 1319. (e) Manni, G. L.; Dzubak, A.; Mulla, A.; Brogden, D. W.; Berry, J. F.; Gagliardi, L. *Chem. Eur. J.* **2012**, *18*, 1737.

5. (a) Chisholm, M. H.; Macintosh, A. M. *Chem. Rev.* **2005**, *105*, 2949. (b) Cotton, F. A.; Lin, C.; Murillo, C. A. *Acc. Chem. Res.* **2001**, *34*, 759. (c) Filatov, A. S.; Napier, M.; Vreshch, V. D.; Sumner, N. J.; Dikarev, E. V.; Petrukhina, M. A. *Inorg. Chem.* **2012**, *51*, 566. (d) Filatov, A. S.; Petrukhina, M. A. *Coord. Chem. Rev.* **2010**, *254*, 2234.

6. (a) Nippe, M.; Timmer, G. H.; Berry, J. F. *Chem. Commun.* **2009**, 4357. (b) Nippe, M.; Victor, E.; Berry, J. F. *Inorg. Chem.* **2009**, *48*, 11889. (c) Long, A. K. M.; Yu, R. P.; Timmer, G. H.; Berry, J. F. *J. Am. Chem. Soc.* **2010**, *132*, 12228. (d) Nippe, M.; Goodman, S. M.; Fry, C. G.; Berry, J. F. *J. Am. Chem. Soc.* **2011**, *133*, 2856. (e) Long, A. K. M.; Timmer, G. H.; Pap, J. S.; Snyder, J. L.; Yu, R. P.; Berry, J. F. *J. Am. Chem. Soc.* **2011**, *133*, 13138. (f) Nippe, M.; Turov, Y.; Berry, J. F. *Inorg. Chem.* **2011**, *50*, 10592.

(g) Turov, Y.; Berry, J. F. *Dalton Trans.* **2012**, *41*, 8153. (h) Timmer, G. H.; Berry, J. F. *Chem. Sci.* **2012**, *3*, 3038.

7. (a) Cotton, F. A.; Ilsley, W. H.; Kaim, W. *Inorg. Chem.* **1980**, *19*, 3586. (b) Cotton, F. A.; Favello, L. R.; Han, S.; Wang, W. *Inorg. Chem.* **1983**, *22*, 4106. (c) Cayton, R. H.; Chisholm, M. H.; Huffman, J. C.; Lobkovsky, E. B. *J. Am. Chem. Soc.* **1991**, *113*, 8709. (d) Pimblett, G.; Garner, C. D.; *J. Chem. Soc. Dalton Trans.* **1986**, 1257. (e) Clegg, W.; Pimblett, G.; Garner, C. D. *Polyhedron*, **1986**, *5*, 31. (f) Cotton, F. A.; Reid, A. H. Jr.; Schwotzer, W. *Inorg. Chem.* **1985**, *24*, 3965. (g) Cotton, F. A.; Kühn F. E. *Inorg. Chim. Acta.* **1996**, *252*, 257. (h) Cotton, F. A.; Daniels, L. M.; Murillo, C. A.; Wang, X *Polyhedron*, **1998**, *17*, 2781. (i) Day, E. F.; Huffman, J. C.; Folting, K.; Christou, G. *J. Chem. Soc. Dalton Trans.* **1997**, 2837. (j) Cotton, F. A.; Wiesinger, K. J. *Inorg. Chem.* **1991**, *30*, 871. (k) Xue, W.-M.; Kühn, F. E.; Zhang, G.; Herdtweck, E.; Raudaschl-Sieber, G. *J. Chem. Soc*. *Dalton Trans.* **1999**, 4103. (l) Kuang, S-M.; Fenwick, P. E.; Walton, R. A. *Inorg. Chim. Acta*. **2000**, *305*, 102.

8. (a) Robbins, G. A.; Martin, D. S. *Inorg. Chem.* **1984**, *23*, 2086. (b) Wu, Y.-Y.; Chen, J.-D.; Liou, L.-S.; Wang, J.-C. *Inorg. Chim. Acta.* **1997**, *258*, 193. (c) Suen, M.-W.; Tseng, G.-W.; Chen, J.-D.; Keng, T.-C.; Wang, J.-C. *Chem Comm.* **1999**, 1185. (d) Udovic, B.; Leban, I.; Segedin, P. *Croat. Chim. Acta.* **1999**, *72*, 477. (e) Yi, J.; Miyabayashi, T.; Ohashi, M.; Yamagata, T.; Mashima, K. *Inorg. Chem.* **2004**, *43*, 6596. (f) Arnold, D. I.; Cotton, F. A.; Kühn, F. E. *Inorg. Chem.* **1996**, *35*, 4733. (g) Nippe, M. N.; Bill, E.; Berry, J. F. *Inorg. Chem.* **2011**, *50*, 7650. (h) Nippe, M.; Victor, E.; Berry, J. F. *Eur. J. Inorg. Chem.* **2008**, *47*, 5569. (i) Cotton, F. A.; Fanwick, P. E. *Inorg. Chem.* **1983**, *22*, 1327.

9. Cotton, F. A.; Mester, Z. C.; Webb, T. R. *Acta Cryst*. **1970**, *B30*, 2768.

10. (a) Gabbaï, F. P.; Schier, A.; Riede, J.; Sladek, A.; Görlitzer, H. W. *Inorg. Chem.* **1997**, *36*, 5694. (b) Wade, C. R.; Lin, T.-P.; Nelson, R. C.; Mader, E. A.; Miller, J. T.; Gabbaï, F. P. *J. Am. Chem. Soc.* **2011**, *133*, 8948. (c) Lin, T.-P.; Nelson, R. C.; Wu, T.; Miller, J. T.; Gabbaï, F. P. *Chem. Sci.* **2012**, *3*, 1128.

11. (a) Greenwood, B. P.; Forman, S. I.; Rowe, G. T.; Chen, C.-H.; Foxman, B. M.; Thomas, C. M. *Inorg. Chem.* **2009**, *48*, 6251. (b) Krogman, J. P.; Foxman, B. M.; Thomas, C. M. *J. Am. Chem. Soc.* **2011**, *133*, 14582.

12. (a) Ferguson, G. S.; Wolczanski, P. T. *Organometallics* **1985**, *4*, 1601. (b) Ferguson, G. S.; Wolczanski, P. T. *J. Am. Chem. Soc.* **1986**, *108*, 8293. (c) Ferguson, G. S.; Wolczanski, P. T.; Párkányi, M. C.; Zonnevyille, M. C. *Organometallics*, **1988**, *7*, 1967. (d) Baxter, S. M.; Ferguson, G. S.; Wolczanski, P. T. *J. Am. Chem. Soc.* **1988**, *110*, 4231.

13. (a) Nagashima, H.; Sue, T.; Oda, T.; Kanemitsu, A.; Matsumoto, T.; Motoyama, Y.; Sunada, Y. *Organometallics* **2006**, *25*, 1987. (b) Sunada, Y.; Sue, T.; Matsumoto, T.; Nagashima, H. *J. Organomet. Chem.* **2006**, *691*, 3176. (c) Sue, T.; Sunada, Y.; Nagashima, H. *Eur. J. Inorg. Chem.* **2007**, 2897. (d) Tsutsumi, H.; Sunada, Y.; Shiota, Y. Yoshizawa, K.; Nagashima, H. *Organometallics* **2009**, *28*, 1988.

14. Zhou, H.-C.; Abbaoui, B.; Scott, T. A. *Inorg. Chem.* **2004**, *43*, 2459.

15. Holste, G. and Schäfer, H. *Z. anorg. allg. Chem.* **1972**, *391*, 263.

16. Cotton, F. A.; Norman, G. J. *J. Coord. Chem.* **1971**, *1*, 161.

17. Berg, U.; Sandström, J. *Acta Chemica Scandinavica*. **1966**, *20*, 689.

18. Zhu, X.; Giordano, T.; Yu, Q. -S.; Holloway, H. W.; Perry, T. A.; Lahiri, D. K.; Brossi, A.; Greig, N. H. *J. Med. Chem.* **2003**, *46*, 5222.

19. APEX-II; Bruker-AXS: Madison, WI.

20. Flack, H. D. *Acta Crystallogr.* **1983**, *A39*, 876.

21. (a) Neese, F. *ORCA-an ab inito DFT and Semi-empirical Electronic Structure Package*, version 2.8.0; University of Bonn: Germany, 2010. (b) Perdew, J. P. *Phys. Rev. B: Condens. Matter*. **1986**, *33*, 8822. (c) Becke, A. D. *Phys. Rev. A: At. Mol. Opt. 38*, **1988**, 3098.

22. Weigend, F.; Ahlrichs, R. *Phys. Chem. Chem. Phys.* **2005**, *7*, 3297.

23. Crystals of $LiMo_2(SNO6)_4Cl$ were obtained, and the linear Li···Mo≡Mo structure was determined by crystallographic characterization. Crystallographic data are: *monoclinic*, *Cc*, *a* = 14.9958(5) Å, *b* = 11.1604(4) Å, *c* = 18.4996(7) Å, β = 108.995(2)°, *V* = 2927.5(2) $Å^3$. The Mo≡Mo and $Mo_2$–Cl distances are 2.135(1) Å and 2.715(2) Å, respectively.

24. (a) Cotton, F. A.; Niswander, R. H., Sekutowski, J. C. *Inorg. Chem.* **1979**, *18*, 1149. (b) Ambrosius, H. P. M. M.; Cotton, F. A.; Falvello, L. R.; Hintzen, H. T. J. M.; Melton, T. J.; Schwotzer, W.; Tomas, M.; van der Linden, J. G. M. *Inorg. Chem.* **1984**, *23*, 1611. (c) Fanwick, P. E.; Qi, J.-S.; Wu, Y.-P.; Walton, R. A. *Inorg. Chim. Acta*. **1990**, *168*, 159. (d) Sheldrick, W. S.; Mintert, M. *Inorg. Chim. Acta.* **1994**, *219*, 23. (e) Hicks, J.; Ring, S. P.; Patmore, N. J. *Dalton Trans.* **2012**, *41*, 6641.

25. (a) Bailey, P. J.; Bone, S. F.; Mitchell, L. A.; Parsons, S.; Taylor, K. J.; Yellowlees, L. J. *Inorg. Chem.* **1997**, *36*, 867. (b) Bailey, P. J.; Bone, S. F.; Mitchell, L. A.; Parsons, S.; Taylor, K. J.; Yellowlees, L. J. *Inorg. Chem.* **1997**, 5420. (c) Cotton, F. A.; Daniels, L. M.; Hillard, E. A.; Murillo, C. A. *Inorg. Chem.* **2002**, *41*, 1639. (d) Lin, C.; Protasiewicz, J. D.; Smith, E. T.; Ren, T. *Inorg. Chem.* **1996**, *35*, 6422. (e) Cotton, F. A.; Daniels, L.

M.; Murillo, C. A.; Timmons, D. J.; Wilkinson, C. C. *J. Am. Chem. Soc.* **2002**, *124*, 9249. (f) Chisholm, M. H.; D'Acchioli, J. S.; Pate, B. D.; Patmore, N. J.; Dalal N. S.; Zipse, D. J. *Inorg. Chem.* **2005**, *44*, 1061. (g) Nippe, M.; Victor, E.; Berry, J. F. *Inorg Chem.* **2009**, *48*, 11889.

26. (a) Fukuzumi S.; Ohkubo, K. *Coord. Chem. Rev.* **2010**, *254*, 372. (b) Fukuzumi, S.; Ohkubo, K.; Morimoto, Y. *Phys. Chem. Chem. Phys.* **2012**, *14*, 8472.

27. (a) Yokota, Y.; Young Jr., V. G.; Verkade, J. G. *Acta Crystallogr.* **1999**, *C55*, 196. (b) Seo, D. M.; Boyle, P. D.; Henderson, W. A. *Acta Crystallogr.* **2011**, *E67*, m1148.

28. Danil de Namor, A. F.; Ng, J. C. Y.; Tanco, M. A. L.; Salomon, M. *J. Phys. Chem.* **1996**, *100*, 14485.

# Chapter 4

*Influence of Lewis Acid Charge and Proximity in Mo≡Mo···M Linear Chain Compounds with M = $Na^{+}$, $Ca^{2+}$, $Sr^{2+}$, and $Y^{3+}$*



## 4.1 Abstract

The syntheses, X-ray structural characterizations, and electrochemical properties of four new paddlewheel $[MMo_2(SNO5)_4Cl]^{n-1+}$ ($M^{n+}$ = $Na^{+}$, $Ca^{2+}$, $Sr^{2+}$, $Y^{3+}$; HSNO5 = monothiosuccinimide) compounds are described here. By changing the $M^{n+}$ cation charge and size, we demonstrate a method for easily tuning the Lewis acidity of the Mo≡Mo quadruple bond and the $[Mo_2]^{4+/5+}$ redox potential. As the charge of the $M^{n+}$ cation is increased, the distal Mo atom becomes slightly more Lewis acidic, leading to a shorter $Mo_2$–Cl bond distance, and the $[Mo_2]^{4+/5+}$ redox couple becomes less accessible. As the $M^{n+}$···$Mo_2$ distance is increased, the distal Mo atom becomes less Lewis acidic, leading to a longer $Mo_2$–Cl bond distance.

## 4.2 Introduction

The chemistry of quadruply bonded $[Mo_2]^{4+}$ compounds has been studied for the past 50 years, and now it is a mature field.[1] Much of the current work in the field has focused on electronic and photophysical properties,[2] reactivity,[3] redox chemistry,[4] and the use of $[Mo_2]^{4+}$ units as building blocks in the synthesis of novel heterometallic compounds and supramolecular architectures.[5] The stability of the Mo≡Mo quadruple bond makes these compounds particularly robust and versatile.

Despite a wealth of chemistry based on equatorial ligand substitutions, $[Mo_2]^{4+}$ complexes are not nearly as keen to bind ligands in the axial sites. For example, $[Mo_2]^{4+}$ tetracarboxylates bind terminal chloride ions at distances ranging from 2.84 – 2.89 Å,[6] significantly longer (by ≥ 0.3 Å!) than the equatorial terminal Mo–Cl distances in the $[Mo_2Cl_8]^{2-}$ ion.[7] This attenuated axial Lewis acidity of $[Mo_2]^{4+}$ complexes contrasts meaningfully with the strong Lewis acidity of the analogous $[Rh_2]^{4+}$ compounds. The unparalleled catalytic behavior of $[Rh_2]^{4+}$ compounds may be attributed to this Lewis acidity,[8] which is instrumental in the stabilization of key intermediates in catalysis.[8c,9] A major goal in the chemistry of metal-metal multiple bonds would be to engender complexes of the cheap, Earth abundant metal Mo possessing some of the chemical behavior more characteristic of Rh.

A topic of recent interest in coordination chemistry has been the effect of hard, redox-inactive, Lewis acidic main group metal ions on the chemical properties of transition metal complexes.[10] We hypothesized that a closely bound redox-inactive metal ion might increase the Lewis acidity of a quadruply-bonded $[Mo_2]^{4+}$ unit. With this idea in mind, we designed the heterotrimetallic $[Mo_2]^{4+}$ compound $pyLiMo_2(SNO5)_4Cl$ (**1**, $SNO5^-$ = monothiosuccinimidate, see Scheme 4.1), in which Lewis acidic $Li^+$ is held in the axial position of a $[Mo_2]^{4+}$ unit.[5c] The $Li^+$ ion serves to polarize the Mo≡Mo bond, increasing the Lewis acidity of the distal Mo atom and strengthening the $Mo_2$–Cl axial bond. The synthesis of **1** is facilitated by the ambidentate nature of the $SNO5^-$ ligand. The hard O donor atom preferentially binds to the hard acid $Li^+$ and the soft S donor atom preferentially binds to the soft acid Mo, allowing **1** to self-assemble from a mixture of $Mo_2(OAc)_4$, HSNO5, and LiCl (Scheme 4.1).[5c] The ease with which **1** is synthesized

suggests that the ambidentate nature of $SNO5^-$ can be harnessed to synthesize a variety of $M\cdots Mo_2$ heterotrimetallic chain compounds.

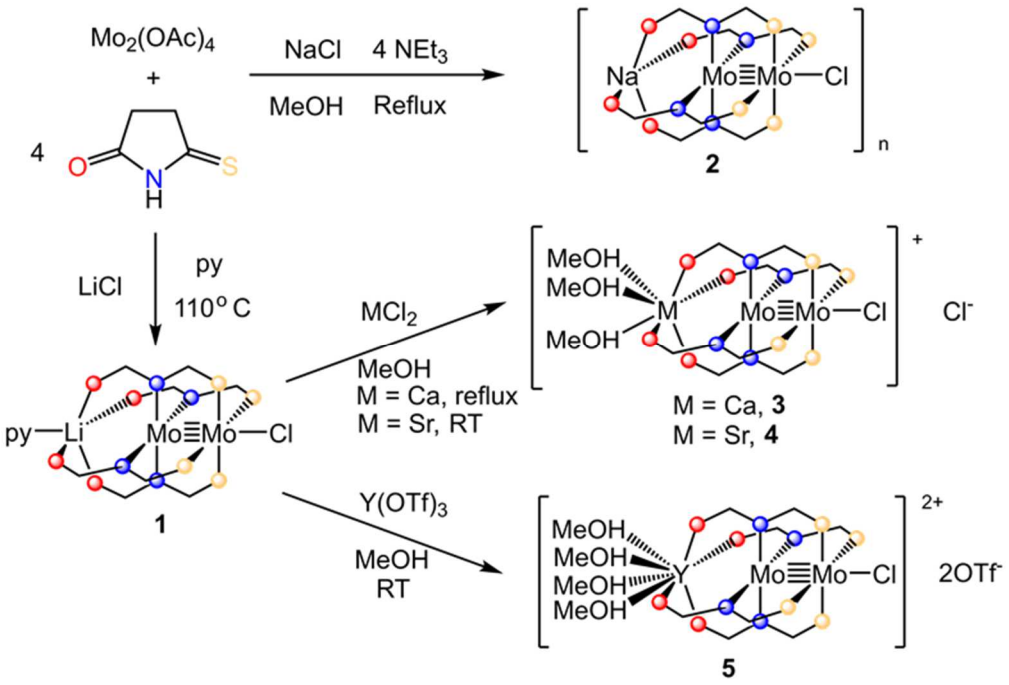


**Scheme 4.1.** Synthetic routes to compounds **1** – **5**.

Herein, we describe the syntheses, X-ray structural characterization, and electrochemistry of four new $M\cdots Mo_2$ compounds ($M = Na^+$, $Ca^{2+}$, $Sr^{2+}$, $Y^{3+}$). The syntheses of these new compounds greatly expand the scope of $M\cdots Mo_2$ heterotrimetallic compounds known and shows that the $[Mo_2(SNO5)_4Cl]^-$ system can be generalized to interact with Lewis acids over a range of sizes and charges. Through the structural and electrochemical characterization of these compounds, the effect that cation charge and cation size have on the Lewis acidity and electronic properties of the $[Mo_2]^{4+}$ unit is probed.

## 4.3 Experimental

### 4.3.1 General

All synthetic work was carried out under an inert atmosphere using standard Schlenk and glovebox techniques. All solvents were rigorously dried prior to use. THF, MeCN, hexanes, and $Et_2O$ were dried over molecular sieves and subsequently dried using a Vacuum Atmospheres solvent purification system and degassed prior to use. Pyridine was dried over molecular sieves, distilled from barium oxide under $N_2$, and stored in an inert atmosphere glovebox prior to use. MeOH was dried sequentially over molecular sieves and $Mg/Mg(OMe)_2$. It was then distilled under $N_2$ immediately prior to use. Propylene carbonate was purchased in anhydrous form from Sigma Aldrich and further dried by stirring over CaO for 72 hours. It was then distilled under vacuum and stored in the glovebox prior to use. Monothiosuccinimide (HSNO5) was synthesized from succinimide and $P_4S_{10}$.[11] Molybdenum acetate ($Mo_2(OAc)_4$) was synthesized from $Mo(CO)_6$, acetic acid, and acetic anhydride.[12] **1**·py was synthesized from $Mo_2(OAc)_4$, HSNO5, and LiCl.[5c] All other reagents were purchased from Sigma-Aldrich and used without further purification. Elemental analyses were carried out by Midwest Microlabs in Indianapolis, IN, USA. NMR Spectroscopy was performed on a Bruker AC 300 MHz spectrometer or Bruker Avance III 500 MHz Spectrometer. FTIR (ATR) data were obtained using a Bruker TENSOR 27 spectrometer.

### 4.3.2 Syntheses

***poly*-Sodiumdimolybdenum-chlorotetrakis(monothiosuccinimidato) $(NaMo_2(SNO5)_4Cl)_n$ (2)**

A 100 mL Schlenk flask was charged with 138 mg HSNO5 (1.20 mmol), 440 mg NaCl (7.5 mmol), and 60 mL MeOH. To the resulting suspension was added 190 μL $NEt_3$ (1.36 mmol), and the mixture was stirred at 60 ° C to until the NaCl had fully dissolved. This solution was then transferred *via* cannula to a flask containing 127 mg $Mo_2(OAc)_4$ (0.297 mmol). The reaction mixture became an orange color, and there was a slow precipitation of orange-brown solid over a period of 5 minutes. The reaction mixture was heated at 70 ° C overnight. Then, the reaction mixture was cooled to room temperature, filtered, and the solid was washed with 2 x 25 mL MeOH and 2 x 25 mL DCM. The remaining solid was extracted with 15 mL pyridine and layered with hexanes, yielding small crystals of **2**. The crystals were collected, washed with 3 x 30 mL hexanes, and dried under vacuum. Yield: 56 mg (27 %). Anal. Calc. for $C_{18.5}H_{18.5}N_{4.5}O_4S_4Mo_2NaCl$ (**2**·0.5 $C_5H_5N$) C: 29.77 %, H 2.50%, N: 8.44%, Found C: 29.81%, H: 2.64%, N: 7.81%. $^1$H NMR (500 MHz, DMSO-d6) δ 3.53 (br, 8H, S=CC*H*$_2$CH$_2$C=O), 2.77 (m, 8H, S=CCH$_2$C*H*$_2$C=O). IR (ATR, cm$^{-1}$) 1728 (s), 1437 (m), 1457 (m), 1396 (s), 1240 (w), 1193 (vs), 1115 (w), 1050 (w), 911 (m), 806 (m), 667 (s).

**tris-methanol-calciumdimolybdenumchloro-tetrakis(monothiosuccinimidato) chloride $[(MeOH)_3CaMo_2(SNO5)_4Cl][Cl]$ (3)**

A 50 mL flask was charged with 164 mg **1**·py (0.193 mmol), 700 mg $CaCl_2$ (6.31 mmol), and 20 mL MeOH. The reaction mixture was heated with stirring at 70 ° C for 5 hours. The mixture was filtered, and the filtrate was collected. After standing overnight,

crystals of (**3**) formed. These crystals were filtered and washed with 2 x 10 mL MeOH. The solid was then dried under vacuum and collected. Yield: 65 mg (39 %). Anal. Calc. for $C_{19}H_{28}N_4S_4O_7Mo_2CaCl_2$ C: 26.67%, H: 3.30%, N: 6.55%, Found C: 27.16%, H: 2.60%, N: 7.12%. $^1$H NMR (300 MHz, DMSO-d$^6$) δ 3.49 (m, 8H, S=CC*H*$_2$CH$_2$C=O), 3.15 (s, C*H*$_3$OH), 2.73 (m, 8H, S=CCH$_2$C*H*$_2$C=O) ppm. IR (ATR, cm$^{-1}$) 1723 (vs) 1654 (vw), 1388 (m) 1270 (vs), 1248 (vs) 1230 (vs) 1026 (w), 679 (w).

**tris-methanol-strontiumdimolybdenumchloro-tetrakis(monothiosuccinimidato) chloride [(MeOH)$_3$SrMo$_2$(SNO5)$_4$Cl][Cl] (4)**

Analogously to the synthesis of **3**, A 100 mL Schlenk flask was charged with 173 mg **1**·py (0.204 mmol) and 1.9 g $SrCl_2$ (12 mmol). These were dissolved in MeOH at room temperature and stirred overnight resulting in the production of an orange precipitate. The solid was collected by filtration and washed with 2 x 25 mL $Et_2O$. Yield: 46 mg (25%). X-ray quality crystals could be obtained from concentration of the red-orange filtrate to 5 mL. $^1$H NMR (DMSO-d$^6$) δ 3.51 (m, 8H, S=CC*H*$_2$CH$_2$C=O), 3.17 (s, C*H*$_3$OH), 3.15 (s, C*H*$_3$OH), 2.74 (m, 8H, S=CCH$_2$C*H*$_2$C=O), IR (ATR, cm$^{-1}$) 1716 (s), 1611 (vw), 1429 (w), 1385 (m), 1260 (vs), 1238 (vs), 1222 (vs), 1101 (m, br), 804 (w), 681 (m).

**tetrakis-methanol-yttriumdimolybdenum-chloro-tetrakis-monothiosuccinimidato bis-triflate [(MeOH)$_4$YMo$_2$(SNO5)$_4$Cl][OTf]$_2$ (5)**

A flask was charged with 1.32 g Y(OTf)$_3$ (2.46 mmol) and 199 mg **1**·py (0.234 mmol). These were dissolved in 10 mL of MeOH. The reaction mixture was stirred at room temperature overnight. Then the reaction mixture was filtered and layered with 80 mL $Et_2O$. Within a week, X-ray quality crystals of (**5**) grew. The crystals were collected

by filtration, washed with 3 x 50 mL $Et_2O$, and dried under vacuum. Yield: 140 mg (50 %). Anal. Calc. for $C_{22.15}H_{32}N_4S_{6.15}O_{14.45}F_{6.45}YMo_2Cl_{0.85}$ (0.85·**5** + 0.15·$[(MeOH)_4YMo_2(SNO5)_4][OTf]_3$, C: 21.88%, H: 2.65%, N: 4.61%, Found C: 21.43%, H: 2.65%, N: 4.45%. $^1$H NMR (500 MHz, DMSO-d6) δ 3.49 (m, 8H, S=CC*H*$_2$CH$_2$C=O), 3.17 (s, C*H*$_3$OH), 3.15 (s, C*H*$_3$OH), 2.74 (m, 8H, S=CCH$_2$C*H*$_2$C=O). IR (ATR, cm$^{-1}$) 1696 (m), 1657 (w), 1405 (m), 1394 (m), 1382 (m), 1290 (s), 1258 (vs), 1225 (s), 1166 (w), 1066 (s), 1028 (vs), 880 (w), 802 (w), 761 (vw), 698 (m), 637 (s).

**4.3.3 X-ray crystallography**

Single crystals of **2**·4 py, **3**·2 MeOH, **3-dim**·5.5 MeCN, **4**·2 MeOH and **5**·1.6MeOH were selected under paratone oil and attached to a MiTeGen MicroMount. They were mounted in a stream of cold $N_2$ at 100(1) K using an Oxford Cryostat and centered in the X-ray beam using a video monitoring system. The crystal evaluation and data collection were performed on a Bruker Quazar APEX-II diffractometer with Mo Kα radiation (λ = 0.71073 Å). The data were collected using a routine to survey an entire sphere of reciprocal space. The data were integrated using the SAINT routine in APEX-II and corrected for absorption using SADABS.[13] The structures were solved *via* direct methods and refined by iterative cycles of least-squares refinement on $F^2$ followed by difference Fourier synthesis using SHELX2013.[14] All non-hydrogen atoms were refined anisotropically except where noted below. The alcohol hydrogen atoms on MeOH components of structures **3**·2MeOH, **4**·2MeOH, and **5**·1.6MeOH were located from the Fourier difference map and refined independently. All other hydrogen atoms were included in the final structure factor calculation at idealized positions and were allowed to ride on the neighboring atoms with relative isotropic displacement coefficients.

**Table 4.1.** X-ray experimental data for structures **2-5**

| Compound | **2**·4py | **3**·2MeOH | **3-dim**·5.5$CH_3CN$ | **4**·2MeOH | **5**·1.6MeOH |
|---|---|---|---|---|---|
| Empirical formula | $C_{36}H_{36}ClMo_2N_8NaO_4S_4$ | $[C_{19}H_{30}N_4O_7S_4ClCaMo_2]Cl{\cdot}2(CH_3OH)$ | $C_{32}H_{32}Ca_2Cl_4Mo_4N_8O_8S_8{\cdot}5.5(CH_3CN)$ | $[C_{19}H_{30}N_4O_7S_4ClSrMo_2]Cl{\cdot}2(CH_3OH)$ | $C_{20}H_{32}Cl_{0.85}Mo_2N_4O_8S_4Y[CF_3SO_3]_{2.15}{\cdot}1.6(CH_3OH)$ |
| Formula weight | 1023.29 | 919.64 | 1773.08 | 967.18 | 1260.11 |
| Temperature/K | 100.0 | 100.0 | 100.0 | 100.0 | 100.0 |
| Crystal system | Tetragonal | Orthorhombic | Orthorhombic | Orthorhombic | Monoclinic |
| Space group | *P*4/*ncc* | *Pbca* | *Pnma* | *Pbca* | $P2_1/c$ |
| a/Å | 13.402(4) | 19.139(7) | 26.379(9) | 19.1231(9) | 12.156(4) |
| b/Å | 13.402(4) | 14.502(5) | 16.334(6) | 14.5719(7) | 14.561(5) |
| c/Å | 22.289(6) | 24.573(8) | 15.656(6) | 24.850(1) | 25.45(1) |
| β/° | 90 | 90 | 90 | 90 | 102.61(1) |
| Volume/$Å^3$ | 4003(3) | 6821(4) | 6746(4) | 6924.7(6) | 4396(3) |
| Z | 4 | 8 | 4 | 8 | 4 |
| $\rho_{calc}$ mg/$mm^3$ | 1.698 | 1.791 | 1.746 | 1.855 | 1.904 |
| μ/$mm^{-1}$ | 0.964 | 1.338 | 1.342 | 2.694 | 2.308 |
| F(000) | 2064.0 | 3712.0 | 3534.0 | 3856.0 | 2509.0 |
| Radiation | MoKα (λ = 0.71073) | MoKα (λ = 0.71073) | MoKα (λ = 0.71073) | MoKα (λ = 0.71073) | MoKα (λ = 0.71073) |
| 2Θ range for data collection | 3.654 to 64.276° | 3.314 to 55.23 | 3.024 to 54.798 | 3.278 to 52.804 | 3.242 to 52.878 |
| Independent reflections | 3527 | 7917 | 7924 | 7089 | 8995 |
| *R*(int) | 0.0314 | 0.0786 | 0.0848 | 0.1088 | 0.0547 |
| Data/restraints/parameters | 3527/168/185 | 7917/38/433 | 7924/930/566 | 7089/39/430 | 8995/192/632 |
| Goodness-of-fit on $F^2$ | 1.121 | 1.061 | 1.134 | 1.021 | 1.418 |
| Final R indexes [I>=2σ (I)] [a,b] | R1 = 0.0257<br>wR2 = 0.0709 | R1 = 0.0243<br>wR2 = 0.0482 | R1 = 0.0415<br>wR2 = 0.0945 | R1 = 0.0346<br>wR2 = 0.0625 | R1 = 0.0699<br>wR2 = 0.1430 |
| Final R indexes [all data] | R1 = 0.0287<br>wR2 = 0.0744 | R1 = 0.0387<br>wR2 = 0.0531 | R1 = 0.0568<br>wR2 = 0.1010 | R1 = 0.0608<br>wR2 = 0.0699 | R1 = 0.0808<br>wR2 = 0.1460 |

[a] $R1 = [\Sigma||F_o|-|F_c||]/[\Sigma|F_o|]$. [b] $wR2 = [\Sigma[w(F_o^2-F_c^2)^2]]/[\Sigma(w(F_o^2)^2]]^{1/2}$, $w = 1/[\sigma^2(F_o^2) + (aP)^2 + bP]$, where $P = [\max(0 \text{ or } F_o^2) + 2(F_c^2)]/3$

### 4.3.4 Electrochemistry

Compounds **1**, **2**, **3**, and **5** were dissolved in propylene carbonate and chloride was removed by addition of a slight excess of $TlPF_6$, giving dehalogenated compounds **1a**, **2a**, **3a**, and **5a**. The gray TlCl that precipitated was removed by filtration. Cyclic voltammograms for compounds **1a**, **2a**, **3a**, and **5a** were taken in propylene carbonate at room temperature with 2 mM analyte and 100 mM electrolyte ($NEt_4PF_6$) using a standard glassy carbon electrode for the working electrode, a platinum wire for the auxiliary electrode, and an $Ag/Ag^+$ electrode as the reference electrode. The solutions were titrated with the appropriate $M(OTf)_n$ until the redox wave no longer changed. All electrochemical potentials were internally referenced to the ferrocene/ferrocenium couple. The voltammetry was performed in the range of 1000 mV to 0 mV at a scan rate of 100 mV $s^{-1}$.

## 4.4 Results and Discussion

### 4.4.1 Synthesis

Each compound reported here was synthesized by one of two methods: self-assembly or cation exchange of $Li^+$ for $M^{n+}$. Compound **2** was synthesized by the self-assembly method shown in Scheme 4.1. In this method, the acetate ligands of $Mo_2(OAc)_4$ are substituted for HSNO5 while simultaneously installing the $Na^+$ ion into the compound. In this reaction, the $Na^+$ is first allowed to bind to the deprotonated $SNO5^-$ ligand in MeOH at 60° C. Then, the $Na^+$-ligand solution is added to $Mo_2(OAc)_4$ and heated to reflux to give the desired compound. Without NaCl in the reaction, *cis*-2,2-$Mo_2(SNO5)_4$ is predominantly produced.[2b] Indeed, this reaction also generates some *cis*-2,2-$Mo_2(SNO5)_4$ as a byproduct, but allowing $Na^+$ and HSNO5 to precomplex before adding the

$Mo_2(OAc)_4$ limits the amount of this undesired byproduct that is formed. The presence of $Na^+$ thus appears to template the desired 4,0 arrangement of the ligands, similar to the role of $Li^+$ in the synthesis of **1**.[5c]

In solution, the $Li^+$ ion of **1** only has a modest thermodynamic preference for binding ($K_{eq}$ = 95 at 298 K).[5c] Thus, **1** is potentially a good starting material for the preparation of a variety of M···$Mo_2$ compounds compounds by cation exchange. Compounds **3** - **5** were synthesized in this manner, by exchanging $Li^+$ for either $Ca^{2+}$, $Sr^{2+}$, or $Y^{3+}$ (Scheme 4.1). In these reactions, either $CaCl_2$, $SrCl_2$, or $Y(OTf)_3$ is reacted with **1** in MeOH. Compound **1** is only sparingly soluble in MeOH, but when the incoming metal is present in solution, **1** easily dissolves and reacts to form the desired compound as a precipitate. These reactions can be either done at reflux (compound **3**) or room temperature (compounds **4** and **5**). While the former does yield a successful synthesis of the compound, it also forms a significant amount of *cis*-2,2-$Mo_2(SNO5)_4$ that must be removed, and reactions at room temperature avoid this complication.

**4.4.2 X-ray Crystal Structures**

The X-ray crystal structures of **2** – **5** are shown in Figures 4.1 – 4.4, and important bond distances of **2** – **5** are compiled in Table 4.2 and compared with those of **1**·py and its dimer $[LiMo_2(SNO5)_4Cl]_2$ (**1-dim**). Each compound has a very similar Mo≡Mo bond distance between 2.12 Å and 2.14 Å. These distances are longer than the average Mo≡Mo bond distance of $[Mo_2]^{4+}$ paddlewheel compounds found in the CSD (~2.10 Å), likely due to electron donation into σ* and π* orbitals of the $[Mo_2]^{4+}$ unit by the axial ligands.[5c,15] Compounds **2** – **5** each exhibit the same 4,0 arrangement of $SNO5^-$ ligands

found in **1**·py and **1-dim**. The differences between these structures lie in the coordination environment, charge, and ionic radius of their Lewis acidic main group cations.

**Table 4.2.** Selected bond distances for compounds **1-5**.

| **Compound** | Mo–Mo (Å) | M···$Mo_2$ (Å) | $Mo_2$–Cl (Å) | $M^{n+}$-$O_{SNO5}$ (Å) | $M^{n+}$ ionic radius (Å)[a] | Reference |
|---|---|---|---|---|---|---|
| **1**·py | 2.1357(3) | 3.075(5) | 2.6533(6) | 2.182[6] | 0.90 | [5c] |
| **1**-dim | 2.1354(8) | 3.049(6) | 2.644(1) | 2.185[7] | 0.90 | [5c] |
| **2**·4 py | 2.1377(7) | 3.505(2) | 2.776(1) | 2.434(2) | 1.14 | This work |
| **3**·2 MeOH | 2.1306(6) | 3.699(1) | 2.7023(9) | 2.4422[9] | 1.20 | This work |
| **3-dim**·5.5 MeCN | 2.1361[8] | 3.711[1] | 2.630[1] | 2.439[2] | 1.20 | This work |
| **4**·2 MeOH | 2.1333(5) | 3.8138(5) | 2.707(1) | 2.554[2] | 1.35 | This work |
| **5**·1.6 MeOH | 2.120(1) | 3.745(2) | 2.699(3) | 2.374[3] | 1.16 | This work |

[a]Values taken from ref. [18].

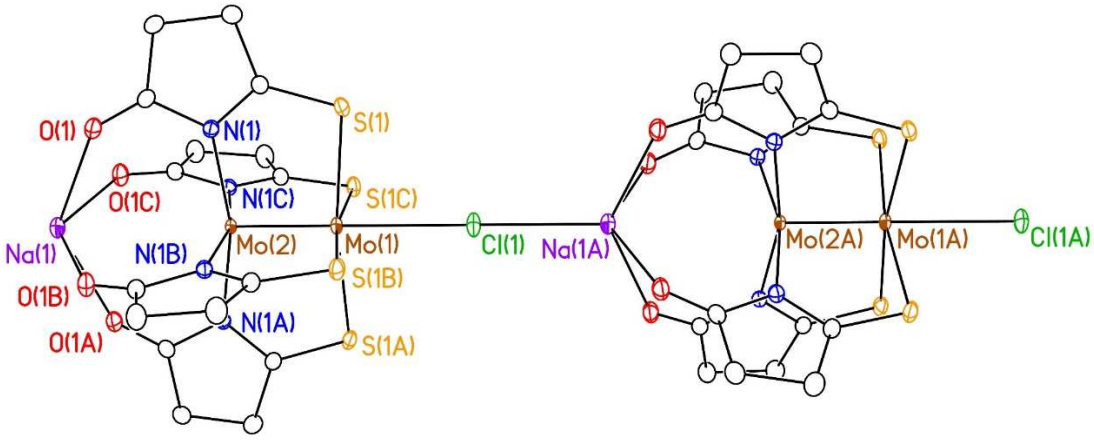


**Figure 4.1**. X-ray crystal structure of polymeric **2**·4 py. Atoms are drawn as 50% thermal probability ellipsoids. All hydrogen atoms and solvent molecules are omitted for clarity.

Structure **2**·4py is polymeric, with the $Na^+$ ion coordinated to a bridging chloride of an adjacent molecule as well as the four $SNO5^-$ ligands, giving a square pyramidal coordination geometry around the $Na^+$ ion. The Na···$Mo_2$ distance is 3.505(2) Å, which is substantially longer than the Li···$Mo_2$ distances found in **1**·py and **1-dim** (3.075(5) Å and

3.049(6) Å, respectively). The $Mo_2$–Cl bond distance increases from 2.6533(6) Å in **1**·py to 2.776(1)Å in **2**·4py. Since $Na^+$ is more remote from the $[Mo_2]^{4+}$ core than $Li^+$ is, it has less of an influence on the acidity of the $[Mo_2]^{4+}$. The lower Lewis acidity as well as the bridging nature of the axial $Cl^-$ contribute to the increased $Mo_2$–Cl bond distance in this compound as compared to the $Li^+$ complex.

The $Ca^{2+}$ and $Sr^{2+}$ ions of **3**·2MeOH and **4**·2MeOH are coordinated by three MeOH ligands as well as the four $SNO5^-$ ligands, giving a seven-coordinate mono-capped trigonal prismatic geometry with one $SNO5^-$ O atom in the capping position. These structures also have two solvent MeOH molecules. One of these forms a hydrogen bond with the free $Cl^-$, and one of these forms a hydrogen bond with the axial $Cl^-$, which serves to lengthen the $Mo_2$–Cl bond. The complexes have M···$Mo_2$ distances of 3.699(1) Å and 3.8138(5) Å, respectively, which are significantly larger than that of **2**·4py. For **4**·2MeOH, this is expected, since $Sr^{2+}$ has a much larger ionic radius than $Na^+$, but for **3**·2MeOH, this is unexpected. The ionic radii of 5-coordinate $Na^+$ and 7-coordinate $Ca^{2+}$ are 1.14 Å and 1.20 Å, respectively. However, the average M-$O_{SNO5}$ bond distance is essentially identical, indicating that the difference in ionic radii between $Na^+$ and $Ca^{2+}$ has a negligible impact on the structure and does not adequately explain the ~0.19 Å increase in M···$Mo_2$ separation. Instead, we believe this change to result from Coulombic repulsion between $[Mo_2]^{4+}$ and $M^{n+}$. The $Mo^{2+}$ ions of the dimolybdenum unit more strongly repel the $Ca^{2+}$ ion than the $Na^+$ ion because of the higher charge on $Ca^{2+}$, resulting in the longer M···$Mo_2$ separation. In spite of the longer M···$Mo_2$ distance as well as the hydrogen bonding interaction between solvent MeOH and the axial $Cl^-$, both

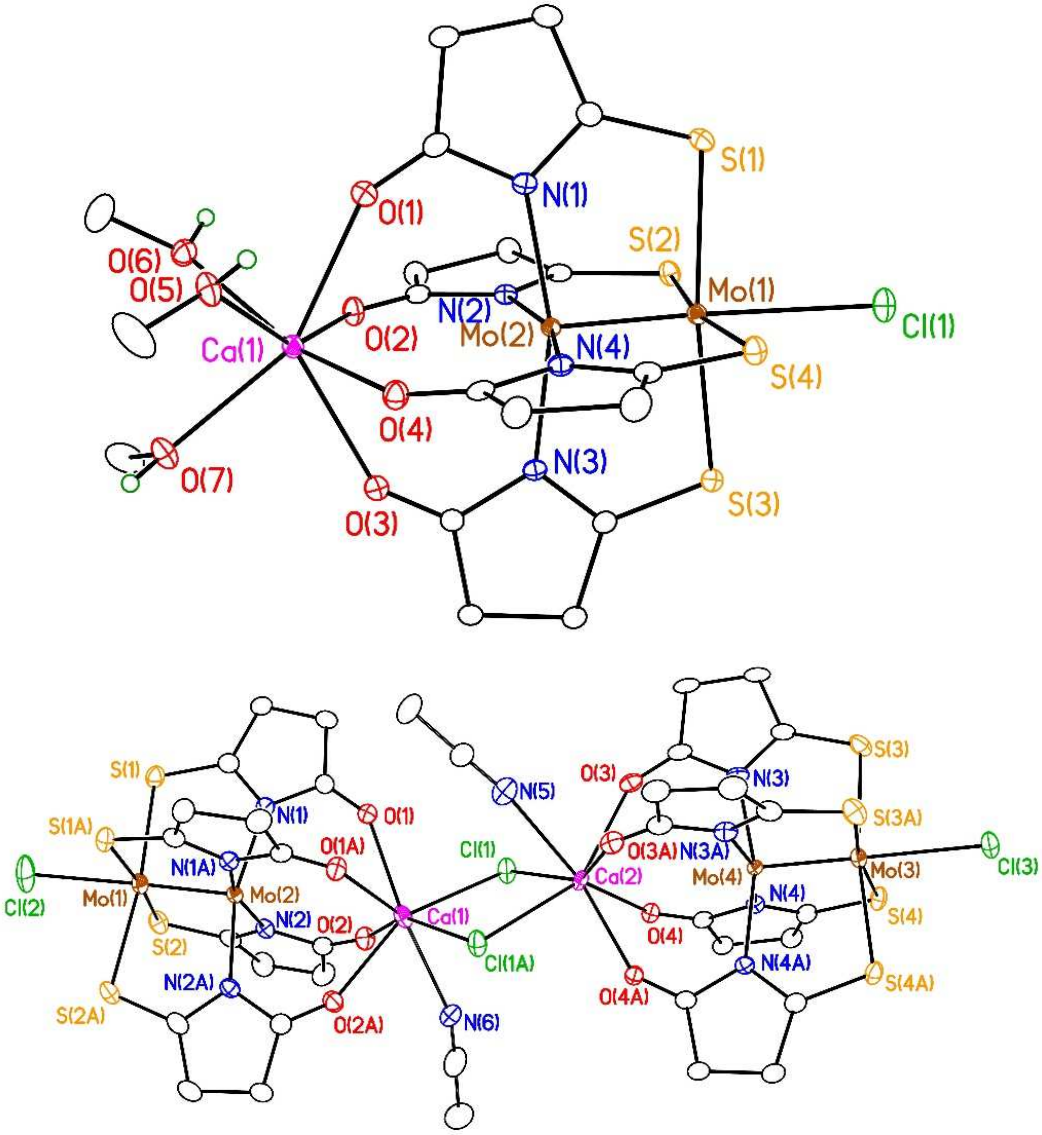


**Figure 4.2.** X-ray crystal structures of a) monomeric **3** and b) dimeric **3-dim**. All atoms are drawn as 50% thermal probability ellipsoids. All hydrogen atoms, except the alcohol hydrogens of methanol, all counter ions, minor components of disorder, and free solvent molecules are omitted for clarity.

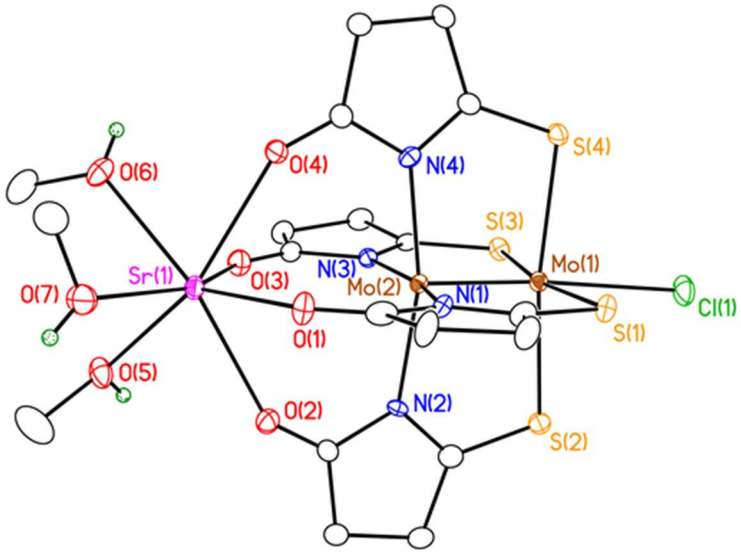


**Figure 4.3.** X-ray crystal structure of the cation of **4**. All non-hydrogen atoms are drawn as 50% thermal probability ellipsoids. All hydrogen atoms except the alcohol hydrogens of methanols are omitted for clarity.

**3**·2 MeOH and **4**·2 MeOH have $Mo_2$–Cl bond distances (2.7023(9) Å and 2.707(1) Å, respectively) that are significantly shorter than the $Mo_2$–Cl bond distance in **2**·4py. While the increased charge of $Ca^{2+}$ is responsible for the increased M···$Mo_2$ distance, the increased charge also exerts a greater influence on $[Mo_2]^{4+}$, resulting in a $Mo_2$–Cl bond distance closer to that in the corresponding $Li^+$ compound. The $Mo_2$–Cl bond distance of **4**·2MeOH is slightly longer than that of **3**·2MeOH. This slight increase is likely caused by the slightly longer M···$Mo_2$ distance of the $Sr^{2+}$ compound.

When crystallized from MeCN, **3** dimerizes to form the structure **3-dim**·5.5MeCN. In this structure, both $Ca^{2+}$ ions are coordinated by four $SNO5^-$ ligands, two chlorides, which bridge the two halves of the dimer, and one MeCN ligand. This structure has a slightly longer M···Mo distance than does **3**·2MeOH, but it has a much shorter $Mo_2$–Cl bond distance of 2.630[1] Å. This $Mo_2$–Cl bond distance is also shorter than those of

**1**·py and **1-dim.** Another set of heterotrimetallic linear chain compounds recently reported by our group ($Mo_2Ru(dpa)_4Cl_2$, $Mo_2$–Cl = 2.5262(6) Å, and $[Mo_2Ru(dpa)_4Cl_2]OTf$, $Mo_2$–Cl = 2.4637(5) Å) have shorter $Mo_2$–Cl bond distances caused by covalent bonding between Ru and $Mo_2$.[5a,16] The $Mo_2$–Cl bond distance of **3-dim**·5.5MeCN is the shortest known for a M···$Mo_2$ heterotrimetallic compound in which M interacts with the $[Mo_2]^{4+}$ unit in a purely Coulombic fashion. Unlike the MeOH solvent molecules of **3**·2MeOH, the MeCN solvent molecules of **3-dim**·5.5MeCN are unable to form hydrogen bonds with the axial chlorides. Without the hydrogen bonding interaction competing with the $[Mo_2]^{4+}$ core for the axial $Cl^-$, structure **3-dim**·5.5MeCN can support a shorter $Mo_2$–Cl bond distance.

Structure **5**·1.6MeOH contains an eight-coordinate $Y^{3+}$ ion that is coordinated by the four $SNO5^-$ ligands and four MeOH ligands in a square anti-prismatic arrangement. Like **3**·2MeOH and **4**•2MeOH, 5·1.6MeOH has a hydrogen bond between one of the partially occupied MeOH solvent molecules and the axial $Cl^-$. The axial $Cl^-$ attached to the $[Mo_2]^{4+}$ unit is compositionally disordered with a triflate anion ($Cl^-$ component: 85.5(5)%). This compositional disorder is representative of the bulk sample as evidenced by the elemental analysis data (*vide supra*). This structure has a Y···$Mo_2$ distance of 3.745(2) Å, which is slightly longer than the Ca···$Mo_2$ distance in **3**•2MeOH as the $Y^{3+}$ ion is repelled by the $Mo^{2+}$ ions more strongly than $Ca^{2+}$ is. The $Mo_2$–Cl bond distance is slightly shorter than that of **3**•2MeOH and **4**•2MeOH, an effect that can be attributed to the increased charge of $Y^{3+}$ as compared with either $Ca^{2+}$ or $Sr^{2+}$.

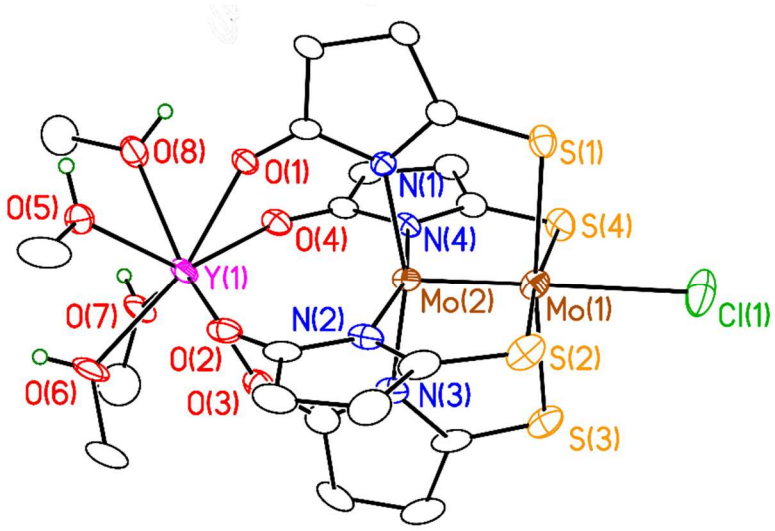


**Figure 4.4.** X-ray crystal structure of the cation of **5**. All non-hydrogen atoms are drawn as 50% thermal probability ellipsoids. All hydrogen atoms, except those on the alcohol groups, and all disordered components are omitted for clarity.

In general, the increased charge of the Lewis acidic cation influences the dimolybendum center, making it more Lewis acidic and shortening the $Mo_2$–Cl bond distance. However, this effect is mitigated by the increased repulsion between the $[Mo_2]^{4+}$ moiety and the cation resulting from the cation's increased charge as well as by the formation of hydrogen bonds with solvent methanol.

### 4.4.3 Electrochemistry

Cyclic voltammograms (CV) of compounds $[LiMo_2(SNO5)_4][PF_6]$ (**1a**), $[NaMo_2(SNO5)_4][PF_6]$ (**2a**), $[CaMo_2(SNO5)_4][PF_6]_2$ (**3a**), and $[YMo_2(SNO5)_4][PF_6]_3$ (**5a**) were taken in propylene carbonate with 2 mM analyte and 100 mM $NEt_4PF_6$ as the electrolyte. Compounds **1a**, **2a**, **3a**, and **5a** were generated *in situ* by reacting **1**, **2**, **3**, and **5** with $TlPF_6$ in propylene carbonate in order to strip away the axial chloride. This was a necessary step for obtaining high quality CVs of the compounds because the $[Mo_2]^{4+/5+}$

redox waves of some compounds overlapped with the $Cl^{-}/Cl^{\cdot}$ redox waves. Solid TlCl was removed by filtration, and CVs were taken on the filtered solutions of **1a**, **2a**, **3a**, and **5a**. Each of these exhibits a quasi-reversible $[Mo_2]^{4+/5+}$ redox wave that moves to a higher potential as $M^{n+}$ is added to the solution. These CVs are consistent with metal ion-coupled electron transfer,[17] and they indicate that each of these compounds reversibly binds $M^{n+}$, as we previously reported for the electrochemistry of **1**. Further, these CVs are substantially different from those of the previously reported *trans*-2,2-$Mo_2(SNO5)_4$ and *cis*-2,2-$Mo_2(SNO5)_4$, ruling out the possibility that **1a**, **2a**, **3a**, and **5a** undergo ligand rearrangement upon halide abstraction. Thus, the conclusions we draw from this electrochemical study are based on the reasonable assumption that the solution structures of **1a**, **2a**, **3a**, and **5a**, are similar to those of their halogenated counterparts.

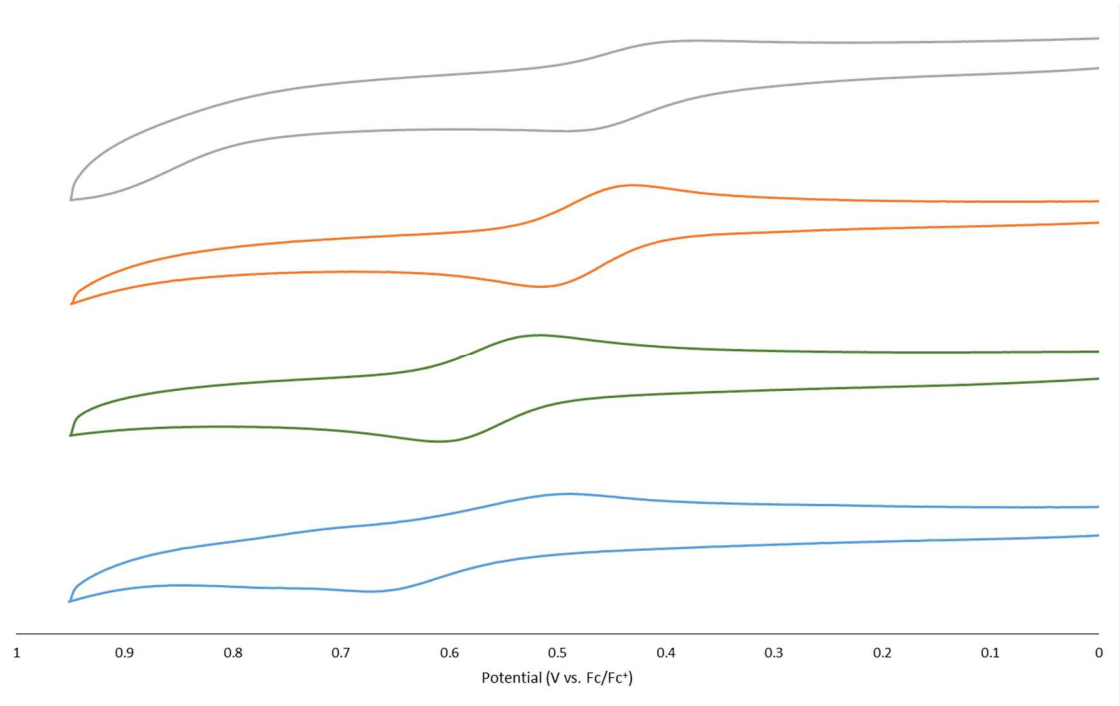


**Figure 4.5.** Cyclic voltammograms of $[LiMo_2(SNO5)_4]^{+}$ (**1a**, gray) $[NaMo_2(SNO5)_4]^{+}$ (**2a**, orange), $[CaMo_2(SNO5)_4]^{2+}$ (**3a**, green), and $[YMo_2(SNO5)_4]^{3+}$ (**5a**, blue). The CVs were taken in PC with 2 mM analyte and 100 mM $NEt_4PF_6$. The currents are normalized.

Each solution was titrated with a solution of $M(OTf)_n$ until the redox wave was no longer affected by additional aliquots of $M(OTf)_n$ solution. The final CVs for each compound are shown in Figure 4.5 and the redox potentials as well as the amount of $M^{n+}$ added to solution are reported in Table 4.3. The charge of the Lewis acid, and thus the charge of the $[MMo_2(SNO5)_4]^{n+}$ cation, greatly influences the $[Mo_2]^{4+/5+}$ redox potential. The ionic radii of $Na^+$, $Ca^{2+}$, and $Y^{3+}$ have a narrow range of 0.06 Å. Thus, the differences in the CVs of **2a**, **3a**, and **5a** are based primarily on the charge of $M^{n+}$, rather than differences in the ionic radius. As the charge of $M^{n+}$ in these compounds increases from +1 to +3, this potential shifts from 480 mV to 579 mV. Given the ease of swapping one cation for another in these systems, these results demonstrate a simple method to reliably tune the redox potential of the $[Mo_2]^{4+/5+}$ couple over a range of 100 mV.

**Table 4.3.** Electrochemical potentials of **1a**, **2a**, **3a**, and **5a**.

| Compound | $E_{1/2}$ vs. $Fc/Fc^+$ (mV) | Equivalents $M^{n+}$ added |
|---|---|---|
| **1a** | 446 | 20 |
| **2a** | 480 | 19 |
| **3a** | 567 | 25 |
| **5a** | 579 | 8 |

## 4.5 Conclusions

We describe here the synthesis of four new M···$Mo_2$ compounds in which M is a Group I, II, or III cation. Three of these compounds (**2**, **3**, and **5**) follow a diagonal trend and have very similar ionic radii, allowing the effect of cation charge on the Lewis acidity of $[Mo_2]^{4+}$ and the $[Mo_2]^{4+/5+}$ redox couple to be probed. Compound **4** has the same cation charge as **3**, but it has a larger ionic radius, allowing the effect of increasing

the M···$Mo_2$ distance on $[Mo_2]^{4+}$ Lewis acidity to be examined. Increasing the charge of the $M^{n+}$ does increase the Lewis acidity of $[Mo_2]^{4+}$, shortening the $Mo_2$–Cl bond distance, however the effect is attenuated by an increase in the M···$Mo_2$ distance resulting from increased repulsion between $M^{n+}$ and $[Mo_2]^{4+}$. Increasing the M···$Mo_2$ distance has a modest effect that decreases $[Mo_2]^{4+}$ Lewis acidity and slightly increases the $Mo_2$–Cl bond distance. The charge of $M^{n+}$ has a profound impact on the redox potential of the $[Mo_2]^{4+/5+}$ couple. Increasing the charge of $M^{n+}$ from n = 1 to n = 3 allows the $[Mo_2]^{4+/5+}$ redox couple to be tuned over a 100 mV range.

**4.6 Acknowledgements**

The authors thank Tristan R. Brown for his help in obtaining elemental analysis data on these compounds. Financial support was provided under NSF Grant CHE-1300464 and a generous gift from Paul J. Bender (X-ray diffraction and NMR spectroscopy instrumentation).

## 4.7 Supporting Information

### 4.7.1 Crystallographic Asymmetric Units

Below are images of the asymmetric units of the crystal structures presented in this paper.

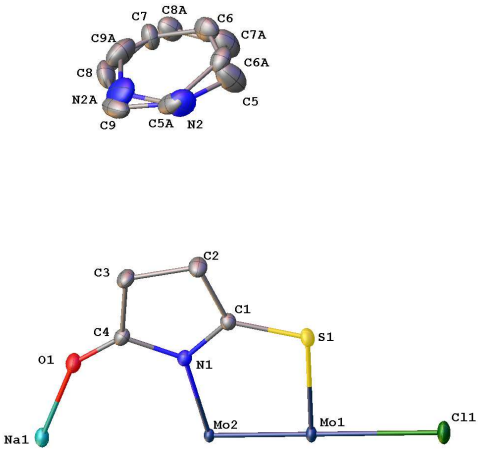


**Figure 4.S1.** The asymmetric unit of **2**·4py, including all disordered components. All atoms are drawn as 50% thermal probability ellipsoids. All hydrogen atoms have been omitted for clarity. The molecule resides on a crystallographic 4-fold axis.

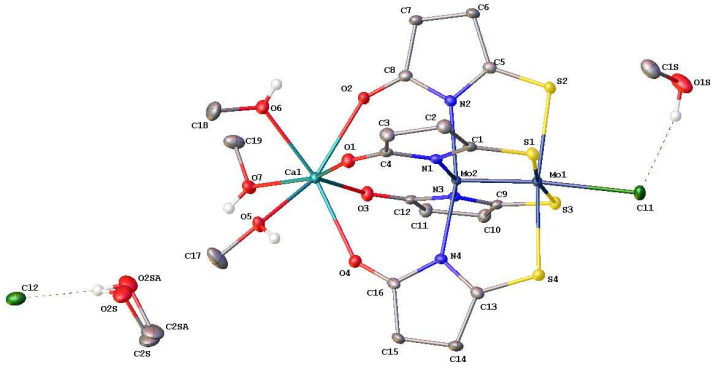


**Figure 4.S2.** The asymmetric unit of **3**·2MeOH, including all disordered components, solvent, and counterions. All atoms are drawn as 50% thermal probability ellipsoids. All hydrogen atoms, except for alcohol protons have been omitted for clarity.

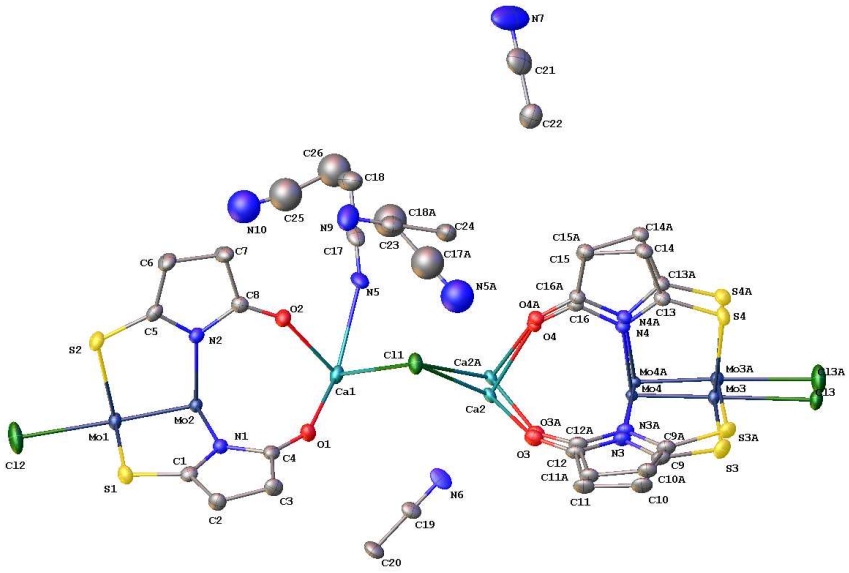


**Figure 4.S3.** The asymmetric unit **of 3-dim**·5.5MeCN, including all disordered components and solvent molecules. The compound resides on a crystallographic mirror plane. All atoms are drawn as 50% thermal probability ellipsoids. All hydrogen atoms have been omitted for clarity.

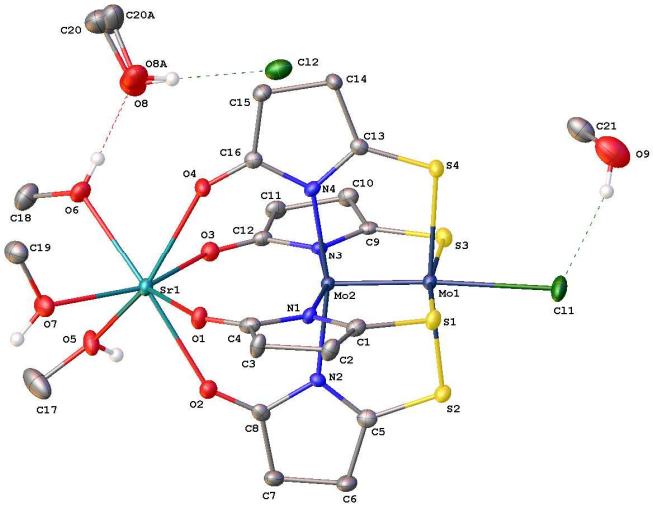


**Figure 4.S4.** The asymmetric unit of **4**·2MeOH, including all disordered components, solvent molecules, and counterions. All atoms are drawn as 50% thermal probability ellipsoids. All hydrogen atoms except for alcohol protons have been omitted for clarity.

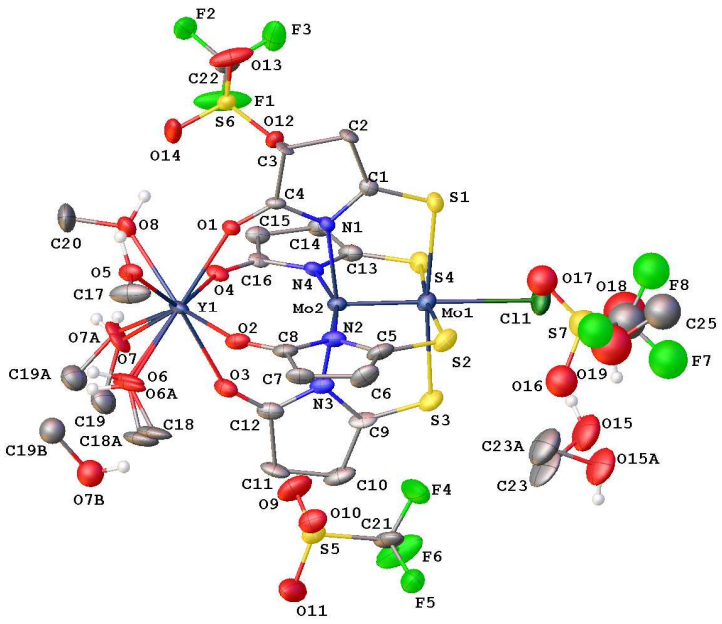


**Figure 4.S5.** The asymmetric unit of **5**·1.5MeOH, including all disordered components, solvent molecules and counterions. All atoms are drawn as 50% thermal probability ellipsoids. All hydrogen atoms except for alcohol protons have been omitted for clarity.

### 4.7.2 Disorder in X-ray Crystal Structures

Positional disorder was present in the solvent pyridine of **2**·4py, in the MeOH (O2S) in **3**·2MeOH, in several of the MeCN moieties as well as the $[Mo_2]^{4+}$ fragment Mo3 in **3-dim**·5.5MeCN, in MeOH O8 in **4**·2MeOH and MeOH O7 of **5**·1.6MeOH. These disordered components were refined with bond distance and thermal parameter restraints in order to ensure a chemically reasonable and computationally stable refinement. Most of the MeCN molecules were modeled with idealized geometries in order to achieve a computationally stable refinement. The lowest occupied components of disordered MeCN molecules of **3-dim** (N5A and N10) were refined isotropically with no hydrogen atoms in order to facilitate a stable refinement.

In addition to the solvent positions modeled for **3-dim**, several other solvent positions for MeCN were found. After many attempts to model the diffusely diffracting species, a stable refinement was not obtainable for those positions. Option SQUEEZE of the program PLATON was used to adjust the diffraction data to eliminate these diffuse scattering effects.[19] PLATON calculated the upper limit of the solvent-occupied volume as 365.1 $Å^3$, or 20.4% of the unit cell volume. The program calculated 111 electrons in the unit cell for the diffuse species. This approximately corresponds to 1.75 molecules of squeezed acetonitrile in the asymmetric unit (28 electrons).

Chloride Cl1 of **5**·1.6MeOH was compositionally disordered with a triflate (chloride component 85.5(5)%. Due to its low occupancy, the triflate was modeled isotropically with thermal parameter restraints and an idealized geometry.[20]

**4.8 References**

1. (a) Cotton, F. A.; Murillo, C. A.; Walton, R. A. *Multiple Bonds Between Metal Atoms*. 3rd ed.; Springer Science and Business Media, Inc.: New York, 2005; (b) Falvello, L. R.; Foxman, B. M.; Murillo, C. A., *Inorg. Chem.* **2014**, *53*, 9441.

2. (a) Li Manni, G.; Dzubak, A. L.; Mulla, A.; Brogden, D. W.; Berry, J. F.; Gagliardi, L. *Chem. Eur. J.* **2012**, *18*, 1737. (b) Dolinar, B. S.; Berry, J. F. *Dalton Trans.* **2014**, *43*, 6165-76; (c) Hicks, J.; Ring, S. P.; Patmore, N. J. *Dalton Trans.* **2012**, *41*, 6641. (d) Chisholm, M. H.; Patmore, N. J. *Acc. Chem. Res.* **2007**, *40*, 19. (e) Wilkinson, L. A.; McNeill, L.; Meijer, A. J.; Patmore, N. J. *J. Am. Chem. Soc.* **2013**, *135*, 1723. (f) Wilkinson, L. A.; McNeill, L.; Scattergood, P. A.; Patmore, N. J. *Inorg. Chem.* **2013**, *52*, 9683. (g) Alberding, B. G.; Brown-Xu, S. E.; Chisholm, M. H.; Gustafson, T. L.; Reed, C. R.; Naseri, V. *Dalton Trans.* **2012**, *41*, 13097. (h) Chisholm, M. H.; Gustafson, T. L.;

Turro, C. *Acc. Chem. Res.* **2013**, *46*, 529. (i) Alberding, B. G.; Chisholm, M. H.; Durr, C. B.; Gallucci, J. C.; Ghosh, Y.; Spilker, T. F. *Dalton Trans.* **2014**, *43*, 11397. (j) Alberding, B. G.; Chisholm, M. H.; Chou, Y.-H.; Gallucci, J. C.; Ghosh, Y.; Gustafson, T. L.; Patmore, N. J.; Reed, C. R.; Turro, C. *Inorg. Chem.* **2009**, *48*, 4394. (k) Alberding, B. G.; Chisholm, M. H.; Chou, Y. H.; Ghosh, Y.; Gustafson, T. L.; Liu, Y.; Turro, C. *Inorg. Chem.* **2009**, *48*, 11187. (l) Alberding, B. G.; Chisholm, M. H.; Gallucci, J. A.; Ghosh, Y.; Gustafson, T. L. *Proc. Natl. Acad. Sci. U.S.A.* **2011**, *108*, 8152. (m) Alberding, B. G.; Chisholm, M. H.; Gustafson, T. L.; Reed, C. R.; Singh, N.; Turro, C. *J. Clust. Sci.* **2009**, *20*, 307. (n) Alberding, B. G.; Chisholm, M. H.; Lear, B. J.; Naseri, V.; Reed, C. R. *Dalton Trans.* **2011**, *40*, 10658. (o) Chisholm, M. H.; D'Acchioli, J. S.; Pate, B. D.; Patmore, N. J. *Inorg. Chem.* **2005**, *44*, 1061.

3. Murillo, C. A. *Aust. J. Chem.* **2014**, *67*, 972.

4. (a) Nippe, M.; Victor, E.; Berry, J. F. *Inorg. Chem.* **2009**, *48*, 11889. (b) Brogden, D. W.; Turov, Y.; Nippe, M.; Li Manni, G.; Hillard, E. A.; Clerac, R.; Gagliardi, L.; Berry, J. F. *Inorg. Chem.* **2014**, *53*, 4777.

5. (a) Brogden, D. W.; Berry, J. F. *Inorg. Chem.* **2014**, *53*, 11354. (b) Brogden, D. W.; Christian, J. H.; Dalal, N. S.; Berry, J. F. *Inorg. Chim. Acta* **2015**, *424*, 241. (c) Dolinar, B. S.; Berry, J. F. *Inorg. Chem.* **2013**, *52*, 4658. (d) Nippe, M.; Berry, J. F. *J. Am. Chem. Soc.* **2007**, *129*, 12684.; (e) Nippe, M.; Bill, E.; Berry, J. F. *Inorg. Chem.* **2011**, *50*, 7650. (f) Nippe, M.; Turov, Y.; Berry, J. F. *Inorg. Chem.* **2011**, *50*, 10592. (g) Nippe, M.; Victor, E.; Berry, J. F. *Eur. J. Inorg. Chem.* **2008**, 5569. (h) Nippe, M.; Wang, J.; Bill, E.; Hope, H.; Dalal, N. S.; Berry, J. F. *J. Am. Chem. Soc.* **2010**, *132*, 14261. (i) Mashima, K.; Shimoyama, Y.; Kusumi, Y.; Fukumoto, A.; Yamagata, T.; Ohashi, M. *Eur. J. Inorg.*

*Chem.* **2007**, 235. (j) Ohashi, M.; Shima, A.; Rüffer, T.; Mizomoto, H.; Kaneda, Y.; Mashima, K. *Inorg. Chem.* **2007**, *46*, 6702 (k) Pal, K.; Nakao, K.; Mashima, K. *Eur. J. Inorg. Chem.* **2010**, 5668. (l) Chisholm, M. H.; Macintosh, A. M. *Chem. Rev.* **2005**, *105*, 2949. (m) Li, B.; Zhang, H.; Huynh, L.; Shatruk, M.; Dikarev, E. V. *Inorg. Chem.* **2007**, *46*, 9155. (n) Koeberl, M.; Cokoja, M.; Herrmann, W. A.; Kühn, F. E., *Dalton Trans.* **2011**, *40*, 6834.

6. (a) Jansen, K.; Dehnicke, K.; Fenske, D. *Z. Naturforsch.* **1985**, *40b*, 13. (b) Apfelbaum, F.; Bino, A. *Inorg. Chim. Acta* **1989**, *155*, 191. (c) Cotton, F. A.; Falvello, L. R.; Reid Jr., A. H.; Roth, W. J., *Acta Crystallogr.* **1990**, *C46*, 1815. (d) Udovic, B.; Leban, I.; Šegedin, P. *Croat. Chim. Acta* **1999**, *72*, 477.

7. (a) Brencic, J. V.; Cotton, F. A. *Inorg. Chem.* **1969**, *8*, 7. (b) Brencic, J. V.; Cotton, F. A. *Inorg. Chem.* **1969**, *8*, 2698. (c) Leban, I.; Šegedin, P. *Inorg. Chim. Acta* **1984**, *85*, 181. (d) Cotton, F. A.; Matonic, J. H.; Silva, D. d. O. *Inorg. Chim. Acta* **1995**, *234*, 115.

8. (a) Adly, F. G.; Ghanem, A. *Chirality* **2014**, *26*, 692. (b) Hansen, J.; Davies, H. M. L. *Coord. Chem. Rev.* **2008**, *252*, 545. (c) Trindade, A. F.; Coelho, J. A. S.; Afonso, C. A. M.; Veiros, L. F.; Gois, P. M. P. *ACS Catal.* **2012**, *2*, 370. (d) Kornecki, K. P.; Berry, J. F.; Powers, D. C.; Ritter, T. Metal-Metal Bond-Containing Complexes as Catalysts for C-H Functionalization. In *Prog. Inorg. Chem.*, Karlin, K. D., Ed. 2014; Vol. 58, pp 225. (e) Kornecki, K. P.; Berry, J. F. *Chem. Eur. J.* **2011**, *17*, 5827. (f) Kornecki, K. P.; Berry, J. F. *Eur. J. Inorg. Chem.* **2012**, 562. (g) Kornecki, K. P.; Berry, J. F. *Chem. Commun.* **2012**, *48*, 12097.

9. Kornecki, K. P.; Briones, J. F.; Boyarskikh, V.; Fullilove, F.; Autschbach, J.; Schrote, K. E.; Lancaster, K. M.; Davies, H. M. L.; Berry, J. F. *Science* **2013**, *342*, 351.

10. (a) Tsui, E. Y.; Tran, R.; Yano, J.; Agapie, T. *Nature Chem.* **2013**, *5*, 293. (b) Park, Y. J.; Ziller, J. W.; Borovik, A. S. *J. Am. Chem. Soc.* **2011**, *133*, 9258. (c) Ke, I. S.; Jones, J. S.; Gabbaï, F. P. *Angew. Chem. Int. Ed.* **2014**, *53*, 2633. (d) Lin, T. P.; Gabbaï, F. P. *J. Am. Chem. Soc.* **2012**, *134*, 12230. (e) Yang, H.; Gabbaï, F. P. *J. Am. Chem. Soc.* **2014**, *136*, 10866.

11. Berg, U.; Sandström, J. *Acta Chem. Scand.* **1966**, *20*, 689.

12. Holste, G.; Schäfer, H. *Z. Anorg. Allg. Chem.* **1972**, *391*.

13. (a) Bruker-AXS *APEX2*, 2014.11-0; Bruker AXS: Madison, WI, 2014; (b) Kraus, L.; Herbst-Irmer, R.; Sheldrick, G. M.; Stalke, D. *J. Appl. Crystallogr.* **2015**, *48*, 3.

14. (a) Sheldrick, G. M. *XS*, Georg-August-Universität Göttingen: Göttingen, Germany, 2013; (b) Sheldrick, G. M. *Acta Crystallogr.* **2015**, *C71*, 3.

15. Allen, F. H. *Acta Crystallogr.* **2002**, *B58*, 380.

16. Brogden, D. W.; Berry, J. F. *Inorg. Chem.* **2015**, *54*, 7660.

17. (a) Fukuzumi, S.; Ohkubo, K. *Coord. Chem. Rev.* **2010**, *254*, 372. (b) Fukuzumi, S.; Ohkubo, K.; Morimoto, Y. *Phys. Chem. Chem. Phys.* **2012**, *14*, 8472.

18. Shannon, R. D., *Acta Crystallogr.* **1976**, *A32*, 751-767.

19. Spek, A. L. *Acta Crystallogr.* **2015**, *C71*, 9-18.

20. Guzei, I. A. *J. Appl. Crystallogr.* **2014**, *47*, 806.

# Chapter 5

*Tri- and Pentametallic Metal Atom Chain Compounds Containing Lanthanide Ions*

## 5.1 Abstract

The reaction of pyLi$Mo_2(SNO5)_4Cl$·py (**1**·py, $SNO5^-$ = monothiosuccinimidato) with $Ln(OTf)_3$ (Ln = Ce – Nd, Sm – Lu) in MeOH yields $[(MeOH)_xLnMo_2(SNO5)_4Cl][OTf]_2$ (**2-Ln**; x = 5, Ln = Ce – Nd; x = 6, Ln = Sm – Lu) and recrystallization of **2-Eu** yields $[Eu[Mo_2(SNO5)_4]_2Cl]_n$ (**3-Eu**) These compounds are the first examples of $Ln^{3+}$–containing heterometallic extended metal atom chains (HEMACs). X-ray crystallographic studies indicate that the $Ln^{3+}$ proximity to the $[Mo_2]^{4+}$ unit has a modest effect on the Lewis acidity of the $[Mo_2]^{4+}$ unit, resulting in a slight shortening of the $Mo_2$–Cl bond distance as the charge density of $Ln^{3+}$ is increased. The decreasing size of the $Ln^{3+}$ ion across the series results in the $SNO5^-$ ligands being pulled more tightly into the $[Mo_2]^{4+}$ core, donating more electron density, and resulting in lowering of the $[Mo_2]^{4+/5+}$ redox potential across the series.

## 5.2 Introduction

Coordination compounds of the lanthanide (Ln) ions are of considerable technological importance.[1] Complexes that contain both lanthanide and transition metal ions are of interest for their magnetic[2] and photoluminescent properties,[3] and present substantial synthetic challenges. While a number of successful strategies to target mixed d-block/f-block compounds now exist, $Ln^{3+}$ ions have never before been incorporated into extended metal atom chains (EMACs): linear multimetallic coordination compounds that feature metal-metal bonds. Our group has investigated methods for preparing heterometallic EMACs – or HEMACs – in which a heterometal is appended to a bimetallic metal-metal bonded unit (Scheme 5.1).

The third metal atom in the chain modifies the bimetallic metal-metal bonding manifold through interactions ranging from weak Coulombic interactions to strong covalent bonds.[4] These perturbations to the metal-metal bond result in compounds containing interesting electronic and magnetic properties, including thermal spin-crossover compounds, single molecule magnets, molecular wires, and molecular transistors. [4o,5] Recently, we have introduced HEMACs using the new tridentate equatorial ligand, monothiosuccinimide (HSNO5, Scheme 5.1). Unlike polypyridyl amides, such as dipyridylamide (dpa), which have three N donor atoms, HSNO5 contains three different donor atoms – S, N, and O. The difference in hardness between the O and S donor atoms allows HEMACs to be designed by taking advantage of HSAB principles. Thus far, this ligand has been successfully used to synthesize M'$M_2$ compounds where M' = $Li^+$, $Na^+$, $Ca^{2+}$, $Sr^{2+}$, and $Y^{3+}$ and $M_2$ = $[Mo_2]^{4+}$ as well as a supramolecular $K_3[Mo_2]_4$ structure.[4m,4n,6] In these compounds, the M'$^{n+}$ ion influences the Lewis acidity and electrochemistry of $[Mo_2]^{4+}$ through a Coulombic interaction. As the charge of M'$^{n+}$ increases, the $[Mo_2]^{4+}$ core becomes more Lewis acidic, forming stronger $Mo_2$-$L_{ax}$ bonds, and the $[Mo_2]^{4+/5+}$ redox couple becomes less accessible.

**Scheme 5.1.** The structure of M'···M≡M HEMACs.

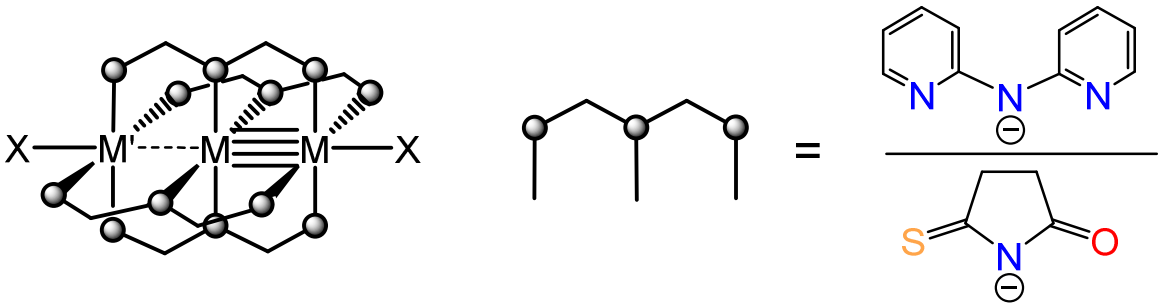


Previous Work: M = Cr, Mo, W; M' = Cr - Ni, Li, Na, Ca, Sr, Y
This Work: M = Mo, M' = Ce - Nd, Sm - Lu

After our success at synthesizing the aforementioned $MMo_2$ heterotrimetallic EMACs, we sought to expand the scope of this chemistry even further by installing a lanthanide ion as the third metal in the heterotrimetallic chain, as described here. We thus present a new class of HEMACs that incorporates d-block and f-block metals, affording us the opportunity to directly examine how the $Ln^{3+}$ charge density impacts the properties of the $[Mo_2]^{4+}$core.

**5.3 Results and Discussion**

**5.3.1 Syntheses**

Using reaction conditions devised for the synthesis of $CaMo_2$, $SrMo_2$, and $YMo_2$ compounds as a starting point, we developed reliable methods for the synthesis of $LnMo_2$ compounds (Scheme 5.2a). These compounds are best synthesized by generating a solution that is 0.1 M in $Ln(OTf)_3$ and 0.02 M in $pyLiMo_2(SNO5)_4Cl{\cdot}py$ (**1**·py) in MeOH. The starting material **1**·py is sparingly soluble in MeOH, but inclusion of the $Ln(OTf)_3$ salt in the reaction mixture results in the immediate formation of a bright red solution with a very small amount of suspended red solid. After stirring the reaction mixture for 1 – 6 hours at room temperature, the red solid is removed via filtration, and the filtrate is layered with $Et_2O$. After diffusing overnight, X-ray quality crystals of $[(MeOH)_xLn(SNO5)_4Cl][OTf]_2$ (**2-Ln**; x = 5, Ln = Ce – Nd; x = 4, Ln = Sm – Lu) begin forming, growing larger over the course of a week. Filtering and washing the crystals with THF yields pure **2-Ln** in yields of up to 62%. Heating **2-Eu** in MeCN followed by filtration and layering with $Et_2O$ yields crystals of the polymeric chain compound $[Eu(Mo_2(SNO5)_4)_2Cl][OTf]_2$ (**3-Eu**) containing pentametallic Mo≡Mo···Eu···Mo≡Mo units. The formation of this polymer is consistent with the behavior of other $MMo_2(SNO5)_4Cl$ complexes in which crystallization from MeCN results in the formation of dimers or supramolecular structures connected through the heterometal of the compound.[4n,6]

**Scheme 5.2.** a) The synthetic methods for forming trimetallic $LnMo_2$ compounds and pentametallic $Mo_2LnMo_2$ chains. b) The equilibrium between a high coordinate lanthanide structure and low coordinate lanthanide structure in solution.

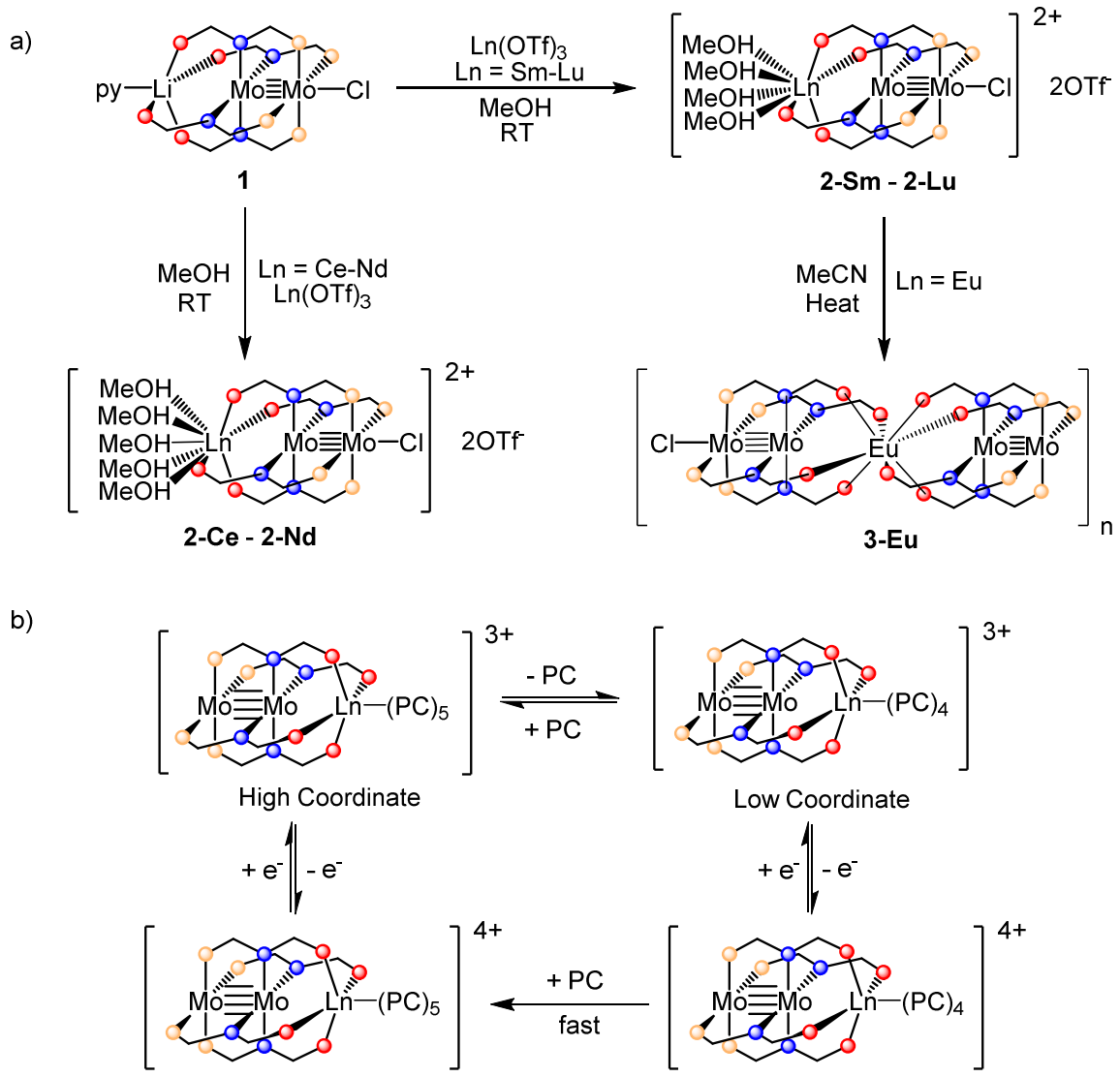


### 5.3.2 Structures

The X-ray crystallographic structures of **2-Ce** – **2-Lu** each exhibit the characteristic paddlewheel structure about the $[Mo_2]^{4+}$ unit, with all four $SNO5^-$ ligands arranged such that the O atoms are bonded to the $Ln^{3+}$ ion, the N atoms are bonded to the proximal Mo atom, and the S atoms are bonded to the distal Mo atom. The distal Mo atom also is bonded to an axial $Cl^-$ ion.

The lanthanide coordination sphere conforms to one of two motifs (Figures 5.1a – 5.1b). For structures **2-Ce** – **2-Nd**, the lanthanide has a 9-coordinate capped square anti-prismatic geometry, and structures **2-Sm** – **2-Lu** have an 8-coordinate square anti-prismatic coordination geometry. These geometries result from facial capping by the $Mo_2(SNO5)_4$ group, and the filling of the remainder of the Ln coordination sphere with four or five MeOH ligands. Structures **2-Sm** – **2-Dy** exhibit crystallographic disorder of the position of the lanthanide ion. The minor component for the $Ln^{3+}$ ion in each of those structures is at a distance that is indicative of co-crystallization of the nine-coordinate $Ln^{3+}$ structures, and the minor component occupancy decreases from 20% in **2-Sm** to 1.6% in **2-Dy**. The structures containing a smaller $Ln^{3+}$ ion do not exhibit any $Ln^{3+}$ positional disorder. Since the minor component represents the higher coordinate species, the decrease in minor component occupancy directly translates to an increased thermodynamic preference for lower coordinate complexes across the series.

This series of compounds exhibits the well-known lanthanide contraction, in which the primary coordination sphere of the lanthanide ion shrinks as a result of the decreasing ionic radius of the $Ln^{3+}$ ion from 1.15 Å for $Ce^{3+}$ to 1.01 Å for $Lu^{3+}$.[7] The Ln-$O_{SNO5}$ bond distances and Ln-$O_{MeOH}$ bond distances of both the 9-coordinate and 8-coordinate structural motifs decrease across the series (Ln-$O_{SNO5}$: 9-coordinate, 2.547[2] – 2.527[6] Å; 8-coordinate: 2.414[3] – 2.3379[7] Å | Ln-$O_{solv}$: 9-coordinate, 2.528[2] – 2.484[6] Å; 8-coordinate, 2.441[3] – 2.2977[7] Å). Consequently, the Ln···$Mo_2$ distance also decreases (9-coordinate: 3.9940[5] – 3.972(2) Å; 8-coordinate: 3.746(4)Å – 3.7143(9) Å). These changes to the primary coordination sphere of the $Ln^{3+}$ ion influence the coordination environment of the $[Mo_2]^{4+}$ unit. As the $Ln^{3+}$ ionic radius shrinks and the Ln-$O_{SNO5}$ distance decreases, the angle between the vector connecting the S and N atoms of each $SNO5^-$ ligand and the Mo≡Mo vector (χ, Chart 5.1)

a)

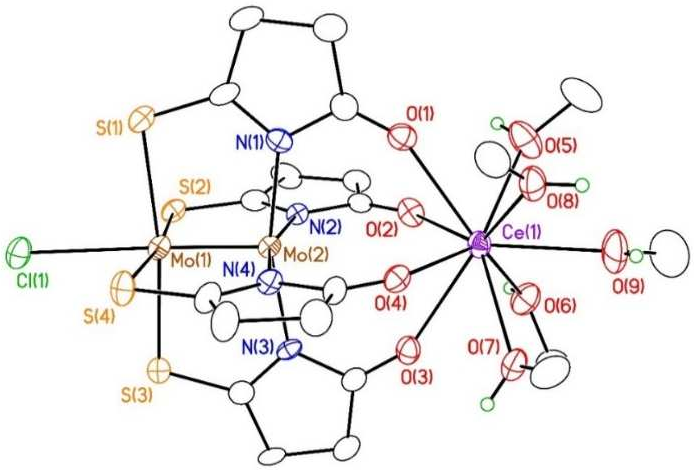


b)

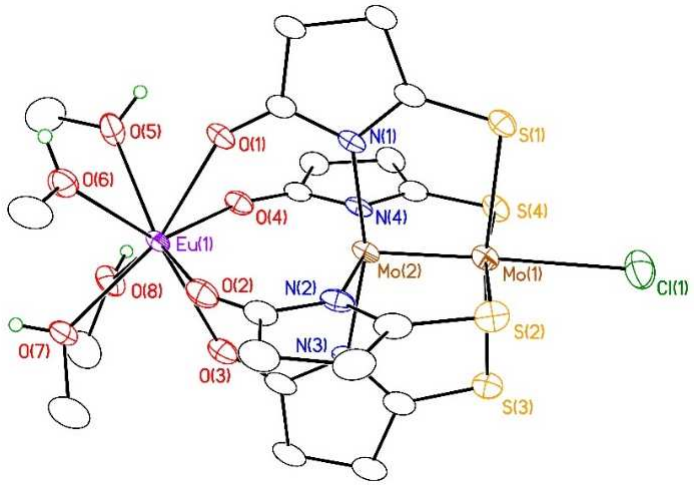


c)

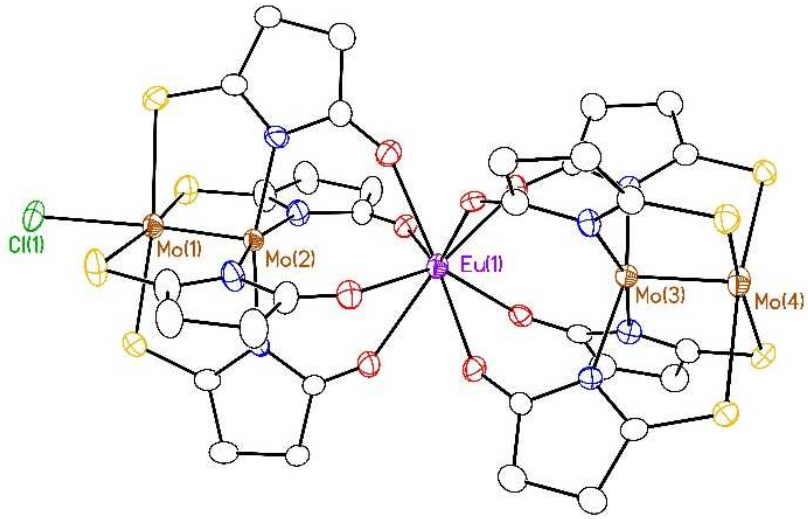


**Figure 5.1.** The a) 9-coordinate and b) 8-coordinate $LnMo_2$ structural motifs. c) The monomer of the polymeric chain of **3-Eu**.

**Table 5.1.** Important bond and angle parameters from the crystallographic structures of **2-Ce** – **2-Lu**.

| | Ln···$Mo_2$ (Å) | Ln-$O_{solv}$ (Å) | Ln-$O_{SNO5}$ (Å) | Mo-N (Å) | Mo-S (Å) | Mo-Cl (Å) | χ (°) | Ionic Radius (Å) |
|---|---|---|---|---|---|---|---|---|
| | 9-Coordinate Lanthanide | | | | | | | |
| **2-Ce** | 3.9940[5] | 2.528[2] | 2.547[2] | 2.118[2] | 2.5179[7] | 2.735[2] | 9.129 | 1.15 |
| **2-Pr** | 3.9809(6) | 2.515[6] | 2.533[2] | 2.112[3] | 2.521[1] | 2.733(2) | 9.205 | 1.13 |
| **2-Nd** | 3.972(2) | 2.484[6] | 2.527[6] | 2.116[6] | 2.521[2] | 2.722(5) | 9.240 | 1.12 |
| | 8-Coordinate Lanthanide | | | | | | | |
| **2-Sm** | 3.746(4) | 2.441[3] | 2.414[3] | 2.119[2] | 2.5201[4] | 2.722(2) | 9.258 | 1.11 |
| **2-Eu** | 3.7608(2) | 2.435[1] | 2.4122[1] | 2.116[2] | 2.5203[7] | 2.7188(2) | 9.345 | 1.08 |
| **2-Gd** | 3.7592(9) | 2.389[3] | 2.405[2] | 2.116[2] | 2.5212[8] | 2.713(2) | 9.380 | 1.07 |
| **2-Tb** | 3.747(1) | 2.378[8] | 2.392[2] | 2.111[2] | 2.5195[6] | 2.710(2) | 9.491 | 1.06 |
| **2-Dy** | 3.740(1) | 2.36[1] | 2.381[2] | 2.111[3] | 2.5211[9] | 2.708(2) | 9.582 | 1.05 |
| **2-Ho** | 3.7370(5) | 2.348[7] | 2.373[2] | 2.111[2] | 2.5248[5] | 2.714(2) | 9.628 | 1.04 |
| **2-Er** | 3.7327(4) | 2.35[1] | 2.362[2] | 2.107[2] | 2.5256[4] | 2.711(1) | 9.733 | 1.03 |
| **2-Tm** | 3.7212(8) | 2.313[4] | 2.3518[9] | 2.1052[9] | 2.5244[4] | 2.7107(8) | 9.751 | 1.02 |
| **2-Yb** | 3.7196(5) | 2.308[9] | 2.341[2] | 2.103[2] | 2.5262[7] | 2.714(2) | 9.838 | 1.01 |
| **2-Lu** | 3.7143(9) | 2.2977[7] | 2.3379[7] | 2.1062[8] | 2.5321[4] | 2.6740(8) | 9.896 | 1.00 |

becomes steeper, resulting in the Mo-$N_{eq}$ bond distance decreasing over the series and the Mo-$S_{eq}$ bond distance increasing slightly from **2-Ce** – **2-Lu**. The $Mo_2$-$Cl_{ax}$ bond distance also decreases over this series from 2.735[2] Å to 2.722(5) Å for the 9-coordinate motif and 2.722(2) Å - 2.6740(8) Å for the 8-coordinate motif. The origin of this increased affinity for the axial chloride is attributed to the decrease in the Ln···$Mo_2$ distance across the series, which increases the polarization of electrons within the $[Mo_2]^{4+}$ core, resulting in increased Lewis acidity. Shorter distances allow for a stronger Coulombic interaction between the $Ln^{3+}$ ion and the $[Mo_2]^{4+}$ core. The $Eu^{3+}$ ion of the polymeric chain **3-Eu** is coordinated by two 4,0-$Mo_2(SNO5)_4$ units, giving it an 8-coordinate square-antiprismatic geometry similar to that of its monomeric counterpart **2-Eu** (Figure 5.1c). Each pentanuclear $[Eu[Mo_2(SNO5)_4]_2]^{3+}$ unit is connected *via* a bridging chloride giving the polymeric chain. The asymmetric unit also contains two triflate counterions to balance

the remaining charge on the monomer. The molecule resides on a crystallographic mirror plane. The polymer propagates in a spiral, following the crystallographic $\bar{4}$ axis.

**Chart 5.1.** The angle between the $SNO5^-$ ligand and $[Mo_2]^{4+}$ (χ).

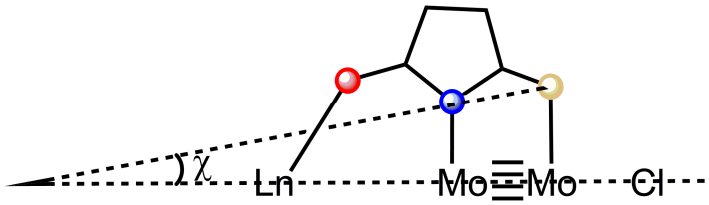


### 5.3.4 Electrochemistry

Propylene carbonate (PC) solutions of **2-Ce** – **2-Lu** were dehalogenated with $TlPF_6$ to give solutions of $[(PC)_xLnMo_2(SNO5)_4]^{3+}$ (**2a-Ce** – **2a-Lu**). The electrochemical potentials of the resulting solutions were measured by cyclic voltammetry (CV, Supporting Information, Figures 5.S15 – 5.S27). Each CV exhibits an oxidation wave attributed to the $[Mo_2]^{4+/5+}$ redox couple. The redox potential of each of these one-electron oxidations is highly dependent on the lanthanide concentration, which is consistent with reversible binding of the $Ln^{3+}$ ion in solution. Each electrochemical solution was titrated with 25 eq. of the appropriate $Ln(OTf)_3$, at which point the $[Mo_2]^{4+/5+}$ potential was invariant upon further addition of $Ln^{3+}$, indicating that the waves observed are attributable to intact Ln···Mo≡Mo compounds. The electrochemistry data exhibit two distinct trends across the lanthanide series (Figure 5.2). For **2a-Ce** – **2a-Eu**, the $[Mo_2]^{4+/5+}$ oxidation potential gradually increases from 584 mV to 609 mV vs $Fc/Fc^+$, whereas from **2a-Eu** to **2a-Lu**, the oxidation wave becomes more accessible by 55 mV.

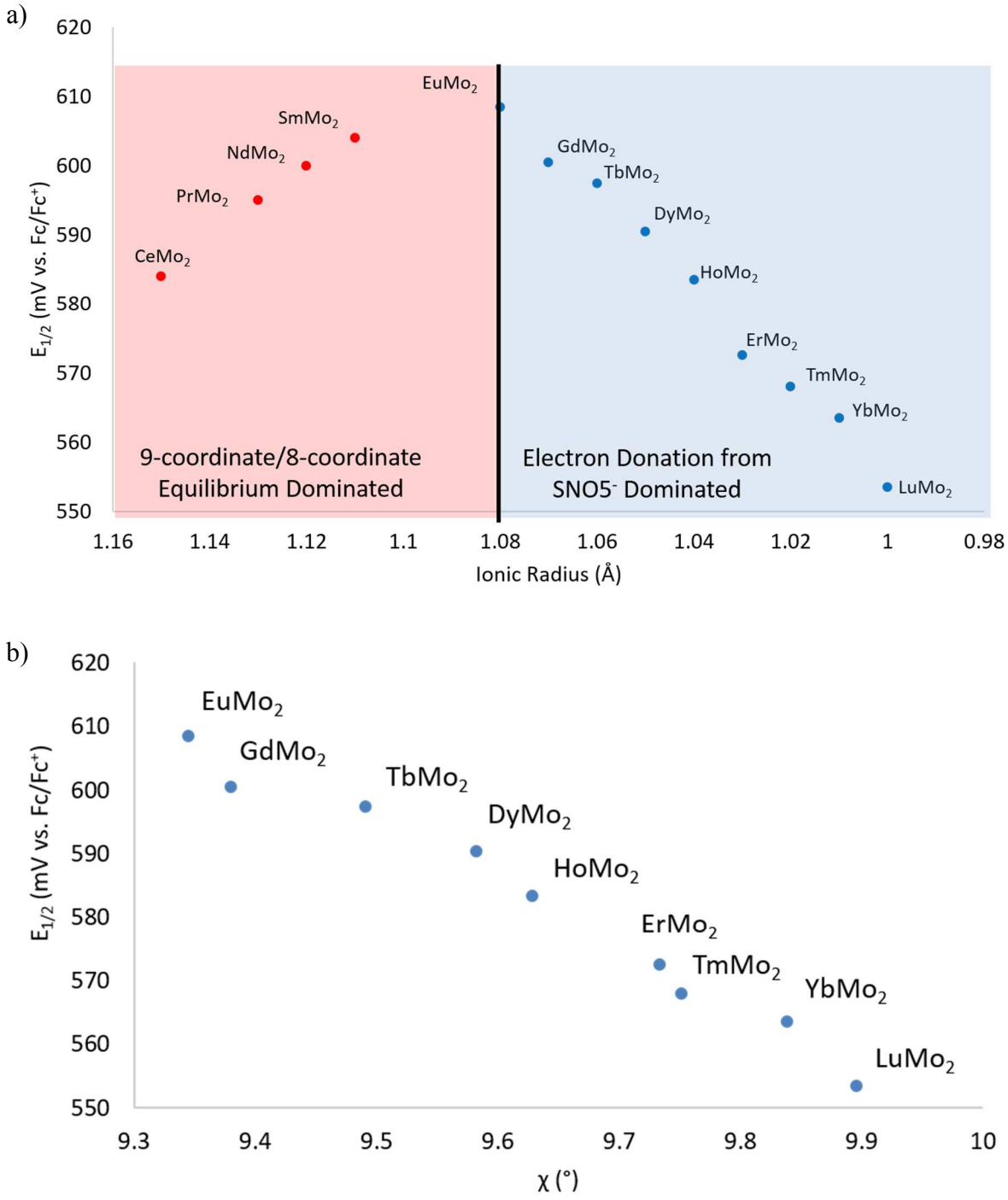


**Figure 5.2** a) The two trends in $[Mo_2]^{4+/5+}$ redox potential for the $LnMo_2$ series and b) The electrochemical potentials of the late $LnMo_2$ compounds (**2a-Eu** – **2a-Lu**) vs. angle χ (see Chart 5.1 for definition of χ).

The increasing trend for $[Mo_2]^{4+/5+}$ redox potential in the first half of the series may be explained by the structural trends in $Ln^{3+}$ coordination geometry across the series. The two structural motifs of the crystal structures grown from MeOH (i.e., 9- and 8- coordinate species) can be reasonably assumed to be present in equilibrium in PC. The electrochemical data support this analysis. While the CV for **2a-Ce** exhibits very clean anodic and return waves, the CVs of **2a-Pr** – **2a-Eu** show the presence of two, overlapping anodic waves with a single return wave. The two anodic waves may be attributed to oxidation of 9-coordinate and 8-coordinate structural motifs in equilibrium in solution, respectively (Scheme 5.2b). The recorded $E_{1/2}$ value is necessarily a weighted average of these two species in solution. The presence of only one return wave suggests that the increased charge on the oxidized complex favors the 9-coordinate motif, since the extra MeOH ligand will help counter the charge. As the $Ln^{3+}$ ionic radius decreases, the composition of the electrochemistry solution shifts from being predominantly the 9-coordinate structure towards predominantly the 8-coordinate structure. The 8-coordinate structure has fewer MeOH ligands donating electron density to the $Ln^{3+}$ ion, decreasing the degree to which its positive charge is shielded. Thus, the charge seen by the $[Mo_2]^{4+}$ unit is higher in the 8-coordinate structure than it is in the 9-coordinate structure, and as the composition of the solution changes to favor the 8-coordinate structure, the apparent $[Mo_2]^{4+/5+}$ $E_{1/2}$ value moves to a higher potential. This trend in the electrochemical data is corroborated by the increasing preference for the 8-coordinate structure exhibited in lanthanide disorder for structures **2-Sm** – **2-Dy** (*vide supra*).

The decreasing trend in oxidation potential across the latter half of the $LnMo_2$ series (Figure 5.2b) is unintuitive. $Ln[Fc^{Ph_2PO}]_2$ complexes (Figures 5.3), the closest relatives of the $LnMo_2$ compounds described here, exhibit an increasing trend in ferrocene oxidation potential

across the lanthanide series 628 mV to 683 mV vs. $Fc/Fc^{+}$.[8] In these compounds, the increase in oxidation potential is attributed to an enhanced electron withdrawing ability of later lanthanides owing to their higher charge density. As the lanthanide draws electron density away from the ferrocene moiety, it becomes harder to oxidize. The structural trends seen in the crystal structures of **2-Eu** – **2-Lu** (*vide supra*) provide a partial explanation for the opposite trend seen here. As described above, the decreasing ionic radius of the $Ln^{3+}$ ion results in steeper χ angles and shorter Mo-N bond distances, which donate more electron density to the $[Mo_2]^{4+}$ core. Stronger Mo-N bonding leads to lower $[Mo_2]^{4+/5+}$ oxidation potentials due to N p π donation into the $[Mo_2]^{4+}$ δ HOMO, which is consistent with the electrochemical behavior seen in bimetallic *cis*-2,2-$Mo_2(SNO5)_4$ and *trans*-2,2-$Mo_2(SNO5)_4$.[9] Second, the smaller lanthanides form shorter bonds with the oxygen atoms of both the $SNO5^{-}$ ligand and the MeOH ligands. With these shorter bonds, the charge on the $Ln^{3+}$ becomes masked better by the electron clouds of its ligands, dampening its effect on the electrochemistry of $[Mo_2]^{4+}$ and resulting in a more accessible oxidation potential.

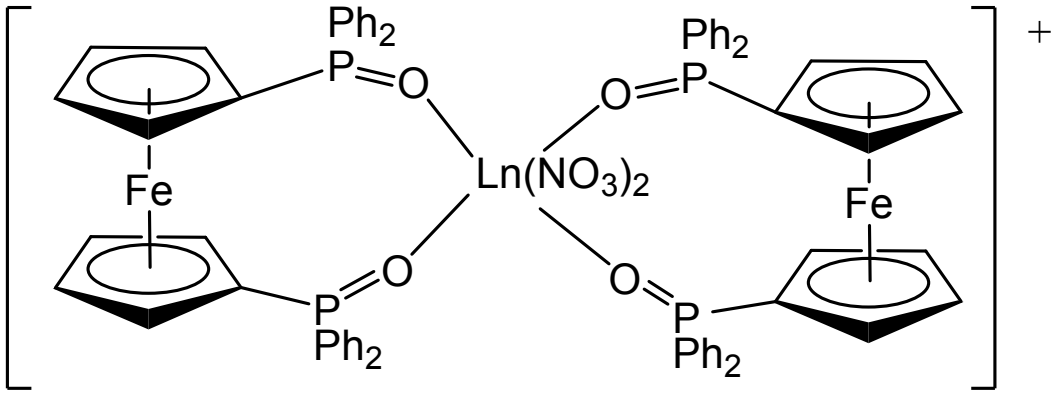


**Figure 5.3.** The structure of $Ln[Fc^{Ph_2PO}]_2$ complexes. $Ln^{3+} = La^{3+}$, $Eu^{3+}$, $Dy^{3+}$, $Lu^{3+}$.

## 5.4 Conclusions

In summary, we have synthesized the first examples of $LnMo_2$ compounds, which represent a completely new frontier in the chemistry of HEMACs by incorporating both f-block and d-block metals into the same metal atom chain. The compounds are synthesized through cation substitution of $Li^+$ in **1** for $Ln^{3+}$. The choice of $Ln^{3+}$ ion influences the Lewis acidity, structural properties, and redox properties of the $[Mo_2]^{4+}$ unit through its effective charge and proximity to the $[Mo_2]^{4+}$ unit. As the $Ln^{3+}$ ionic radius decreases, so too do the distance between the $Ln^{3+}$ ion and the $[Mo_2]^{4+}$ core, and the $Mo_2$-Cl bond distance decreases correspondingly. The electrochemical oxidation potential of the $[Mo_2]^{4+}$ core also is dependent on the identity of the $Ln^{3+}$ ion. As the $Ln^{3+}$ ion decreases in size, it pulls the equatorial $SNO5^-$ ligands closer to the $[Mo_2]^{4+}$ core, reducing the oxidation potential. The degree of shielding of the $Ln^{3+}$ charge by coordinated solvent molecules also influences the electrochemical potential. A higher solvent coordination number allows more shielding of the $Ln^{3+}$ charge, providing a lower oxidation potential than a lower solvent coordination number. Further explorations of the physical properties of these novel HEMACs are currently underway.

## 5.5 Acknowledgements

The authors wish to acknowledge Ilia A. Guzei for his helpful advice in dealing with the pseudo-merohedral twinning in one of the structures. Financial support was provided under NSF Grant CHE-1300464, NIH NCRR award 1S10RR024601-1 (Mass spectrometry), and a generous gift from Paul J. Bender (X-ray diffraction). BSD thanks the Seaborg Institute for a summer research fellowship that contributed to this paper.

## 5.6 Supporting Information

### 5.6.1 Experimental

#### 5.6.1.1 General

All synthetic work was carried out under an inert atmosphere using standard Schlenk and glovebox techniques. All solvents were rigorously dried prior to use. THF, MeCN, and $Et_2O$ were dried over molecular sieves and subsequently dried using a Vacuum Atmospheres solvent purification system and degassed prior to use. Pyridine was dried over molecular sieves, distilled from BaO under $N_2$, and stored in an inert atmosphere glovebox prior to use. MeOH was dried sequentially over molecular sieves and $Mg/Mg(OMe)_2$. It was then distilled under $N_2$ immediately prior to use. 99.9% anhydrous propylene carbonate was purchased from Sigma Aldrich and further dried by stirring over CaO. It was then distilled under vacuum and stored in the glovebox prior to use. **1**·py was synthesized from $Mo_2(OAc)_4$, HSNO5, and LiCl in pyridine. All other reagents were purchased from Sigma-Aldrich and used without further purification. Elemental analyses were carried out by Midwest Microlabs in Indianapolis, IN, USA. NMR Spectroscopy was performed on a Bruker AC 300 MHz spectrometer or Bruker Avance III 500 MHz Spectrometer. FTIR (ATR) data were obtained using a Bruker TENSOR 27 spectrometer.

#### 5.6.1.2 Syntheses

General

A Schlenk flask was charged with 300 mg $Ln(OTf)_3$ and 150-160 mg **1**·py. These were dissolved in 10 mL MeOH giving a solution that is approximately 0.05 M $Ln(OTf)_3$ and 0.02 M **1**·py. These were stirred at room temperature for 6 hours. The reaction was then filtered and layered with 40 mL $Et_2O$, yielding crystals of the desired compound. Specifics for each compound are listed below.

**tetrakis-methanol-ceriumdimolybdenum-chloro-tetrakis-monothiosuccinimidato bis-triflate [(MeOH)$_5$CeMo$_2$(SNO5)$_4$Cl][OTf]$_2$ (2-Ce)**

770 mg Ce(OTf)$_3$ and 178 mg **1**·py (0.210 mmol) were dissolved in 30 mL MeOH and stirred at room temperature overnight. The reaction is filtered and layered with Et$_2$O, yielding bright red crystals. The crystals are collected by filtration and washed with 3 x 20 mL Et$_2$O, dried under vacuum and collected. Yield: 107 mg (39.8%). IR (ATR, cm$^{-1}$): 3397 (w, br), 2980 (w), 2941 (w), 1708 (m), 1427 (w), 1383 (w), 1280 (vs), 1233 (vs), 1171 (m), 1029 (s), 806 (w), 760 (w), 692 (m), 636 (s). Elem. Anal. Calcd. for $C_{19}H_{20}CeClF_6Mo_2N_4O_{11}S_6$ ([(MeOH)CeMo$_2$(SNO5)$_4$Cl]$^{2+}$·2[OTf]$^-$) C, 19.77%; H, 1.75%; N, 4.85%; Found C, 19.29%; H, 2.00%; N, 4.65%. MALDI-TOF MS (m/z): 826 ($M^{2+}$ - 4MeOH)

**tetrakis-methanol-praseodymiumdimolybdenum-chloro-tetrakis-monothiosuccinimidato bis-triflate [(MeOH)$_5$PrMo$_2$(SNO5)$_4$Cl][OTf]$_2$ (2-Pr)**

446 mg Pr(OTf)$_3$ and 160 mg **1**·py (0.188 mmol) were dissolved in 10 mL MeOH and stirred for 6 hours. Then, the reaction was filtered and layered with 40 mL Et$_2$O. The crystals were filtered, washed with 2 x 20 mL THF, and dried under vacuum overnight. Yield: 112 mg X-ray quality crystals were obtained by adding ~5 mL THF to the reaction mixture before layering with Et$_2$O. (46.2%). IR (ATR, cm$^{-1}$): 3384 (w, br), 2944 (vw), 1706 (m), 1427 (w), 1384 (w), 1281 (vs), 1234 (vs), 1169 (m), 1029 (s), 989 (vw), 806 (vw), 760 (w), 693 (m), 636 (vs). MALDI-TOF MS (m/z): Elem. Anal. Calcd. for $C_{19}H_{20}PrClF_6Mo_2N_4O_{11}S_6$ ([(MeOH)PrMo$_2$(SNO5)$_4$Cl][OTf]$_2$): C, 19.76%; H, 1.75%; N, 4.85%; Found: C, 19.66%; H, 1.98%; N, 4.67%. MALDI-TOF MS (m/z): 972 ($M^{2+}$ - $CH_3^+$).

**tetrakis-methanol-neodymiumdimolybdenum-chloro-tetrakis-monothiosuccinimidato bis-triflate [(MeOH)$_5$NdMo$_2$(SNO5)$_4$Cl][OTf]$_2$ (2-Nd)**

365 mg $Nd(OTf)_3$ and 154 mg **1**·py (0.181 mmol) were dissolved in 10 mL MeOH and stirred 6 hours. Then, the reaction is filtered and layered with $Et_2O$. After 24 hours, beautiful crystals grew. These crystals were filtered, washed with 2 x 20 mL THF, and dried under vacuum. Yield: 147 mg (63.0%). X-ray quality crystals were grown by adding ~5 mL THF to the reaction mixture before layering with $Et_2O$. IR (ATR, $cm^{-1}$): 3377 (vw, br), 2953 (vw), 1697 (m), 1664 (w) 1427 (w), 1383 (w), 1283 (vs), 1234 (vs), 1165 (m), 1029 (s), 865 (w), 806 (vw), 761 (vw), 694 (m), 637 (vs). Elem. Anal. Calcd. for $C_{20.5}H_{26}ClF_6Mo_2N_4NdO_{12.5}S_6$ ($[(MeOH)_{2.5}NdMo_2(SNO5)_4Cl][OTf]_2$): C, 20.41%; H, 2.17%; N, 4.64%. Found: C, 20.78%; H, 1.83%; N, 4.67%. MALDI-TOF MS (m/z): 975 ($M^{2+}$ - $CH_3^+$).

**tetrakis-methanol-samariumdimolybdenum-chloro-tetrakis-monothiosuccinimidato bis-triflate $[(MeOH)_4SmMo_2(SNO5)_4Cl][OTf]_2$ (2-Sm)**

486 mg $Sm(OTf)_3$ and 151 mg **1**·py (0.178 mmol) were added to a flask, dissolved in 15 mL MeOH and stirred for 1 hour. The reaction was filtered and layered with $Et_2O$, yielding bright red crystals. The crystals were filtered, washed with 2 x 20 mL THF, and dried under vacuum overnight. Yield: 133 mg (59.3%). IR (ATR, $cm^{-1}$): 3355 (br, vw), 2949 (vw), 1697 (m), 1664 (w), 1423 (vw), 1382 (w), 1286 (vs), 1259 (s), 1241 (s), 1163 (m), 1030 (m), 1012 (m), 964 (w), 939 (m), 804 (vw), 695 (m), 637 (vs). Elem. Anal. Calcd. for $C_{20}H_{24}ClF_6Mo_2N_4O_{12}S_6Sm$ ($[(MeOH)_2SmMo_2(SNO5)_4Cl][OTf]_2$): C, 20.08%; H, 2.02%; N, 4.68%. Found: C, 20.03%; H, 2.31%; N, 4.78%. MALDI-TOF MS (m/z) 948 ($M^{2+}$ - $CH_3^+$).

**tetrakis-methanol-europiumdimolybdenum-chloro-tetrakis-monothiosuccinimidato bis-triflate $[(MeOH)_4EuMo_2(SNO5)_4Cl][OTf]_2$ (2-Eu)**

560 mg $Eu(OTf)_3$ and 156 mg **1**·py (0.184 mmol) are added to a flask and dissolved in 10 mL MeOH. The reaction stirred at room temperature for 4 hours. Then, it was filtered and

layered with $Et_2O$, yielding large red crystals. The crystals were filtered and washed with 2 x 20 mL THF, and dried under vacuum overnight. Yield: 100 mg (43.1%). IR (ATR, $cm^{-1}$): 3363 (w, br), 2954 (vw), 1695 (m), 1663 (w), 1614 (vw), 1422 (w), 1383 (w), 1286 (vs), 1259 (vs), 1243 (s), 1226 (m), 1186 (w), 1164 (m), 1108 (vw), 1031 (m), 1011 (m), 803 (w), 791 (vw), 695 (w), 637 (vs). Elem. Anal. Calcd. for $C_{19}H_{20}ClEuF_6Mo_2N_4O_{11}S_6$ ($[(MeOH)EuMo_2(SNO5)_4Cl][OTf]_2$): C, 19.57%; H, 1.73%; N, 4.80%. Found: C, 19.32%; H, 2.10%; N, 4.49%. MALDI-TOF MS (m/z): 950 ($M^{2+}$ - $CH_3^+$).

**tetrakis-methanol-gadoliniumdimolybdenum-chloro-tetrakis-monothiosuccinimidato bis-triflate $[(MeOH)_4GdMo_2(SNO5)_4Cl][OTf]_2$ (2-Gd)**

510 mg $Gd(OTf)_3$ and 156 mg **1**·py (0.184 mmol) are added to a flask and dissolved in 10 mL MeOH. The reaction stirred at room temperature for 4 hours. Then, it was filtered and layered with $Et_2O$, yielding large red crystals. The crystals were filtered and washed with 2 x 20 mL THF, and dried under vacuum overnight. Yield: 125 mg (53.7%)
IR (ATR, $cm^{-1}$): 3384 (w, br), 2942 (vw), 1696 (m), 1663 (w), 1425 (vw), 1382 (w), 1287 (vs), 1258 (s), 1238 (s), 1224 (s), 1167 (m), 1029 (s), 963 (m), 939 (m), 917 (m), 805 (w), 761 (vw), 695 (m), 636 (vs). Elem. Anal. Calcd. for $C_{20.065}H_{24}Cl_{0.935}F_{6.195}GdMo_2N_4O_{12.195}S_{6.065}$ ($0.935[(MeOH)GdMo_2(SNO5)_4Cl][OTf]_2 + 0.065\ [(MeOH)GdMo_2(SNO5)_4][OTf]_3$): C, 19.90%; H, 2.00%; N, 4.63%. Found: C, 19.80%; H, 2.12%; N, 4.11%. MALDI-TOF MS (m/z): 955 ($M^{2+}$-$CH_3^+$).

**tetrakis-methanol-terbiumdimolybdenum-chloro-tetrakis-monothiosuccinimidato bis-triflate $[(MeOH)_4TbMo_2(SNO5)_4Cl][OTf]_2$ (2-Tb)**

280 mg $Tb(OTf)_3$and 148 mg **1**·py (0.151 mmol) are added to a flask and dissolved in 10 mL MeOH, and stirred for 15 minutes. The reaction is filtered and layered with $Et_2O$, yielding

large red crystals. The crystals are collected by filtration, washed with 2 x 20 mL THF, and dried under vacuum. Yield: 128 mg (66.9%). IR (ATR, $cm^{-1}$): 3364 (w, br), 2955 (vw), 1696 (m), 1660 (w), 1424 (vw), 1383 (w), 1288 (vs), 1259 (vs), 1242 (vs), 1225 (s), 1167 (m), 1030 (s), 804 (w), 761 (vw), 696 (w), 636 (vs). Elem. Anal. Calcd. for $C_{23}H_{27}ClF_6Mo_2N_4O_{12}S_6Tb$ $[(MeOH)TbMo_2(SNO5)_4Cl][OTf]_2]\cdot THF$: C, 22.20%; H, 2.19%; N, 4.50%. Found: C, 22.49%; H, 2.12%; N, 4.46%. MALDI-TOF MS (m/z): 956 ($M^{2+}$ - $CH_3^+$).

**tetrakis-methanol-dysprosiumdimolybdenum-chloro-tetrakis-monothiosuccinimidato bis-triflate $[(MeOH)_4DyMo_2(SNO5)_4Cl][OTf]_2$ (2-Dy)**

300 mg $Dy(OTf)_3$ and 142 mg **1**·py are added to a flask and dissolved in 10 mL MeOH. The reaction was stirred at room temperature for 6 hours. The reaction was filtered and layered with $Et_2O$, yielding red crystals. The crystals were collected by filtration and washed with 2 x 20 mL THF and dried under vacuum overnight. Yield: 67 mg (31%). IR (ATR, $cm^{-1}$): 3344 (w, br), 2951 (vw), 1695 (m), 1659 (w), 1423 (vw), 1382 (w), 1289 (vs), 1259 (vs), 1243 (s), 1223 (s), 1188 (m), 1166 (m), 1030 (s), 804 (w), 760 (vw), 697 (w), 637 (vs). Elem. Anal. Calcd. for $C_{19.5}H_{22}ClDyF_6Mo_2N_4O_{11.5}S_6$ ($[(MeOH)_{1.5}DyMo_2(SNO5)_4Cl][OTf]_2$): C, 19.64%; H, 1.86%; N, 4.70%. Found: C, 19.31%; H, 2.14%; N, 4.24%. MALDI-TOF MS (m/z): 961 ($M^{2+}$ - $CH_3^+$).

**tetrakis-methanol-holmiumdimolybdenum-chloro-tetrakis-monothiosuccinimidato bis-triflate $[(MeOH)_4HoMo_2(SNO5)_4Cl][OTf]_2$ (2-Ho)**

A flask is charged with 130 mg $Ho(OTf)_3$and 75 mg **1**·py (0.088 mmol), dissolved in 5 mL MeOH, an stirred at room temperature for 5 hours. The reaction is filtered and layered with $Et_2O$, yielding bright red crystals. The crystals are collected by filtration, washed with 2 x 20 mL THF, and dried under vacuum. Yield: 58 mg (51%).

IR (ATR, $cm^{-1}$): 3364 (vw, br), 2946 (vw), 1695 (m), 1662 (w), 1427 (vw), 1377 (w), 1288 (vs), 1260 (s), 1233 (vs), 1215 (vs), 1028 (s), 805 (w), 760 (vw), 696 (w), 635 (vs). Elem. Anal. Calc. for $C_{22}H_{32}ClF_6HoMo_2N_4O_{14}S_6$ ($[(MeOH)_4HoMo_2(SNO5)_4Cl][OTf]_2$): C, 20.72%, H, 2.53%, N, 4.39%. Found: C, 21.07%; H, 2.69%; N, 4.14%. MALDI-TOF MS (m/z): 963 ($M^{2+}$ - $CH_3^+$).

**tetrakis-methanol-erbiumdimolybdenum-chloro-tetrakis-monothiosuccinimidato bis-triflate $[(MeOH)_4ErMo_2(SNO5)_4Cl][OTf]_2$ (2-Er)**

170 mg $Er(OTf)_3$ and 80 mg **1**·py (0.0942 mmol) are added to a flask, dissolved in 5 mL MeOH, and stirred at room temperature for 1 hour. The reaction is then filtered and layered with $Et_2O$, yielding bright red crystals. The crystals are collected by filtration, washed with 2 x 20 mL THF, and dried under vacuum overnight. Yield: 75 mg (62.3%) IR (ATR, $cm^{-1}$): 3356 (w, br), 2953 (vw), 1697 (m), 1660 (w), 1424 (vw), 1384 (w), 1289 (vs), 1259 (vs), 1243 (vs), 1225 (vs), 1188 (m), 1167 (m), 1029 (s), 803 (w), 761 (w), 698 (m), 636 (vs). Elem. Anal. Calcd. for $C_{19}H_{20}ClErF_6Mo_2N_4O_{11}S_6$ ($[(MeOH)ErMo_2(SNO5)_4Cl][OTf]_2$): C, 19.32%; H, 1.71%; N, 4.74%. Found: C, 18.93%; H, 1.94%; N, 4.26%. MALDI-TOF MS (m/z): 964 ($M^{2+}$ – $CH_3^+$).

**tetrakis-methanol-thuliumdimolybdenum-chloro-tetrakis-monothiosuccinimidato bis-triflate $[(MeOH)_4TmMo_2(SNO5)_4Cl][OTf]_2$ (2-Tm)**

346 mg $Tm(OTf)_3$ and 150 mg **1**·py (0.177 mmol) are added to a flask, dissolved in 10 mL MeOH and stirred at room temperature for 1 hour. The reaction was then filtered and layered with $Et_2O$, yielding bright red crystals. The crystals were collected by filtration, washed with 2 x 20 mL THF, and dried under vacuum overnight. Yield: 115 mg (50.9%).

IR (ATR, $cm^{-1}$): 3360 (w, br), 2950 (vw), 1727 (w), 1697 (m), 1664 (w), 1429 (vw), 1384 (w), 1258 (vs), 1238 (vs), 1224 (vs), 1170 (m), 1029 (s), 923 (vw), 806 (w), 761 (vw), 696 (m), 636 (vs). Elem. Anal. Calcd. for $C_{19.5}H_{22}ClF_6Mo_2N_4O_{11.5}S_6Tm$

([(MeOH)$_{1.5}$TmMo$_2$(SNO5)$_4$Cl][OTf]$_2$): C, 19.53; H, 1.85, N, 4.67. Found: 19.23%, H, 2.06%, N, 4.21%. MALDI-TOF MS (m/z): 966 ($M^{2+}$ - $CH_3^+$).

**tetrakis-methanol-ytterbiumdimolybdenum-chloro-tetrakis-monothiosuccinimidato bis-triflate [(MeOH)$_4$YbMo$_2$(SNO5)$_4$Cl][OTf]$_2$ (2-Yb)**

530 mg Yb(OTf)$_3$ and 158 mg **1**·py (0.186 mmol) were added to a flask, dissolved in 15 mL MeOH and stirred for 30 minutes. The reaction was filtered and layered with Et$_2$O, yielding red crytals. The crystals were collected by filtration, washed with 2 x 20 mL THF, and dried under vacuum overnight. Yield: 55 mg (23 %) IR (ATR, $cm^{-1}$): 3343 (w, br), 2957 (vw), 1696 (m), 1659 (w), 1421 (vw), 1383 (w), 1291 (vs), 1259 (vs), 1225 (vs), 1188 (s), 1167 (m), 1030 (s), 963 (m), 939 (m), 917 (m), 803 (w), 761 (vw), 761 (m), 636 (vs). Elem. Anal. Calcd. for $C_{21}H_{28}ClF_6Mo_2N_4O_{13}S_6Yb$ ([(MeOH)$_3$YbMo$_2$(SNO5)$_4$Cl][OTf]$_2$): C, 20.16%; H, 2.26%; N, 4.48%. Found: C, 19.80%; H, 2.47%; N, 3.95%. MALDI-TOF MS (m/z): 970 ($M^{2+}$ - $CH_3^+$).

**tetrakis-methanol-lutetiumdimolybdenum-chloro-tetrakis-monothiosuccinimidato bis-triflate [(MeOH)$_4$LuMo$_2$(SNO5)$_4$Cl][OTf]$_2$ (2-Lu)**

310 mg Lu(OTf)$_3$ and 114 mg **1**·py (0.134 mmol) are added to a flask, dissolved in 15 mL MeOH, and stirred for 30 minutes. The reaction was filtered and layered with Et$_2$O, yielding large red crystals. The crystals were collected by filtration, washed with 2 x 20 mL THF, and dried under vacuum. Yield: 54 mg (31 %).IR (ATR, $cm^{-1}$): 3405 (br, vw), 1726 (m), 1666 (w), 1334 (vw), 1391 (vw), 1275 (vs), 1241 (vs), 1225 (vs), 1029 (s), 964 (w), 941 (w), 915 (w), 861 (w) 763 (w), 735 (w), 682 (w), 667 (m), 637 (vs). Elem. Anal. Calcd. for $C_{22}H_{32}ClF_6LuMo_2N_4O_{14}S_6$ ([(MeOH)$_4$LuMo$_2$(SNO5)$_4$Cl][OTf]$_2$): C, 20.56%; H, 2.51%; N, 4.36%. Found: C, 20.70%; H, 2.50%; N, 4.17%. MALDI-TOF MS (m/z): 974 ($M^{2+}$ - $CH_3^+$).

#### 5.6.1.3 X-ray crystallography

Single crystals of **2-Ce – 2-Lu** were selected under paratone oil and attached to a MiTeGen MicroMount. They were mounted in a stream of cold $N_2$ at 100(1) K using an Oxford Cryostat and centered in the X-ray beam using a video monitoring system. The crystal evaluation and data collection were performed on a Bruker Quazar APEX-II diffractometer with Mo Kα radiation (λ = 0.71073 Å) or a Bruker SMART APEX-II diffractometer with Cu Kα radiation (λ = 1.54178 Å). The data were collected using a routine to survey an entire sphere of reciprocal space. The data were integrated using the SAINT routine in APEX-II and corrected for absorption using SADABS. The structures were solved *via* direct methods and refined by iterative cycles of least-squares refinement on $F^2$ followed by difference Fourier synthesis using SHELX2013. All non-hydrogen atoms were refined anisotropically except where noted below. The alcohol hydrogen atoms on MeOH components of structures were located from the Fourier difference map and refined independently. All other hydrogen atoms were included in the final structure factor calculation at idealized positions and were allowed to ride on the neighboring atoms with relative isotropic displacement coefficients.

**Table 5.S1** Crystal data and structure refinement for **2-Ce – 2-Sm**

| Compound | **2-Ce** | **2-Pr** | **2-Nd** | **2-Sm** |
|---|---|---|---|---|
| Empirical formula | $[C_{21}H_{36}CeClMo_2N_4O_9S_4]^{2+}$, $2[CF_3O_3S]^-$, $2.28(CH_3OH)$ | $[C_{24}H_{39.41}Cl_{0.85}F_{0.44}Mo_2N_4O_{9.3}PrS_{4.15}]^{2+}$, $2[CF_3O_3S]^{2+}$, $2(CH_3OH)$ | $[C_{24}H_{40}ClMo_2N_4NdO_9S_4]^{2+}$, $2[CF_3O_3S]^-$, $2(CH_3OH)$ | $[C_{20}H_{32.39}ClMo_2N_4O_{8.19}S_4Sm]^{2+}$, $2[CF_3O_3S]^-$, $1.59(CH_3OH)$ |
| Formula weight | 1355.28 | 1399.42 | 1390.63 | 1314.93 |
| Temperature/K | 100.0 | 100.0 | 100.0 | 100.0 |
| Crystal system | monoclinic | orthorhombic | orthorhombic | monoclinic |
| Space group | $P2_1$ | $P2_12_12_1$ | $P2_12_12_1$ | $P2_1/c$ |
| a/Å | 12.2813(4) | 12.2702(5) | 12.252(5) | 12.1708(6) |
| b/Å | 25.9072(8) | 14.8949(6) | 14.934(5) | 14.675(2) |
| c/Å | 14.7974(5) | 26.3026(11) | 26.162(9) | 25.2765(19) |
| β/° | 90.0007(13) | 90 | 90 | 102.489(5) |
| Volume/Å$^3$ | 4708.1(3) | 4807.2(3) | 4787(3) | 4407.7(8) |
| Z | 4 | 4 | 4 | 4 |
| $\rho_{calc}$g/cm$^3$ | 1.912 | 1.934 | 1.930 | 1.982 |
| μ/mm$^{-1}$ | 1.889 | 1.920 | 1.994 | 18.503 |
| Crystal size/mm$^3$ | 0.373 × 0.262 × 0.112 | 0.4 × 0.3 × 0.2 | 0.102 × 0.055 × 0.029 | 0.214 × 0.147 × 0.107 |
| Radiation | MoKα (λ = 0.71073) | MoKα (λ = 0.71073) | MoKα (λ = 0.71073) | CuKα (λ = 1.54178) |
| 2Θ range for data collection/° | 2.752 to 61.092 | 3.096 to 55.088 | 3.114 to 51.522 | 7.008 to 147.134 |
| Reflections collected | 136238 | 113950 | 91193 | 74599 |
| Independent reflections | 28303 [$R_{int}$ = 0.0493, $R_{sigma}$ = 0.0365] | 11069 [$R_{int}$ = 0.0972, $R_{sigma}$ = 0.0471] | 9140 [$R_{int}$ = 0.1238, $R_{sigma}$ = 0.0722] | 8801 [$R_{int}$ = 0.0529, $R_{sigma}$ = 0.0267] |
| Data/restraints/parameters | 28303/48/1203 | 11069/317/728 | 9140/224/679 | 8801/122/611 |
| Goodness-of-fit on $F^2$ | 1.086 | 1.057 | 1.114 | 1.100 |
| Final R indexes [I>=2σ (I)] | $R_1$ = 0.0293 $wR_2$ = 0.0753 | $R_1$ = 0.0358 $wR_2$ = 0.0682 | $R_1$ = 0.0419 $wR_2$ = 0.1007 | $R_1$ = 0.0453 $wR_2$ = 0.1100 |
| Final R indexes [all data] | $R_1$ = 0.0294 $wR_2$ = 0.0754 | $R_1$ = 0.0428 $wR_2$ = 0.0708 | $R_1$ = 0.0476 $wR_2$ = 0.1025 | $R_1$ = 0.0479 $wR_2$ = 0.1116 |

[a]$R1 = \Sigma||F_o| - |F_c||/[\Sigma|F_o|]$. [b]$wR2 = |[\Sigma[w(F_o^2 - F_c^2)^2]/[\Sigma[w(F_o^2)^2]]]^{1/2}$, $w = 1/\sigma^2(F_o^2) + (aP)^2 + bP$, where $P = [\max(0 \text{ or } F_o^2) + 2(F_c^2)]/3$.

**Table 5.S2.** Crystal data and structure refinement for **2-Eu – 2-Dy**

| Compound | **2-Eu** | **2-Gd** | **2-Tb** | **2-Dy** |
|---|---|---|---|---|
| Empirical formula | $[C_{20}H_{32}ClEuMo_2N_4O_8S_4]^{2+}$, $2(CH_3OH)$, $2[CF_3O_3S]^-$ | $[C_{20}H_{32}Cl_{0.94}GdMo_2N_4O_8S_4]^{2+}$, $1.6(CH_3OH)$, $2.06[CF_3O_3S]^-$ | $[C_{20}H_{32}Cl_{0.95}TbMo_2N_4O_8S_4]^{2+}$, $1.62(CH_3OH)$, $2.05[CF_3O_3S]^-$ | $[C_{20}H_{32}ClDyMo_2N_4O_8S_4]^{2+}$, $2[CF_3O_3S]^-$, $1.65(CH_3OH)$ |
| Formula weight | 1326.25 | 1326.24 | 1327.18 | 1325.70 |
| Temperature/K | 100.0 | 100.0 | 100.0 | 100.0 |
| Crystal system | monoclinic | monoclinic | monoclinic | monoclinic |
| Space group | $P2_1/c$ | $P2_1/c$ | $P2_1/c$ | $P2_1/c$ |
| a/Å | 12.1538(14) | 12.156(2) | 12.139(3) | 12.167(3) |
| b/Å | 14.6610(10) | 14.6376(12) | 14.591(4) | 14.543(5) |
| c/Å | 25.3417(18) | 25.379(2) | 25.402(7) | 25.278(7) |
| α/° | 90 | 90 | 90 | 90 |
| β/° | 102.483(9) | 102.468(8) | 102.552(11) | 103.045(12) |
| γ/° | 90 | 90 | 90 | 90 |
| Volume/Å$^3$ | 4408.8(7) | 4409.5(9) | 4392(2) | 4358(2) |
| Z | 4 | 4 | 4 | 4 |
| $\rho_{calc}$g/cm$^3$ | 1.998 | 1.998 | 2.007 | 2.021 |
| μ/mm$^{-1}$ | 18.689 | 18.225 | 2.593 | 2.705 |
| Radiation | CuKα (λ = 1.54178) | CuKα (λ = 1.54178) | MoKα (λ = 0.71073) | MoKα (λ = 0.71073) |
| 2Θ range for data collection/° | 7.008 to 147.078 | 7.014 to 147.058 | 3.238 to 61.218 | 3.252 to 51.456 |
| Reflections collected | 74341 | 74964 | 125173 | 85282 |
| Independent reflections | 8783 [$R_{int}$ = 0.0493, $R_{sigma}$ = 0.0257] | 8802 [$R_{int}$ = 0.0704, $R_{sigma}$ = 0.0382] | 13521 [$R_{int}$ = 0.0394, $R_{sigma}$ = 0.0204] | 8303 [$R_{int}$ = 0.0314, $R_{sigma}$ = 0.0144] |
| Data/restraints/parameters | 8783/202/652 | 8802/166/647 | 13521/159/647 | 8303/203/646 |
| Goodness-of-fit on $F^2$ | 1.099 | 1.097 | 1.259 | 1.338 |
| Final R indexes [I>=2σ (I)] | $R_1$ = 0.0400<br>$wR_2$ = 0.0917 | $R_1$ = 0.0442<br>$wR_2$ = 0.0955 | $R_1$ = 0.0400<br>$wR_2$ = 0.0864 | $R_1$ = 0.0463<br>$wR_2$ = 0.1007 |
| Final R indexes [all data] | $R_1$ = 0.0442<br>$wR_2$ = 0.0937 | $R_1$ = 0.0539<br>$wR_2$ = 0.0995 | $R_1$ = 0.0445<br>$wR_2$ = 0.0881 | $R_1$ = 0.0475<br>$wR_2$ = 0.1012 |

[a]$R1 = \Sigma||F_o| - |F_c||/[\Sigma|F_o|]$. [b]$wR2 = |[\Sigma[w(F_o^2 - F_c^2)^2]/[\Sigma[w(F_o^2)^2]]]^{1/2}$, $w = 1/\sigma^2(F_o^2) + (aP)^2 + bP$, where $P = [\max(0 \text{ or } F_o^2) + 2(F_c^2)]/3$.

**Table 5.S3.** Crystal data and structure refinement for **2-Ho – 2-Lu**

| Compound | **2-Ho** | **2-Er** | **2-Tm** | **2-Yb** | **2-Lu** |
|---|---|---|---|---|---|
| Empirical formula | $[C_{20}H_{32}ClHoMo_2N_4O_8S_4]^{2+}$ $2[CF_3O_3S]^-$, $1.74(CH_3OH)$ | $[C_{20}H_{32}ClErMo_2N_4O_8S_4]^{2+}$ $2[CF_3O_3S]^-$, $1.70(CH_3OH)$ | $[C_{20}H_{32}Cl_{0.96}TmMo_2N_4O_8S_4]^{2+}$, $1.62(CH_3OH)$, $2.04[CF_3O_3S]^-$ | $[C_{20}H_{32}ClYbMo_2N_4O_8S_4]^{2+}$, $2[CF_3O_3S]^-$, $1.82(CH_3OH)$ | $[C_{20}H_{32}ClLuMo_2N_4O_8S_4]^{2+}$, $2[CF_3O_3S]^-$, $2(CH_3OH)$ |
| Formula weight | 1330.47 | 1332.80 | 1335.25 | 1341.86 | 1349.26 |
| Temperature/K | 100.0 | 100.0 | 100.0 | 100.0 | 100.0 |
| Crystal system | monoclinic | monoclinic | monoclinic | monoclinic | monoclinic |
| Space group | $P2_1/c$ | $P2_1/c$ | $P2_1/c$ | $P2_1/c$ | $P2_1/n$ |
| a/Å | 12.1361(7) | 12.1274(5) | 12.120(3) | 12.1194(6) | 12.130(3) |
| b/Å | 14.5800(11) | 14.5686(19) | 14.548(5) | 14.5641(9) | 15.095(4) |
| c/Å | 25.422(3) | 25.4000(15) | 25.363(6) | 25.3857(17) | 25.171(7) |
| β/° | 102.514(5) | 102.479(4) | 102.452(14) | 102.539(3) | 103.742(12) |
| Volume/Å$^3$ | 4391.4(6) | 4381.7(6) | 4367(2) | 4373.9(5) | 4477(2) |
| Z | 4 | 4 | 4 | 4 | 4 |
| $\rho_{calc}$g/cm$^3$ | 2.012 | 2.020 | 2.031 | 2.038 | 2.002 |
| μ/mm$^{-1}$ | 11.894 | 12.103 | 3.020 | 12.522 | 3.170 |
| Crystal size/mm$^3$ | 0.115 × 0.095 × 0.055 | 0.115 × 0.095 × 0.055 | 0.115 × 0.095 × 0.055 | 0.115 × 0.095 × 0.055 | 0.115 × 0.095 × 0.055 |
| Radiation | CuKα (λ = 1.54178) | CuKα (λ = 1.54178) | MoKα (λ = 0.71073) | CuKα (λ = 1.54178) | MoKα (λ = 0.71073) |
| 2Θ range for data collection/° | 7.032 to 144.654 | 7.036 to 144.706 | 3.246 to 61.376 | 7.04 to 144.652 | 3.17 to 65.686 |
| Reflections collected | 74565 | 74455 | 124888 | 73910 | 142906 |
| Independent reflections | 8635 [$R_{int}$ = 0.0300, $R_{sigma}$ = 0.0143] | 8630 [$R_{int}$ = 0.0363, $R_{sigma}$ = 0.0178] | 13451 [$R_{int}$ = 0.0248, $R_{sigma}$ = 0.0125] | 8618 [$R_{int}$ = 0.0494, $R_{sigma}$ = 0.0228] | 16550 [$R_{int}$ = 0.0345, $R_{sigma}$ = 0.0200] |
| Data/restraints/parameters | 8635/184/625 | 8630/172/620 | 13451/206/658 | 8618/206/642 | 16550/12/561 |
| Goodness-of-fit on $F^2$ | 1.270 | 1.157 | 1.114 | 1.263 | 1.072 |
| Final R indexes [I>=2σ (I)] | $R_1$ = 0.0356 $wR_2$ = 0.0788 | $R_1$ = 0.0287 $wR_2$ = 0.0647 | $R_1$ = 0.0229 $wR_2$ = 0.0528 | $R_1$ = 0.0416 $wR_2$ = 0.0995 | $R_1$ = 0.0220 $wR_2$ = 0.0512 |
| Final R indexes [all data] | $R_1$ = 0.0362 $wR_2$ = 0.0791 | $R_1$ = 0.0305 $wR_2$ = 0.0655 | $R_1$ = 0.0248 $wR_2$ = 0.0538 | $R_1$ = 0.0417 $wR_2$ = 0.0996 | $R_1$ = 0.0267 $wR_2$ = 0.0530 |

[a]$R1 = \Sigma||F_o| - |F_c||/[\Sigma|F_o|]$. [b]$wR2 = |[\Sigma[w(F_o^2 - F_c^2)^2]/[\Sigma[w(F_o^2)^2]]]^{1/2}$, $w = 1/\sigma^2(F_o^2) + (aP)^2 + bP$, where $P = [\max(0 \text{ or } F_o^2) + 2(F_c^2)]/3$.

**Table 5.S4** Crystal data and structure refinement for **3-Eu.**

| Identification code | **3-Eu** |
|---|---|
| Empirical formula | $C_{34}H_{32}ClEuF_6Mo_4N_8O_{14}S_{10}$ |
| Formula weight | 1782.44 |
| Temperature/K | 100.0 |
| Crystal system | tetragonal |
| Space group | $I\bar{4}2m$ |
| a/Å | 21.981(9) |
| b/Å | 21.981(9) |
| c/Å | 32.322(15) |
| α/° | 90 |
| β/° | 90 |
| γ/° | 90 |
| Volume/Å$^3$ | 15617(15) |
| Z | 8 |
| $\rho_{calc}$g/cm$^3$ | 1.516 |
| μ/mm$^{-1}$ | 1.779 |
| F(000) | 6928.0 |
| Crystal size/mm$^3$ | 0.099 × 0.097 × 0.037 |
| Radiation | MoKα (λ = 0.71073) |
| 2Θ range for data collection/° | 2.24 to 56.51 |
| Index ranges | -29 ≤ h ≤ 29, -29 ≤ k ≤ 29, -42 ≤ l ≤ 42 |
| Reflections collected | 163840 |
| Independent reflections | 10018 [$R_{int}$ = 0.0895, $R_{sigma}$ = 0.0410] |
| Data/restraints/parameters | 10018/1094/647 |
| Goodness-of-fit on F$^2$ | 1.056 |
| Final R indexes [I>=2σ (I)][a,b] | $R_1$ = 0.0298, $wR_2$ = 0.0697 |
| Final R indexes [all data][a,b] | $R_1$ = 0.0377, $wR_2$ = 0.0726 |
| Largest diff. peak/hole / e Å$^{-3}$ | 0.72/-0.73 |
| Flack parameter | 0.237(9) |

[a]$R1 = \Sigma||F_o| - |F_c||/[\Sigma|F_o|]$. [b]$wR2 = |[\Sigma[w(F_o^2 - F_c^2)^2]/[\Sigma[w(F_o^2)^2]]]^{1/2}$, $w = 1/\sigma^2(F_o^2) + (aP)^2 + bP$, where $P = [\max(0 \text{ or } F_o^2) + 2(F_c^2)]/3$.

### 5.6.1.4 Electrochemistry

Compounds **2-Ce – 2-Lu** were dissolved in propylene carbonate and chloride was removed by addition of 1.1 eq of $TlPF_6$, giving dehalogenated compounds **2a-Ce – 2a-Lu**. The TlCl that precipitated was removed by filtration. Cyclic voltammograms for compounds **2a-Ce – 2a-Lu** were taken in propylene carbonate at room temperature with 2 mM analyte and 100 mM electrolyte ($NEt_4PF_6$) using a standard glassy carbon electrode for the working electrode, a platinum wire for the auxiliary electrode, and an $Ag/Ag^+$ electrode as the reference electrode. The solutions were titrated with 10 mL of a

0.05 M solution of $Ln(OTf)_n$ in propylene carbonate, resulting in an unchanging $[Mo_2]^{4+/5+}$ redox peak. All electrochemical potentials were internally referenced to the ferrocene/ferrocenium couple. The voltammetry was performed in the range of 1000 mV to -100 mV vs. $Ag/Ag^+$ at a scan rate of 100 mV $s^{-1}$.

### 5.6.2 Results

#### 5.6.2.1 X-ray Crystallography

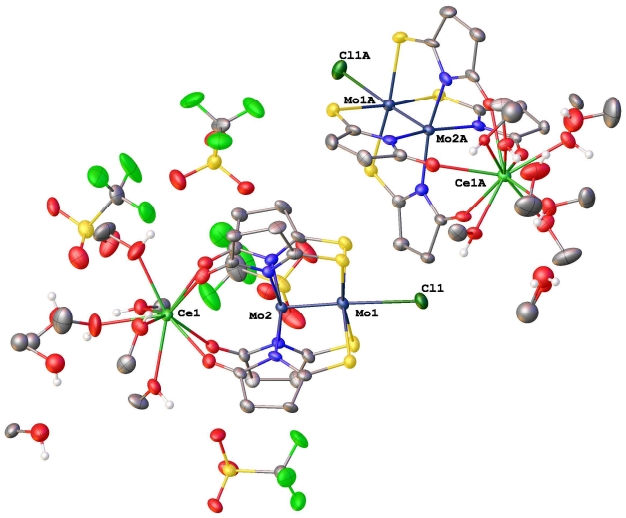


**Figure 5.S1.** The asymmetric unit of **2-Ce**, including all disordered components. All atoms are drawn as 50% thermal probability ellipsoids. All H atoms, except methanol OH protons, are omitted for clarity.

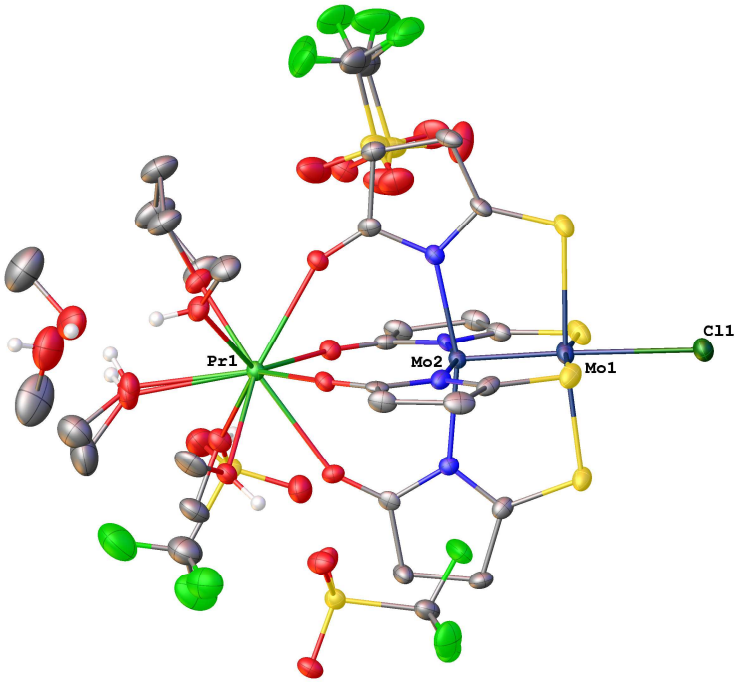


**Figure 5.S2**. The asymmetric unit of **2-Pr**, including all disordered components. All atoms are drawn as 50% thermal probability ellipsoids. All H atoms, except methanol OH protons, are omitted for clarity.

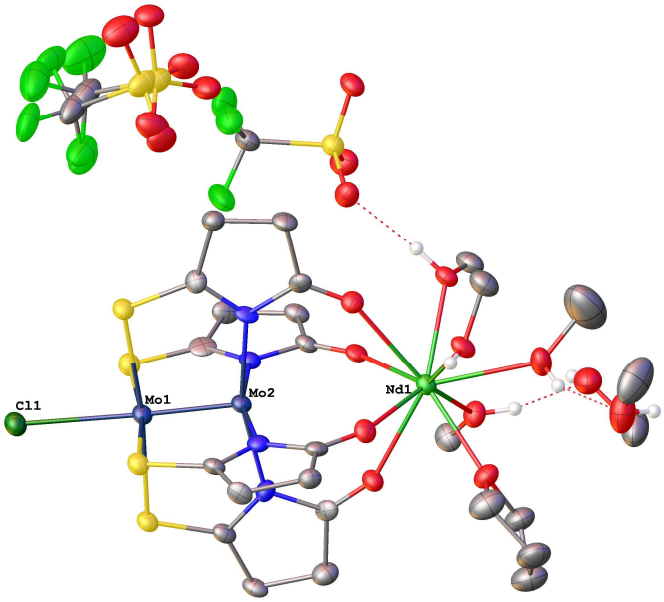


**Figure 5.S3**. The asymmetric unit of **2-Nd**, including all disordered components. All atoms are drawn as 50% thermal probability ellipsoids. All H atoms, except methanol OH protons, are omitted for clarity.

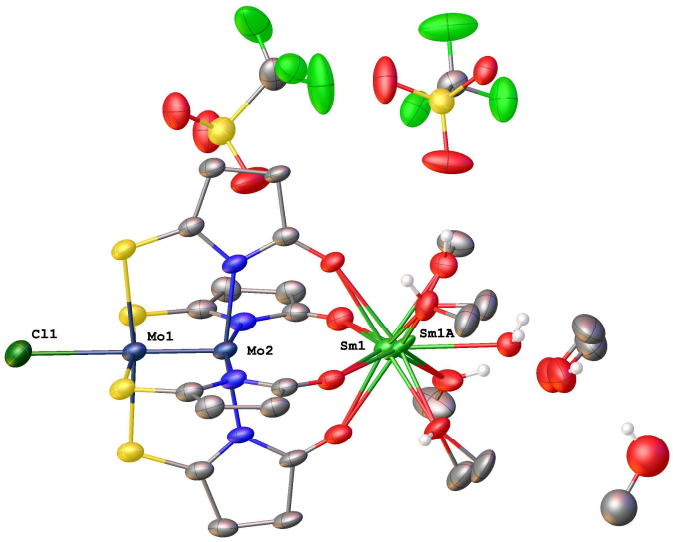


**Figure 5.S4.** The asymmetric unit of **2-Sm**, including all disordered components. All atoms are drawn as 50% thermal probability ellipsoids. All H atoms, except methanol OH protons, are omitted for clarity.

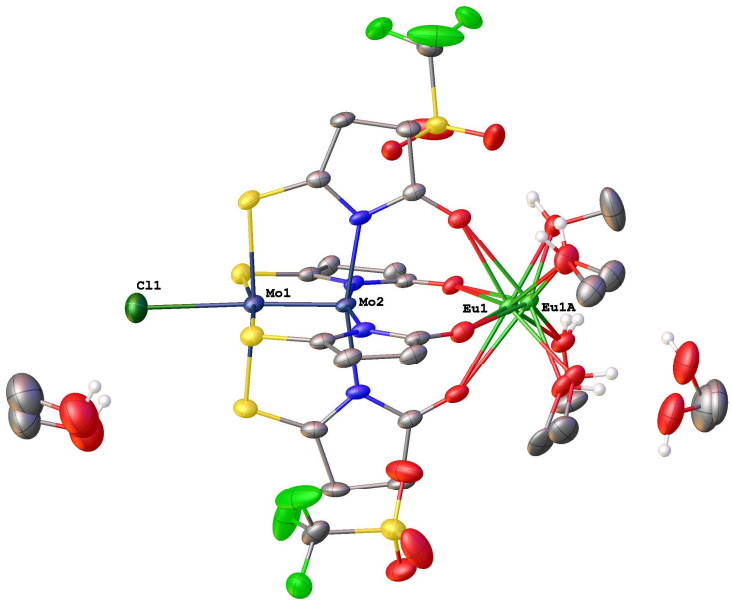


**Figure 5.S5.** The asymmetric unit of **2-Eu**, including all disordered components. All atoms are drawn as 50% thermal probability ellipsoids. All H atoms, except methanol OH protons, are omitted for clarity.

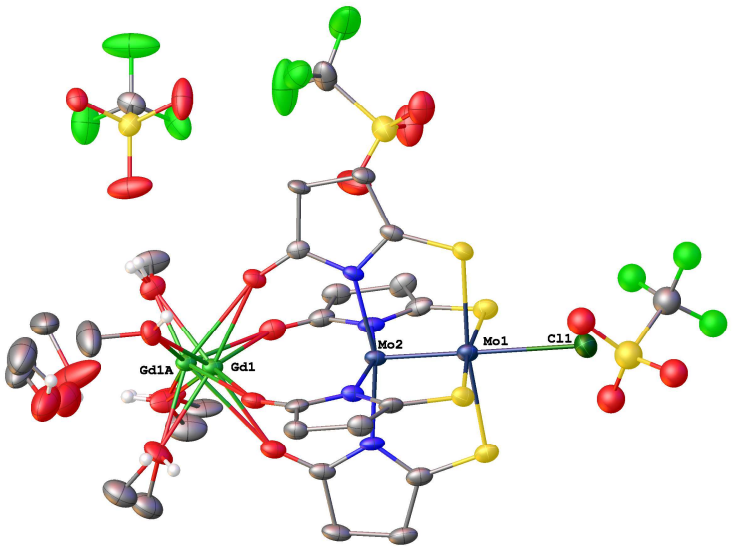


**Figure 5.S6.** The asymmetric unit of **2-Gd**, including all disordered components. All atoms are drawn as 50% thermal probability ellipsoids. All H atoms, except methanol OH protons, are omitted for clarity.

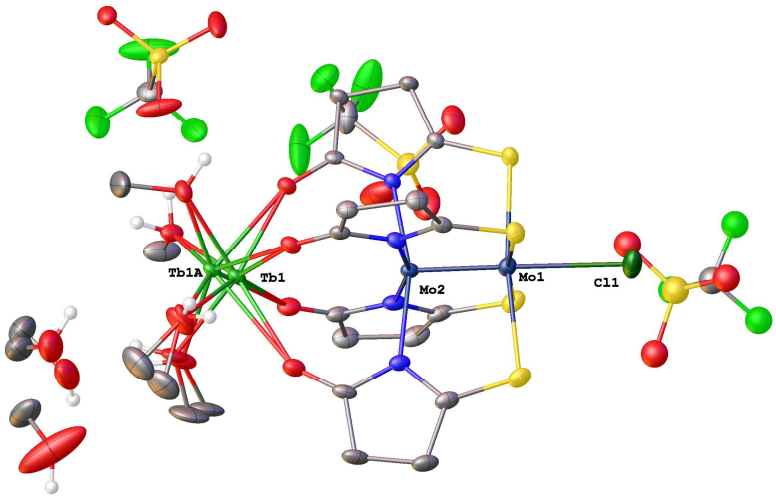


**Figure 5.S7.** The asymmetric unit of **2-Tb**, including all disordered components. All atoms are drawn as 50% thermal probability ellipsoids. All H atoms, except methanol OH protons, are omitted for clarity.

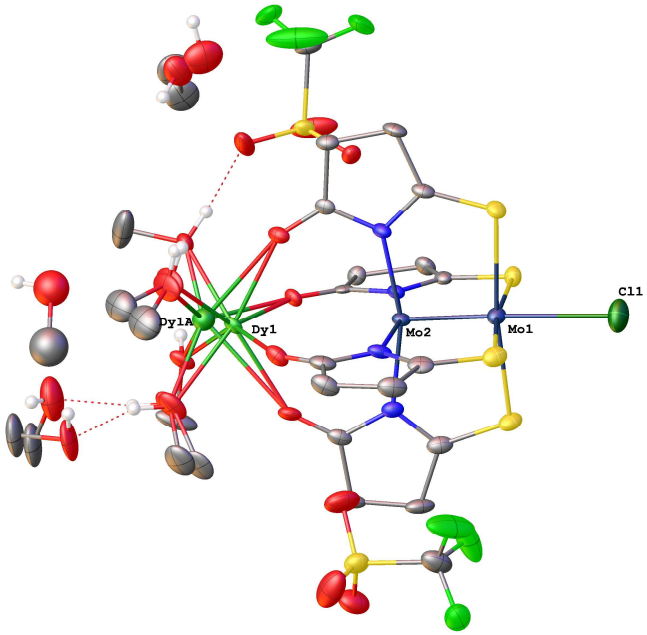


**Figure 5.S8.** The asymmetric unit of **2-Dy**, including all disordered components. All atoms are drawn as 50% thermal probability ellipsoids. All H atoms, except methanol OH protons, are omitted for clarity.

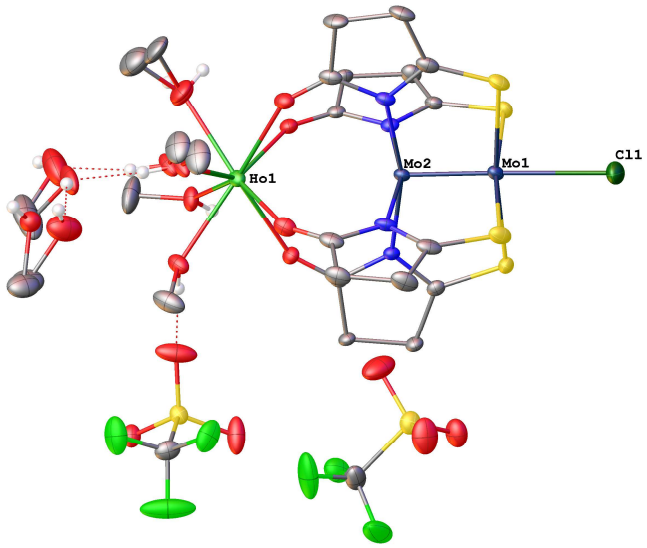


**Figure 5.S9.** The asymmetric unit of **2-Ho**, including all disordered components. All atoms are drawn as 50% thermal probability ellipsoids. All H atoms, except methanol OH protons, are omitted for clarity.

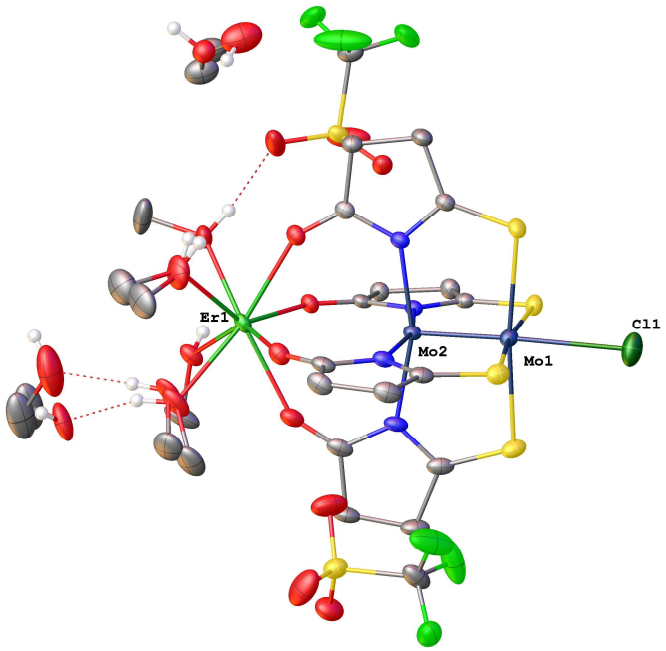


**Figure 5.S10.** The asymmetric unit of **2-Er**, including all disordered components. All atoms are drawn as 50% thermal probability ellipsoids. All H atoms, except methanol OH protons, are omitted for clarity.

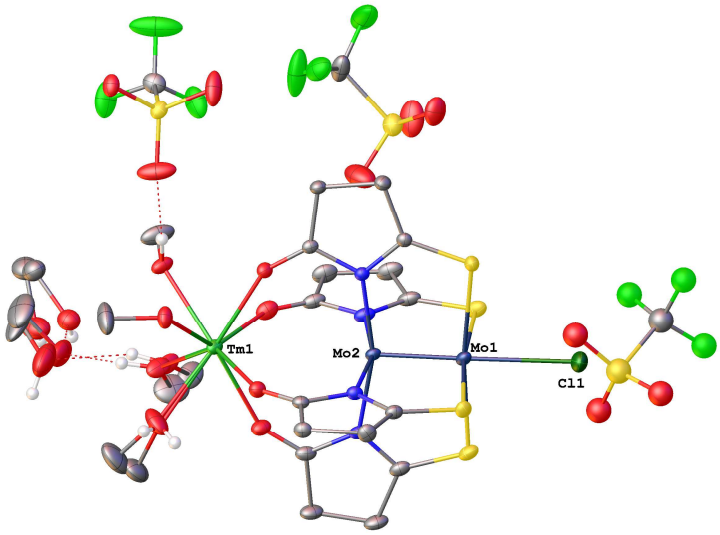


**Figure 5.S11.** The asymmetric unit of **2-Tm**, including all disordered components. All atoms are drawn as 50% thermal probability ellipsoids. All H atoms, except methanol OH protons, are omitted for clarity.

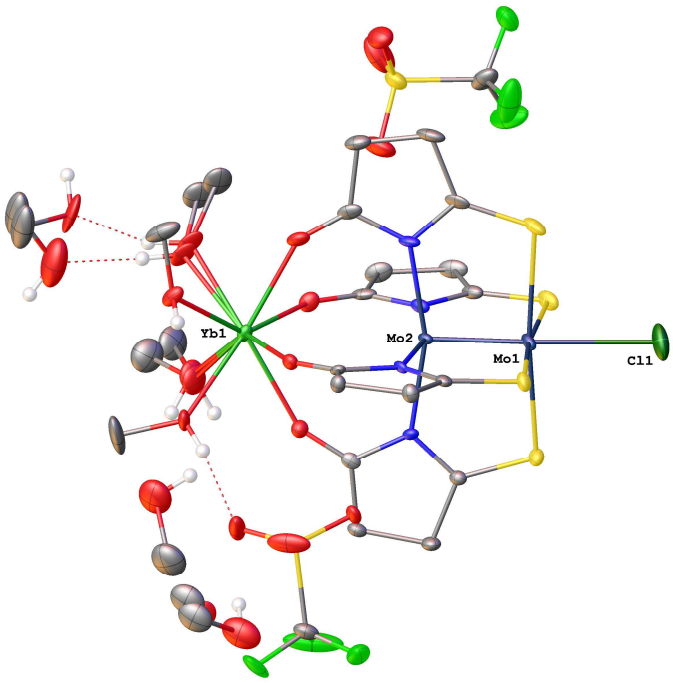


**Figure 5.S12.** The asymmetric unit of **2-Yb**, including all disordered components. All atoms are drawn as 50% thermal probability ellipsoids. All H atoms, except methanol OH protons, are omitted for clarity.

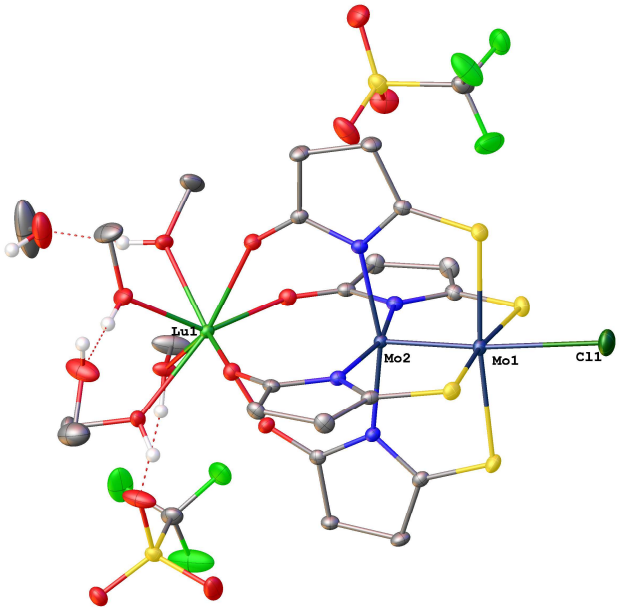


**Figure 5.S13.** The asymmetric unit of **2-Lu**. All atoms are drawn as 50% thermal probability ellipsoids. All H atoms, except methanol OH protons, are omitted for clarity.

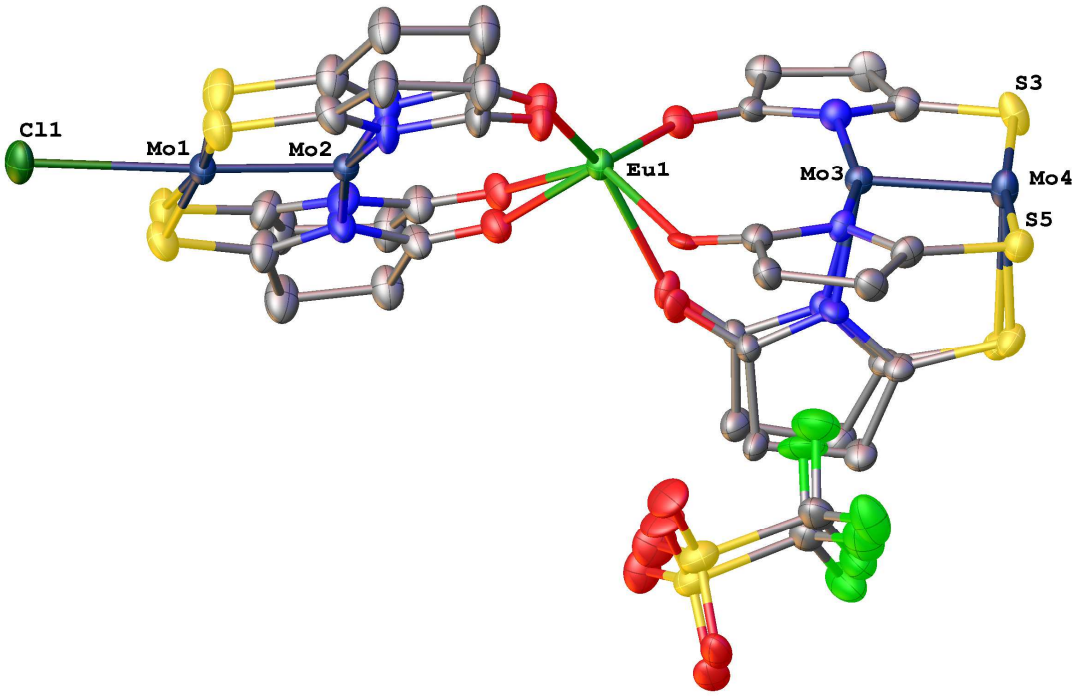


**Figure 5.S14.** The asymmetric unit of **3-Eu** including all disordered components. All atoms are drawn as 50% thermal ellipsoids. All H atoms are omitted for clarity.

### 5.6.2.2 Cyclic Voltammograms

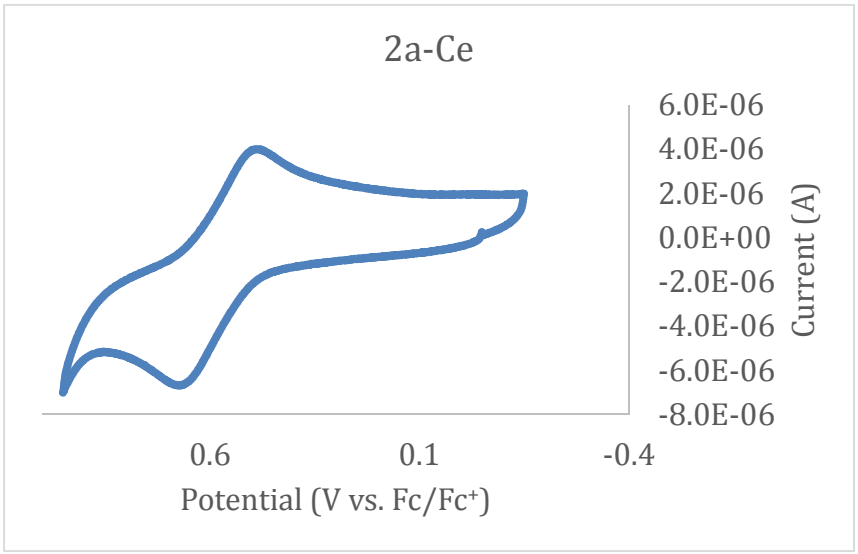


**Figure 5.S15.** The cyclic voltammogram of **2a-Ce**.

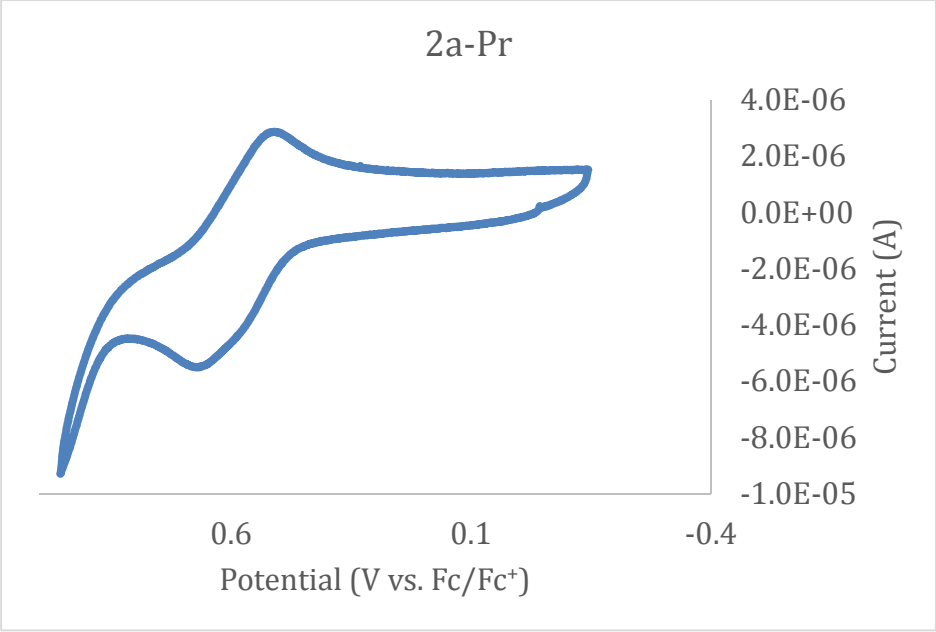


**Figure 5.S16.** The cyclic voltammogram of **2a-Pr**.

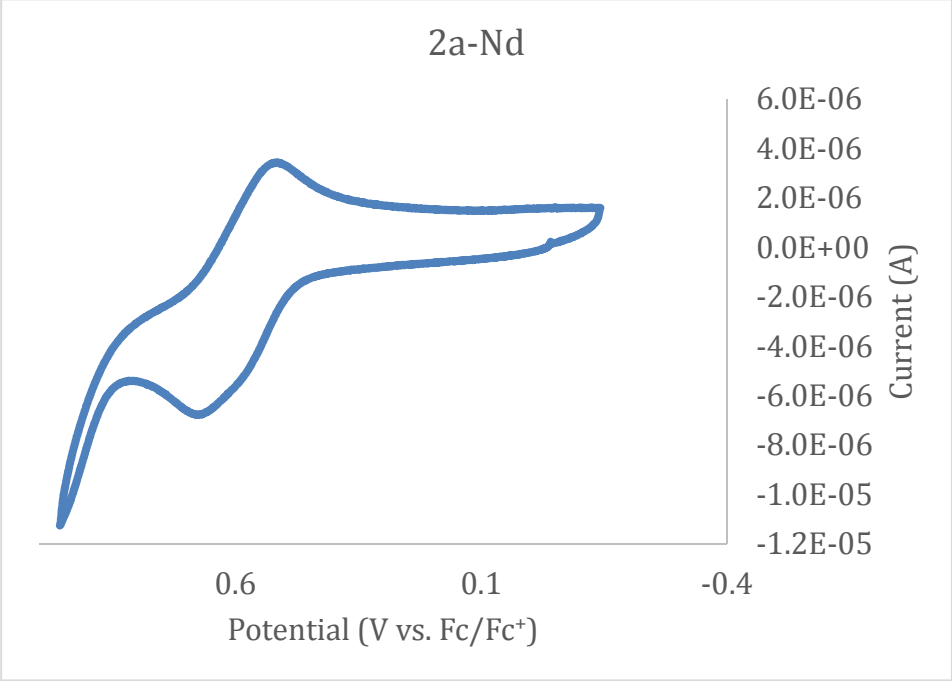


**Figure 5.S17.** The cyclic voltammogram of **2a-Nd**.

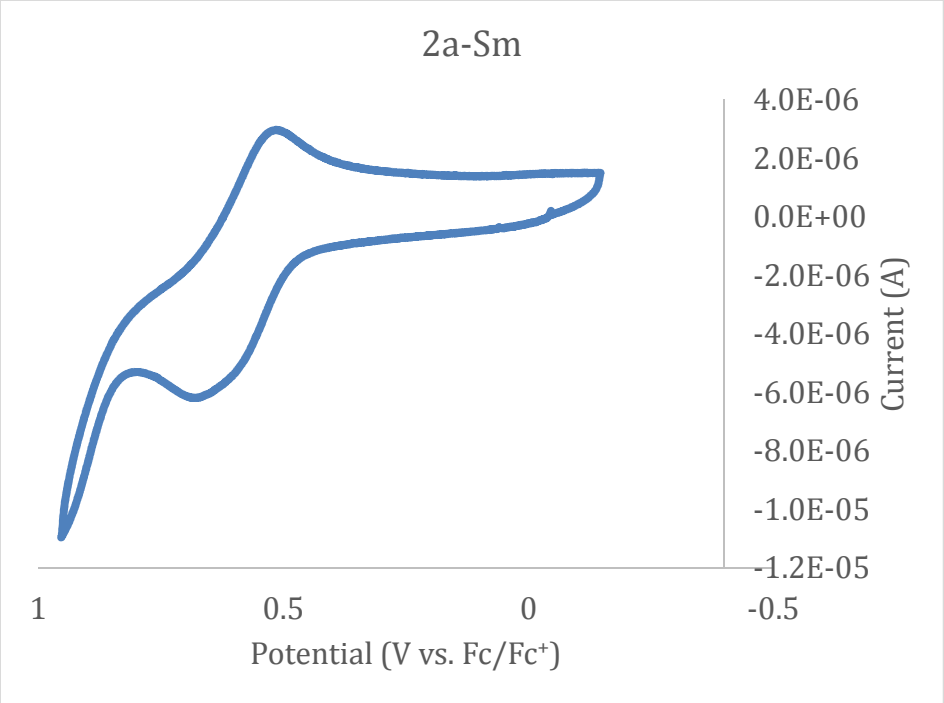


**Figure 5.S18.** The cyclic voltammogram of **2a-Sm**.

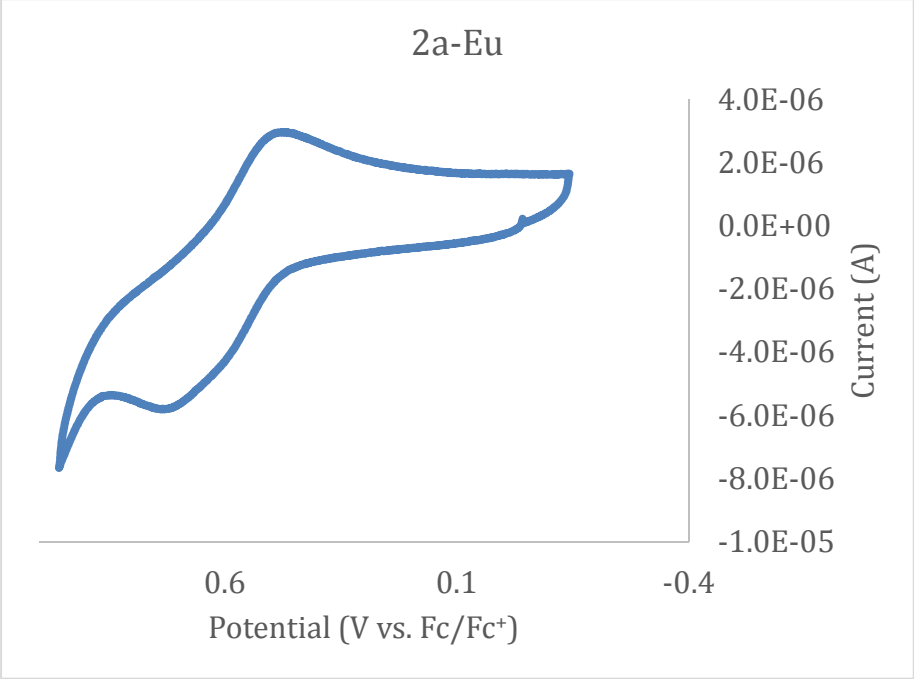


**Figure 5.S19.** The cyclic voltammogram of **2a-Eu**.

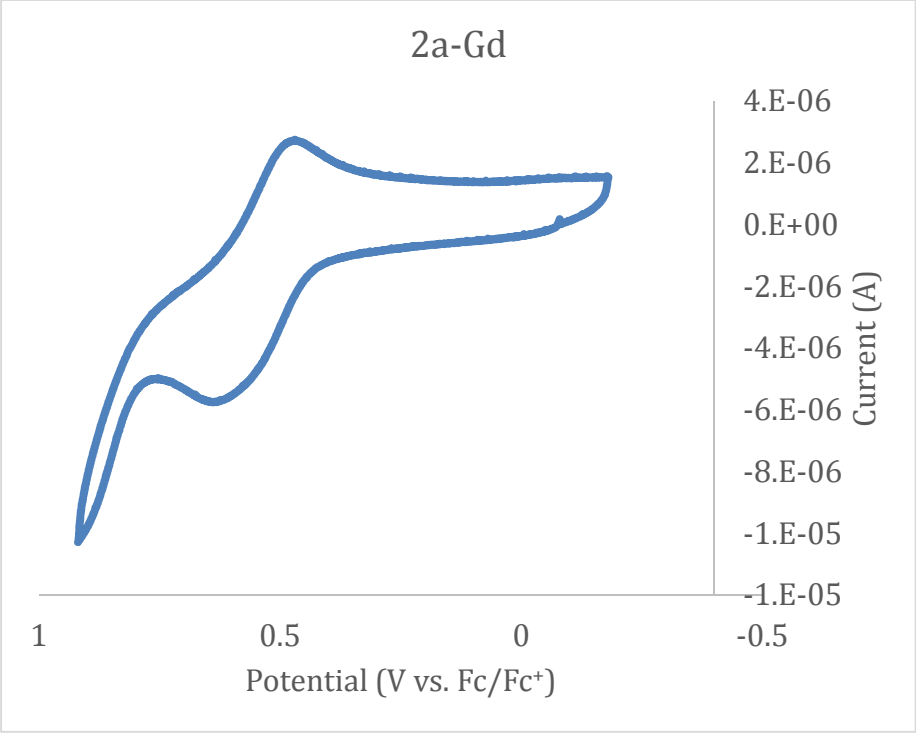


**Figure 5.S20.** The cyclic voltammogram of **2a-Gd**.

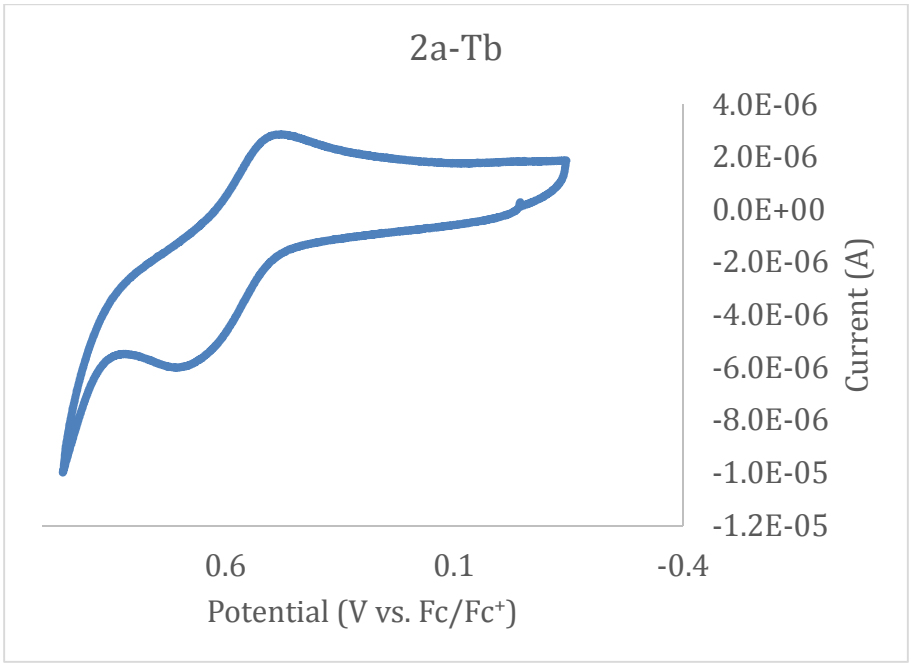


**Figure 5.S21.** The cyclic voltammogram of **2a-Tb**.

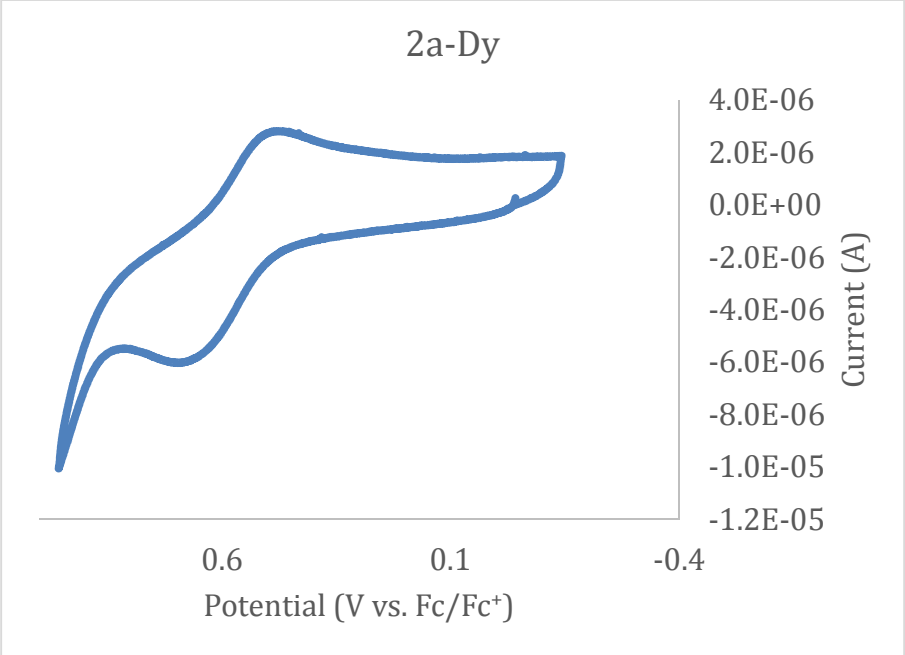


**Figure 5.S22.** The cyclic voltammogram of **2a-Dy.**

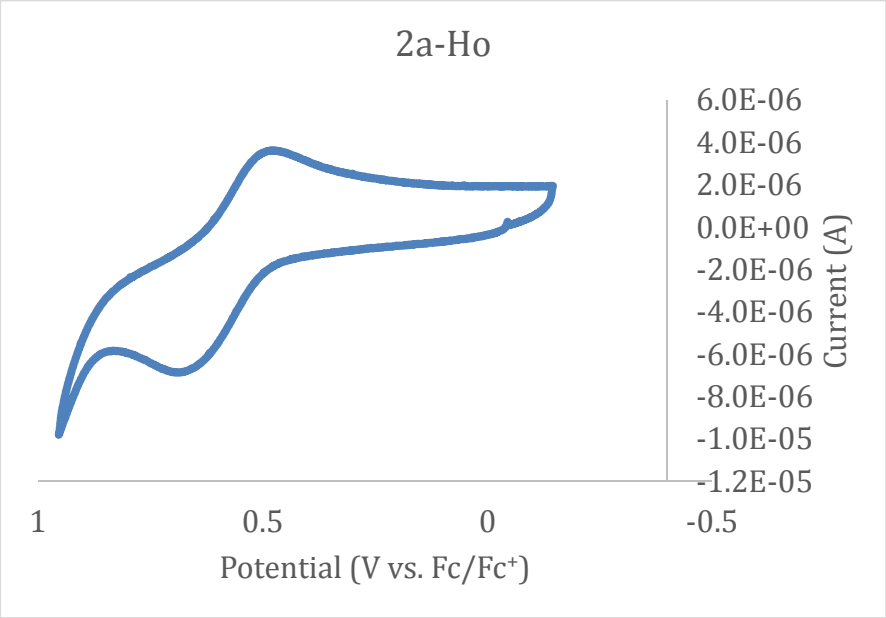


**Figure 5.S23.** The cyclic voltammogram of **2a-Ho.**

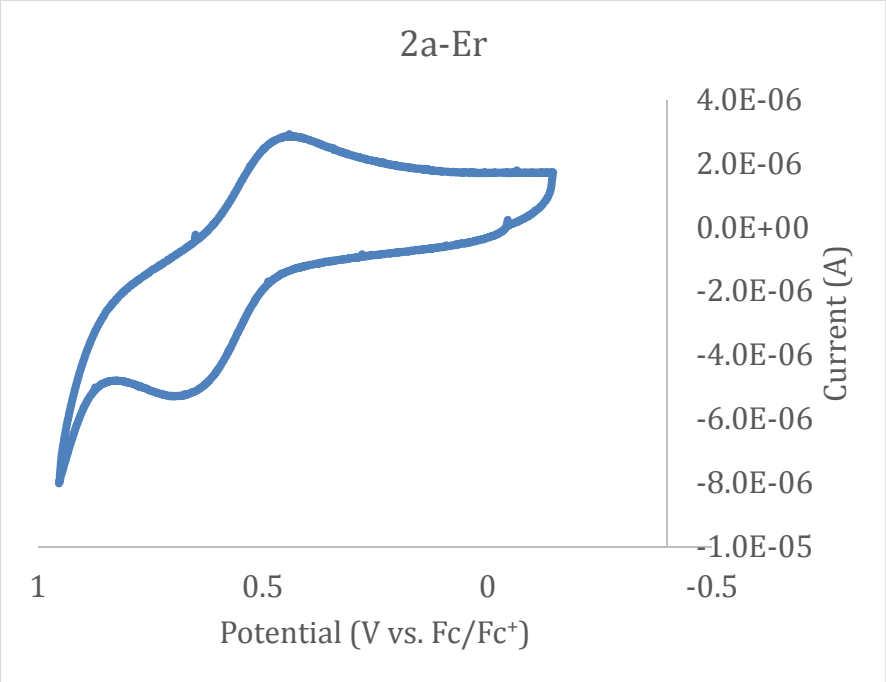


**Figure 5.S24.** The cyclic voltammogram of **2a-Er.**

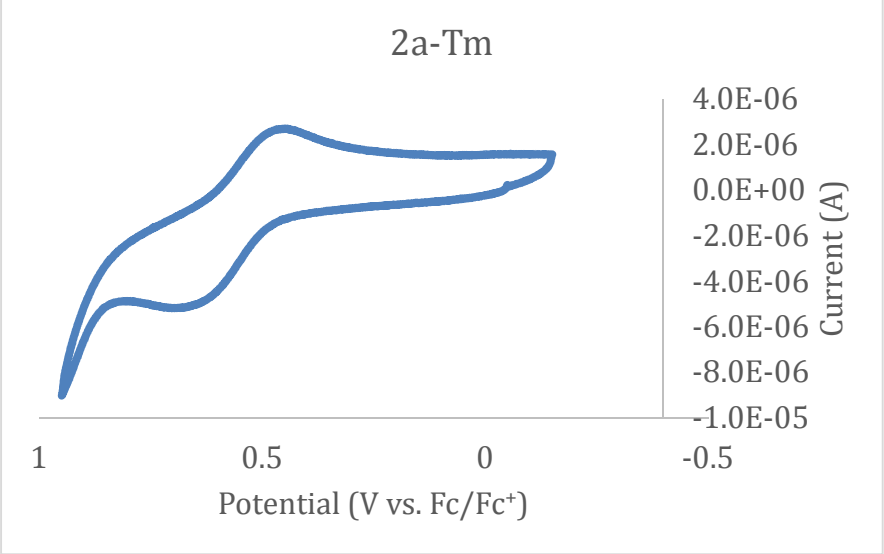


**Figure 5.S25.** The cyclic voltammogram of **2a-Tm**.

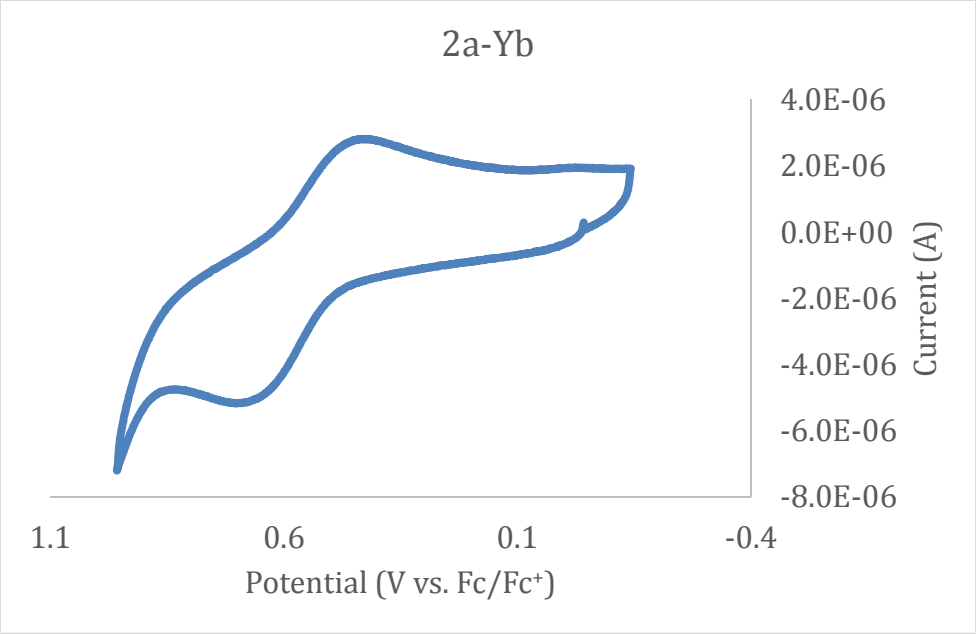


**Figure 5.S26.** The cyclic voltammogram of **2a-Yb.**

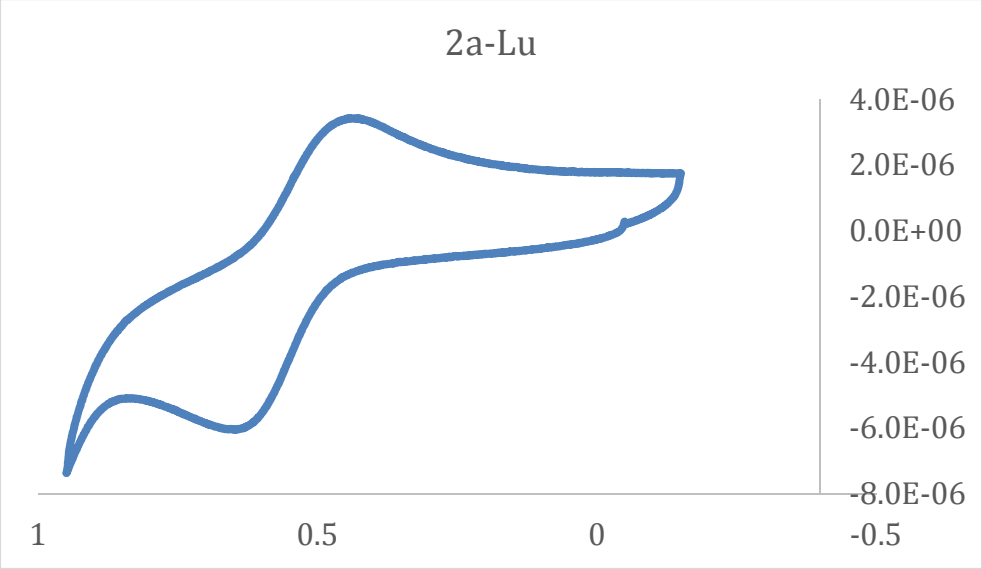


**Figure 5.S27.** The cyclic voltammogram of **2a-Lu.**

### 5.7 References

1. Bünzli, J.-C. *J. Coor. Chem.* **2014**, *67*, 3706.

2. (a) Winpenny, R. E. P. *Chem. Soc. Rev.* **1998**, *27*, 447. (b) Merca, A.; Müller, A.; van Slageren, J.; Läge, M.; Krebs, B. *J. Clust. Sci.* **2007**, *18*, 711. (c) Chen, W.; Li, Y.; Wang,

Y.; Wang, E.; Zhang, Z. *Dalton Trans.* **2008**, 865. (d) Fang, X.; Kogerler, P., *Angew. Chem. Int. Ed.* **2008**, *47*, 8123. (e) Nohra, B.; Mialane, P.; Dolbecq, A.; Riviere, E.; Marrot, J.; Secheresse, F. *Chem. Commun.* **2009**, 2703. (f) Andruh, M.; Costes, J.-P.; Diaz, C.; Gao, S., *Inorg. Chem.* **2009**, *48*, 3342. (g) Reinoso, S.; Galan-Mascaros, J. R. *Inorg. Chem.* **2010**, *49*, 377. (h) Reinoso, S. *Dalton Trans.* **2011**, *40*, 6610. (i) Feng, X.; Zhou, W.; Li, Y.; Ke, H.; Tang, J.; Clerac, R.; Wang, Y.; Su, Z.; Wang, E. *Inorg. Chem.* **2012**, *51*, 2722. (j) Zhang, Z. M.; Li, Y. G.; Yao, S.; Wang, E. B. *Dalton Trans.* **2011**, *40*, 6475. (k) Reinoso, S.; Galan-Mascaros, J. R.; Lezama, L. *Inorg. Chem.* **2011**, *50*, 9587. (l) Wu, H. H.; Yao, S.; Zhang, Z. M.; Li, Y. G.; Song, Y.; Liu, Z. J.; Han, X. B.; Wang, E. B. *Dalton Trans.* **2013**, *42*, 342. (m) Rosado Piquer, L.; Sanudo, E. C. *Dalton Trans.* **2015**, *44*, 8771. (n) Singh, S. K.; Beg, M. F.; Rajaraman, G. *Chem. Eur. J.* **2016**, *22*, 672.

3. (a) Chen, F.-F.; Chen, Z.-Q.; Bian, Z.-Q.; Huang, C.-H. *Coord. Chem. Rev.* **2010**, *254*, 991. (b) Meyer, L. V.; Schonfeld, F.; Muller-Buschbaum, K. *Chem. Commun.* **2014**, *50*, 8093. (c) Xu, L.-J.; Xu, G.-T.; Chen, Z.-N. *Coord. Chem. Rev.* **2014**, *273-274*, 47. (d) Zeng, G.; Xing, S.; Wang, X.; Yang, Y.; Ma, D.; Liang, H.; Gao, L.; Hua, J.; Li, G.; Shi, Z.; Feng, S. *Inorg. Chem.* **2016**, *55*, 1089.

4. (a) Nippe, M.; Berry, J. F. *J. Am. Chem. Soc.* **2007**, *129*, 12684. (b) Mashima, K.; Shimoyama, Y.; Kusumi, Y.; Fukumoto, A.; Yamagata, T.; Ohashi, M. *Eur. J. Inorg. Chem.* **2007**, *2007*, 235. (c) Ohashi, M.; Shima, A.; Rüffer, T.; Mizomoto, H.; Kaneda, Y.; Mashima, K. *Inorg. Chem.* **2007**, *46*, 6702. (d) Yin, C.; Huang, G.-C.; Kuo, C.-K.; Fu, M.-D.; Lu, H.-C.; Ke, J.-H.; Shih, K.-N.; Huang, Y.-L.; Lee, G.-H.; Yeh, C.-Y.; Chen, C.-h.; Peng, S.-M. *J. Am. Chem. Soc.* **2008**, *130*, 10090. (e) Nippe, M.; Timmer, G. H.; Berry, J. F. *Chem. Commun.* **2009**, 4357. (f) Nippe, M.; Victor, E.; Berry, J. F. *Eur. J.*

*Inorg. Chem.* **2008**, *2008*, 5569. (g) Pal, K.; Nakao, K.; Mashima, K. *Eur. J. Inorg. Chem.* **2010**, 5668. (h) Nippe, M.; Turov, Y.; Berry, J. F. *Inorg. Chem.* **2011**, *50*, 10592. (i) Wang, W.-Z.; Ismayilov, R. H.; Wang, R.-R.; Huang, Y.-L.; Yeh, C.-Y.; Lee, G.-H.; Peng, S.-M. *Dalton Trans.* **2008**, 6808. (j) Nippe, M.; Wang, J.; Bill, E.; Hope, H.; Dalal, N. S.; Berry, J. F. *J. Am. Chem. Soc.* **2010**, *132*, 14261. (k) Yeh, C.-W.; Liu, I. P.-C.; Wang, R.-R.; Yeh, C.-Y.; Lee, G.-H.; Peng, S.-M. *Eur. J. Inorg. Chem.* **2010**, 3153. (l) Turov, Y.; Berry, J. F. *Dalton Trans.* **2012**, *41*, 8153. (m) Dolinar, B. S.; Berry, J. F. *Inorg. Chem.* **2013**, *52*, 4658. (n) Dolinar, B. S.; Berry, J. F. *Polyhedron* **2016**, *103*, 71. (o) Brogden, D. W.; Berry, J. F. *Inorg. Chem.* **2015**, *54*, 7660. (p) Brogden, D. W.; Christian, J. H.; Dalal, N. S.; Berry, J. F. *Inorg. Chim. Acta* **2015**, *424*, 241.

5. (a) Clerac, R.; Cotton, F. A.; Daniels, L. M.; Dunbar, K. R.; Kirschbaum, K.; Murillo, C. A.; Pinkerton, A. A.; Schultz, A. J.; Wang, X. *J. Am. Chem. Soc.* **2000**, *122*, 6226. (b) Kuo, C. K.; Chang, J. C.; Yeh, C. Y.; Lee, G. H.; Wang, C. C.; Peng, S. M. *Dalton Trans.* **2005**, 3696. (c) Chae, D. H.; Berry, J. F.; Jung, S.; Cotton, F. A.; Murillo, C. A.; Yao, Z. *Nano Lett.* **2006**, *6*, 165. (d) Chen, I.-W. P.; Fu, M.-D.; Tseng, W.-H.; Yu, J.-Y.; Wu, S.-H.; Ku, C.-J.; Chen, C.-H.; Peng, S.-M. *Angew. Chem. Int. Ed.* **2006**, *45*, 5814. (e) Kuo, C.-K.; Liu, I. P.-C.; Yeh, C.-Y.; Chou, C.-H.; Tsao, T.-B.; Lee, G.-H.; Peng, S.-M. *Chem. Eur. J.* **2007**, *13*, 1442. (f) Huang, G.-C.; Liu, I. P.-C.; Kuo, J.-H.; Huang, Y.-L.; Yeh, C.-Y.; Lee, G.-H.; Peng, S.-M. *Dalton Trans.* **2009**, 2623. (g) DeBrincat, D.; Keers, O.; McGrady, J. E. *Chem. Commun.* **2013**, *49*, 9116. (h) Wang, W.-Z.; Wu, Y.; Ismayilov, R. H.; Kuo, J.-H.; Yeh, C.-Y.; Lee, H.-W.; Fu, M.-D.; Chen, C.-h.; Lee, G.-H.; Peng, S.-M. *Dalton Trans.* **2014**, *43*, 6229. (i) Christian, J. H.; Brogden, D. W.; Bindra, J. K.; Kinyon, J. S.; van Tol, J.; Wang, J.; Berry, J. F.; Dalal, N. S. Submitted.

6. Dolinar, B. S.; Kozimor, S. A.; Berry, J. F. In preparation.

7. Shannon, R. D. *Acta Crystallogr.* **1976**, *A32*, 751.

8. Buckley-Dhoot, E.; Fawcett, J.; Kresinski, R. A.; Platt, A. W. G. *Polyhedron* **2009**, *28*, 1497.

9. Dolinar, B. S.; Berry, J. F. *Dalton Trans.* **2014**, *43*, 6165.

# Chapter 6

## *$K_3[Mo_2(SNO5)_4Cl]_3[Mo_2(SNO5)_4]$: The First Example of a Heterometallic Extended Metal Atom Node (HEMAN)*

### 6.1 Abstract

The synthesis, structural characterization, and electrochemistry of $K_3[Mo_2(SNO5)_4Cl]_3[Mo_2(SNO5)_4]$ (**1**, HSNO5 = monothiosuccinimide) the first example of a heterometallic extended metal atom node (HEMAN), and the synthesis and structure of $[pyH][Mo_2(SNO5)_4Cl]$ (**2**) are presented here. The HEMAN is formed by a core of $K^+$ ions that tether three $[Mo_2(SNO5)_4Cl]^-$ units and one $[Mo_2(SNO5)_4]$ unit together, giving rise to a structural motif consisting of two perpendicular, intersecting lines of metal atoms. The electrochemistry of **1** indicates that the compound remains intact in solution.

### 6.2 Introduction

Extended metal atom chains (EMACs, Chart 6.1) are multimetallic coordination compounds consisting of three or more linked metal atoms held together in a row by supporting ligands and have been known since the structure of $Ni_3(dpa)_4Cl_2$ was determined in 1991 (dpa = 2,2'-dipyridylamide).[1] Since then, the family of linear, trimetallic compounds has expanded to various transition metals including heterometallic (HEMAC) examples.[2] EMACs and HEMACs are enticing synthetic targets for molecular electronics due to their structural analogy to one-dimensional wires and transistors.[3] Production of molecule–scale logic gates will not just require wire components, but also well-defined junctions in which wires meet each other.[4] Such a junction can be described

**Chart 6.1.** The general structures of a) EMACs and b) EMANs.

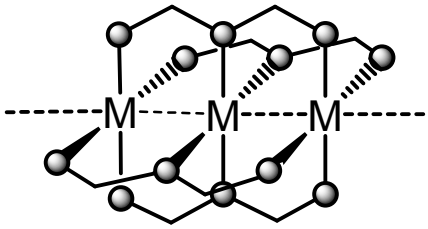


Extended Metal Atom Chain
(EMAC)

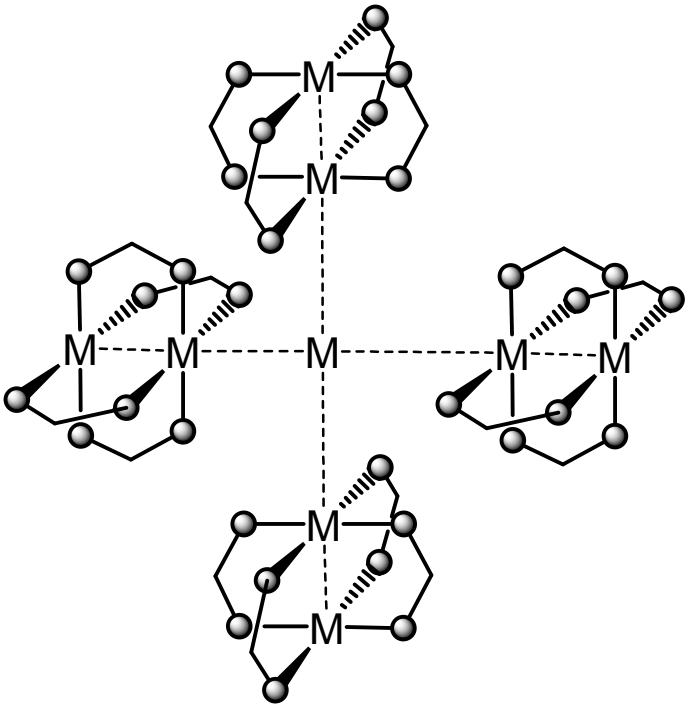


Extended Metal Atom Node
(EMAN)

as an extended metal atom node (EMAN, Chart 6.1) – the smallest component of a possible two-dimensional network of EMACs. To date, no such junction between EMACs has been prepared. Here, we report a heterometallic approach to this problem. Using the monothiosuccinimide ligand (HSNO5, Scheme 6.1) has led us to synthesize a variety of heterotrimetallic EMACs consisting of a dimolybdenum unit paired with a

heterometal selected from the alkali metals ($Li^+$, $Na^+$), alkaline earth metals ($Ca^{2+}$, $Sr^{2+}$), Group III ($Y^{3+}$) or the lanthanides.[2o,2s] Unlike in EMACs supported by equatorial dpa ligands, which consistently feature 3-center metal-metal σ bonds, the heterometal of the $SNO5^-$ compounds is farther away from the $[Mo_2]^{4+}$ unit, and influences its Lewis acidity and redox properties in a purely Coulombic manner. An interesting consequence of the extra distance between the heterometal and the $[Mo_2]^{4+}$ unit is that the coordination sphere of larger heterometals is not fully satisfied by the four $SNO5^-$ ligands, potentially allowing for the self-assembly of supramolecular structures. In contast to our results with $Li^+$ and $Na^+$, in which discrete heterotrimetallic M···Mo≡Mo compounds are produced, we show here that the larger $K^+$ ion leads to the self-assembly of the 11-core heterometallic EMAN (HEMAN) $K_3[Mo_2(SNO5)_4Cl]_3[Mo_2(SNO5)_4]$ (**1**) in MeCN, in which four dimolybdenum units are connected to a central core containing three $K^+$ ions.

**Scheme 6.1.** The synthetic route of **1** and **2**.

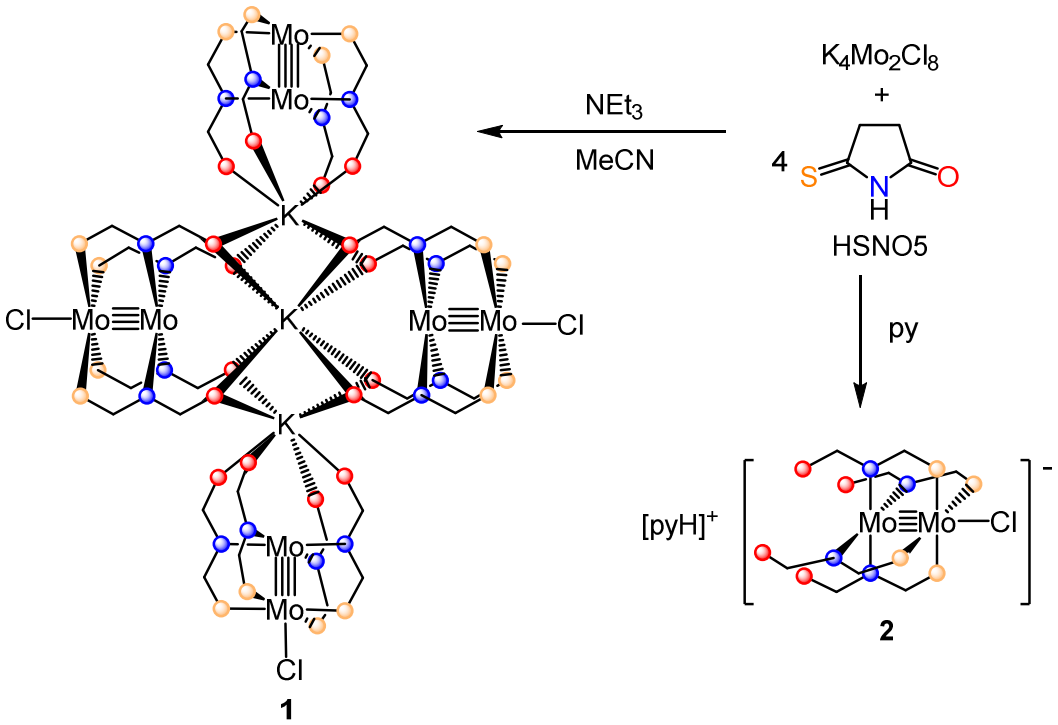

## 6.3 Results and Discussion

### 6.3.1 Synthesis

Reactions of quadruply-bonded $[Mo_2]^{4+}$ starting complexes with the HSNO5 ligand in the presence of $K^+$ ions produce different results depending on the reaction conditions. When $Mo_2(OAc)_4$ is used as a starting material, only *trans*-2,2-$Mo_2(SNO5)_4$ or *cis*-2,2-$Mo_2(SNO5)_4$ compounds are formed. [2o,5] $K_4Mo_2Cl_8$ can be used as a source of both $[Mo_2]^{4+}$ and $K^+$, however, the retention of $K^+$ in the final product depends on the solvent in which the reaction is conducted. When the reaction is conducted in MeCN, $K^+$ is included in the final product, resulting in **1**, but when the solvent is pyridine, (pyH)[(4,0)-$Mo_2(SNO5)_4Cl$] (**2**) is formed instead (See Scheme 6.1).

### 6.3.2 Structure

The structure of **1**·10MeCN is shown in Figure 6.1. The compound crystallizes as two symmetry independent half-molecules of **1** in the space group $P\bar{1}$ consisting of three $[Mo_2(SNO5)_4Cl]^-$ units and one $Mo_2(SNO5)_4$ species. The most defining feature of this compound is the two perpendicular, intersecting lines of metal atoms that is created in the compound. The four $[Mo_2]^{4+}$ units are held together by three $K^+$ ions lying along a non-crystallographic $C_2$ symmetry axis of the $C_{2v}$-symmetric molecule. The three $K^+$ ions, eight Mo atoms, and three $Cl^-$ ions reside in a non-crystallographic mirror plane that bisects the complex. Each of the $[Mo_2]^{4+}$ components is bonded to four $SNO5^-$ ligands situated in a 4,0-paddlewheel arrangement. The $SNO5^-$ ligands on each of the axial $[Mo_2]^{4+}$ units (parallel to the principal axis) reside in the molecular mirror planes. Each of the $SNO5^-$ ligands on the two equatorial $[Mo_2]^{4+}$ units (perpendicular to the principal axis) are rotated out of the plane by approximately 45° to avoid a steric clash between the

$SNO5^-$ ligands of the axial $[Mo_2]^{4+}$ units. Each $K^+$ ion is coordinated by the O atoms of eight $SNO5^-$ ligands. The central $K^+$ ion has a cubic coordination geometry, while the two outer $K^+$ ions have a square anti-prismatic geometry.

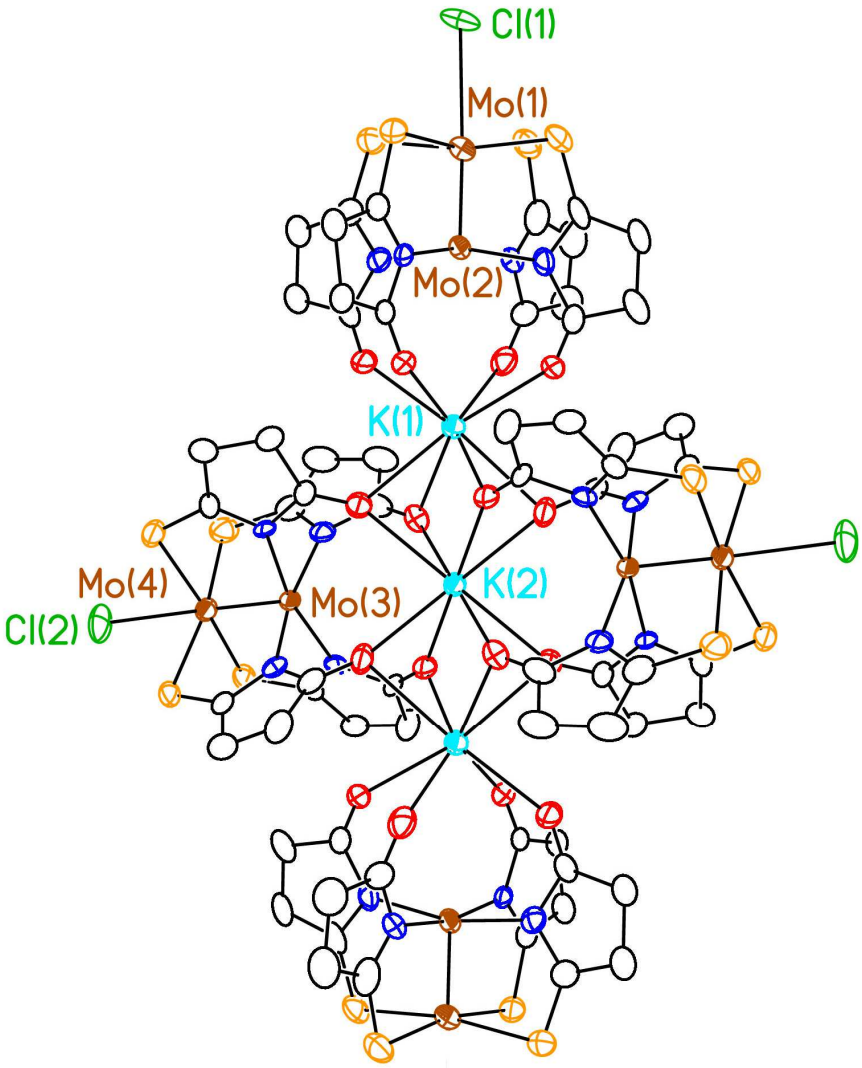


**Figure 6.1.** The X-ray crystal structure of **1**·10MeCN. All atoms are drawn as 50% thermal probability ellipsoids. Brown atoms denote Mo, green atoms denote Cl, sky blue atoms denote K, orange atoms denote S, red atoms denote O, dark blue atoms denote N, and black atoms denote C. All hydrogen atoms are omitted for clarity.

Relevant bond distances for both the axial and equatorial $[Mo_2]^{4+}$ components of **1**·10MeCN are listed in Table 6.1. For both the axial and equatorial $[Mo_2]^{4+}$ components, the Mo≡Mo quadruple bond is 2.14 Å, which is elongated compared with the average quadruple bonded Mo≡Mo distance.[6] This elongation is consistent with other 4,0-$[Mo_2(SNO5)_4Cl]^-$ variants,[2o,2s] and has been attributed to the donation of electron density from the axial $Cl^-$ ligand to the $[Mo_2]^{4+}$ σ* and π* orbitals. The K···$Mo_2$ distance is shorter for the axial component than it is for the equatorial component (3.938[2] and 4.091[1] Å, respectively), likely due to the difference in $K^+$ coordination geometry. This observation is further supported by the shorter K-O distances in the axial $[Mo_2]^{4+}$ units as compared with those of the equatorial $[Mo_2]^{4+}$ units. These K···$Mo_2$ distances are significantly longer than the heterometallic separations in either the $Na^+$ or $Li^+$ analogs (3.505(2) Å and 3.075(5) Å, respectively), primarily due to the larger ionic radius of $K^+$ (1.52 Å).[7] The $Mo_2$-Cl bond distances of the axial $[Mo_2]^{4+}$ units are longer than those of the equatorial $[Mo_2]^{4+}$ units (2.733[2] Å and 2.670[2] Å, respectively). This difference is attributable to the packing arrangement of **1** in the crystal structure. The chlorides on the equatorial $[Mo_2]^{4+}$ units point directly into pockets in the structure of neighboring molecules of **1**, whereas the axial $Cl^-$ ligands are not constrained by these interactions.

**Table 6.1.** Important Bond Distances for Structures **1**·10MeCN.

| **Structure** | **1**·10MeCN |
|---|---|
| d(Mo≡Mo) (Å) | 2.138[1] (ax) |
| | 2.144[1] (eq) |
| d(Mo-S) (Å) | 2.497[1] (ax) |
| | 2.494[1] (eq) |
| d(Mo-N) (Å) | 2.161[3] (ax) |
| | 2.150[3] (eq) |
| d($Mo_2$-Cl) (Å) | 2.733[2] (ax) |
| | 2.670[2] (eq) |
| d(K···$Mo_2$) (Å) | 3.938[2] (ax) |
| | 4.091[1] (eq) |

### 6.3.3 Electrochemistry

Cyclic voltammetry was performed between 750 mV and -850 mV vs. $Fc/Fc^+$ on a solution of **1** in propylene carbonate with 0.1 M $NEt_4PF_6$ as the electrolyte. The cyclic voltammogram exhibits two quasi-reversible oxidation waves. The electrochemical solution was titrated with 10 mL of a 0.1 M solution of KOTf. Over the course of the titration, both of the $[Mo_2]^{4+/5+}$ oxidation waves move to a slightly higher potential, reaching final $E_{1/2}$ potentials of 216 mV and 407 mV vs. $Fc/Fc^+$. The two waves likely represent the oxidation of the axial and equatorial $[Mo_2]^{4+}$ groups of **1**. The increasing oxidation potential with increasing $[K^+]$ is consistent with previous examples of $[MMo_2(SNO5)_4Cl]^{n-1+}$ compounds in which an assembled $MMo_2$ complex is in equilibrium with demetallated complex. The oxidation waves were invariant upon further addition of $K^+$ to the solution, indicating that these $E_{1/2}$ values correspond to intact molecules of **1**.

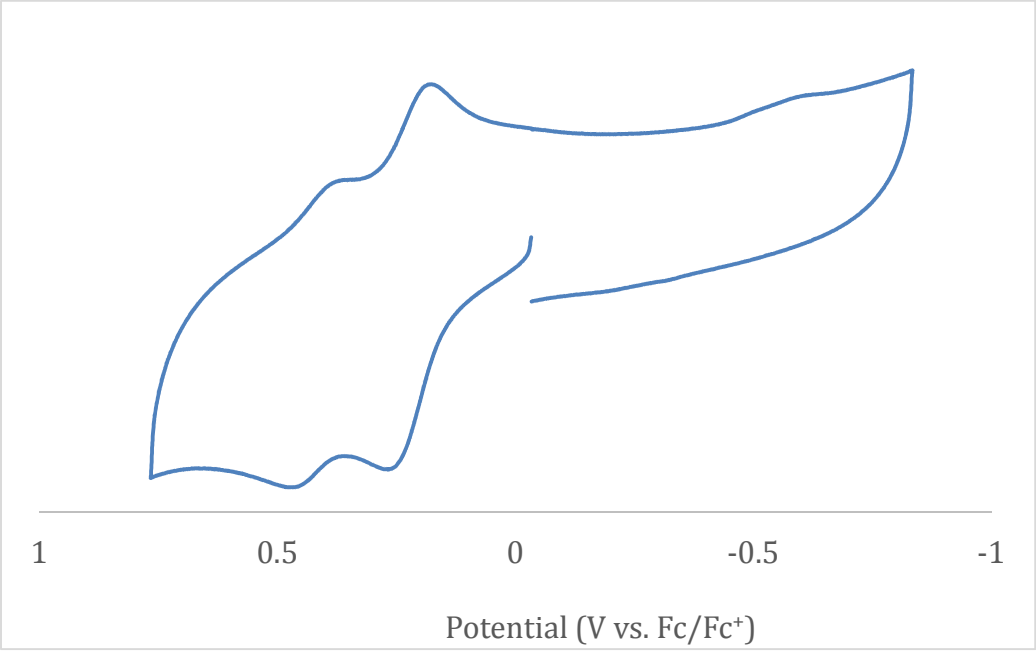


**Figure 6.2.** The electrochemistry of **1**.

## 6.4 Conclusions

In this paper we have described the synthesis and characterization of **1**, the first example of a HEMAN structural motif composed of four converging $[Mo_2]^{4+}$ subunits held together through coordination to three $K^+$ ions. This compound is important for two reasons. First, it illustrates the diversity of structural motifs that are capable of being supported by the $SNO5^-$ ligand. Second, the ease with which **1** is synthesized indicates that HEMANs could be rapidly generated by judiciously choosing the heterometal additive in a ligand substitution reaction. The planar structure of **1** suggests that it may adhere to planar electrode or semiconductor surfaces where it could be tested as a molecular logic gate.

## 6.5 Acknowledgements

The authors wish to acknowledge financial support was provided under NSF Grant CHE-1300464, NIH NCRR award 1S10RR024601-1 (Mass spectrometry), and a generous gift from Paul J. Bender (X-ray diffraction). BSD thanks the Seaborg Institute for a summer research fellowship that contributed to this paper.

## 6.6 Supporting Information

### 6.6.1 Experimental

#### 6.6.1.1 General

All syntheses were carried out under an inert $N_2$ atmosphere using standard Schlenk and glovebox techniques unless otherwise specified. Solvents MeCN and THF were dried sequentially over molecular sieves and a Vacuum Atmospheres solvent purification system and degassed prior to use. Pyridine was dried over molecular sieves, distilled from barium oxide under $N_2$, and stored in an inert atmosphere glovebox prior to

use. $K_4Mo_2Cl_8$ was synthesized from $Mo_2(OAc)_4$, KCl, and HCl gas. [8] HSNO5 was synthesized from succinimide and $P_4S_{10}$. [9] All other reagents were purchased from Sigma Aldrich and used as received. $^1H$, and $^{13}C$ NMR spectra were collected on a Bruker Avance III 500 MHz spectrometer. Mass spectra were collected on a Bruker ULTRAFLEX™ III MALDI-TOF/TOF-MS equipped with a SmartBeam™ laser. FTIR (ATR) data were obtained using a Bruker TENSOR 27 spectrometer. Elemental analysis was carried out by Midwest Microlabs in Indianapolis, IN, USA.

**6.6.1.2 Syntheses**

**tripotassium-tris(dimolybdenum(tetrakis-monothiosuccinimidato)chloro)(dimolybdenum(tetrakis-monothiosuccinimidato) ($K_3[Mo_2(SNO5)_4Cl]_3[Mo_2(SNO5)_4]$), (1)**

A flask was charged with 104 mg HSNO5 (0.903 mmol) and 129 mg $K_4Mo_2Cl_8$ (0.226 mmol). These were suspended in 20 mL MeCN. Then, 250 μL $NEt_3$ (1.79 mmol) was added via syringe, turning the reaction mixture an orange color. The reaction mixture was heated to 75° C for 16 hours. Over the course of the reaction, the solution gradually became a very dark orange color and deposited crystals on the walls and base of the flask. After cooling to room temperature, the reaction mixture was filtered, washed with 3 x 20 mL MeCN, 3 x 20 mL $H_2O$, 3 x 20 mL EtOH, and 3 x 20 mL $Et_2O$. The compound was dried in air. Yield: 35 mg (22 %). X-ray quality crystals of **1** were grown from layering the filtrate of the reaction with $Et_2O$. $^1H$ NMR (500 MHz, DMSO-d6) δ 3.55 (m, 32 H), 2.77 (m, 32H). $^{13}C$ (125 MHz, DMSO-d6) δ 216.53, 189.58, 46.01, 32.54 ppm . IR (ATR, $cm^{-1}$): 2962 (vw), 2930 (vw), 1731 (m), 1431 (w), 1389 (m), 1230 (s), 1211 (vs), 1125 (w), 995 (vw), 963 (m), 931 (m), 806 (w), 679 (w). Elem. Anal. Cald. for:

$C_{64}H_{78}Cl_3K_3Mo_8N_{16}O_{23}S_{16}$ (**1**·7$H_2O$): C, 26.11%; H, 2.67%; N, 7.61%. Found: C, 25.78%; H, 2.22%; N, 7.35%.

**pyridinium 4,0-molybdenum(tetrakis-monothiosuccinimidato)chloride ([pyH][4,0-$Mo_2$(SNO5)$_4$Cl]), (2)**

A flask was charged with 56 mg HSNO5 (0.49 mmol) and 69 mg $K_4Mo_2Cl_8$ (0.12 mmol). These were suspended in 15 mL pyridine and heated without stirring at 75° C for 16 hours. Throughout the course of the reaction, X-ray quality crystals of **2** were deposited on the walls and base of the flask. The crystals were collected by filtration, washed with 2 x 20 mL $H_2O$, 3 x 20 mL EtOH, and dried under vacuum. Yield: 21 mg (23%) $^1$H NMR (500 MHz, DMSO-d6) δ 8.82 ppm (br), 8.34 (br), 7.85 (br), 3.55 (m, 8H) 2.78 (m, 8H). $^{13}$C (125 MHz, DMSO-d6) δ 216.54, 189.54, 144.78, 143.60, 126.68, 32.54. IR (ATR, cm$^{-1}$): 2963 (vw), 1752 (m), 1732 (m), 1524 (vw), 1490 (vw), 1392 (w), 1259 (m), 1229 (m), 1195 (m), 1089 (s), 1019 (s), 963 (m), 940 (m), 866 (m), 799 (vs), 751 9w), 678 (w). Elem. Anal. Calcd for $C_{22.65}H_{23.65}ClMo_2N_{5.33}O_4S_4$ (**2**·0.33py): C, 34.43%; H, 3.02%; N, 9.45%. Found: C, 34.72%; H, 2.95%; N, 9.03%.

**6.6.1.3 X-ray Crystallography**

Single crystals of **1** and **2** were selected under paratone oil and attached to a MiTeGen MicroMount. They were mounted in a stream of cold $N_2$ at 100(1) K in a cold $N_2$ stream using an Oxford Cryostat and centered in the X-ray beam using a video monitoring system. The crystal evaluation and data collection were performed on a Bruker Quazar APEX-II diffractometer with Mo Kα radiation (λ = 0.71073 Å). The data were collected using a routine to survey an entire sphere of reciprocal space. The data were integrated using the SAINT routine in APEX-II and corrected for absorption using

SADABS. [10] The structures were solved *via* direct methods and refined by iterative cycles of least-squares refinement on $F^2$ followed by difference Fourier synthesis using SHELX2013. [11] All non-hydrogen atoms were refined anisotropically. The data collection and acquisition parameters for **1** and **2** are included in Table 6.S1.

#### 6.6.1.4 Electrochemistry

The electrochemistry of **1** was measured by cyclic voltammetry in propylene carbonate at room temperature with 1 mM analyte and 100 mM electrolyte ($NEt_4PF_6$) using a standard glassy carbon electrode for the working electrode, a platinum wire for the auxiliary electrode, and an $Ag/Ag^+$ electrode as the reference electrode. The solution was titrated with 10 mL of a 0.1 M solution of KOTf in propylene carbonate. All electrochemical potentials were internally referenced to the ferrocene/ferrocenium couple. The voltammetry was performed in the range of 400 mV to -1200 mV and 1500 to -1200 mV vs. $Fc/Fc^+$ at a scan rate of 100 mV $s^{-1}$.

### 6.6.2 Crystallographic Details for 1·10MeCN

*Data Collection*

An orange crystal with approximate dimensions 0.05 x 0.05 x 0.01 $mm^3$ was selected under oil under ambient conditions and attached to the tip of a MiTeGen MicroMount©. The crystal was mounted in a stream of cold nitrogen at 100(1) K and centered in the X-ray beam by using a video camera.

The crystal evaluation and data collection were performed on a Bruker Quazar SMART APEXII diffractometer with Mo $K_\alpha$ ($\lambda$ = 0.71073 Å) radiation and the diffractometer to crystal distance of 4.96 cm.

The initial cell constants were obtained from three series of ω scans at different starting angles. Each series consisted of 12 frames collected at intervals of 0.5° in a 6° range about ω with the exposure time of 60 seconds per frame. The reflections were successfully indexed by an automated indexing routine built in the APEXII program suite. The final cell constants were calculated from a set of 9934 strong reflections from the actual data collection.

The data were collected by using the full sphere data collection routine to survey the reciprocal space to the extent of a full sphere to a resolution of 0.70 Å. A total of 57281 data were harvested by collecting 3 sets of frames with 0.5° scans in ω and φ with exposure times of 120 sec per frame. These highly redundant datasets were corrected for Lorentz and polarization effects. The absorption correction was based on fitting a function to the empirical transmission surface as sampled by multiple equivalent measurements.[10b]

*Structure Solution and Refinement*

The diffraction data were consistent for the space groups $P1$, $P\bar{1}$. The *E*-statistics strongly suggested a centrosymmetric space group, and $P\bar{1}$ yielded chemically reasonable and computationally stable results of refinement.

A successful solution by the direct methods provided most non-hydrogen atoms from the *E*-map. [11a] The remaining non-hydrogen atoms were located in an alternating series of least-squares cycles and difference Fourier maps. All non-hydrogen atoms were refined with anisotropic displacement coefficients. All hydrogen atoms were included in the structure factor calculation at idealized positions and were allowed to ride on the neighboring atoms with relative isotropic displacement coefficients.[11b,12]

The asymmetric unit consists of two symmetry independent half molecules of $K_3[Mo_2(SNO5)_4Cl][Mo_2(SNO5)_4]$. The $K_3[Mo_2(SNO5)_4Cl][Mo_2(SNO5)_4]$ molecules reside on a crystallographic inversion center. Chlorides Cl1 and Cl1A are disordered across the inversion center and have 50% occupancy in the asymmetric unit.

There were several partially occupied solvent molecules of acetonitrile present in the asymmetric unit. A significant amount of time was invested in identifying and refining the disordered molecules. Idealized geometries and thermal parameter restraints were applied to model the molecules but the resulting isotropic displacement coefficients suggested the molecules were mobile. In addition, the refinement was computationally unstable. The solvent mask option of OLEX2 was used to correct the diffraction data for diffuse scattering effects and to identify the solvate molecule. OLEX2 calculated the upper limit of volume that can be occupied by the solvent to be 1839.5 $Å^3$, or 30.3% of the unit cell volume. The program calculated 461.8 electrons in the unit cell for the diffuse species. This approximately corresponds to 10.5 molecules of acetonitrile in the asymmetric unit (231 electrons). It is very likely that these solvent molecules are disordered over several positions.

The final least-squares refinement of 1151 parameters against 22344 data resulted in residuals $R$ (based on $F^2$ for $I \geq 2\sigma$) and $wR$ (based on $F^2$ for all data) of 0.0675 and 0.1770, respectively. The final difference Fourier map was featureless.

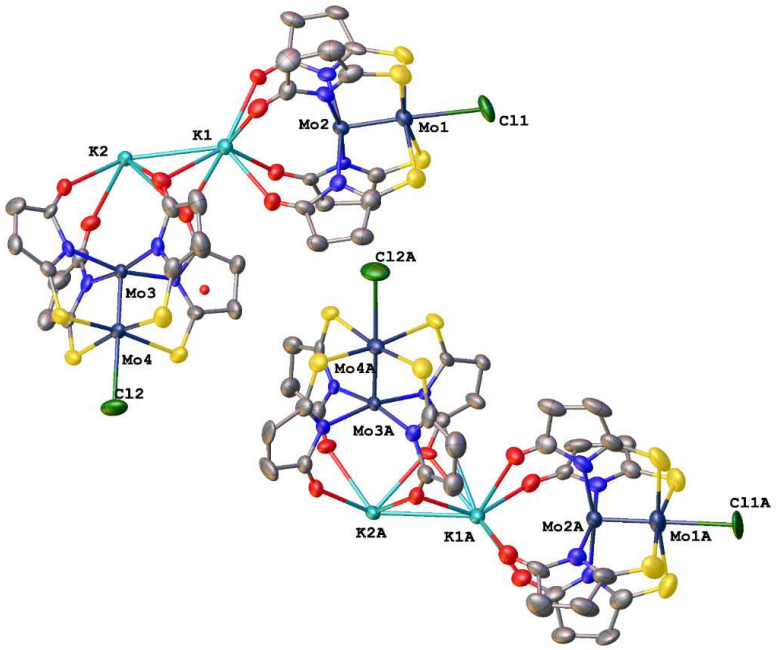


**Figure 6.S1.** The asymmetric unit of **1**·10MeCN. All atoms are shown as 50% thermal probability ellipsoids. All H atoms are omitted for clarity.

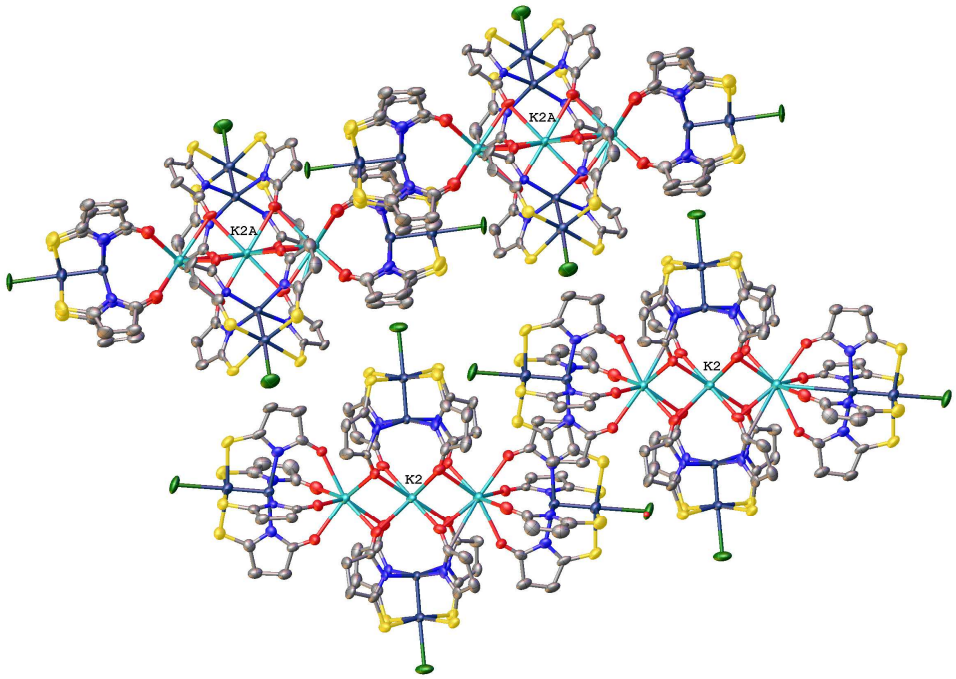


**Figure 6.S2.** The packing diagram of **1**·10MeCN. All atoms are drawn as 50% thermal probability ellipsoids. All H atoms are omitted for clarity.

### 6.6.3 Crystallographic Details for 2·1.5py

*Data Collection*

A red crystal with approximate dimensions 0.056 x 0.094 x 0.098 $mm^3$ was selected under oil under ambient conditions and attached to the tip of a MiTeGen MicroMount©. The crystal was mounted in a stream of cold nitrogen at 100(1) K and centered in the X-ray beam by using a video camera.

The crystal evaluation and data collection were performed on a Bruker Quazar SMART APEXII diffractometer with Mo $K_\alpha$ ($\lambda$ = 0.71073 Å) radiation and the diffractometer to crystal distance of 4.96 cm.

The initial cell constants were obtained from three series of $\omega$ scans at different starting angles. Each series consisted of 12 frames collected at intervals of 0.5° in a 6° range about $\omega$ with the exposure time of 30 seconds per frame. The reflections were successfully indexed by an automated indexing routine built in the APEXII program suite. The final cell constants were calculated from a set of 9995 strong reflections from the actual data collection.

The data were collected by using the full sphere data collection routine to survey the reciprocal space to the extent of a full sphere to a resolution of 0.70 Å. A total of 64686 data were harvested by collecting 5 sets of frames with 0.5° scans in $\omega$ and $\varphi$ with exposure times of 30 sec per frame. These highly redundant datasets were corrected for Lorentz and polarization effects. The absorption correction was based on fitting a function to the empirical transmission surface as sampled by multiple equivalent measurements.[10b]

*Structure Solution and Refinement*

The systematic absences in the diffraction data were uniquely consistent for the space groups $P2_1/c$, which yielded chemically reasonable and computationally stable results of refinement.

A successful solution by the direct methods provided most non-hydrogen atoms from the *E*-map.[11a] The remaining non-hydrogen atoms were located in an alternating series of least-squares cycles and difference Fourier maps. All non-hydrogen atoms were refined with anisotropic displacement coefficients. All hydrogen atoms were included in the structure factor calculation at idealized positions and were allowed to ride on the neighboring atoms with relative isotropic displacement coefficients.[11b,12]

The asymmetric unit consists of a pyridinium cation, a $[Mo_2(SNO5)_4Cl]^-$ anion, and two pyridine solvent molecules. The pyridinium cation and pyridine solvent molecule N6 reside on general positions and are both disordered over two positions (major components: 50.3(6)% and 71.0(9)%, respectively). Pyridine solvent molecule N7 is disordered over a crystallographic inversion center (major component: 50%). Bond distance and thermal parameter restraints were used to ensure a chemically reasonable and computationally stable refinement.

The final least-squares refinement of 552 parameters against 7714 data resulted in residuals *R* (based on $F^2$ for $I \geq 2\sigma$) and *wR* (based on $F^2$ for all data) of 0.0431 and 0.1057, respectively.

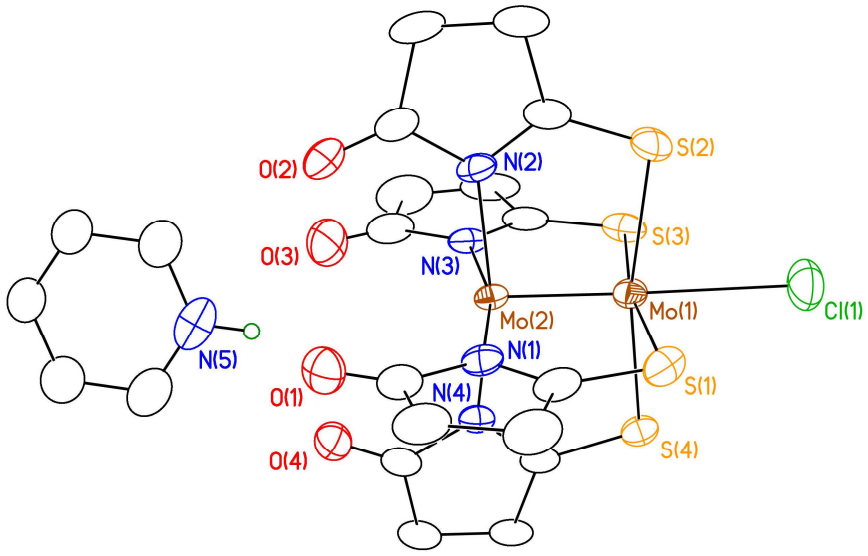


**Figure 6.S3.** The structure of the **2**·1.5py. All atoms are drawn as 50% thermal probability ellipsoids. All H-atoms are omitted for clarity.

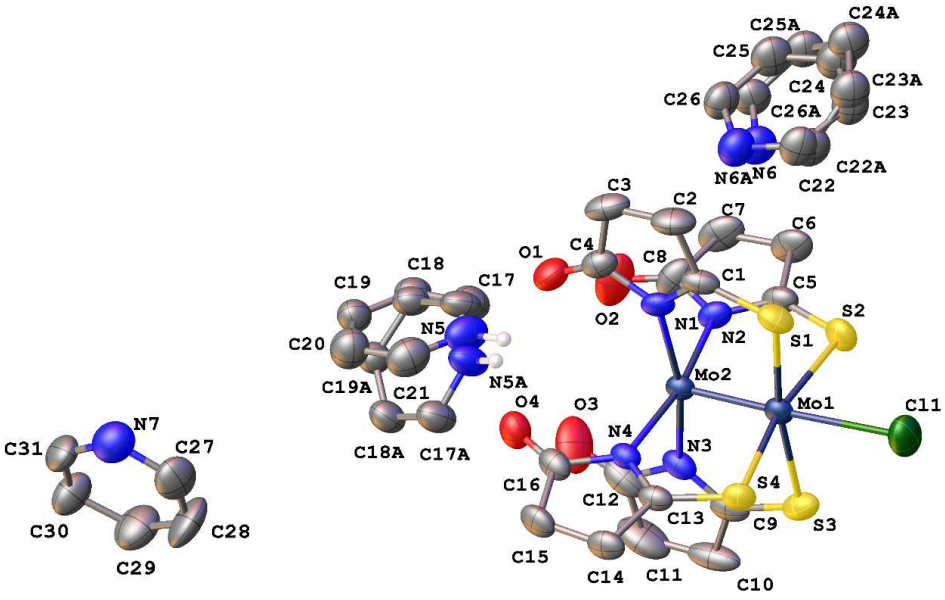


**Figure 6.S4.** The asymmetric unit of **2**·1.5py, including all disordered components. All atoms are drawn as 50% thermal probability ellipsoids. All H atoms, except those on the N of the pyridinium cation, are omitted for clarity.

**Table 6.S1.** The X-ray crystallography experimental parameters for structures **1**·10MeCN and **2**·1.5py

| Structure | **1** · 10 MeCN | **2** · 1.5 py |
|---|---|---|
| Empirical formula | $K_3Mo_8(C_{64}H_{64}N_{16}O_{16}S_{16}Cl_3)\cdot 10(CH_3CN)$ | $[C_5H_6N]^+ [Mo_2C_{16}H_{16}N_4S_4O_4Cl]^-\cdot 1.5(C_5H_5N)$ |
| Formula weight | 2825.44 | 882.65 |
| Temperature/K | 100.0 | 100.0 |
| Crystal system | triclinic | monoclinic |
| Space group | $P\bar{1}$ | $P2_1/c$ |
| a/Å | 16.397(7) | 8.762(3) |
| b/Å | 17.295(6) | 14.296(5) |
| c/Å | 24.416(13) | 26.630(8) |
| α/° | 88.31(3) | 90 |
| β/° | 79.279(18) | 92.425(16) |
| γ/° | 63.20(2) | 90 |
| Volume/Å$^3$ | 6061(5) | 3332.8(19) |
| Z | 2 | 4 |
| $\rho_{calc}$g/cm$^3$ | 1.548 | 1.759 |
| μ/mm$^{-1}$ | 1.298 | 1.129 |
| F(000) | 2784.0 | 1772.0 |
| Crystal size/mm$^3$ | 0.4 × 0.3 × 0.2 | 0.4 × 0.3 × 0.2 |
| Radiation | MoKα (λ = 0.71073) | MoKα (λ = 0.71073) |
| 2Θ range for data collection/° | 2.644 to 50.9 | 3.062 to 55.202 |
| Index ranges | $-19 \le h \le 19$<br>$-20 \le k \le 20$<br>$-29 \le l \le 29$ | $-11 \le h \le 11$<br>$-18 \le k \le 18$<br>$-34 \le l \le 34$ |
| Reflections collected | 57281 | 64686 |
| Independent reflections | 22344 [$R_{int}$ = 0.0969 $R_{sigma}$ = 0.1344] | 7714 [$R_{int}$ = 0.0526 $R_{sigma}$ = 0.0424] |
| Data/restraints/parameters | 22344/0/1151 | 7714/429/552 |
| Goodness-of-fit on $F^2$ | 0.931 | 1.062 |
| Final R indexes [I>=2σ (I)] | R1 = 0.0675<br>wR2 = 0.1610 | R1 = 0.0431<br>$wR_2$ = 0.0998 |
| Final R indexes [all data] | R1 = 0.1280<br>wR2 = 0.1770 | R1 = 0.0568<br>wR2 = 0.1061 |
| Largest diff. peak/hole / e Å$^{-3}$ | 1.52/-1.32 | 1.15/-0.49 |

**Table 6.S2.** Important bond distances for **2**·1.5 py

| | **2**·1.5 py |
|---|---|
| d(Mo-Mo) (Å) | 2.1463(7) |
| d(Mo-S) (Å) | 2.4870[7] |
| d(Mo-N) (Å) | 2.155[2] |
| d(Mo-Cl) (Å) | 2.707(2) |

## 6.7 References

1. (a) Aduldecha, S.; Hathaway, B. *J. Chem. Soc. Dalton Trans.* **1991**, 993. (b) Cotton, F. A.; Murillo, C. A.; Walton, R. A. *Multiple Bonds Between Metal Atoms*. 3rd ed.; Springer Science and Business Media, Inc.: New York, 2005. (c) Berry, J. F. Metal Metal Bonds in Chains of Three or More Metal Atoms: From Homometallic to Heterometallic Chains. In *Metal-Metal Bonding*, Parkin, G., Ed. 2010; Vol. 136, pp 1. (d) Hua, S.-A.; Tsai, Y.-C.; Peng, S.-M. *J. Chin. Chem. Soc.* **2014**, *61*, 9.

2. (a) Chien, C.-H.; Chang, J.-C.; Yeh, C.-Y.; Lee, G.-H.; Fang, J.-M.; Peng, S.-M. *Dalton Trans.* **2006**, 2106. (b) Kuo, C.-K.; Liu, I. P.-C.; Yeh, C.-Y.; Chou, C.-H.; Tsao, T.-B.; Lee, G.-H.; Peng, S.-M. *Chem. Eur. J.* **2007**, *13*, 1442. (c) Wang, W.-Z.; Ismayilov, R. H.; Lee, G.-H.; Liu, I. P.-C.; Yeh, C.-Y.; Peng, S.-M. *Dalton Trans.* **2007**, 830. (d) Nippe, M.; Berry, J. F. *J. Am. Chem. Soc.* **2007**, *129*, 12684. (e) Ohashi, M.; Shima, A.; Rüffer, T.; Mizomoto, H.; Kaneda, Y.; Mashima, K. *Inorg. Chem.* **2007**, *46*, 6702. (f) Nippe, M.; Victor, E.; Berry, J. F. *Eur. J. Inorg. Chem.* **2008**, *2008*, 5569. (g) Wang, W.-Z.; Ismayilov, R. H.; Wang, R.-R.; Huang, Y.-L.; Yeh, C.-Y.; Lee, G.-H.; Peng, S.-M. *Dalton Trans.* **2008**, 6808. (h) Yin, C.; Huang, G.-C.; Kuo, C.-K.; Fu, M.-D.; Lu, H.-C.; Ke, J.-H.; Shih, K.-N.; Huang, Y.-L.; Lee, G.-H.; Yeh, C.-Y.; Chen, C.-H.; Peng, S.-M. *J. Am. Chem. Soc.* **2008**, *130*, 10090. (i) Ismayilov, R. H.; Wang, W.-Z.;

Wang, R.-R.; Huang, Y.-L.; Yeh, C.-Y.; Lee, G.-H.; Peng, S.-M. *Eur. J. Inorg. Chem.* **2008**, 4290. (j) Huang, G.-C.; Liu, I. P.-C.; Kuo, J.-H.; Huang, Y.-L.; Yeh, C.-Y.; Lee, G.-H.; Peng, S.-M. *Dalton Trans.* **2009**, 2623. (k) Liu, I. P.-C.; Chen, C.-H.; Chen, C.-F.; Lee, G.-H.; Peng, S.-M. *Chem. Commun.* **2009**, 577. (l) Yeh, C.-W.; Liu, I. P.-C.; Wang, R.-R.; Yeh, C.-Y.; Lee, G.-H.; Peng, S.-M. *Eur. J. Inorg. Chem.* **2010**, 3153. (m) Pal, K.; Nakao, K.; Mashima, K. *Eur. J. Inorg. Chem.* **2010**, 5668. (n) Nippe, M.; Wang, J.; Bill, E.; Hope, H.; Dalal, N. S.; Berry, J. F. *J. Am. Chem. Soc.* **2010**, *132*, 14261. (o) Dolinar, B. S.; Berry, J. F. *Inorg. Chem.* **2013**, *52*, 4658. (p) Brogden, D. W.; Berry, J. F. *Inorg. Chem.* **2014**, *53*, 11354. (q) Huang, M.-J.; Hua, S.-A.; Fu, M.-D.; Huang, G.-C.; Yin, C.; Ko, C.-H.; Kuo, C.-K.; Hsu, C.-H.; Lee, G.-H.; Ho, K.-Y.; Wang, C.-H.; Yang, Y.-W.; Chen, I. C.; Peng, S.-M.; Chen, C.-H. *Chem. Eur. J.* **2014**, *20*, 4526. (r) Brogden, D. W.; Christian, J. H.; Dalal, N. S.; Berry, J. F. *Inorg. Chim. Acta* **2015**, *424*, 241. (s) Dolinar, B. S.; Berry, J. F. *Polyhedron* **2016**, *103*, 71.

3. (a) Chae, D. H.; Berry, J. F.; Jung, S.; Cotton, F. A.; Murillo, C. A.; Yao, Z., *Nano Lett.* **2006**, *6*, 165. (b) Georgiev, V. P.; Mohan, P. J.; DeBrincat, D.; McGrady, J. E. *Coord. Chem. Rev.* **2013**, *257*, 290. (c) DeBrincat, D.; Keers, O.; McGrady, J. E. *Chem. Commun.* **2013**, *49*, 9116.

4. (a) Collier, C. P.; Wong, E. W.; M., B.; Raymo, F. M.; Stoddart, J. F.; Kuekes, P. J.; Williams, R. S.; Heath, J. R. *Science* **1999**, *285*, 391. (b) Bachtold, A.; Hadley, P.; Nakanishi, T.; Dekker, C. *Science* **2001**, *294*, 1317. (c) Huang, Y.-L.; Duan, X.; Cui, Y.; Lauhon, L. J.; Kim, K.-H.; Lieber, C. M. *Science* **2001**, *294*, 1313. (d) Luo, Y.; Collier, C. P.; Jeppesen, J. O.; Nielsen, K. A.; Delonno, E.; Ho, G.; Perkins, J.; Tseng, H.-R.; Yamamoto, T.; Stoddart, J. F.; Heath, J. R. *Chem. Phys. Chem.* **2002**, *3*, 519. (e) Zong,

Z.; Wang, D.; Cui, Y.; Bockrath, M. W.; Lieber, C. M. *Science* **2003**, *302*, 1377. (f) Pischel, U. *Angew. Chem. Int. Ed.* **2007**, *46*, 4026. (g) Ruiter, G. D.; van der Boom, M. E. *Acc. Chem. Res.* **2011**, *44*, 563.

5. Dolinar, B. S.; Berry, J. F. *Dalton Trans.* **2014**, *43*, 6165.

6. Allen, F. H. *Acta Crystallogr.* **2002**, *B58*, 380.

7. Shannon, R. D. *Acta Crystallogr.* **1976**, *A32*, 751.

8. Brencic, J. V.; Cotton, F. A. *Inorg. Chem.* **1969**, *8*, 7.

9. Berg, U.; Sandström, J. *Acta Chem. Scand.* **1966**, *20*, 689.

10. (a) Bruker-AXS *APEX2*, 2014.11-0; Bruker AXS: Madison, WI, 2014; (b) Kraus, L.; Herbst-Irmer, R.; Sheldrick, G. M.; Stalke, D. *J. Appl. Crystallogr.* **2015**, *48*, 3.

11. (a) Sheldrick, G. M. *XS*, Georg-August-Universität Göttingen: Göttingen, Germany, 2013; (b) Sheldrick, G. M. *Acta Crystallogr.* **2015**, *C71*, 3.

12. Dolomanov, O. V.; Bourhis, L. J.; Gildea, R. J.; Howard, J. A. K.; Puschmann, H. *J. Appl. Crystallogr.* **2009**, *42*, 339.

# Chapter 7

*Summary and Future Directions*

The research presented in this thesis describes the synthesis of a variety of HEMACs containing main group elements and lanthanides as the heterometal. The size and charge of these ions influences the Lewis acidity and electrochemistry of the $[Mo_2]^{4+}$ unit. This work has expanded the scope of $MMo_2$ HEMACs from a small handful of complexes, in which M is confined to the transition metals and interacted with $[Mo_2]^{4+}$ *via* covalent interactions of varying strength, to a large array of complexes containing Group I, II, III, or lanthanide ions that interact with $[Mo_2]^{4+}$ unit *via* through space Coulombic interactions (Figure 7.1). Now, the exploration of more of their chemical and physical properties can commence. Several possible routes by which this chemistry can be expanded are described below.

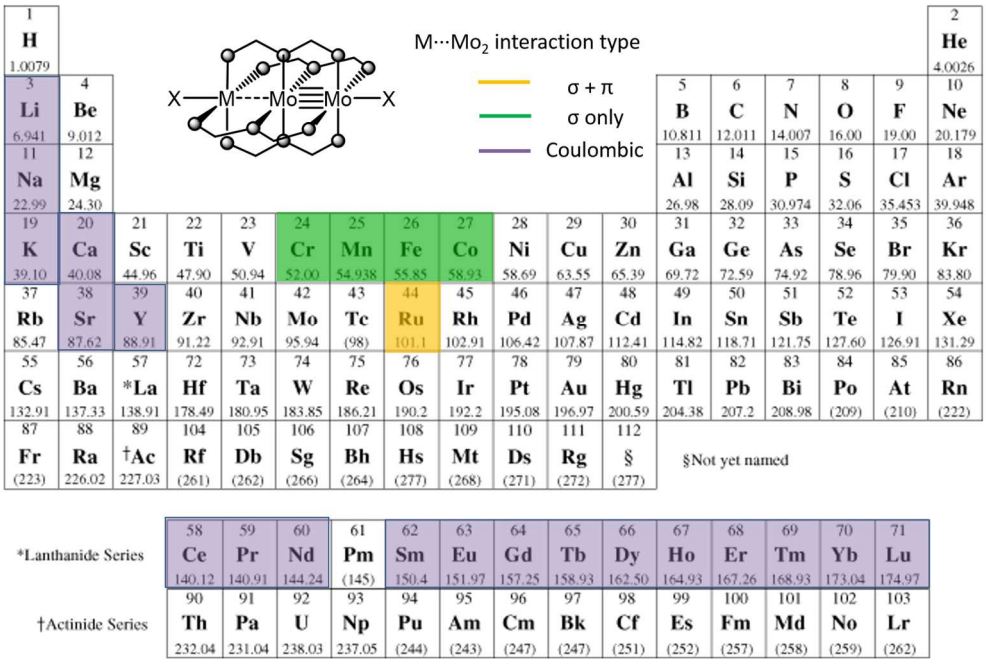


**Figure 7.1.** The periodic table showing the $MMo_2$ complexes that had been previously made (gold and green) and were made in the course of this thesis (purple).

First, the increased Lewis acidity of $[Mo_2]^{4+}$ can be more thoroughly exploited by synthesizing $MMo_2$ HEMACs with a variety of axial ligands. Compounds containing these ligands can possibly be obtained by substituting the axial chlorides of the $[MMo_2(SNO5)_4Cl]^{n+}$ compounds for ligands such as $N_3^-$, $RO^-$, and $Bz^-$. These types of ligands have never been axially substituted onto a $[Mo_2]^{4+}$ paddlewheel complex and thus their effect on the electronics and chemistry of the $[Mo_2]^{4+}$ will be worthy of study. In particular a $[MMo_2(SNO5)_4N_3]^{n+}$ complex is desirable as it may enable access to an axial nitride $[MMo_2(SNO5)_4N]^{n-2+}$ compound via thermolysis or photolysis and possible catalytic chemistry. Such chemistry might provide a cheaper route to the axial azide chemistry of $Ru_2(chp)_4N_3$.[1]

In addition to the chemistry centered at the $[Mo_2]^{4+}$ unit, the physical properties of the heterometal also need to be explored. The magnetism of the $[(MeOH)_xLnMo_2(SNO5)_4Cl]^{2+}$ compounds has yet to be examined. Due the highly axial nature of these compounds, they may exhibit single molecule magnet behavior.[2] In these compounds, the interaction of the diamagnetic anisotropy of the $[Mo_2]^{4+}$ unit with the large paramagnetic anisotropies of the $Ln^{3+}$ ions may also enhance the magnetic behavior (Figure 7.1). Currently these compounds have been submitted for SQUID magnetometry in an effort to elucidate this behavior. The magnetism of Mo≡Mo···Ln··· Mo≡Mo compounds similar to Mo≡Mo···Eu··· Mo≡Mo synthesized in Chapter 5 is also unknown. Comparing the 2:1 $Mo_2$:Ln complexes with the 1:1 $Mo_2$:Ln complexes should provide insight into whether or not the diamagnetic anisotropy of the $[Mo_2]^{4+}$ unit has a significant influence on the $Ln^{3+}$ magnetism.

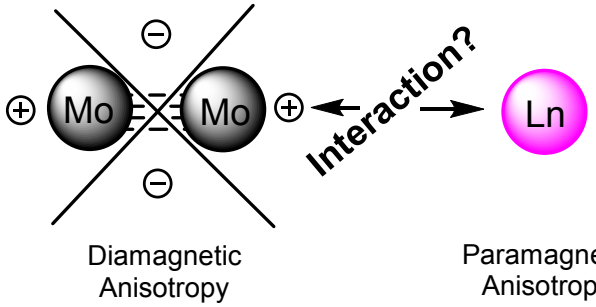


**Figure 7.2.** The proposed interaction between the diamagnetic anisotropy of $[Mo_2]^{4+}$ and the paramagnetic anisotropy of $Ln^{3+}$.

Finally, heterotrimetallic complexes containing other bimetallic units, such as $[Ru_2]^{5+}$ and $[Rh_2]^{4+}$ will also be a set of desirable targets. Heterotrimetallic compounds containing these bimetallic units may be able to influence the rich reactivity they currently display. Also, by taking advantage of the different magnetic properties of these bimetallic units, the influence of their magnetism on that of $Ln^{3+}$ ions can also be studied and compared with the effects of $[Mo_2]^{4+}$.

**7.1 References**

1. Corcos, A. R.; Long, A. K. M.; Guzei, I. A.; Berry, J. F. *Eur. J. Inorg. Chem.* **2013**, 3808.
2. Rinehart, J. D.; Long, J. R. *Chem. Sci.* **2011**, *2*, 2078.